Investigating the actin cytoskeleton in cancer

Jennifer Brown

Submitted in fulfilment of the requirements for the
Degree of Doctor of Philosophy

October 2015

Beatson Institute for Cancer Research

University of Glasgow

Abstract

Dynamic alterations in the actin cytoskeleton, under the regulation of the Rho/ROCK pathway, permit cell motility, cell-to-cell and cell-to-matrix adhesion, and have also been shown to participate in apoptosis and cell proliferation. These facets of cellular behaviour all have the capacity to become dysregulated in cancer; components of the Rho/ROCK pathway are known to play varying roles in these processes, both within primary tumours and within the tumour microenvironment.

The LIM kinases are phosphorylated and activated by ROCK, leading to inactivation of cofilin and subsequent stabilisation of actin filaments. In addition, LIM kinase 2 serves as a p53 target and is upregulated in response to DNA damage. In some solid tumours (e.g. breast and prostate), LIM kinase levels are elevated. However, we found that LIM kinase 2 expression is downregulated in colon cancer, with a progressive reduction noted with advancing tumour stage. I found that LIMK2 expression in colon cancer is under epigenetic regulation, with hypermethylation of the promoters leading to transcriptional silencing; this implicates *LIMK2* as a tumour suppressor gene in this context. This has potential translational implications as loss of LIMK2 could be utilised as a biomarker to stratify patients in the future.

Elevated mechanical tension within the tumour microenvironment is known to be an adverse prognostic indicator due to its association with desmoplasia. ROCK activation has previously been shown to increase epidermal tissue stiffness and thickness, but little was known about the mechanisms by which this occurs. I found that ROCK activation leads to the deposition of extracellular matrix components, with a presumed consequent further increase in stromal stiffness. This indicates that a positive feedback cycle is established in the tumour microenvironment, maintaining a fibrotic stromal reaction that permits tumour progression.

These results highlight the disparate roles that the actin cytoskeleton and constituents of the Rho/ROCK pathway play in tumour initiation and propagation, indicating the need for further research.

Table of Contents

List of Tables

List of Figures

Preface

The process by which a normal cell embarks and continues on the journey towards becoming a cancer is characterised by perturbations of many aspects of normal cell behaviour [1]. This is reflected by the alterations seen in the cytoskeleton as cancer cells become motile, invasive, change their morphology, and respond differently to cues received from their microenvironment.

As we seek to understand the influences at play in tumour initiation and development, the pivotal role of those pathways that directly and indirectly influence the cytoskeleton and those that are in turn altered by cytoskeletal changes are of paramount importance.

Acknowledgement

Thanks to Mike for being such an inspiring and positive supervisor; you made my foray into science much more enjoyable. Thank you also to my advisor Jeff Evans for his support throughout my research.

It has been a real pleasure being a part of R17 – I couldn't have asked for a nicer group, so thank you to all members past and present. Particular thanks to June for all her help in the lab, Nicola for her assistance with the animal work, and Katerina, Mathieu & both Dominikas for tea breaks and encouragement. Last, littlest, but definitely not least, thanks to Linda, the happiest scientist I know. I'd also like to thank the other Beatson research fellows – it was good to have you guys around for moral support.

I am also very grateful to CRUK for funding this research, and the Beatson Institute for providing such a great environment to work in.

Finally, thanks to my parents, Anne and Peter, for their kind words of encouragement, and to my friends, especially Kate, Kirsty, Catie and Jenni, for giving me a laugh when the science didn't.

Author’s Declaration

I am the sole author of this thesis. All the work presented is entirely my own unless stated otherwise.

Abbreviations

4-HT	4-hydroxytamoxifen
5-AZA	5-azacytidine
ADF	Actin depolymerising factor
ADP	Adenosine diphosphate
ANOVA	Analysis of variance
ATP	Adenosine triphosphate
BCA	Bicinchoninic acid
BSA	Bovine serum albumin
CAF	Cancer-associated fibroblast
CIN	Chromosomal instability
CpG	Methyl cytosine modified CG dinucleotide
CRC	Colorectal cancer
cSCC	Cutaneous squamous cell cancer
DAPI	4',6-diamidino-2-phenylindole
DMEM	Dulbecco's Modified Eagle Medium
DMSO	Dimethyl sulfoxide
DNA	Deoxyribonucleic acid
DNMT	DNA methyltransferase
ECM	Extracellular matrix
EGF	Epidermal growth factor
EMT	Epithelial-mesenchymal transition
ER	Estrogen receptor
F-actin	Filamentous actin
FAP	Familial adenomatous polyposis
FBS	Fetal bovine serum
G-actin	Globular actin
GAP	GTPase activating protein
GDF15	Growth differentiation factor 15
GDI	Guanine nucleotide dissociation inhibitor
GDP	Guanosine diphosphate
GEF	Guanine nucleotide exchange factor
GFP	Green fluorescent protein
GTP	Guanosine triphosphate
H&E	Haematoxylin & eosin
HNPCC	Hereditary non-polyposis colon cancer
IBD	Inflammatory bowel disease
IHC	Immunohistochemistry
K14	Cytokeratin 14
KD	Kinase dead
KGM	Keratinocyte growth medium
KO	Knock out
LIMK	LIM domain kinase
MEF	Mouse embryonic fibroblast
MET LUC	*Metridia* luciferase

MKL1	Megakaryoblastic leukaemia 1
MLC	Myosin light chain
MMP	Matrix metalloproteinase
MMR	Mismatch repair system
MSI	Microsatellite instability
MSP	Methylation specific PCR
PAK	p21 activated kinase
PBS	Phosphate buffered saline
PCR	Polymerase chain reaction
RIN	RNA integrity number
RNA	Ribonucleic acid
ROCK	Rho-associated coiled-coil kinase
SEAP	Secreted alkaline phosphatase
SMA	Smooth muscle actin
SRE	Serum response element
TBS	Tris buffered saline
TGFβ	Transforming growth factor beta
TNC	Tenascin C
TSLP	Thymic stromal lymphopoietin
WT	Wild type

1 Introduction

1.1 The actin cytoskeleton

Actin is one of the most abundant proteins observed in eukaryotes; it is found both as a globular monomer (G-actin), and as a polymeric chain of G-actin subunits (filamentous or F-actin) [2]. The F-actin filament has structural polarity, as all subunits are oriented in the same direction. The "pointed" (negative) end possesses an actin subunit with an exposed ATP binding site, while the "barbed" (positive) end displays a cleft directed at an adjacent G-actin monomer. "Treadmilling", or the cycle of actin polymerisation and depolymerisation, is an ongoing process by which ADP exchange for ATP promotes the addition of G-actin monomers to the barbed end of F-actin filaments, and vice versa [3] (Figure 1-1). Following formation and elongation of an F-actin filament, its stability and mechanical properties can be altered by accessory proteins (e.g. profilins) that bind alongside the polymer, determining the state of polymerisation, and cross-linking and severing the actin filament [4]. In addition, capping proteins can bind to the end of the filament and regulate its assembly and disassembly [5]. Furthermore, F-actin filaments, in co-operation with myosin II filaments and integrins, form focal adhesion complexes, anchoring cells via the cytoskeleton to the extracellular matrix and to neighbouring cells, thus permitting cell-cell/cell-matrix dialogue [6].

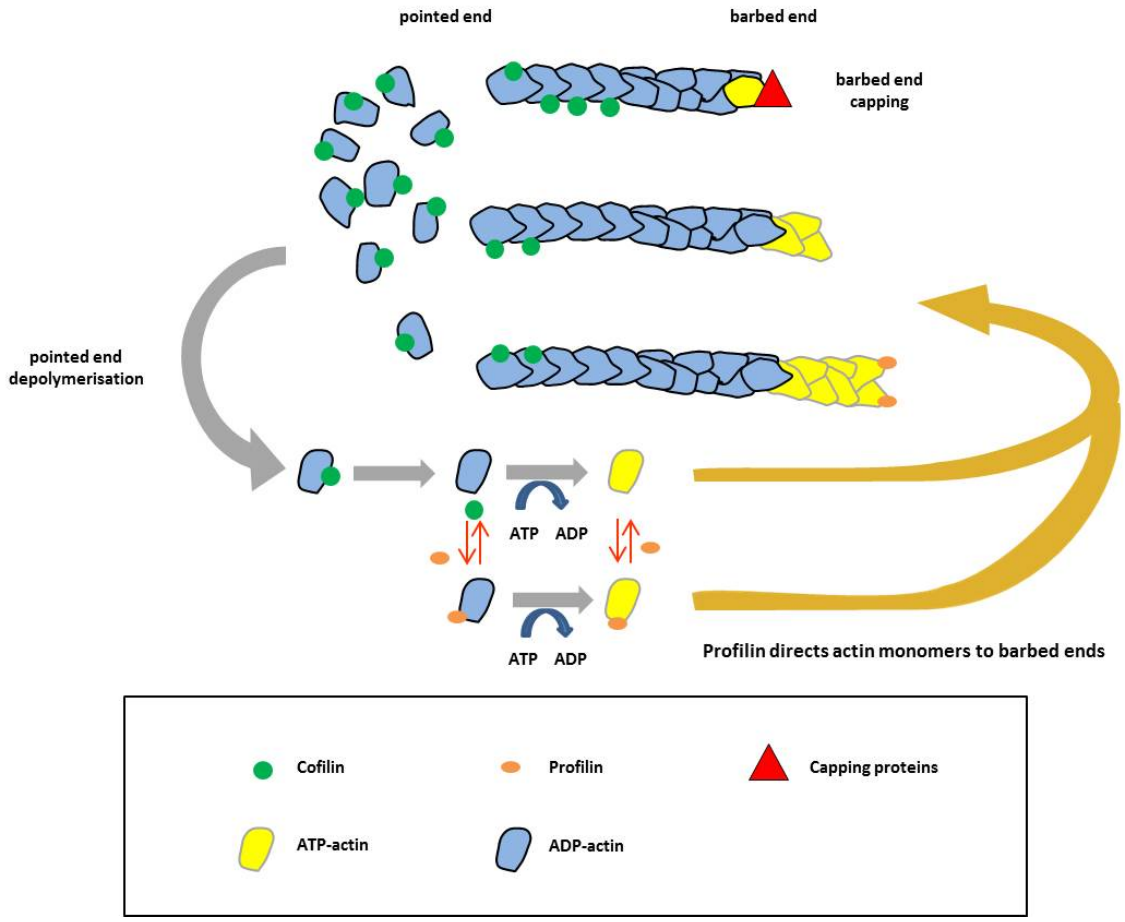

Figure 1-1 Actin treadmilling

Cofilin binds to and severs F-actin, increasing the "treadmilling" rate of actin filaments. Adapted with permission from MBInfo: www.mechanobio.info; Mechanobiology Institute, National University of Singapore.

1.1.1 Regulation of the actin-myosin cytoskeleton

1.1.1.1 The Rho GTPase family and its activators

The Rho GTPase family is a group of molecules with pivotal functions in the regulation of cytoskeletal organisation [7]. They are members of the Ras superfamily of small GTPases, but alter from other small GTPases in that their sequences possess a Rho insert domain within the GTPase domain. This insert is proposed as an activator of downstream proteins [8]. There are 22 mammalian members of the Rho GTPase family; the most extensively studied members comprise Rac1, RhoA and Cdc42, small guanine triphosphatases. Three Rho isoforms exist: A, B and C. They transition between a GDP-bound state (inactive) and GTP-bound state (active). Their protein sequences are approximately 85% identical, with some divergence between members in the "insert loop", a region that enables NADPH oxidase binding to Rac [9]. RhoA is necessary for disassembly of cell adhesions during cell migration, while RhoB inhibits growth factor receptor trafficking [10]. RhoC remodels the cytoskeleton via activation of mDIA1 and FMNL2 [11].

The regulators of Rho protein function fall into 3 main subgroups:

1. Guanine nucleotide exchange factors (GEFs). These function by catalysing the release of GDP, thus facilitating GTP binding; a consequent alteration in conformation of the switch region of the GTPase increases the binding affinity of effector proteins, thus prompting downstream signalling [12].

2. GTPase-activating proteins (GAPs). These proteins improve the capacity of small GTPases to hydrolyse GTP to GDP, thus promoting inactivation and reversing effector binding, effectively terminating the signalling pathway [13].

3. Guanine nucleotide dissociation inhibitors (GDIs). These regulatory proteins are located in the cytosol and, through complex formation with GDP-bound GTPases, prevent cycling of GTPases between the cytosol and the plasma membrane, thus inhibiting GEF-mediated activation of Rho GTPases [14]. Rho GTPases are maintained as soluble cytosolic proteins by insertion into the hydrophobic pocket of the GDI [15]. Upon their release,

Rho GTPases can insert into the lipid bilayer of the plasma membrane, permitting association with effector targets at the cell membrane [16].

There are additional regulatory mechanisms known to play a role in influencing Rho GTPases, including micro RNAs, which regulate post-transcriptional processing of Rho GTPase-encoding mRNAs [17]; palmitoylation (the covalent attachment of fatty acids to the membrane-bound proteins, thus modulating protein trafficking and protein-protein interactions) [18]; post-translational phosphorylation [19], and the similar process AMPylation (the transfer of AMP from ATP to a threonine residue) [20], transglutamination [21], and ubiquitination [22].

1.1.1.2 Rac1 and Cdc42 pathways

Rac1 controls the formation of lamellipodia, the cytoskeletal actin projections observed on the mobile edge of cells [23], while Cdc42 primarily regulates the formation of filopodia, the narrow cytoplasmic projections that extend beyond the leading edge of lamellipodia in migrating cells [24] . Multiple proteins have been identified as downstream binding partners of these Rho GTPases; several of these are serine/threonine kinases with the capacity to trigger signalling pathways by phosphorylating further target proteins. Downstream of Rac1 and Cdc42 are the 6 mammalian-encoded p21-activated kinases (PAKs), of which only PAKs 1–3 are able to bind Rac1 [25]; PAKs 1–6 are all capable of binding Cdc42 [26]. PAKs in turn phosphorylate substrates that affect cytoskeletal dynamics (through disassembly of stress fibres and focal adhesion complexes) including LIM kinases [27] and myosin light chain kinase [28].

In addition to kinase effectors, non-kinase scaffold proteins exist to transfer signals from Rho GTPases: e.g. N-WASP is activated by Cdc42 and consequently binds proteins to bring about actin polymerisation and subsequent filopodia formation [29].

1.1.1.3 RhoA-ROCK pathway

RhoA also binds a number of effector proteins; the best characterised of these are the Rho-associated coiled-coil-containing protein kinases (ROCK1 and ROCK2), serine/threonine kinases with multiple Rho-binding domains within the coiled-coil region [30]. RhoA must be in an activated, GTP-bound state in order to

bind to ROCK; upon Rho-GTP binding, there is thought to be a conformational change that induces kinase activity [31]. ROCK1 and 2 share the same overall domain structure, with the kinase domain situated at the N-terminus, and a coiled-coil region bearing a Rho-binding domain (RBD). A pleckstrin homology domain with a cysteine-rich region exists at the C-terminus [32]. ROCKS are capable of displaying an autoinhibitory conformation, with the C-terminal RBD and pleckstrin homology domains binding to the kinase domain, thus preventing kinase activity. When Rho-GTP binds to the RBD, a conformational change is induced, freeing the kinase domain and permitting activity [33].

There is approximately 90% homology between the kinase domains of ROCK1 and ROCK2; they are therefore observed to phosphorylate a largely shared proportion of substrates [34]. These include regulatory myosin light chain, the contractile force-generating subunit of the myosin macromolecule. Upon phosphorylation, primarily at serine 19, the ATPase activity of myosin increases, resulting in enhanced cell contractility and the formation of stress fibres [35] (Figure 1-2 and 1-3).

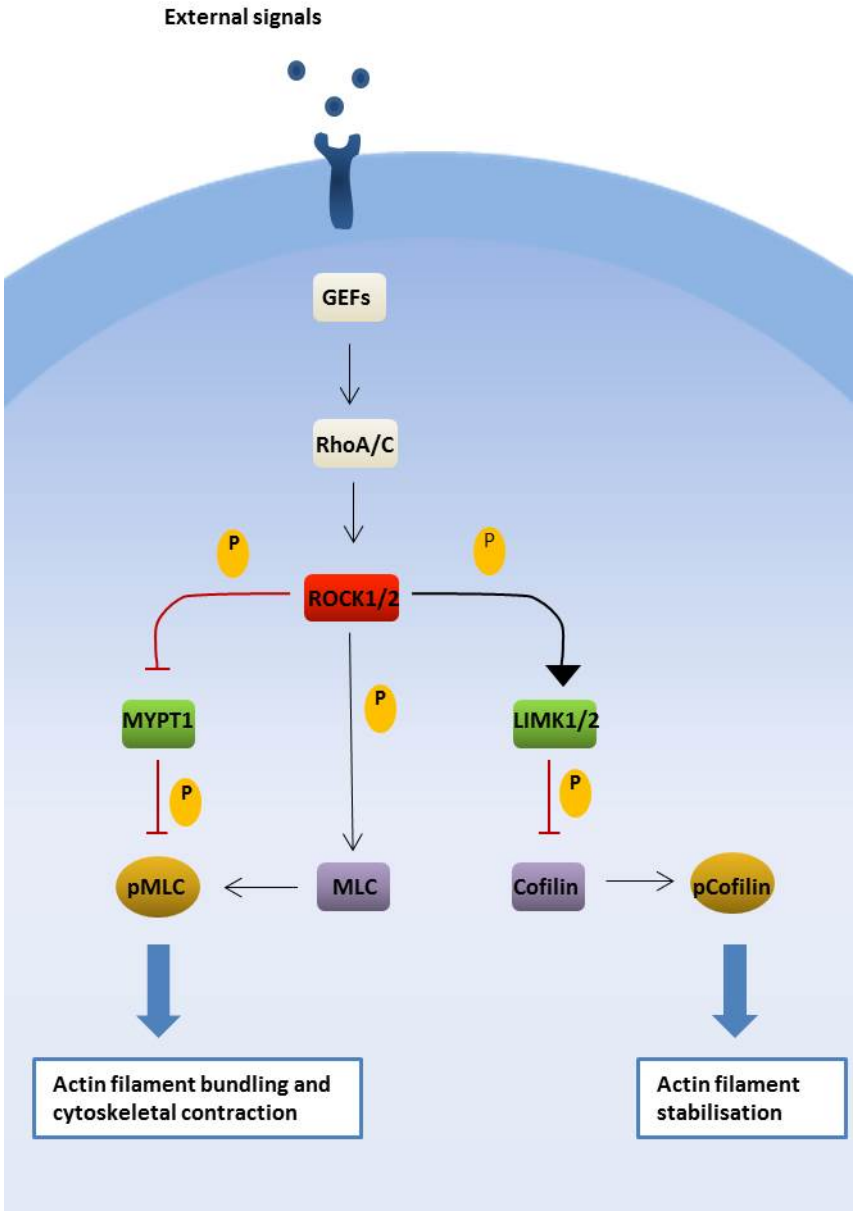

Figure 1-2 The Rho/ROCK signalling cascade

External signals from activated membrane receptors are translated by GEFs to activate RhoA/C. In turn, ROCK 1 and 2 are activated, and phosphorylate the target proteins MLC, LIMK1/2, and MYPT. Phosphorylation of MLC and, via LIMK, cofilin, results in actin fibre bundling and increased contractility. Adapted from Rath and Olson [36].

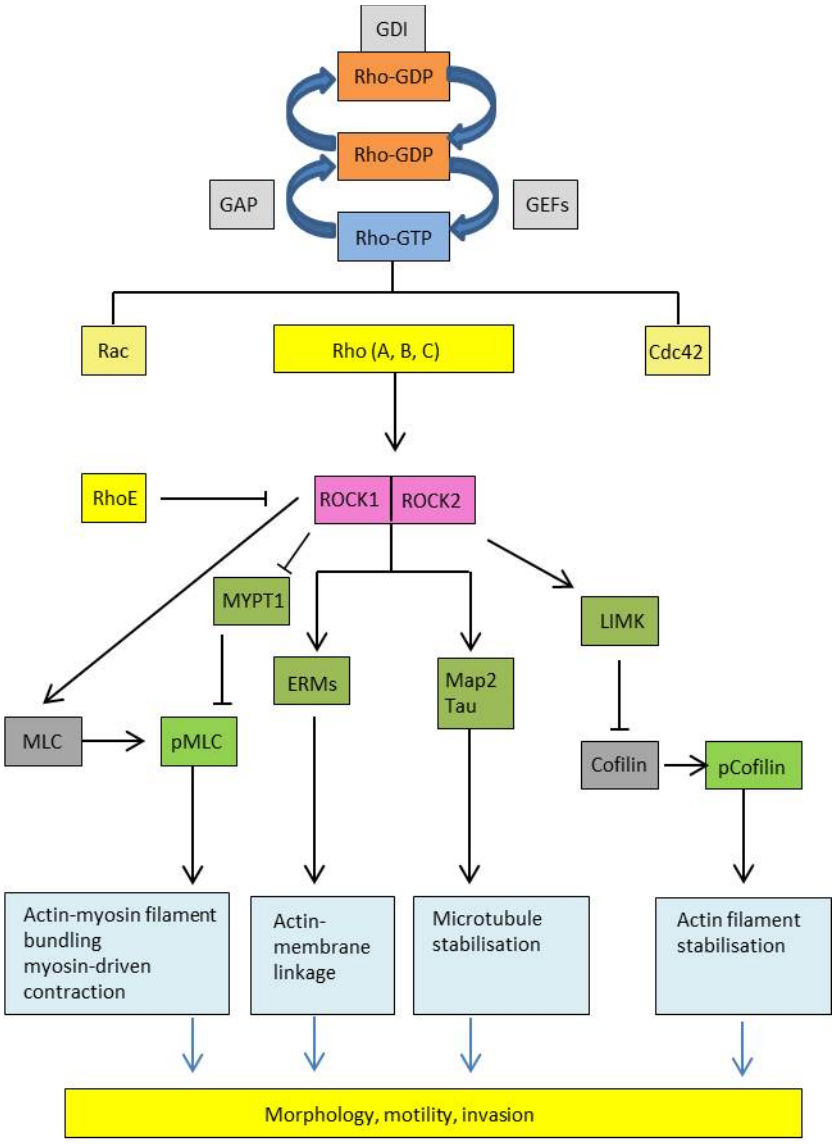

Figure 1-3 The Rho/ROCK signalling pathway showing additional substrates
MYPT1: myosin phosphatase 1; ERM: ezrin/radixin/moesin.
Adapted from Matsuoka and Yashiro [37].

ROCK also acts by phosphorylating the myosin phosphatase targeting (MYPT) proteins at sites Thr 696 and Thr 853. Phosphorylation of the first of these sites reduces myosin light chain phosphatase (MLCP) activity (a negative regulator of actomyosin contractility through dephosphorylation of MLC); phosphorylation of the latter also decreases MLCP activity, and additionally induces dissociation of MYPT1 from myosin [38,39].

In addition, ROCK phosphorylates LIM kinases 1 and 2 on conserved threonine residues (Thr 508 in LIMK1 and Thr 505 in LIMK2). LIM domains are conserved features consisting of twin zinc finger-like motifs, which were first identified in Lin11, Isl1 and Mec-3 [40]. A consequence of LIM kinase (LIMK) phosphorylation is the phosphorylation and inactivation of the cofilin group of proteins (cofilin 1, cofilin 2, and actin depolymerising factor, ADF), leading to stabilisation of F-actin filaments [41].

ROCK1 is widely expressed in human tissue, including the heart, pancreas, lung, liver, skeletal muscle and kidney. It is not found in the brain [42]. ROCK2 is expressed ubiquitously, and is observed within the brain [43]. ROCK1 knock-out mice display failure of eyelid closure and omphalocoele phenotype (in which the intestine protruded through an abdominal wall defect). Most animals die shortly after birth [44]. ROCK2 knock-out mice have also been generated; there is 90% embryonic lethality with this genotype, thought secondary to placental dysfunction, and the surviving pup are runts, albeit with subsequent normal development [45].

1.1.2 ROCKS

1.1.2.1 ROCKs in physiological conditions

Contractility

Cell-matrix communication

The best-recognised function of ROCK 1 and 2 is to enhance myosin-actin binding and thus contractility. This in turn promotes the assembly of stress fibres, composed of multiple actin filaments cross-linked by α-actinin, and generally

anchored to focal adhesions, providing a point of contact between the extracellular matrix and the actin cytoskeleton [46]. This communication permits transmission of mechanical force via stress fibres to focal adhesion complexes, resulting in alterations in the conformation of e.g. integrins, and consequent signal transduction [47]. Furthermore, the ability of stress fibres to sense the degree of mechanical tension in the milieu can directly regulate biomechanical and signalling pathways in cells, determining cell differentiation and ultimate cell fate [48].

Cell motility

Skeletal muscle myosin forms part of the sarcomere, and has the capacity to generate largely stable filaments [49]. The interaction of myosin and actin in skeletal muscle is regulated by the calcium-sensitive tropomyosin-troponin complex [50]. Smooth muscle and cytoplasmic myosin interact with actin through different mechanisms due to the absence of troponin [51]; following stimulation, intracellular calcium concentrations increase, and calcium binds to calmodulin, thus activating myosin light chain kinase (MLCK) [52].

In the presence of unphosphorylated MLC, MLCK phosphorylates MLC in association with the calcium-calmodulin complex, thus elevating myosin ATPase activity. MLCK is also capable of binding directly to myosin without the requirement for the calcium-calmodulin complex [53]. If myosin exists in a fully phosphorylated state, MLCK becomes inhibitory indirectly through the actin-binding domain [54]. In the context of smooth muscle, MLC phosphorylation causes monomeric myosin molecules in solution to assemble into thick filaments. Inhibition of MLCK has been shown to prevent MLC phosphorylation and isometric force generation withn muscle [55].

The polymerisation of G-actin monomers into F-actin filaments drives cell motility [4]. A complex is formed from F-actin and myosin II filaments; the complex utilises energy from the hydrolysis of ATP to facilitate cytoskeletal contraction [56] . The force generated from actin-myosin contraction permits alteration of cell morphology, enabling cell movement.

Phosphorylation of myosin light chain (MLC) is a vital mechanism that regulates cell contractility [57]. Following MLC phosphorylation, the myosin heavy chain is released and forms filaments, permitting the interaction between the myosin head and F-actin, and thus causing ATP-mediated movement of actin filaments. As previously described, activation of the Rho-ROCK signalling pathway results in phosphorylation of MLC and thus contributes to the regulation of cell motility [35].

Apoptosis

Apoptosis is the process of programmed cell death that occurs in response to extra- and intra-cellular stress. ROCK1, via caspase cleavage, is known to regulate the actin-myosin contraction force that mediates membrane blebbing, breakdown of the nucleus, and fragmentation of apoptotic cells [58]. When apoptosis occurs due to flawed cell-ECM attachment, it is termed anoikis [59]. This may arise due to loss of attachment, or when cells attempt to adhere to ECM that does not express the correct integrins, and thus fails to support cell survival[60].

Cell-cell junction regulation

In addition to the regulation of cell contractility and cell-matrix adhesion, there are multiple pathways in which ROCKs are implicated as key players. These include the regulation of tight junctions, adhesive regions between neighbouring epithelial or endothelial cells that serve a barrier function by preventing molecules and ions passing between cells [61]. ROCK activation has been found to increase the permeability of tight junctions in the context of endothelial cells, whereas the inverse appears to be the case in epithelial cells [61,62].

Adherens junctions tend to occur at a more basal level than tight junctions, and are also subject to ROCK regulation. They are composed of cadherins, which span the cell membrane and interact with α, β and ɣ catenins. It has been shown that ROCK-induced cytoskeletal contraction disrupts and destabilises adherens junctions, a step implicated in the process of epithelial-mesenchymal transition [63,64].

Cell proliferation

There is evidence to suggest that ROCK participates in the regulation of cell proliferation; ROCK overexpression increases cell growth [65]. In addition, ROCK inhibition leads to retarded cytokinesis [66], induces disordered separation of centrioles at the G_1 phase of the cell cycle, and promotes early centrosome migration during mitosis [67]. Furthermore, ROCK activation in the context of a conditionally active ROCK-ER fusion protein system in fibroblasts prompts G_1/S cell cycle progression [68].

Stem cell regulation

Dissociation of human embryonic stem cells leads to increased phosphorylation of myosin light chain in a Rho/ROCK-dependent fashion, with subsequent blebbing and apoptosis [69]. ROCK inhibition has been found to promote the survival of human embryonic stem cells [70]. It is thought that this occurs as a consequence of avoidance of anoikis via increased cell-cell interactions and adhesion [71]. Furthermore, ROCK inhibition enhances proliferation of stem cells [72].

1.1.2.2 ROCKs in cancer

Expression

Somatic mutations in both *ROCK* genes have been found in primary human tumours and in cancer cell lines [73]. Mutations in the *ROCK1* gene in breast cancer and non-small cell lung cancer have been shown to result in an increase in kinase activity as a consequence of loss of autoinhibition [73,74]. There are also mutations present in the *ROCK2* gene in primary gastric carcinomas, and in melanoma cell lines [73], which are again thought to lead to increased kinase activity.

Elevated protein levels of ROCK have been documented in breast cancer, with a positive association between high ROCK expression, increased tumour grade, and poor survival outcomes [75]. Other cancer types that also demonstrate a positive correlation between ROCK protein levels and reduced overall survival or a more aggressive phenotype include osteosarcoma [76], hepatocellular cancer [77], and bladder cancer [78].

Tumour microenvironment

In addition to aberrant ROCK expression observed within tumour cells, the increased cytoskeletal contractility that occurs as a consequence of ROCK activation plays an important role in regulation of the tumour microenvironment. It is recognised that in many cancer types, including breast [79] and pancreatic [80] cancers, a desmoplastic stroma is observed , and is noted to have a positive correlation with adverse clinical outcomes [81,82].

ROCK signalling is known to increase tissue density through elevated production of collagen and other ECM components such as periostin and fibronectin [83,84]. The consequences of this include activation of integrin-mediated signalling, epidermal hyperproliferation, and increased levels of tumour initiation, growth and progression in an animal model of ROCK activation [83]. A positive feedback system appears to exist in that increased matrix density, and consequent stiffness, leads to an elevation in ROCK activity; this is thought to be related to the epigenetic silencing of Notch1 [85].

In addition, ROCK activation leads to increased levels of contractility within the cellular compartment of the tumour microenvironment, permitting deformation of the ECM, and creating "tracks" that facilitate cancer cell migration [86]. This appears to be triggered in part by pro-inflammatory cytokines [87]; however, evidence also suggests a positive feedback cycle exists between the ROCK and JAK/STAT pathways that may explain the perpetual signalling that ultimately permits invasion [87]. In the context of lung adenocarcinoma, Rho/ROCK function is required to enable cancer-associated fibroblasts to invade a collagen matrix; ROCK inhibition abrogated the capacity of CAFs to invade [88].

1.1.2.3 ROCK inhibition

ROCK inhibition has been studied in the context of a number of malignancies. The most widely utilised compounds include Fasudil (a moderate inhibitor, with a K_i of 330 nM) [89], Y27632 (a specific inhibitor of ROCK 1 and 2) [90], and H-1152P (a dimethylated analogue of Fasudil, and the most potent compound) [91] . All the aforementioned compounds are competitive inhibitors of the ATP-binding site of ROCK [92]. In a broad range of cancer types, ROCK inhibition has been shown to

reduce cancer cell migration, proliferation and invasion, whilst simultaneously inducing apoptosis (Table 1-1). This confirms the central role played by ROCK in cancer progression, both through its function within tumour cells, and via modulation of the tumour microenvironment.

Tumour type	Experimental model	ROCK inhibitor	Result
Acute myeloid leukaemia [93]	Primary human cells	Fasudil	Increased apoptosis, reduced viability
Triple negative breast cancer [94]	Human cell line	H-1152	Reduced migration and invasion
Urothelial cancer [95]	Human cell line	Fasudil	Reduced proliferation and migration; induced apoptosis
Small cell lung cancer [96]	Human cell line	Fasudil	Reduced growth, proliferation, adhesion, migration and invasion; increased apoptosis
Glioblastoma [97]	Human cell line & *in vivo* (murine xenograft)	Fasudil	Reduced proliferation, migration, invasion; increased apoptosis. Reduced invasion and growth *in vivo*
Prostate cancer [98]	Conditioned HUVECs	Fasudil	Reduced endothelial cell proliferation and migration
Adenocarcinoma lung [88]	Primary human CAFs & human cell line	Y27632	Reduced invasion
Hepatocellular cancer [99]	Human cell line	Y27632	Reduced migration and invasion
Melanoma [100]	Murine and human cell lines & *in vivo*	Y27632	Reduced invasion; reduced tumour volume

Table 1-1 Result of ROCK inhibition in different tumour types

1.1.3 LIM kinases

1.1.3.1 LIM kinase expression and regulation

There are two subtypes of the LIM kinase serine/threonine kinase protein family: LIM kinase 1 *(LIMK1)*, encoded on chromosome 7q11.23, and LIM kinase 2 *(LIMK2)*, encoded on chromosome 22q12.2. As a result of alternative splicing, there are two *LIMK1* mRNAs, one encoding the full-length protein, the other producing a truncated protein lacking the carboxyl-terminal kinase domain. Alternative splicing also produces three *LIMK2* isoforms: 1 (the largest protein), 2a and 2b. *LIMK2a* contains two LIM motifs, while *LIMK2b* contains 1.5 LIM motifs. A *LIMK2a* specific exon (exon 2) and a *LIMK2b* specific exon (exon 2b) at the 5' region of the mouse *Limk2* gene exist, implying that *Limk2a* and *2b* are transcribed from a single *Limk2* gene by alternative usage of exons [101] (Figure 1-4). No functional differences between the isoforms have been identified, although there are indications that their expression may vary in different tissues. Both LIMK1 and 2 are expressed widely in all tissues, with particularly high expression of LIMK1 in the brain, kidney, stomach and testis [102,103].

Both LIMK1 and 2 are phosphorylated by the Rho effector Rho kinase (ROCK) on conserved threonine residues (Thr-508 in LIMK1 and Thr-505 in LIMK2) leading to activation. In addition, PAK and MRCKα have been reported to phosphorylate and activate LIMK. Dephosphorylation and inactivation of LIMK1 is regulated by phosphatases including slingshot 1. Par-3, a polarity protein, appears to play a similar role in influencing the activity of LIMK2 [40].

The cofilin family, comprising cofilin 1, cofilin 2 and actin depolymerising factor (ADF) plays a key role in actin filament dynamics in cells [104]. Cofilins sever Filamentous-actin (F-actin) filaments to generate barbed ends that can serve as de novo actin nucleation sites. In addition, cofilins have been shown to induce protrusion and influence the direction of cell migration [105]. Cofilins are the most extensively characterised substrates of the LIM kinases, which act by phosphorylating cofilin on serine 3 and inactivating its F-actin severing activity.

In addition to its role in regulation of the actin cytoskeleton, LIMK 1 has also been shown to play a role in modulating microtubule disassembly [106].

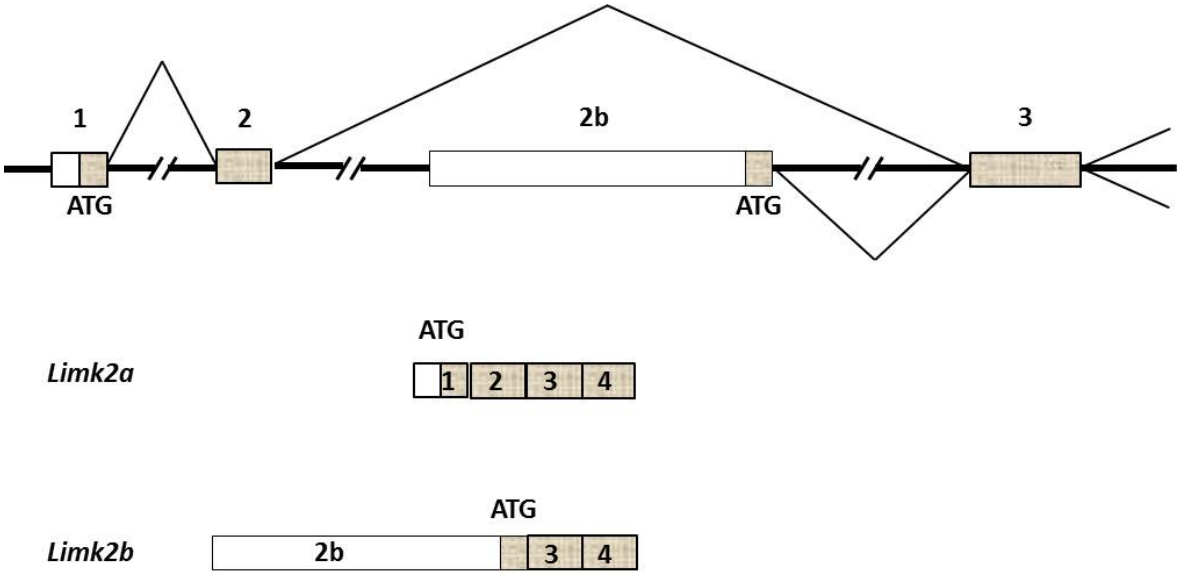

Figure 1-4 Schematic diagram of alternative exon usage near the 5'-terminal region of the mouse *Limk2* gene
Alternatively initiated *Limk2a* and *Limk2b* transcripts are indicated in the lower panels. Adapted from Ikebe et al [101].

1.1.3.2 LIM Kinases in Cancer

It has been proposed that the LIM kinases may play a role in cancer cell invasion and metastasis; the balance between phosphorylated and non-phosphorylated cofilin under the influence of LIMKs may prove to be a significant determinant of metastatic potential.

Evidence suggests that LIMK 1 activity is important for cancer cell metastasis; the level and activity of LIMK 1 are higher in invasive breast and prostate cancer cell lines, leading to enhanced tumour angiogenesis and metastasis [107,108]. LIMK 1 activity was also shown to be necessary for invasiveness of breast cancer cell lines [109]. In addition, work with pancreatic cancer cell lines has established a role for both LIMK 1 and 2 in metastasis and tumour cell-induced angiogenesis [110]. It is proposed that the LIM kinases likely have non-overlapping functions in the formation of metastasis, as a *LIMK1/2* double knockdown is necessary to completely block metastatic behaviour *in vivo*.

It has been shown that *LIMK2* acts as a p53 target and is upregulated in response to DNA damage [111]. This activation of *LIMK2* is thought to have a pro-survival function. However, it appears that the isoforms of *LIMK2 (LIMK2a* and *LIMK2b*) behave differently in response to DNA damage. Certainly, there is differential regulation of *LIMK2a* and *LIMK2b* in different human cancers with, for example, marked reduction of *LIMK2b* and increase of *LIMK2a* in gastro-oesophageal cancers. It has been proposed that *LIMK2b* promotes DNA damage-induced G2/M cell cycle arrest, contributing to checkpoint regulation. Depletion of *LIMK2b* was reported to impair G2/M arrest, while reduction of *LIMK2a* did not appear to have this effect, again indicating their apparent functional differences [112].

1.2 Colorectal cancer

Colorectal cancer (CRC) is the 4th commonest type of cancer diagnosed in the UK, and the 2nd commonest cause of cancer death (Office for National Statistics). The lifetime risk of developing CRC is approximately 6% (Cancer Research UK, http://www.cancerresearchuk.org/health-professional/cancer-statistics/risk/lifetime-risk#heading-One, accessed February 2016). CRC survival is dependent on the stage of disease at diagnosis; staging follows two conventional systems: Duke's (Table 1-1) and TNM (Table 1-2). In addition, a number of factors are used to determine the prognostic outlook of an individual, including the tumour grade (i.e. the degree of differentiation) and the presence or absence of cancer cells within the vasculature around the tumour. In those patients presenting with early stage disease, curative surgery is usually possible, with consequent 5-year survival rates of 93.2% (NCIN 1996 – 2002). However, the majority of patients present with more advanced disease, necessitating more aggressive management strategies in the form of surgery, and adjuvant systemic treatments such as chemotherapy and biological agents. Despite developments in the treatment of CRC, survival rates progressively decline as the stage of disease at diagnosis advances.

	Depth of invasion	Lymph node metastases present	Distant metastases present	% of cases	% 5-year survival
Duke's A	Into, but not through, bowel wall	No	No	8.7	93.2
Duke's B	Penetrates muscularis propria	No	No	24.2	77.0
Duke's C	Any	Yes	No	23.6	47.7
Duke's D	Any	Yes or no	Yes	9.2	6.6
Unknown	-	-	-	34.3	35.4

Table 1-2 Duke's staging of colon cancer

Disease stage is determined by the depth of invasion of the primary tumour and the presence or absence of regional lymph node or distant metastatic deposits. The 5-year survival progressively declines as the stage of disease at diagnosis increases. Data from the National Cancer Intelligence Network 1996 – 2002.

Stage	T	N	M
0	Tis	N0	M0
I	T1 T2	N0 N0	M0 M0
IIA IIB IIC	T3 T4a T4b	N0 N0 N0	M0 M0 M0
IIIA IIIB IIIC	T1 – T2 T1 T3 – T4a T2 – T3 T1 – T2 T4a T3 – T4a T4b	N1 N2a N1 N2a N2b N2a N2b N1 – N2	M0 M0 M0 M0 M0 M0 M0 M0
IVA IVB	Any T Any T	Any N Any N	M1a M1b

Table 1-3 TNM staging of colon cancer

TNM staging assigns a group depending on the depth of primary tumour invasion ("T"), the extent of lymph node involvement ("N") and the degree of metastasis ("M"). Tis = carcinoma in situ; T1 = tumour invades submucosa; T2 = tumour invades muscularis propria; T3 = tumour invades through muscularis propria and into the pericolonic tissues; T4a = tumour penetrates to the surface of the visceral peritoneum; T4b = tumour directly invades or is adherent to other organs/structures. N0 = no regional lymph node metastases; N1 = metastasis in 1-3 regional lymph nodes; N2a = metastasis in 4-6 regional lymph nodes; N2b = metastasis in 7 or more regional lymph nodes. M0 = no distant metastasis; M1a = metastasis confirmed to one organ or site; M1b = metastases in more than one organ or site. Adapted from the American Joint Committee on Cancer colon cancer staging, 7th edition 2009.

Colon cancers tend to arise from non-malignant adenomas, with subsequent acquisition of a series of genetic mutations permitting tumour progression [113] (Figure 1-5). The alterations observed are dependent on the degree of chromosomal and microsatellite instability inherent to the tumour. In chromosomally unstable CRCs [114], loss of *APC* appears to be the triggering event for adenoma formation [115] . Subsequent mutations are acquired in *KRAS* [116], followed by loss of *SMAD4* (due to chromosome 18 deletion) [117], and mutations in *TP53* [118]. In contrast, CRCs displaying microsatellite instability (MSI) are deficient in the mismatch repair system (MMR), leading to an inability to maintain genomic stability [119]. This primarily occurs through downregulation of *MLH1* secondary to promoter hypermethylation [120]. In these tumours, adenoma formation secondary to alterations in Wnt signalling [121], followed by mutations in *BRAF* (and, in a minority, *KRAS*) more commonly occurs [116]. Thereafter, positive selection of cells with microsatellite mutations in *MSH2, MSH6* [122], TGFß receptor 2 [123], insulin-like growth factor receptor 2 [124], and *BAX2* [125] enables a *TP53*-independent mechanism of progression.

Parallel to these genetic alterations, it is increasingly recognised that epigenetic changes play a key role in CRC carcinogenesis. There is a mounting body of evidence to suggest that many more genes within the CRC genome are affected by epigenetic aberrations than genetic mutations, with consequent transcriptional silencing of tumour suppressor genes and gain of function in oncogenes [126].

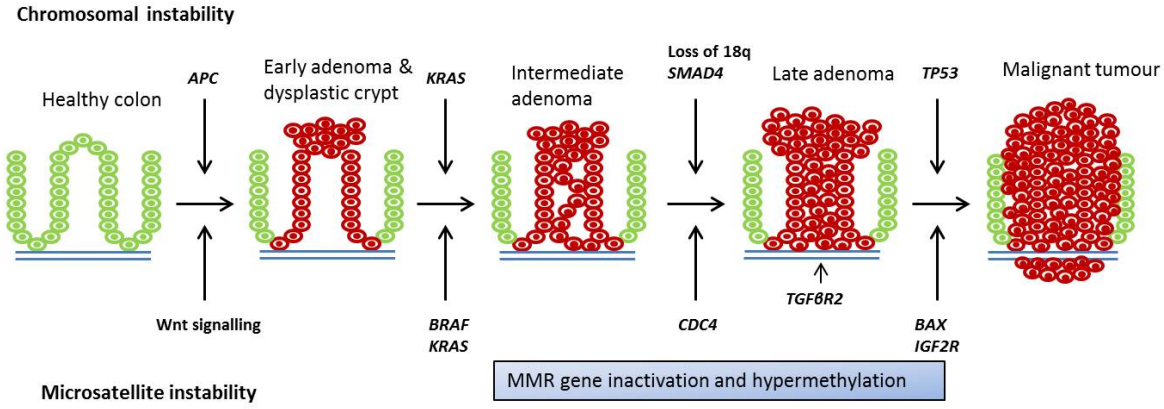

Figure 1-5 Sequence of events in the transition from adenoma to carcinoma

The observed clinicopathological alterations in CRC can be aligned with genetic events initiating and promoting the disease. Differences exist between the pathways activated in tumours exhibiting chromosomal instability and those in which microsatellite instability predominates, but a degree of overlap also exists. Adapted from Walther et al [127].

1.2.1 Aetiology of colorectal cancer

In the vast majority of CRC cases (over 90%), no single causative agent is apparent. These cases are predominantly attributed to a diet high in red meat and processed foods, and high levels of physical inactivity and obesity. The remainder of CRCs are caused by inherited conditions or predisposing diseases [128].

1.2.1.1 Hereditary non-polyposis colon cancer

Hereditary non-polyposis colon cancer (HNPCC or Lynch syndrome) is the most frequently encountered cause of CRC in those cases deemed not due to the "Western lifestyle", and is thought to be responsible for 2-7% of CRC diagnoses [129] . Presentation with an HNPCC-related CRC occurs at an average age of 44 years, in contrast to an average age at diagnosis of 64 years in non-HNPCC CRC. HNPCC is a genetic condition usually inherited in an autosomal dominant fashion, although it can also arise *de novo*. Faulty DNA mismatch repair leading to microsatellite instability is the hallmark of HNPCC; this can occur as a consequence of mutations in a number of genes involved in the DNA MMR pathway: *MSH2, MLH1, MSH6, PMS2, PMS1, TGFBR2*, and *MLH3* [130]. Affected individuals are at increased risk of CRC, and other cancer types including endometrial, urothelial, small bowel, gastric and glioblastoma [131]. The lifetime risk of CRC in a patient with HNPCC is approximately 80%. In order to identify patients at risk of HNPCC, the International Study Group on HNPCC developed the Amsterdam Criteria II [132]:

- Three or more family members with HNPCC-related cancers, one of whom is a first-degree relative of the other two
- Two successive affected generations
- One or more of the HNPCC-related cancers diagnosed at age less than 50 years
- Familial adenosis polyposis (FAP) has been excluded

1.2.1.2 Familial Adenomatous Polyposis

Familial adenomatous polyposis (FAP) is an unusual inherited condition, with an incidence of 1 in 10,000 to 1 in 15,000. It is characterised by the formation of multiple adenomatous polyps in the large intestine [133]. There are 3 subtypes of FAP:

- "Classic" FAP, in which there is an inactivating mutation of the tumour suppressor gene *APC* [134], leading to the development of 100s – 1000s of polyps, with a 93% risk of malignant conversion by the age of 50 years [135].

- Attenuated FAP, a less penetrant subtype [136], usually with truncating mutations in the 5' region of the *APC* gene , manifested by fewer polyps and a lower lifetime risk of cancer (70%) .

- Autosomal recessive FAP, in which there are mutations in the *MUTYH* gene encoding the base excision repair enzyme MYH glycosylase [137] . This generally results in a milder phenotype than classic or attenuated FAP.

1.2.1.3 Colitis-related colorectal cancer

Inflammatory bowel disease (IBD) is a blanket term for 2 distinct conditions: Crohn's disease (in which inflammation can affect any part of the gastrointestinal tract) [138] and ulcerative colitis (in which inflammation is limited to the colon). Both are autoimmune diseases with a degree of genetic predisposition [139], characterised by disproportionate T-cell responses to some types of commensal bacteria [140] , leading to inflammatory cell infiltration, ulceration, oedema and fibrosis of the bowel wall. In patients with ulcerative colitis, the incidence of CRC increases 8 – 10 years after the initial diagnosis , reaching 18% after 30 years [141]; furthermore, the severity of inflammation is correlated with the risk of developing CRC [142]. While the majority of sporadic CRCs appear to arise from adenomatous polyps, colitis-associated CRCs tend to evolve from regions of epithelial dysplasia [143]. Affected patients are generally younger than those with sporadic cancers, and a higher proportion of patients present with 2 or more synchronous primary tumours [144].

A number of possible mechanisms of tumorigenesis specific to colitis-associated CRC have been proposed, including (1) The overexpression of Toll-like receptor 4 (TLR4), which appears to increase EGFR-2 signalling [145]; (2) Oxidative stress in inflamed tissue mediating DNA damage through reactive nitrogen species [146]; and (3) Release of inflammatory cytokines and growth factors such as Interleukin-6 and interleukin-23, causing the induction of anti-apoptotic genes such as *BCL-XL* [147] .

CRC as a consequence of IBD is relatively uncommon, accounting for less than 1% of all CRC diagnoses [128].

1.2.2 Disordered signalling pathways in colorectal cancer

1.2.2.1 Genetic aberrations

Two differing types of genomic instability are regarded as mechanisms of CRC tumorigenesis. Chromosomal instability (CIN) is found in approximately 70% of CRCs, and constitutes the duplication or deletion of fragments of chromosomes or entire chromosomes, resulting in heterogeneous chromosomal abnormalities [148] . Microsatellite instability (MSI) is observed in about 15% of CRCs and results from DNA mismatch repair, leading to the accumulation of DNA sequence errors [149] . This generates novel "microsatellite" fragments. Tumours displaying microsatellite instability have less propensity to metastasise, and can be regarded as less sensitive to chemotherapeutic agents [150]. Microsatellite instability is assessed through the analysis of five microsatellite markers, permitting identification of "high MSI" (>30% MSI in standard markers), "low MSI" (<30%) and microsatellite stable tumours (demonstrating absence of microsatellite alterations). High MSI tumours tend to be more proximal, poorly differentiated, mucinous lesions, with marked lymphocyte infiltration [151]. A systematic review of patients with MSI CRCs revealed that MSI high tumours are associated with a significantly better prognosis when compared to microsatellite stable (MSS) tumours [152]. A pooled survival analysis has found that patients with MSS tumours are more likely to derive benefit from 5-fluorouracil-based chemotherapy than those with MSI high tumours, although the mechanism underlying this remains unclear [153]. The genetic alterations which are

encountered in CIN and MSI cancers, while sharing some common pathways, also demonstrate a number of differences.

Further to the germline mutations in the *APC* gene that are responsible for the majority of cases of FAP, most sporadic CRCs are also observed to harbour somatic *APC* mutations. *APC* is a tumour suppressor gene, and its inactivation through chromosomal instability is deemed to be the triggering event in most CRCs [113] . Loss of *APC* function leads to the accumulation and nuclear-localisation of ß-catenin, resulting in constitutively active Wnt signalling [154]. This in turn promotes cell signalling, proliferation and epithelial-mesenchymal transition through downstream effectors including the TCF/LEF family of transcription factors [155]. It has been shown that, via Wnt activation, loss of APC in an animal model ($Cre^{+}Apc^{fl/fl}$) induced with napthoflavone resulted in abnormal intestinal crypt morphology, changes in ECM proteins, and increased proliferation and apoptosis [156]. When a Wnt stimulus is absent a destruction complex, composed of tumour suppressors AXIN and APC, GSK-3 and CK1 (serine/threonine kinases), protein phosphatase 2A and the E3-ubiquitin ligase ß-TrCP, degrades ß-catenin. The role that APC plays in this process appears complex [157]. APC proteins bear multiple binding sites for ß-catenin; it is thought that APC may promote ß-catenin phosphorylation by AXIN-bound kinases. It has also been postulated that CK1 and GSK-3 may phosphorylate APC after phosphorylating ß-catenin, thus displacing ß-catenin from AXIN and enabling AXIN to interact with a new ß-catenin molecule [158]. Furthermore, APC may function in promoting ß-catenin ubiquitination, thus tagging it for proteosomal degradation [159].

In contrast, in those tumours in which microsatellite instability is predominant, the Wnt signalling pathway appears to be disordered through mutations of *AXIN1* and *AXIN2* [160].

KRAS mutations in colonic epithelium are not sufficient to initiate tumorigenesis; however, occurring on a background of *APC* mutation, *KRAS* mutation results in a clonal expansion that can develop into cancer. *KRAS* mutations are present in approximately 30-50% of CRCs, and occur early in the sequence of transition from adenoma to carcinoma [113]. The majority of mutations are in exon 2 codon 12, with the remainder predominantly located in exon 2 codon 13 and exon 3

codon 61; they lead to inhibition of the GTPase activity of RAS, thus preventing hydrolysis of GTP on RAS via GTPase activating proteins (GAPs) and resulting in the accumulation of RAS in the active GTP-bound form [161]. Constitutively active KRAS activates the RAF/MAPK and PI3K/AKT pathways, driving cell proliferation and survival. *BRAF* mutations are less frequently encountered than *KRAS*, and are unlikely to co-exist with *KRAS* mutations [116]. However, mutations in *BRAF* are more common in microsatellite unstable tumours [162]. The presence of mutations in *KRAS* and/or *BRAF* is predictive of lack of response to EGFR-inhibitory agents such as cetuximab and panitumumab, and confers a worse prognosis on patients [163] .

The most commonly detected cytogenetic abnormality in CRC is deletion of the long arm of chromosome 18 [113] . This is encountered in instances of CIN and MSI [164]. Loss of heterozygosity of 18q leads to loss of *DCC* (deleted in colorectal cancer), which is located in region 18q21 [165]. DCC functions as a receptor for netrin-1 and, when bound to netrin-1, activates the CDC42-RAC and MAPK pathways, promoting tumour development. However, when DCC and netrin-1 are not associated, DCC is a tumour suppressor with a pro-apoptotic function [166]. *SMAD4* is also located on 18q, and is a participant in the TGFβ signalling pathway [167] . High levels of SMAD4 expression in colorectal tumours are associated with significantly better survival outcomes [168], while loss of SMAD4 has been found to upregulate VEGF expression in CRC cell lines and is predictive of early CRC recurrence [169] .

In tumours displaying CIN, an event which occurs relatively late in the progression from adenoma to carcinoma is *TP53* inactivation, either through loss of heterozygosity of chromosome 17, or acquisition of loss of function mutations [118,170]. p53 inactivation is frequently linked with chromosomal instability, although each can exist independently [171]. Loss of p53 function can lead to aberrant cell growth; however, there is not a clear negative correlation between low p53 expression and clinical outcome [172]. In contrast, tumours which display MSI are more inclined to develop through p53-independent mechanisms, such as mutations in bcl-2-associated X protein (*BAX*), a pro-apoptotic gene [125], and insulin-like growth factor 2 receptor (*IGF2R*), a participant in TGFβ signalling [124].

Inactivation of the TGFβ signalling pathway is a key event during CRC progression in a proportion of tumours [173]; this is observed in CIN cancers through loss of *SMAD4* [174], and in MSI cancers through mutations in the TGFβ type II receptor [123]. However, the role of TGFβ in CRC is not clearly delineated, as elevations in TGFβ both in the primary tumour and in the stromal compartment are strongly correlated with risk of relapse [175-177].

1.2.2.2 Epigenetic alterations

Epigenetic modifications are heritable changes in the genome, with no change in the DNA sequence. Methylation is one such modification, and is the outcome of the covalent addition of a methyl group to the cytosines within CpG dinucleotides. CpG islands consist of clusters of CpG subunits, and are observed in the promoter regulatory regions of many genes. Alterations in the methylation status of CpG islands can lead to reduced gene transcription through effective silencing of genes, including tumour suppressor genes [178].

Approximately 30-40% of proximal colon cancers display a disproportionately high frequency of CpG island methylation; this group has been labelled "CpG island methylated phenotype" (CIMP) , and is found to have a strong association with MSI and *BRAF* mutation [179]. CIMP-associated hypermethylation of the MMR gene *MLH1* appears to be the primary mechanism driving the development of sporadic CRC with MSI [120]. Furthermore, cancer-specific CpG hypermethylation has been shown to affect gene expression in colorectal tumours, with consequent down-regulation of a number of genes that may function as tumour suppressor genes [180].

Global hypomethylation is also commonly encountered in CRC, potentially resulting in the upregulation of previously silenced genes and loss of genomic stability [181].

1.2.2.3 Colorectal cancer cell of origin

The identification of cancer stem cells [182] indicates that a subset of progenitor cells exists within the intestinal mucosal epithelium [183], and transformation of these cells (classically through the loss of *APC*) causes initiation of intestinal

adenomas [184]. CRC cancer stem cells are regulated through a number of mechanisms, outlined below.

Wnt-mediated regulation of CRC cancer stem cells

The canonical Wnt pathway is perhaps the most clearly defined regulator of colon cancer stem cells [185]. Investigations using Wnt reporter expression have revealed that Wnt signalling correlates inversely with expression of differentiation markers such as mucin 2 (MUC2) and cytokeratin 20 (CK20). In those cells with the highest levels of Wnt, an increase in vitro clonogenicity was detected; furthermore, these cells expressed the stem cell marker CD133. Achaete scute-like 2 (ASCL2) is a Wnt target transcription factor [186], and is upregulated at an early point in colon tumorigenesis through activation of the Wnt signalling pathway [187]. The function of ASCL2 in the context of CRC remains somewhat undefined, but evidence suggests that loss of ASCL2 leads to reduced cell proliferation and invasion, and loss of the stem cell phenotype, possibly through miRNA-mediated mechanisms [188] .

Another marker of intestinal stem cells is Ephrin receptor B2 (EPHB2) [189]; EPHB2 is also a Wnt target gene, and again high expression levels of EPHB2 are found in a subset of cells within colon tumours [190]; these cells display a high degree of clonogenicity and tumour-initiating capacity, and low levels of differentiation markers.

In addition, Lgr5 has been found to serve as a stem cell marker of the intestinal epithelium. It is also a Wnt target gene, and is solely expressed in cycling crypt base columnar cells [184].

Notch-signalling in CRC cancer stem cells

Notch signalling has been observed to inhibit cell differentiation [191]; in addition, interactions between the Notch and Wnt pathways have been documented [192], indicating that Notch also functions in CRC cancer stem cell regulation. Notch knock-down in CRC cell lines results in increased levels of apoptosis and reduced cell proliferation, while Notch over-expression promotes colony formation and proliferation [193].

Bone morphogenic proteins

The bone morphogenic proteins (BMPs) belong to the TGFβ superfamily, and are also thought to participate in cancer stem cell regulation. Expression of a number of BMP components is elevated in the upper levels of colon crypts, corresponding to the greatest degree of cellular differentiation [194]. Furthermore, several BMP inhibitors, including Gremlin-1, are more highly expressed at the crypt base, implying that BMP signalling exerts a degree of control over intestinal differentiation. Exogenous BMP4 has been found to lead to downregulation of Wnt, thus inducing differentiation in CRC cancer stem cells [195]; it has been proposed that the inverse may also be the case, with Wnt activation inhibiting BMP activity in cancer stem cells [196].

Tumour microenvironment

The microenvironment, comprising stromal cells and extracellular matrix, is also believed to impact on the regulation of CRC cancer stem cells, in part through creating a stem cell niche that maintains the stem cell compartment [197], and also through production of signalling molecules [194] and cytokines [198] .

A hypoxic environment is also likely to influence the degree of differentiation of cancer stem cells, with CRC cell lines grown in < 5% O_2 displaying greater clonogenicity and reduced expression of transcription factors associated with differentiation such as CDX1 [199]. Additionally, hypoxia-inducible factor 1 (HIF1) has been found to induce expression of multiple stem cell markers, including OCT4, in CRC cells [200].

Methylation-mediated regulation of CRC cancer stem cells

Many Wnt target and non-Wnt target genes are affected by aberrant CpG island methylation [201] , possibly silencing genes with a role in differentiation and thus maintaining the "stemness" of colorectal tumours. Furthermore, methylation-prone loci are generally found to lack specific transcription factor sequences, including specificity protein 1 (Sp1), yin yang 1 (YY1) and nuclear respiratory factor 1 (NRF1), which are thought to be protective against methylation in cancer [202] .

1.2.3 The actin cytoskeleton in colorectal cancer

The ability of cancer cells to migrate is recognised as the major determinant of the development of metastatic disease. Dysregulation of components of the actin cytoskeleton is a vital step in the development and progression of CRC; this is mediated through a number of mechanisms.

Reductions in cell-cell adhesion and alterations in cytoskeletal organisation are characteristics of the acquisition of a malignant phenotype. In physiological conditions, the adherens junction is connected to the actin cytoskeleton, maintaining cell polarity and tissue architecture. Epithelial cadherin (E-cadherin) is the primary functional component of adherens junctions of colonic epithelial cells, and is bound to cytoskeletal actin by catenins (α, ß, ɣ, and p 120). As previously described, in CRC ß-catenin accumulates in the nucleus following loss of APC function. As a consequence of this, the E-cadherin-catenin complex is disassembled, leading to disruption of the normal cell adhesion processes [155,203] . Loss of adhesion can act to promote tumour cell detachment from the primary site, direct invasion of adjacent tissue, and dissemination to distant sites. In several tumour types, including CRC, loss of membranous E-cadherin expression is observed to be associated with reduced levels of tumour differentiation; furthermore, reduced expression correlates with increased risk of metastasis [204]. The importance of E-cadherin loss in the development of metastatic disease is highlighted by the finding that expression levels are higher in primary tumours when compared with metastatic deposits, indicating that the ability of tumour cells to disseminate relies upon loss of the adhesion complex [205].

Loss of *APC* is a common feature in CRC tumorigenesis. In addition to the alterations in Wnt signalling that occur as a consequence of this, APC also plays a key role in regulation of the actin cytoskeleton, through binding to and stabilising microtubules [206]. Furthermore, APC has been observed to localise to the cortical actin cytoskeleton in confluent cultured cells [207]. Indirect effects on the actin cytoskeleton can be mediated through APC interactions with IQGAP (a scaffold protein that activates Cdc42), ARHGEF4 (a Rho GTPase), and mDia1 (a Rho GTPase effector protein involved in stress fibre formation) [208-210].

The integrins are a group of transmembrane receptors that serve to mediate cell-cell and cell-extracellular matrix interactions [211]. Integrin-mediated signal transduction occurs via intermediary proteins, including talin, vinculin [212] and α-actinin [213], which link integrins to actin cytoskeleton components. A consequence of these interactions is activation of the focal adhesion-linked protein tyrosine kinases Src and FAK, with subsequent alterations in the actin cytoskeleton promoting cell migration [214] . An association has been observed between increased integrin αv expression and malignant angiogenesis and tumour progression in several cancer types [215]. In CRC, a link between increased integrin αv expression and (i) advanced disease stage [216], and (ii) the presence of hepatic metastases [217] has been found. Furthermore, overexpression of integrin αv as determined by IHC on patient samples is an independent predictor of poorer survival outcomes [218].

1.2.4 The Rho/ROCK pathway in colorectal cancer

In several cancer types, including breast cancer [75] , activation of the ROCK pathway appears to promote tumour progression [219] . However, the impact of dysregulation of the Rho/ROCK pathway in the context of CRC is less clearly defined. There is increasing evidence to suggest that, contrary to the oncogenic role of Rho/ROCK activation in other tumour types, loss of RhoA can accelerate CRC progression [220]. This is thought to occur through a number of mechanisms [221]:

- RhoA signalling is essential to maintain adherens junctions, both in normal intestinal epithelium and in CRC cells [63,222]; inactivation of RhoA in CRC cells results in reduced E-cadherin bound ß-catenin, with consequent increased Wnt pathway activation

- RhoA inactivation leads to increased TCF4/ß-catenin activity, also promoting Wnt signalling and leading to upregulation of mitogenic proteins such as c-MYC and cyclin D1

- Loss of RhoA activity appears to prevent differentiation of CRC cells, through mechanisms that are not yet clearly defined.

Furthermore, pharmacological inhibition of ROCK has been shown to facilitate the culture of CRC organoids with cancer stem cell properties through induction of CD44 [220].

Another component of the Rho/ROCK pathway, LIM kinase, is also frequently found to be upregulated in certain cancer types, including breast [107,109] and prostate [108] cancers, and is thought to promote tumour progression, predominantly through the acquisition of a motile phenotype. LIMK inhibition is found to reduce cell motility, and thus reduce the capacity of cancer cells to invade and metastasise [223].

LIMK is also known to function as a p53 target, upregulated by DNA damage [111,112]. Knockdown or inhibition of *LIMK* appears to increase the sensitivity of cells to apoptosis following exposure to ionising radiation or chemotherapeutic agents, suggesting that *LIMK* functions in a pro-survival manner. Thus it can be determined that LIMK serves additional functions besides regulation of the actin cytoskeleton, and that selective pressure may exist in the context of some cancer types.

The pattern of LIMK2 expression was studied in CRC [224], and it was discovered that LIMK2 levels in a human CRC TMA progressively decreased with advancing stage of disease. In addition, a correlation between LIMK2 level and overall survival was discovered. The mechanism governing the relationship between reduction in LIMK2 expression and CRC was examined further by using *Drosophila melanogaster*, as the posterior midgut is representative of the mammalian intestine. An RNA interference approach was used to reduce dLIMK expression, and a consequent increase in stem cell proliferation was detected. This was recapitulated in a murine *Limk2* knockout model, with an increase in the number of stem cells seen in *Limk2* knockout intestinal crypt organoids relative to wild type. The conclusion drawn from this work was that the presence of LIMK2 limits the proliferation of intestinal stem cells, and thus a reduction in LIMK2 permits their propagation.

1.3 Squamous cell skin cancer

Non-melanoma skin cancer is the commonest cancer diagnosis in the UK, making up 20% of all diagnoses of malignancy. Basal cell carcinoma, originating from the basal cells of the epidermis, represents 74% of non-melanoma skin cancers. Cutaneous squamous skin cancer accounts for approximately 23% of non-melanoma skin cancers. Squamous cell carcinoma (SCC) arises through the malignant transformation of stratifying epithelium, the epithelial subtype present in tissues that serve a barrier function against the environment (e.g. the skin, cervix, and upper aero-digestive tract).

1.3.1 Pathogenesis of cutaneous squamous skin cancer

The most commonly encountered precursor lesion of cutaneous squamous skin cancer is actinic keratosis, characterised by dysplasia, with keratinocytes displaying atypical, hyper-pigmented, pleomorphic nuclei. The normal differentiation process is partially disrupted, resulting in epidermal atypia [225]. *TP53* mutations are frequently observed in actinic keratosis, indicating that dysplastic lesions have acquired triggering genetic mutations before developing into cutaneous squamous cell cancers [226,227]. Following a route of stepwise progression, actinic keratosis can develop into cutaneous squamous cell cancer *in situ*, with a more complete disruption of differentiation. 40% of *in situ* lesions have p53 mutations, again suggesting that this is an early event occurring before the development of an invasive phenotype [228]. In the cutaneous context, loss of p53 function is thought to occur due to UVB-induced inactivation [229] and is widely encountered in pre-malignant and malignant squamous lesions [226,230].

Aberrant Ras activation has also been noted in cutaneous SCC (cSCC) [231,232] and, in its role as an activator of the Raf/Mek/Erk pathway, can promote cSCC formation [233]. However, Ras activation in isolation is insufficient to trigger cSCC formation [234]; simultaneous alterations in pathways including NFκB or activation of CDK4 (a cell cycle progression mediator) are necessary [235,236].

Notch signalling has also been found to participate in the development of cSCC [237]. Notch signalling decreases keratinocyte proliferation and enhances differentiation via p21 (a cell cycle inhibitor), caspase 3 and PKC-δ (a regulator

of UVB-induced apoptosis) activation [238]. *NOTCH1* expression is reduced in cSCC relative to healthy epidermal controls [239], possibly as a consequence of p53 downregulation. Furthermore, *NOTCH1* mutations appear to be early events in the carcinogenesis of cSCC and evidence indicates that *NOTCH1* serves a tumour suppressor function in the epidermis [240,241]. Interestingly, Notch activation appears to suppress Rho/ROCK signalling, while loss of Notch signalling is accompanied by an increase in Rho/ROCK activity in cSCC [239].

1.3.2 Tumour microenvironment

The tumour microenvironment also plays a key role in the initiation and progression of cSCC.

1.3.2.1 cSCC arising in scar tissue

Chronic wounds/scars have the capacity to undergo malignant transformation; of cancers arising on a background of scar tissue, cSCC is the most common subtype [242]. The pathways involved in this process have not been fully elucidated, but it has been suggested that increased cell proliferation secondary to chronic inflammation, exposure of tissue to environmental toxins and carcinogens through loss of barrier function, and impaired immunological responses as a result of inadequate vascularisation of scar tissue may all play roles [242,243].

1.3.2.2 Inflammation

Tumour stroma in general has been shown to attract infiltrating immune cells that produce interleukins, cytokines and growth factors that permit evasion of the host immune responses [244].

In a mouse model of cSCC, cancer associated fibroblasts mediated tumour-promoting inflammation through a gene expression signature that recruited macrophages, and enhanced tumour growth and neoangiogenesis [245].

1.3.2.3 Adhesion

Fluctuations are observed in the type and number of adhesion molecules detected in different cancer contexts, as cells encounter altering environments through the processes of invasion and metastasis.

A more aggressive subtype of cSCC, acantholytic SCC, displays lower levels of intercellular adhesion proteins, such as E-cadherin and Syndecan-1, than those observed in non-acantholytic SCCs [246]; this is thought to contribute to the more invasive nature of this variant.

The dysregulated function of adhesion molecules may also impact on treatment outcomes in SCC: following radiotherapy treatment to head and neck SCC, intercellular adhesion molecule 2 (ICAM2) appears to activate PI3K/AKT signalling, thus blocking apoptosis and enhancing survival [247].

1.3.2.4 Stromal fibroblasts

Cancer-associated fibroblasts are able to remodel the microenvironment, forming tracks that permit the collective invasion of SCC cells [86]. This appears to be both force-mediated, through Rho-regulated actin cytoskeleton alterations in CAFs, and protease-mediated, e.g. via matrix metalloproteinases [248]. The SCC cells that follow the tracks created by the leading CAFs do so in a MRCK and Cdc42-dependent fashion [86].

1.3.2.5 The extracellular matrix

Extracellular matrix components

Laminins are a group of large extracellular glycoproteins that function in tissue development, wound repair and tumorigenesis [249]. Laminin 332 plays an integral role in epidermal adhesion in normal conditions [250]. However, laminin 332 has been shown to be over-expressed in several types of SCC, including cutaneous, oral, laryngeal, oesophageal and cervical cancers, and expression levels correlate with increased invasiveness and adverse clinical outcome [251]. In SCC, laminin 332 tends to localise at the interface between tumour and stroma [252]. In the context of cSCC, laminin 332 appears to promote tumour progression through an interaction with collage VII, which triggers phosphoinositol-3-kinase signalling and thus cell proliferation [253]. Co-deposition of laminin 332 and other extracellular matrix components, including TNC, has been documented [254] ; this is thought to serve a supportive role permitting tumour cell invasion.

Tension within the extracellular matrix

Mechanotransduction signalling within the tumour microenvironment has also been shown to play a pivotal role in the progression of cSCC. A murine model of cSCC, utilising a 2-stage chemical carcinogenesis protocol in FVB/N mice (one application of the mutagen dimethylbenz[a]anthracene followed by multiple applications of 12-O-tetradecanoylphorbol-13-acetate [255]) was used to induce papillomas, with conversion to invasive tumours resembling human cSCC observed in a subset of these lesions. Only a cohort of animals in which ROCK activation within the epidermal keratinocytes was achieved (through the K14 ROCK:ER transgene system) demonstrated progression to invasive cSCC within 15 weeks, indicating the importance of cellular tension in cancer progression. The changes observed in this model included an increase in nuclear and total ß-catenin and an increase in collagen deposition within the extracellular matrix, with a consequent elevation in the level of stiffness within the ECM [83]. Subsequent studies have confirmed that levels of ROCK 1 and ROCK 2 activation are increased in human cSCC relative to normal skin, and that integrin-mediated FAK signalling appears to be driven by increased ECM density [84].

1.4 Epigenetics

1.4.1 Mechanisms of protein level regulation

Earlier work in the lab had determined that LIMK2 expression was downregulated at a protein level in CRC. There are a number of mechanisms by which protein level regulation occurs:

1.4.1.1 Transcriptional regulation

Through binding enhancer elements, and the recruitment of co-factors and RNA polymerase II, transcription factors can regulate gene expression [256-258]. Each individual cell type expresses a specific set of transcription factors, and therefore controls the selective transcription of a subset of genes by RNA polymerase II, and consequently determines the gene expression programme of the cell [259]. Mutations in transcription factors are known to contribute to tumorigenesis, often as a result of overexpression of oncogenic transcription factors such as c-MYC [260]. However, it has also been shown that long non-coding

RNAs can be misregulated, leading to silencing of tumour suppressor genes and consequently promoting cancer progression [261].

1.4.1.2 MicroRNAs

MicroRNAs (miRNAs) are short non-coding RNAs that are often present in reduced levels in tumours [262]. This can occur secondary to genetic loss [263], epigenetic silencing [264], or transcriptional repression via loss of tumour suppressor transcription factors such as p53 [265]. miRNAs regulate the protein synthesis of messenger RNAs by deadenylation or translational repression [266].

1.4.1.3 Protein degradation

Through ubiquitin labelling, proteins are tagged for degradation via proteolysis [267]. The tumour suppressor gene p53 can be targeted by Mdm2 for ubiquitination and proteasomal degradation [268], leading to loss of p53 expression. This mechanism may also apply to destruction of the protein products of other tumour suppressor genes.

The knowledge that a significant proportion of colorectal tumours are characterised by a CpG island methylated phenotype indicated that epigenetic silencing may be the mechanism by which LIMK2 expression is reduced in this context, and therefore my work focused on epigenetic regulation.

1.4.2 Epigenetic regulation

Mutations, whether inherited through the germ line or arising in somatic cells, can cause cancer [269]. This can occur through oncogenes, in which mutations lead to enhanced cell proliferation, or via the loss of function of tumour suppressor genes. However, it is increasingly evident that epigenetic factors are also at play, with heritable alterations in gene expression that are not mediated by changes in the gene's nucleotide sequence [270] leading to silencing of genes in cancer cells [271-273].

The changes in gene expression that are mediated by epigenetic alterations are a consequence of methylation of DNA in promoter regions, where transcription takes place. DNA methylation involves the modification of post-replicative DNA,

with the addition of a methyl group to the cytosine ring to generate methyl cytosine. S-adenosyl-methionine (SAM) is the methyl group donor, and the reaction is catalysed by DNA methyltransferases (DNMTs) (Figure 1-6). In mammals, methyl cytosine modification only occurs in cytosines that immediately precede a guanosine in the nucleotide sequence. This is known as a CpG dinucleotide; these are observed relatively infrequently in the genome, in likelihood due to progressive CpG depletion through DNA methylation. Depletion occurs as a consequence of the tendency for methylated cytosine to deaminate, thus forming thymidine [274].

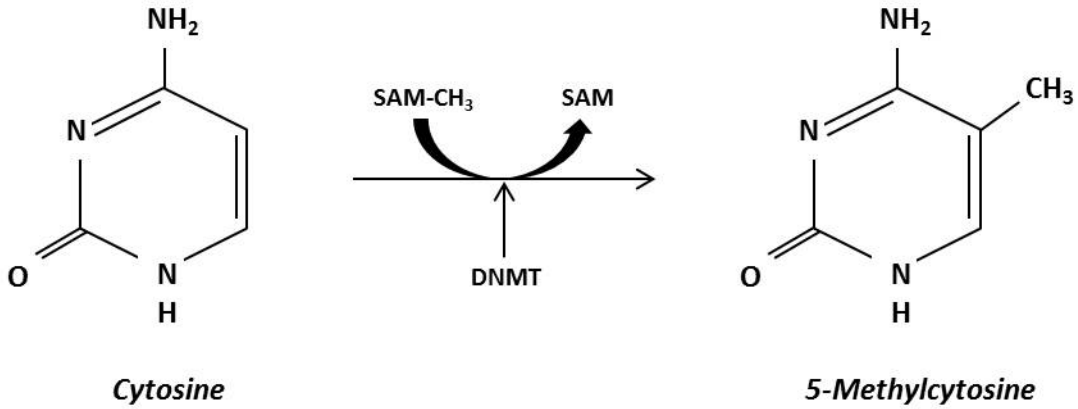

Figure 1-6 Conversion of cytosine to 5-methylcytosine

DNMT catalyses the donation of a methyl group from SAM to the 5-carbon position of cytosine. Adapted from Gibney and Nolan [275].

1.4.3 The physiological role of DNA methylation

1.4.3.1 Maintenance of non-coding DNA

Several studies have linked the state of DNA methylation to gene expression, with a direct correlation observed between promoter region methylation and transcriptional silencing [270-273]. Hypermethylated DNA replicates at a later time point than unmethylated DNA [276], ensuring the majority of the genome undergoes delayed replication. Inactive chromatin is generated during late replication, facilitating transcriptional silencing of non-coding sequences [277]. Through this mechanism, potentially harmful DNA sequences such as transposons, repeat elements, and inserted viral sequences are repressed [278].

1.4.3.2 CpG islands

While CpG dinucleotides are fairly scarce throughout the genome, they are seen grouped within short DNA sequences, often in promoter regions [270]. These CpG clusters are termed CpG islands, and are found in nearly 50% of genes in the genome. The majority of CpG dinucleotides that exist out-with the confines of a CpG island are methylated; however, the CpG dinucleotides within CpG islands tend to be unmethylated, irrespective of whether the gene is undergoing transcription [270]. There are physiological instances in which CpG islands within gene promoter regions are heavily methylated, for example in association with transcriptionally silent genes on the inactive X chromosome of females [270].

1.4.4 DNA methylation in cancer

It has long been recognised that aberrant DNA methylation patterns are observed in cancer cells (Figure 1-7).

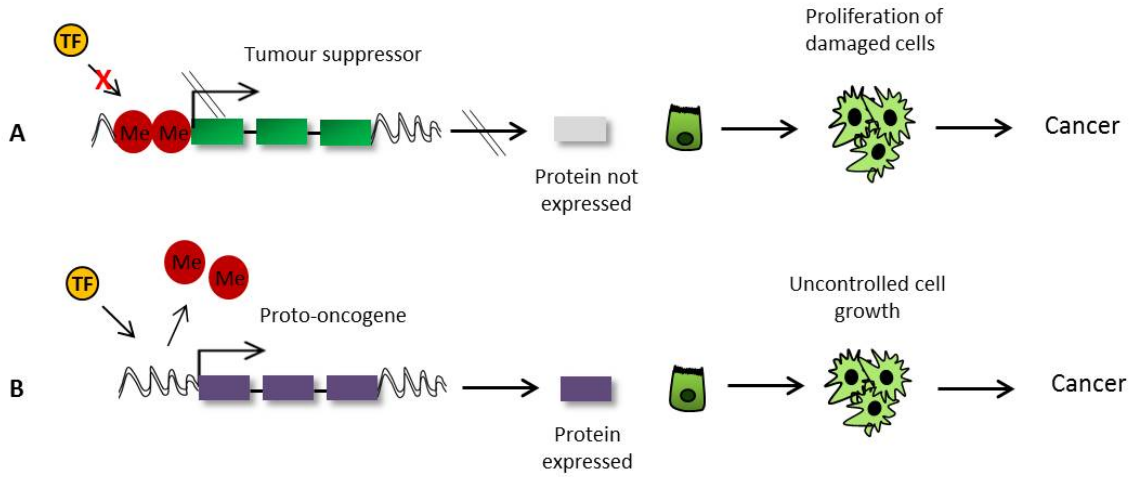

Figure 1-7 Two mechanisms by which epigenetic mechanisms contribute to carcinogenesis

A) Methylation of a tumour suppressor gene prevents transcription factors (TF) binding to the promoter region; the gene is therefore not expressed, and damaged cells proliferate and become malignant. B) Demethylation of a proto-oncogene allows TFs to initiate transcription and genes to express the protein product. Uncontrolled cell proliferation follows. Adapted from Nelson, S. (2008) Comparative methylation hybridization. Nature Education 1(1):55 .

1.4.4.1 Increased DNA methylation

Loss of function of tumour suppressor genes is an important factor in tumorigenesis; this occurs through germ-line or somatic mutations [279], but can also be caused by hypermethylation of gene promoters, leading to transcriptional silencing [280]. The loss of gene function that results from hypermethylation of the promoter and from mutations in the coding region has a similar biological impact [273]. This is illustrated by the fact that microsatellite instability in colon cancer can result from mutation or hypermethylation of *MLH1* [281].

Patterns of DNA methylation have been assessed as diagnostic, prognostic and predictive biomarkers in a number of cancer types, including prostate cancer [282]. Furthermore, hypermethylation, and consequent tumour suppressor gene silencing, has been found to be reversible through the use of demethylating agents [283], permitting re-expression of functional genes in cancer cell lines. These agents include DNMT inhibitors such as 5-azacytidine, which has gained approval for use in some haematological malignancies [284]. Thus, it is evident that the identification of tumour suppressor genes that undergo methylation-mediated silencing during tumorigenesis is important for developing future clinical management strategies.

1.4.4.2 Reduced DNA methylation

Loss of DNA methylation is thought to play a role in tumorigenesis through a decrease in transcriptional repression of normally silent regions of the genome, potentially leading to expression of harmful elements and/or genes that would usually be silent [285]. Furthermore, a reduction in methylation can also impact on nuclear structures, e.g. pericentromeric regions of the chromosome, resulting in instability and incongruous DNA replication [286]. The degree of hypomethylation of DNA correlates with tumour progression and/or grade in some tumour types, including epithelial ovarian cancer [287]; in addition, hypomethylation of centromeric satellite DNA has been identified as a marker predictive of relapse in ovarian cancer [288].

1.4.5 Determining methylation status

Most of the methods utilised to determine the methylation status of a DNA sequence rely on the principle of bisulphite conversion: bisulphite treatment of DNA converts cytosine residues to uracil, but does not alter 5-methylcytosine residues [289] (Figure 1-8). DNA must be denatured prior to bisulphite modification, as only methylcytosines on single strands are vulnerable to bisulphite treatment [290]. DNA degradation can occur during bisulphite treatment, but can be minimised by maintaining an optimum bisulphite concentration, and thus reducing the time required to complete the reaction [291].

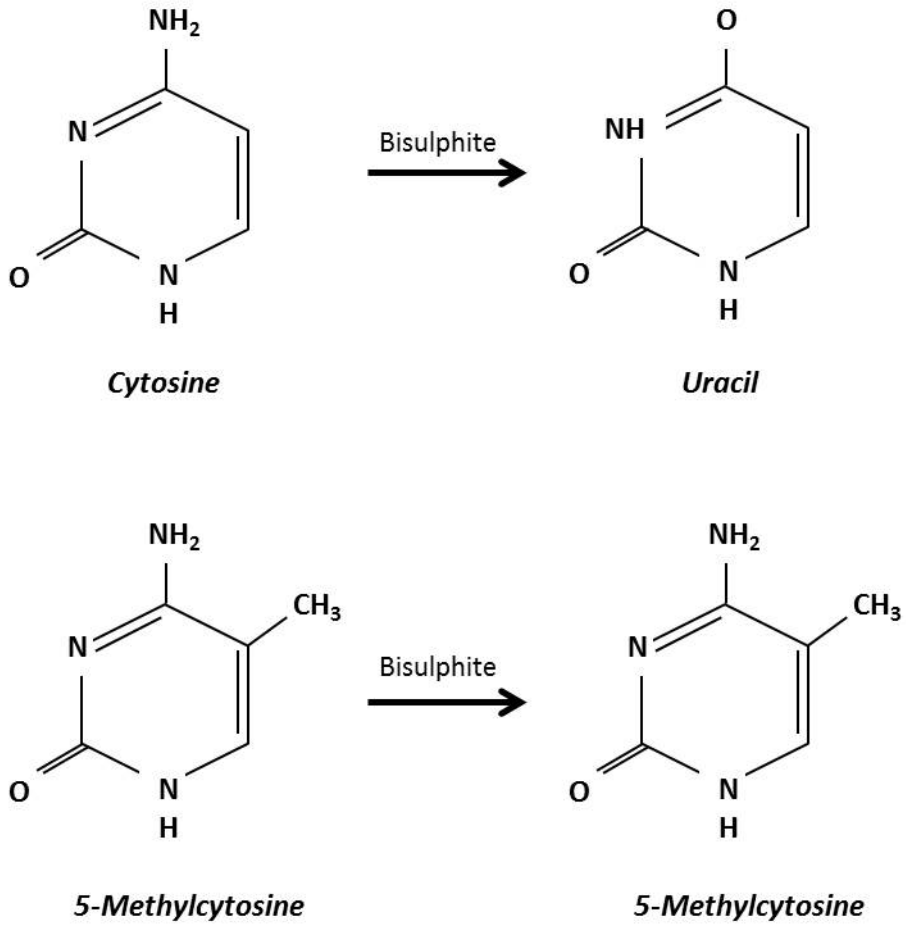

Figure 1-8 Bisulphite conversion

Following treatment with bisulphite, cytosines undergo conversion to uracil. In contrast, 5-methylcytosines are resistant to conversion and remain unaltered.

1.4.5.1 Methylation-specific PCR

Methylation-specific (MSP) PCR is one common method used to assess methylation status; it requires primer design that is customised to detect both unmethylated and methylated sequences [292]. Methylation is determined by the capacity of the specific primer pair (unmethylated or methylated) to achieve amplification. It does not permit resolution at the nucleotide level, and is therefore a non-quantitative measure.

1.4.5.2 Bisulphite sequencing

Bisulphite sequencing relies on PCR amplification of bisulphite treated DNA, with primers that flank but do not involve the methylation site of interest [293]. This permits amplification of both methylated and unmethylated sequences. The PCR product is subsequently cloned into plasmid vectors, and the individual clones are sequenced; this permits the generation of methylation maps of individual DNA molecules (Figure 1-9). All unmethylated cytosines are displayed as thymines in the sequence.

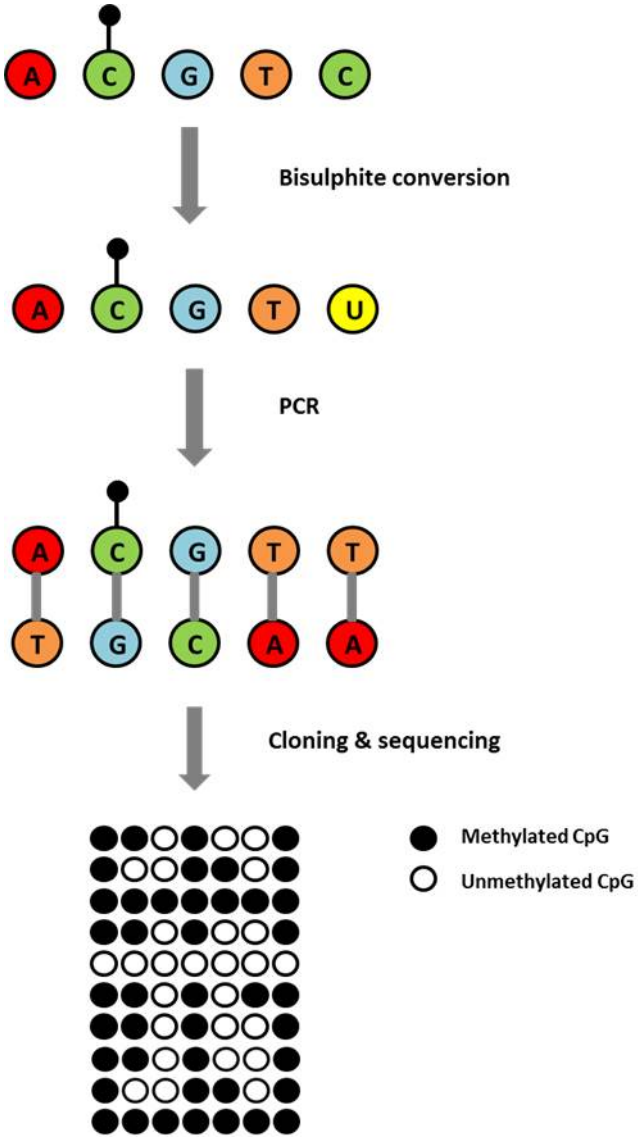

Figure 1-9 Schematic illustrating the process of bisulphite sequencing.

Bisulphite conversion of gDNA results in conversion of unmethylated CpG dinucleotides to uracil. Methylated CpG dinucleotides remain resistant to conversion. Following amplification, gDNA is cloned and sequenced, and the CpG dinucleotides analysed to produce a map of methylation status.

1.5 Tissue mechanics

Solid tumours consist of a mass of cancer cells, host cells (including immune cells), and blood and lymphatic vessels, embedded within an ECM [294]. As tumours progress and grow, they become detectably stiffer than the surrounding tissue due to an increase in the structural components of the tumour. This process inevitably involves the generation of mechanical forces, both within the tumour, and between the tumour and its microenvironment. The increase in rigidity observed in tumours is due in part to:

- Elevations in the elastic modulus as a consequence of changes in the cell architecture [295]
- Stiffening of the ECM through pro-fibrotic mechanisms [296]
- Increases in interstitial tissue pressure as a result of alterations in the tumour vasculature [297].

As the tumour and its surroundings become stiffer, the capacity for tumour cell survival, proliferation and progression is enhanced [298,299].

1.5.1 Non-malignant fibrosis

Alterations in mechanical force can directly affect the morphological features of cells; these changes are mediated through the Rho GTPases, regulatory hubs that determine the cytoskeletal response to changes in extracellular tension [300]. An increase in external force is coupled with cytoskeletal Rho/ROCK activation, a response that serves to increase cellular tension and returns the cell to a state of tension balance with its environment [301] . Simultaneously, ECM components are manufactured in response to alterations in mechanical force to ensure that equilibrium is maintained between the internal and external cellular environments [302] .

Fibrosis is initiated during physiological wound healing; however, when these mechanisms are dysregulated, pathological fibrosis occurs [303]. This is characterised by the deposition of excessive amounts of ECM components, including fibrillar collagen and hyaluronan. The myofibroblast is the cell type

primarily responsible for the synthesis and deposition of ECM components in this setting. Myofibroblasts are essentially activated fibroblasts that express α smooth muscle actin, permitting a contractile phenotype [304]. Fibrotic tissue is stiffer than comparative healthy tissue [305]; the dermis is estimated to have a Young's elastic modulus of 1-5 kPa, while fibrosed dermis measures 20-100 kPa. During the generation of a fibrotic scar, myofibroblast precursors are recruited, attain contractile features and thus contribute to the development of fibrosis [304]. Mechanical stress generated by the stiff, fibrotic ECM accelerates the expression of αSMA in fibroblasts [306] and promotes the survival of myofibroblasts in granulation tissue, leading to the formation of hypertrophic scar tissue [307].

Myofibroblast contraction can also bring about the release of active TGFβ from its stored, latent form within the ECM [308]. This is thought to occur through myofibroblast integrins mediating opening of the latent complex through stress fibre contraction. TGFβ is the primary pro-fibrotic factor and its release compounds the cycle of increasing ECM stiffness leading to myofibroblast activation, in part through enabling myofibroblasts to resist apoptosis [309].

1.5.2 Fibrosis of the tumour stroma

Several tumour types are known to arise on a background of pre-existing fibrosis, such as hepatocellular cancer as a consequence of chronic hepatitis [310], and lung cancer occurring in the context of interstitial lung diseases such as idiopathic pulmonary fibrosis [311]. Tumours arising within fibrotic lesions are thought to develop through dysregulation of cell polarity, cell proliferation, and myofibroblast-stimulated inflammation and neo-angiogenesis [312].

In addition to fibrosis observed in the context of wound healing, scar formation, and benign pathological processes, similar changes are observed in the fibrotic stroma that surrounds some tumours. The same pathways that activate fibroblasts, leading to deposition of ECM components and increased levels of contractility are at play within the reactive tumour stroma. Furthermore, myofibroblasts are present at the invading front of a number of different tumour types, including lung [313], liver [314], breast [312] and gastric [315] cancers. In this context, myofibroblasts are termed cancer associated fibroblasts (CAFs); they

are thought to contribute to cancer progression through the secretion of pro-invasive cytokines and proteases [316-319].

1.5.3 Cancer associated fibroblasts

The primary difference between CAFs and myofibroblasts is the resistance to apoptosis displayed by the former; as a result of this, CAFs tend to persist for significantly longer, and their activation is irreversible [320]. They are derived from a number of cell types, including resident fibroblasts [321], bone marrow-derived mesenchymal stem cells [322], and epithelial cells, the latter conversion occurring through the process of EMT [312] (Figure 1-10).

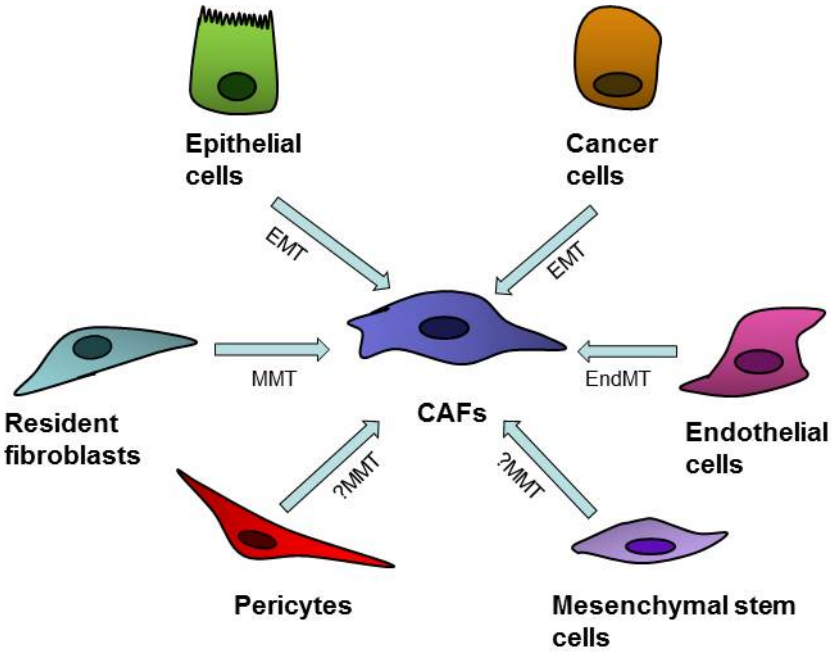

Figure 1-10 Origins of CAFs within the tumour microenvironment

CAFs can develop through differentiation of dormant resident fibroblasts or pericytes via mesenchymal mesenchymal transition (MMT). They can also arise from bone marrow mesenchymal stem cells and from normal or malignant epithelial cells via EMT or from endothelial cells via endothelial to mesenchymal transition (EndMT). Adapted from Cirri and Chiarugi [320].

1.5.3.1 The role of CAFs in tumour initiation

It has been shown that dermal fibroblasts isolated from patients with several types of cancer, including breast, melanoma and colon, display an increased proliferation rate *in vitro,* suggesting that changes in fibroblast phenotype may play a role in cancer initiation [323]. Studies involving murine models of genetically modified fibroblasts have also indicated that fibroblasts participate in the initiation of tumours, with overexpression of growth factors such as TGFß and HGF within fibroblasts promoting malignant transformation of mammary [324] and prostate epithelium [325].

1.5.3.2 The role of CAFs in tumour progression

CAFs produce several growth factors, permitting direct stimulation of tumour cell proliferation, and thus enabling tumour progression. For example, CAFs isolated from lung tumours secrete hepatocyte growth factor (HGF), activating c-MET signalling in cancer cells [326]. In addition to growth factors, stromal CAFs produce cytokines, which promote immune cell infiltration and consequent vascularisation and metastasis [327], and MMPs, which can both degrade the adjacent ECM, allowing tumour expansion, and activate growth factors through cleavage [328,329]. CAFs also play a role in determining cancer cell motility, mainly through the induction of EMT in cancer cells [330]. Growth factors produced by cancer cells are also able to act on CAFs, leading to a pro-tumorigenic interplay between the tumour and stroma [331] (Figure 1-11).

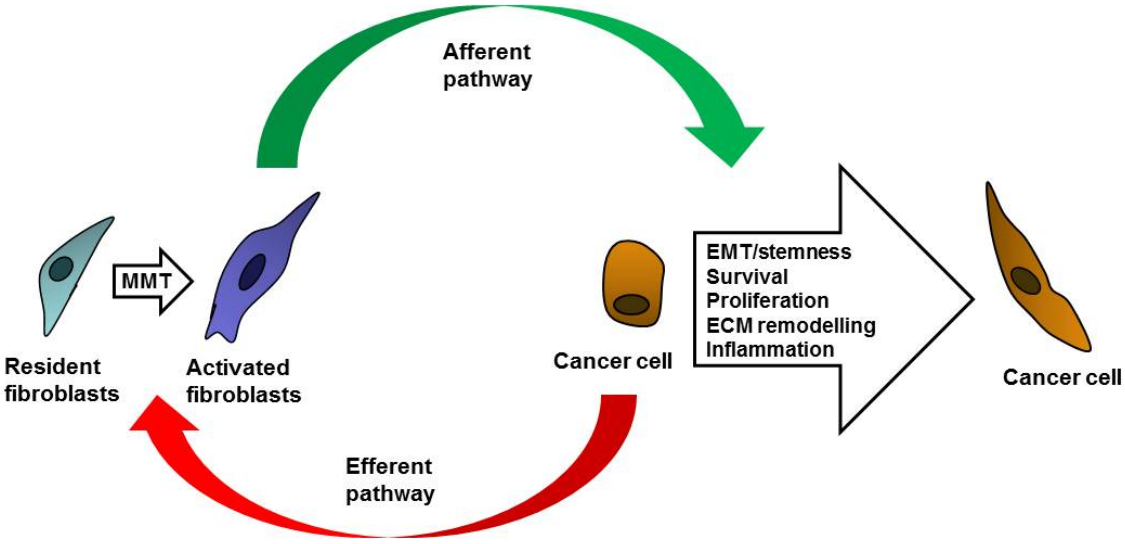

Figure 1-11 Dialogue between CAFs and cancer cells

Tumour progression depends on the interplay between CAFs and cancer cells. Cancer cells stimulate and maintain the activated fibroblast phenotype via growth factors (including TGFß) and cytokines. In turn, fibroblasts produce PDGF, VEGF, MMPs and cytokines, promoting ECM remodelling, EMT, proliferation and angiogenesis, and thus tumour progression. Adapted from Cirri and Chiarugi [320].

The architecture of the tumour microenvironment is also subject to regulation by CAFs, as the components of the ECM are produced by activated fibroblasts. The density and constituents of the ECM impact on the stiffness of the microenvironment, and consequently alter cell morphology, cell signalling and cytoskeletal organisation [332] . Within the ECM around a tumour, fibrillar collagens display enhanced maturation, with increased cross-linking, catalysed by lysyl oxidase (LOX). LOX is expressed in fibroblasts during the initial phase of breast tumorigenesis; the cross-linked collagen fibres that develop as a consequence of this promote cancer cell migration and invasion. Treatment with LOX inhibitors reduces collagen cross-links and thus inhibits tissue stiffening and cancer progression [333]. In addition to the action of LOX on collagen, increased ECM stiffness occurs through integrin signalling and discoidin domain receptor-1 activation, and consequently leads to enhanced growth factor-mediated cell migration [334].

In addition to collagen, CAFs also produce fibronectin, hyaluronan and tenascin C (TNC). Fibronectin participates in numerous cellular interactions with the ECM, mediating cell adhesion, migration and proliferation [335]; its presence in stroma is positively correlated with metastatic potential and MMP production [336]. Expression of hyaluronan by CAFs has been shown to enhance recruitment of tumour-associated macrophages, thus promoting tumour progression [337]. Myofibroblast-derived TNC has been shown to stimulate colon cancer cell invasion through promotion of a migratory phenotype [338].

Fibronectin and collagen bind to cells via integrins; however, hyaluronan functions through binding to a range of cellular receptors, including CD44, and the receptor for hyaluronan-mediated motility (RHAMM) [339].

Increased stromal stiffness as a result of the accumulation of types I and III collagens, with concurrent increased breakdown of collagen type IV, results in the fibrotic condition termed desmoplasia [340] (Figure 1-12). Desmoplastic stroma is associated with a poor clinical outcome in a number of cancer types, including breast [341] and pancreatic [80,82]; in part, this is due to the pro-invasive components of the ECM, and in part to the fact that fibrotic stroma impacts intra-tumoral drug delivery, rendering pancreatic cancer in particular relatively chemo-insensitive [342].

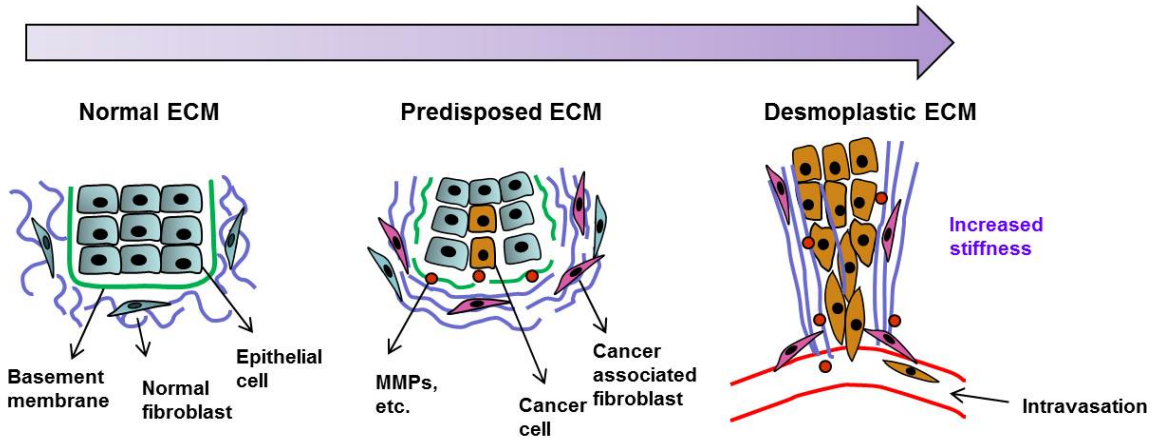

Figure 1-12 The stages of stromal ECM remodelling

In normal conditions, stromal collagen fibrils are wavy. In the pre-invasive stage, collagen fibres straighten and align around the tumour. In the invasive stage, collagen fibres are arranged parallel to the tumour border. Adapted from Malik et al [343].

1.5.4 Increased cellular tension

In addition to the increased stiffness observed within the microenvironment, tumour cells themselves are frequently found to demonstrate higher levels of tension through over-expression of Rho GTPases [344]. Furthermore, ROCK activation appears to promote tumour cell invasion [345]. The increase in cytoskeletal tension that is generated by Rho-ROCK activation induces F actin assembly and promotes cell proliferation [346]. The forces generated by cytoskeletal contraction also promote focal adhesion maturation [347]. The balance of mechanical stress can shift, either through interactions with other cells [348], or due to distortion of the cell membrane as an adaptation to changes in force in the environment [349]. As a consequence, rearrangement of the cytoskeleton, proliferation and morphogenesis occur [350].

1.6 Tenascins

Using an RNA microarray approach, I found that ROCK activation in primary cells led to an increase in Tenascin C gene transcripts and protein level. It had previously been shown in the group that ECM components such as collagen are deposited in higher quantities in murine epidermis following ROCK activation [83]. I hypothesised that TNC may be a constituent part of the dense, stiff ECM observed following ROCK activation, and opted to investigate this further.

Tenascins are a family of oligomeric glycoproteins, located in the extracellular matrix [351]; four members exist, denoted tenascin C, R, X and W. Of these, tenascin C (TNC) is the most extensively studied. All subtypes of tenascin share the same basic structure: amino-terminal heptad repeats, epidermal growth factor (EGF)-like repeats, fibronectin type III domain repeats, and a carboxyl-terminal fibronectin-like globular domain. Individual subunits are able to assemble into trimers or hexamers due to heptad repeats lying in a highly conserved amino-terminal oligomerisation region. Each member of the family displays a different number of EGF-like and fibronectin type III repeats. TNC is the member of the family that I found to be upregulated in response to ROCK activation, and thus has been the focus of this section of my research. .

1.6.1 TNC structure and expression

The human *TNC* gene is found on chromosome 9q33 [352]. The 8150bp transcript encodes a protein 180-250 kDa in size [353]. TNC is conventionally assembled into hexamers, and indeed is also known as hexabrachion. The protein subunits of TNC typically possess 14.5 EGF-like repeats, and 8 fibronectin type III repeats (Figure 1-13). A significant number of splice variants exists, due to alternative splicing of an additional 9 repeats that can be individually incorporated in the TNC structure [354] . Numerous TNC binding partners have been identified, including integrins [355], annexin II [356] , heparin [357], and fibronectin [358]. The majority of binding sites are found in the fibronectin type III repeats or the fibrinogen globe; however, the EGF-like repeats are also thought to behave as ligands for EGF receptors (albeit with low affinity) [359].

During embryogenesis, TNC is expressed at high levels in neural, vascular and skeletal tissues [360]. In adults, low level expression persists only in tissues subject to mechanical loading (e.g. tendinous tissue [361]; however, significant TNC upregulation occurs during wound healing [362,363], and in pathological conditions involving tissue remodelling such as inflammation, tumorigenesis [364] and hyperproliferative conditions (e.g. psoriasis [365]).

1.6.2 TNC in wound healing

Tissue injury prompts a well-recognised series of processes: inflammation, tissue rebuilding, and tissue remodelling [366] (Figure 1-14).

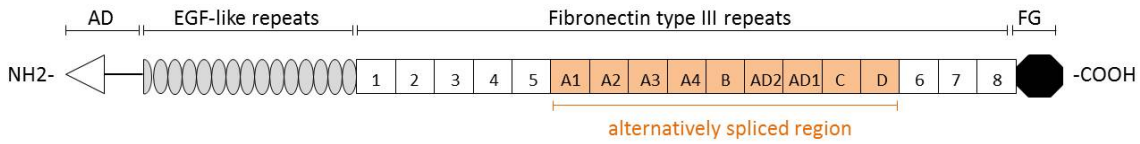

Figure 1-13 Structure of TNC

The assembly domain (AD) at the N-terminus mediates the oligomerisation of the protein, where 2 trimers form a hexamer. The fibronectin repeats are between the EGF-like repeats and the carboxy terminal fibrinogen globe. In humans, 9 of the 17 fibronectin repeats are alternatively spliced. Adapted from Lowy and Oskarsson [367].

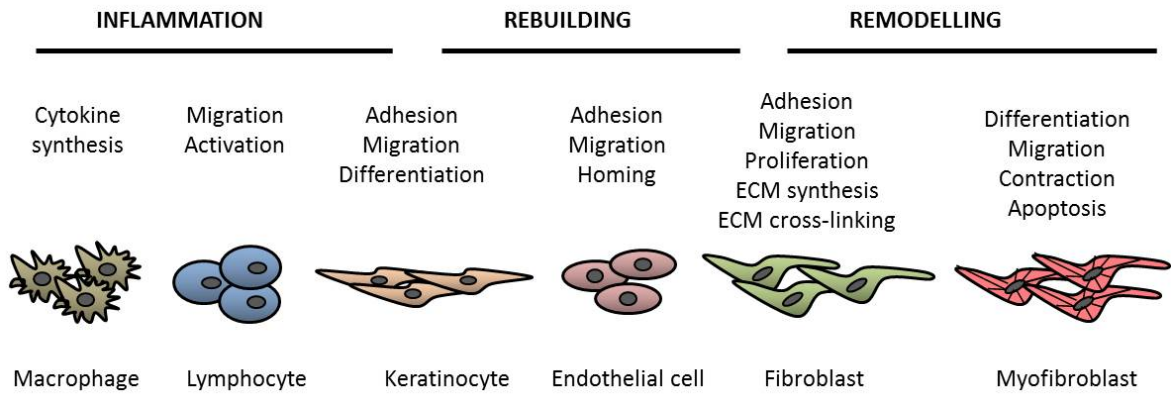

Figure 1-14 TNC in tissue repair

TNC interacts with disparate cell types during the different phases of wound healing. Adapted from Midwood and Orend [363].

1.6.2.1 Inflammation

Upon tissue injury, *TNC* expression is rapidly induced. It appears to modulate inflammatory responses by stimulating the production of pro-inflammatory cytokines including TNFα, IL-6 and IL-8 [368]. Furthermore, during the acute inflammatory phase, TNC co-localises with polymorphonuclear lymphocyte infiltration in the dermis [369]. TNC also appears to directly regulate T cell behaviour, with both anti-adhesive effects mediated by fibronectin binding [370] and pro-adhesive effects through support of lymphocyte rolling [371]. The differing roles are likely to be both context- and splice variant-dependent [372]. TNC expression is observed at sites of inflammation secondary to e.g. incisional wounding [373] but also in states of pathological inflammation such as pulmonary tuberculosis [374] and autoimmune myocarditis [375], suggesting that TNC upregulation is an aspect of a non-specific inflammatory response.

1.6.2.2 Tissue rebuilding

Re-epithelialisation

Early wound closure is achieved by the proliferation and migration of keratinocytes through the fibrin clot. Within 24 hours of wounding, TNC expression is detected at the dermal/epidermal junction beneath the proliferating and migrating keratinocytes [362,373]. Keratinocytes are the primary source of TNC in this context [376]. Pathological skin conditions in which hyper-proliferation of the epidermis is a feature, such as psoriasis [377] and bullous conditions [378] also display high levels of TNC expression under the epidermis.

There is evidence to suggest that TNC may promote differentiation of epithelial cells during wound healing: in one study, TNC was discovered to provide a signal that drives differentiation via androgen receptor upregulation in the developing prostate gland [379]. Furthermore, primary human epidermal keratinocytes display a rounded morphology when cultured on TNC substrates (containing TNC purified from the culture medium of glioblastoma cell lines), indicating that TNC may play a pro-adhesion, pro-migration role during re-epithelialisation[376].

Fibroblast proliferation and migration

Following wounding of the dermis fibroblasts infiltrate into the fibrin and fibronectin matrix-covered wound bed [380]. The presence of TNC within the fibrin-fibronectin scaffold enhances fibroblast migration [381]; one region of fibronectin type III-like repeats appears to be the critical domain of TNC in the promotion of migration. In contrast, another region of these repeats inhibits migration, indicating that differential proteolysis of TNC may dictate the termination of the wound healing process versus the prolonged, unwarranted fibroblast migration seen in pathological fibrosis.

The EGF-like domain of TNC also regulates fibroblast proliferation and migration; the EGF-like repeats phosphorylate EGFR, thus activating the MAP kinase pathway in the NR6 fibroblast cell line [359].

ECM synthesis

In order to restore normal tissue architecture, new ECM must be deposited on the wound bed [382]. TNC increases pro-collagen synthesis, promoting matrix deposition. It is difficult to determine if this is mediated via pro-inflammatory pathways leading to recruitment of collagen-synthesising cells or if TNC has direct effects on ECM deposition. In *Tnc*-null mice, collagen production was reduced in a model of immune-mediated hepatitis [383]; however, the model involved intravenous injections of a pro-inflammatory compound (concanavalin A). In this context, *Tnc*-null mice exhibit attenuated inflammatory responses, potentially leading to a failure to recruit myofibroblasts and collagen-producing cells.

Independent of its effects on inflammation, TNC does appear to impact growth factor production and myofibroblast activity. In a model of glomerulonephritis induced by snake venom [384], the inflammatory infiltrate seen in WT and *Tnc*-null mice was equivalent; however, the number of mesangial cells, which are responsible for tissue regeneration, was significantly lower in the *Tnc*-null mice, leading to irreversible, persistent kidney damage. In addition, platelet-derived growth factor (PDGF) expression was reduced, and TGFß1, collagen type VI, and fibronectin induction were delayed in *Tnc*-null mice, while mesangial cells

isolated from these mice did not proliferate when stimulated with PDGF or TGFß, indicating that the response to these growth factors is affected by the presence or absence of TNC.

The functional subunit of TNC in this context appears to be TNIIIA2, a fibronectin-like repeat peptide that induces ß1 integrin activation through syndecan-4 binding [357]. Fibroblasts induced by TNC and the active peptide TNIIIA2 display enhanced integrin αvß1 activation, resulting in hyper-stimulation of PDGF-dependent proliferation and attenuation of contact inhibition [385].

There is also evidence that the addition of TNC to culture medium enhances EGF-induced proliferation of murine 3T3 fibroblasts [386]. These data suggest that TNC regulates the synthesis of ECM components through regulation of cell migration and proliferation, and controlling the level of and cellular response to growth factors.

ECM assembly

TNC is known to directly interact with several ECM components: it is observed to co-localise with fibronectin fibrils and to areas of fibronectin accumulation [387]. The assembly of a TNC matrix appears to depend on the existence of a fibronectin template [388]. TNC can also bind to fibrillar collagen types I – VI and IX [389], to periostin, forming a bridge between TNC and the ECM [390] and to proteoglycans including versican, aggrecan and neurocan [391]. These data appear to support the theory that TNC can function as a matrix template, facilitating assembly of ECM components during the wound healing process.

Neo-angiogenesis

To enable new tissue to form and repair wounds, new blood vessel formation must take place. A strong association between TNC expression and sites of vascular remodelling during wound healing has been documented [362,373,392] . Endothelial cells are activated during the process of new blood vessel development, adopting a migratory phenotype [393]. TNC expression appears to be increased preferentially in active endothelial cells as opposed to non-migratory endothelial cells [394] . Furthermore, the addition of TNC promotes endothelial

cell migration and reduces endothelial cell focal adhesions [356]. These changes in the interface between endothelial cells and the ECM are accompanied by alterations in growth factors including vascular endothelial growth factor (VEGF) and basic fibroblast growth factor (bFGF) [395]. TNC has been observed to regulate the levels of and the manner in which cells respond to these growth factors; absence of TNC leads to suppression of VEGF expression and a resultant reduction in neovascularisation [396]. TNC also co-localises with endothelial progenitor cells at sites of angiogenic induction [397]. Dual stimulation with bFGF and TNC also enhances endothelial cell proliferation [356]. These data indicate that TNC plays a crucial role in vascular remodelling during tissue repair.

Tissue remodelling

In the final stages of wound healing, closure is facilitated by myofibroblast-mediated wound contraction [398]. Following contraction, myofibroblasts and vascular cells undergo apoptosis, reducing the cellularity of the region and permitting the transition from granulation tissue to scar [399]. Upon completion of normal wound repair, TNC is no longer expressed [362,373,400] .

Keloid scars are the consequence of excessive deposition of fibrotic tissue rich in fibrillar collagen [401]; they extend outwith the borders of the original wound and are persistent, recurring after re-excision [402]. TNC expression is elevated in keloid scars in vivo, and in fibroblasts isolated from keloid tissue, indicating that a failure to down regulate TNC expression at the end of the wound healing process may lead to inappropriate dermal fibrosis [403]. Tumours have been thought of as wounds that do not heal [404]; the clear role of TNC in the wound healing process has prompted further investigation into the part played by TNC in tumorigenesis and cancer progression.

1.6.3 TNC in cancer

The tumour stroma consists of immune cells, fibroblasts, blood vessels, and extracellular matrix components [405]; the interplay between the “reactive” stroma and the tumour cells is increasingly recognised as an integral aspect of tumorigenesis. TNC is highly expressed in the stroma of most types of solid tumour [406], and has been found to facilitate the acquisition of a pro-invasive

phenotype by cancer cells through a number of mechanisms (Figure 1-15). Its expression is positively correlated with a poor clinical outcome in a number of tumour types, including glioma, breast, colon and lung cancers.

The presence of several cytokines and growth factors in a tumour can induce TNC expression; these include TNFα, IFNɣ, interleukins 1, 4, 6, 8 and 13 [407], and EGF, TGFß [408], and CTGF. Within the stromal compartment, NFκB [409], ROS [410], hypoxia [411] and mechanical tension [302,412,413] are also capable of inducing TNC.

Matrix metalloproteinases (MMPs) secreted by tumour and stromal cells can cleave TNC from the ECM, thus freeing it to participate in pro-tumorigenic signalling pathways [414,415] . Cleavage by MMP2 causes the release of a peptide that contains FNIIIA, a pro-adhesive site that enhances PDGF-mediated proliferation and resistance to anoikis [385]. In the context of non-small cell lung cancer, TNC fragmentation is observed [416] and appears to be linked with poor clinical outcomes [417].

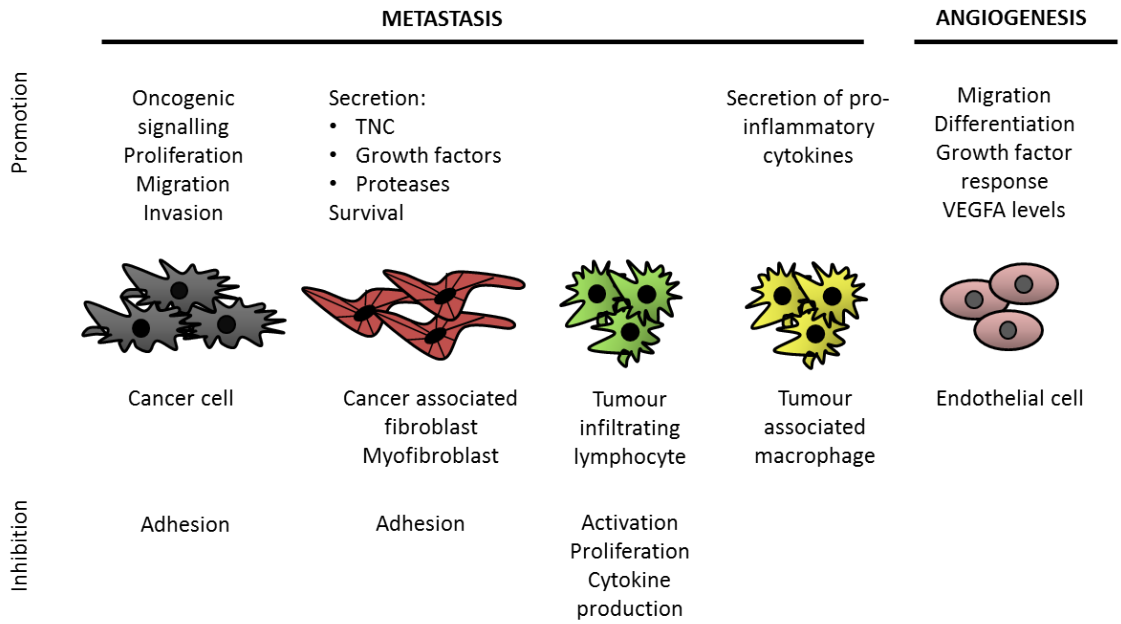

Figure 1-15 TNC in cancer

TNC impacts on several cell types within the tumour and the tumour microenvironment. TNC promotes cell proliferation, migration, invasion, angiogenesis and metastasis, and inhibits cell adhesion. Adapted from Midwood and Orend [363].

1.6.3.1 Cell proliferation

The addition of TNC to tumour cell culture has been found to enhance cell proliferation [406,418]. Furthermore, glioblastoma and breast carcinoma cells cultured on composite fibronectin/TNC substrates display a more proliferative phenotype and reduced adhesion [418]. Increased proliferation has also been observed in 3-dimensional reconstructions of mammary epithelial tissues *in vitro* [419]. In addition, proliferation of cells in 3-D melanoma spheres is significantly attenuated by loss of TNC [420]. An association has also been noted between the expression of TNC and the proliferation marker Ki67 in many solid tumours [421] .

TNC appears to function in the stem cell niche, supporting cell proliferation and differentiation [422]. This is the case with neural stem cells [423]; studies illustrating a link between increasing TNC expression and advancing grade of glioblastoma indicate that TNC may also facilitate cancer stem cell proliferation [424]. TNC is also detected in the haematopoietic stem cell niche [425], where it may facilitate stem cell recruitment, as evidenced by the attenuation in haematopoiesis seen in TNC null mice [426].

TNC has also been noted to increase the stability and nuclear accumulation of ß-catenin in glioblastoma cells, with consequent induction of Wnt signalling and enhanced proliferation [427]. Furthermore, the EGF-like repeats within TNC possess a significant, albeit low, affinity to EGFR, enabling them to bind the receptor and stimulate proliferation [359].

1.6.3.2 Metastasis

Cell adhesion

Cell adhesion to ECM components causes engagement of integrins and syndecan-4, in turn bringing about cell spreading. The initiation of integrin signalling leads to the formation of focal adhesions, facilitating cell-cell and cell-ECM interactions. The presence of TNC during cell adhesion impacts on how cells interact with the ECM; this relationship depends on the cell type, and whether entire TNC molecules or sub-fragments are available [428]. Syndecan-4 is a co-receptor that initiates integrin signalling when cells bind to fibronectin [429]; in fibroblasts [430] and several tumour cell lines [418], TNC binds competitively to a

fibronectin type III repeat and prevents syndecan-4 activation. This is one mechanism by which TNC inhibits cell adhesion to fibronectin substrates.

In addition, TNC appears to prevent the assembly of fibronectin matrices in cells cultured on mixed, fibrin-based fibronectin/TNC substrates [431]. The absence of a fibronectin matrix has been observed as a characteristic of some tumour types [432]. Fibronectin matrix construction requires integrin activation, and also relies on cells adhering to fibronectin, which is inhibited by the action of TNC on syndecan-4.

Epithelial-mesenchymal transition

Epithelial-mesenchymal transition (EMT) is a process in which cells display reduced adhesion, increased cell motility, and loss of E-cadherin expression. TNC may play a role in EMT, as breast cancer cells undergoing TGFß-mediated EMT produce TNC [433]. Studies in colon cancer found that TNC derived from cancer cells was associated with the expression of genes comprising the EMT signature [434]. Furthermore, adding TNC to the culture medium of breast cancer cells induced EMT-like change [435].

Cell migration

Cells adhere to a TNC matrix in a fashion labelled “intermediate”, i.e. the links between the cell and the ECM are not strong to the point of preventing detachment, but are sufficiently strong to permit the generation of contractile forces [436,437] . This facilitates cell motility and invasion in a number of malignant cell types, including colon cancer [338], ovarian cancer [438], laryngeal cancer [439] and glioma [440]. TNC expression tends to be highest at the invasive front of solid tumours [364]; an association between the presence of TNC at the invading front and poor clinical outcome is observed in a number of cancer types, including, prostate [441], mesothelioma [442], melanoma [443], and cholangiocarcinoma [444].

A significant increase in the capacity of breast cancer cells to migrate has been observed following the over-expression of TNC splice variants, through both MMP-dependent and MMP-independent means [445].

Dissemination

As cancer cells become non-adherent and develop migratory characteristics, they gain the ability to invade local structures and metastasise to distant locations. Cancer cells with the capacity to produce factors that support survival under stress have a distinct advantage over those cells that require factors produced by the metastatic "soil". Breast cancer cells that express TNC demonstrate increased survival during the initial phases of colonisation, prior to the activation of stromal fibroblasts [446]. As the micrometastatic deposit becomes established, the microenvironment becomes reactive, and subsequently produces TNC that contributes to maintaining the viability of the cancer cells [446,447]. Thereafter, upon settling within the metastatic niche, TNC engages the Wnt and Notch pathways [448], with a consequent impact on stem/progenitor cell signalling.

TNC is consistently present in gene expression profiles predictive of metastatic disease in breast cancer [449,450]; in addition, TNC expression levels are higher in cases of recurrent non-small cell lung cancer compared with the primary tumour [451], and high expression is linked to the development of early metastatic disease in laryngeal and hypopharyngeal cancers [452].

1.6.3.3 Promotion of angiogenesis

In physiological conditions in adult vasculature, TNC expression is minimal; however, it is induced when blood vessels sustain damage, and is also evident during pathological angiogenesis in a number of conditions, including diabetes, inflammatory bowel disease and cancer [453]. In a *Tnc* knock-out mouse model, tumours formed following the injection of melanoma cells displayed a significant decrease in angiogenesis, indicating that TNC is necessary for the development of new vasculature [454]. It has been proposed that TNC may encourage a sprouting phenotype in endothelial cells in culture [394]; furthermore, TNC reduces focal adhesions and thus promotes endothelial cell migration [356]. VEGF levels, among other factors known to drive angiogenesis, are noted to be secreted at lower levels when stromal-derived TNC is absent [454], but the mechanism behind this remains unclear.

1.6.4 Impact of tissue mechanics on TNC

A role for mechanical stress in the regulation of TNC is suggested by tissues subject to high mechanical loads (e.g. tendons) displaying high levels of TNC [387,455] . Furthermore, upregulation of TNC expression is induced by tensile strain [410,456-458]. These findings are particularly of interest in the context of cancer, as an association has been noted between the rigidity of the tumour microenvironment and tumour progression [332,333]. This raises the possibility that increased mechanical tension in the tumour stroma may prompt the production of TNC, both within the ECM and in cancer cells, thus driving cancer progression through the mechanisms previously outlined.

1.6.5 Megakaryoblastic leukaemia 1

Mechanical strain has been shown to induce TNC expression[458]; this appears to occur in an MKL1-dependent manner. MKL1 (megakaryoblastic leukaemia 1) belongs to the myocardin-related transcription factor (MRTF) family, a group of transcription factors that function as co-activators of serum response factor (SRF). MKL1 (also known as MRTFA) is one of the most potent SRF inducers [459]. SRF relays cytoskeletal signals to the nucleus and is in turn influenced by alterations in actin dynamics [460]. However, it has been shown that MKL1 can mediate TNC transcription secondary to increased mechanical stress in an SRF-independent manner [461]. Furthermore, there is evidence that MKL1 switches between SRF-dependent and SRF-independent gene regulation, with those genes being induced in a non-SRF manner showing correlation with more aggressive breast cancer subtypes [450]. The implication is thus that mechanical strain, MKL1, TNC and aggressive malignant phenotypes are inter-linked.

1.7 Project aims

Colorectal cancer is a complex, multi-stage process with, in the majority of cases, a gradual transition from benign adenoma to malignant tumour. Determining that loss of LIMK2 occurs as tumours become more invasive was an important first step in assessing the potential role of *LIMK2* as a tumour suppressor gene. This led to the first aim of my project:

1. To characterise the mechanism by which LIMK2 expression is reduced in colorectal cancer.

   Hypothesis: LIMK2 downregulation occurs via epigenetic silencing and is associated with worse clinical outcomes.

Subsequently, I wished to investigate the impact of altering the mechanical tension of the microenvironment through modulation of the actin cytoskeleton. This generated the second aim:

2. To determine the consequence of ROCK activation on the composition of the extracellular matrix of the epidermis and to investigate if similar effects could be recapitulated through altering the cellular environment.

   Hypothesis: ROCK activation leads to deposition of ECM components in addition to collagen, and that increased tension within the cellular environment would replicate/enhance the effects seen following ROCK activation.

2 Materials and methods

2.1 Materials

2.1.1 Reagents and chemicals

Reagent/Chemical	Supplier
4-Hydroxytamoxifen	Sigma
5-Azacytidine	Sigma
Ampicillin sodium salt	Sigma
Agarose	Melford
ß-mercaptoethanol	Invitrogen
Bicinchoninic acid solution	Sigma
Bovine pituitary extract	Lonza
Bovine serum albumin	Sigma
Calcium chloride	Lonza
Copper (II) sulphate solution	Sigma
Dimethylformamide	Sigma
Dispase II	Roche
DMEM (Dulbecco's Modified Eagle Medium)	Gibco
DMSO (dimethyl sulfoxide)	Sigma
dNTPs	Zymo Research
Donor calf serum	Gibco
E.coli DH5α cells	Invitrogen
Eco R1	Invitrogen
Epidermal growth factor	Lonza
Epinephrine	Lonza
Ethidium bromide	Sigma
Fetal bovine serum	Gibco
Fibronectin from bovine plasma	Sigma
G1000A	Lonza
G418	Formedium
Ham's F12 nutrient mixture	Gibco
Hepes Free Acid	Sigma
Hydrochloric acid	Fisher Scientific
Hydrocortisone	Lonza

Hyperladder I	Bioline
Hyperladder IV	Bioline
Insulin	Lonza
Kanamycin sulphate	Sigma
Keratinocyte Growth Medium 2	Lonza
L-glutamine (200mM)	Gibco
NuPAGE 4-12% Bis-Tris gels	Invitrogen
NuPAGE MES SDS running buffer	Invitrogen
NuPAGE MOPS SDS running buffer	Invitrogen
NuPAGE Transfer buffer	Invitrogen
Page ruler Pre-stained Protein Ladder	Thermoscientific
Paraformaldehyde 16% aqueous solution	Electron Microscopy Sciences
Penicillin/Streptomycin	Life Technologies
Precision Plus Protein™ all blue standards	Bio-Rad
PureCol	Advanced BioMatrix
React 3	Invitrogen
RG108	Tocris
RNase A	Qiagen
RNase free DNase set	Qiagen
S.O.C. medium (Super Optimal broth with Catabolite repression)	Invitrogen
Sodium hydroxide	Fisher Scientific
Transferrin	Lonza
Transforming growth factor ß (recombinant)	Peprotech
Trypsin EDTA (0.05%)	Gibco
Trypsin EDTA (2.5%)	Gibco
Vectashield mounting medium with DAPI	Vector Laboratories
ZymoTaq polymerase	Zymo Research

Table 2-1 List of reagents and chemicals

2.1.2 Kits

Kit	Supplier
DyNamo Hot Start SYBR Green q PCR kit	Thermoscientific
EZ DNA Methylation Gold Kit	Zymo Research
Luciferase Assay System with Reporter Lysis Buffer	Promega
QiaQuick Gel Extraction Kit	Qiagen
QiaQuick PCR Purification Kit	Qiagen
QiAmp Mini Kit	Qiagen
Quantitect Reverse Transcription Kit	Qiagen
RNeasy Mini Kit	Qiagen
TOPO TA Cloning Kit (pCR 2.1 TOPO vector with one shot top 10 chemically competent *e.coli*)	Invitrogen
Quantikine ELISA TGFβ1	R&D Systems
SEAP Reporter Gene Assay, Chemiluminescent	Roche
pMet Luc Ready to Glow Luciferase Reporter Assay	Clontech
NE-PER Nuclear and Cytoplasmic Extraction Reagents	Thermoscientific

Table 2-2 List of kits

2.1.3 Solutions

Solution	Recipe
Agar plates	85 mM NaCl, 1% (w/v) bacto trypton, 0.5% (w/v) yeast extract, 1.5% (w/v) agarose, antibiotic (100µg/ml ampicillin or 50µg/ml kanamycin)
DNA loading buffer	20 mM EDTA, 0.05% (w/v) bromophenol blue, 50% (v/v) glycerol
L-broth	85 mM NaCl, 1% (w/v) bacto trypton, 0.5% (w/v) yeast extract
PBS	170 mM NaCl, 3.3mM KCl, 1.8mM Na_2HPO_4, 10.6mM H_2PO_4
SDS sample buffer	125 mM Tris-HCl pH 6.8, 6% (w/v) SDS, 30% glycerol,
TBS	20 mM Tris-HCl pH 7.5, 136 mM NaCl
TBST	21 mM Tris-HCl pH 7.5, 136 mM NaCl, 0.1% Tween 20

Table 2-3 List of solutions

2.1.4 Antibodies

Antigen	Species	Supplier	Catalogue no.
Alpha smooth muscle actin	Mouse	Abcam	AB7817
Alpha-tubulin	Mouse	Santa Cruz	SC5286
ER alpha	Rabbit	Santa Cruz	SC543
ERK2	Rabbit	Cell signalling	9108S
GAPDH	Mouse	Sigma	G9295
Lamin A/C	Goat	Santa Cruz	SC6215
Lamin B	Goat	Santa Cruz	SC6217
LIMK2	Rabbit	Santa Cruz	SC5577
MKL1 (MRTF-A)	Mouse	Santa Cruz	SC39867S
Myosin light chain 2	Rabbit	Cell signalling	3672
Phospho myosin light chain (Thr 18/Ser 19)	Rabbit	Cell signalling	3674S
ROCK I/2	Rabbit	Millipore	07-1458
Tenascin C	Mouse	Sigma	T3413

Table 2-4 List of primary antibodies

Antibody	Supplier	Catalogue number
Alexa Fluor 680 goat anti-rabbit IgG	Invitrogen	A21076
Alexa Fluor 680 goat anti-mouse IgG	Invitrogen	A21057
DyLight 800 goat anti-rabbit IgG	Thermo Scientific	35571
DyLight 800 goat anti-mouse IgG	Thermo Scientific	35521
Donkey 800 anti-goat IgG	Rockland	605-732-125

Table 2-5 List of secondary antibodies

All secondary antibodies were used at a concentration of 1:10000.

2.2 Cell culture techniques

2.2.1 Origin, maintenance and storage of cell lines

HCT116 and SW48 are adherent epithelial cell lines originally isolated from human colon adenocarcinomas. Both were grown in DMEM medium supplemented with 10% fetal bovine serum (FBS) and 2 mM L-glutamine. Cells were maintained at 37 °C, 5% CO_2 in a humidified incubator and passaged every 3-4 days as follows: culture medium was removed; cells were washed once with PBS, and incubated in 0.05% trypsin for approximately 5 minutes. Cells were resuspended in culture medium, counted using a Casy® Innovatis cell counter, and an appropriate number of cells transferred to a new tissue culture dish with fresh medium.

Human cell lines were authenticated by the Beatson Institute Molecular Technology Service using the Promega GenePrint 10 system.

NIH 3T3 is an adherent mouse embryo fibroblast cell line. Cells were grown in DMEM medium supplemented with 10% donor calf serum. Cells were maintained and passaged as above, with the substitution of 0.25% trypsin. In addition to the parental cell line, NIH 3T3 cells stably expressing a conditionally active form of ROCK II (ROCK:ER, under the control of 4-hydroxytamoxifen), and a kinase dead (KD:ER) variant were also utilised. These had previously been generated in the laboratory, and were maintained in identical conditions to the parental cells.

For long-term storage, all cell lines were frozen in liquid nitrogen vapour phase tanks. To prepare cells for freezing, healthy cells were harvested by trypsinisation as described above. They were then centrifuged at 1,200 rpm in an Eppendorf 5804R centrifuge for 5 minutes, and the cell pellet resuspended in DMEM medium supplemented with 10% FBS and 10% DMSO. 1 ml aliquots were transferred to cryogenic vials, and these were stored at -80 °C for 24 hours prior to placement in the liquid nitrogen tank.
To thaw cells, cryogenic vials were transferred from the liquid nitrogen tank to a 37 °C water bath; the contents were transferred to a new culture dish with fresh medium.

2.2.2 Treatment of cell lines with DNMT inhibitors

5-Azacytidine (5-AZA) was prepared by dissolving 1.2 mg in 10 ml of DMEM to create a 500 μM stock solution. RG108 was prepared by dissolving 10 mg in 2990 ml of DMSO to give a 1 mM stock solution. 24 hours after plating, culture medium was aspirated from HCT116 and SW48 cells and replaced with medium containing 5-AZA (final concentration 10 μM), RG108 (final concentration 100 μM) or DMSO control (1%). Cells were cultured in treated medium for 48 hours before proceeding with RNA or protein lysate preparation.

2.2.3 Culture of cell lines on differing substrates

ExCellness® biomimetic culture surfaces were utilised to determine the impact of differing culture substrate stiffness on cells. Prior to use, the surface was washed with isopropanol, and subsequently coated with fibronectin (1 mg/ml) diluted in serum-free medium to a stock concentration of 2 μg of protein in 200 μl of medium. The coated plate was incubated at 37 °C for 16 hours, after which time the coating was aspirated from the plate prior to seeding cells.

2.2.4 Plasmid preparation

SRE-SEAP and pMET LUC DNA constructs were a gift of Professor Chiquet-Ehrismann (Friedrich Miescher Institute for Biomedical Research, Basel). 30 ng of DNA was added to a 50 μl aliquot of *E.coli* DH5α competent cells, and incubated on ice for 30 minutes. Following a 45 second heat-shock in a 42 °C water bath, the sample was incubated on ice for 2 minutes. 150 μl of SOC medium was added, and the sample was incubated in a polypropylene round-bottomed snap-cap tube in a 37 °C shaking incubator for 1 hour.

The transformation mixture was subsequently spread on an agar plate containing the appropriate antibiotic for selection, and incubated for 16 hours at 37 °C. Subsequently, 250 ml cultures of bacteria transformed with plasmid were grown at 37 °C in a shaking incubator for at least 16 hours. The culture was transferred to a 250 ml centrifuge tube, and centrifuged at 4000 rpm for 20 minutes at 4 °C in a Beckman-Coulter J6-M1 centrifuge. After removal of supernatant, DNA was isolated from the resulting pellet using the Invitrogen Purelink HiPure Plasmid

Filter Purification Kit following the manufacturer's instructions. DNA isolation was performed by the Beatson Molecular Technology Services.

2.2.5 Transfection of plasmid DNA

For promoter-reporter studies, NIH 3T3 ROCK:ER and KD:ER cells were transiently transfected with SRE-SEAP and pMET LUC plasmids as follows. Cells were seeded 24 hours prior to transfection at 4 x 10^4 cells per well in 24-well plates with complete DMEM. Lipofectamine 2000 transfection reagent, plasmid DNA and Optimem I Reduced Serum Medium (Optimem) were equilibrated to room temperature before commencing. SRE-SEAP plasmid DNA (5 µg) and pMET LUC plasmid DNA were diluted in 250 µl of Optimem, and 3 µl of Lipofectamine 2000 was diluted in 50 µl of Optimem. 50 µl of diluted DNA was added to the diluted Lipofectamine 2000 and the mixture was incubated for 5 minutes at room temperature to permit transfection reagent/DNA complexes to form. 50 µl of the resulting mixture was added to the 500 µl of complete DMEM in each well, and the plate was incubated at 37 °C for 3-4 hours. Following this, the medium containing transfection complexes was removed and the cells were washed twice with complete DMEM, before fresh medium was added.

2.2.6 Secreted alkaline phosphatase assay

To detect secreted alkaline phosphatase (SEAP), the Roche chemiluminescent SEAP reporter assay was used. The plate of transfected cells was allowed to equilibrate to room temperature, and medium was transferred to 1.5 ml Eppendorf tubes. The medium was centrifuged at 13,200 rpm for 10 minutes; 50 µl of medium was then added to 150 µl of dilution buffer in a clean tube, and incubated in a 65 °C water bath for 30 minutes to heat inactivate contaminating alkaline phosphatase activity. The samples were centrifuged at 13,200 rpm for 30 seconds at room temperature, and transferred to ice. 50 µl of each sample was transferred to 1 well of a white 96 well plate, and 50 µl of inactivation buffer was added to each well and incubated for 5 minutes at room temperature. Substrate reagent was formed by adding 50 µl of alkaline phosphatase substrate to 950 µl of substrate buffer; 50 µl of the resulting mixture was added to each well of the plate, and the plate was gently rocked at

room temperature for 10 minutes. The plate was subsequently read on a Turner BioSystems Veritas ™ Microplate Luminometer.

2.2.7 Secreted luciferase assay

To determine transfection efficiency, cells were transfected with pMET LUC plasmid. In order to detect secreted *Metridia* luciferase, the Clontech Ready-to-Glow™ secreted reporter system was used. Following appropriate treatment of NIH 3T3 ROCK:ER and KD:ER cells, the culture plate was brought to room temperature, and 50 µl of medium was transferred to a white 96 well plate. Substrate/reaction buffer was formed by diluting lypophilized secreted luciferase substrate in substrate buffer and incubating at room temperature for 15 minutes. This was further diluted 1:10 in reaction buffer, and 5 µl of substrate/reaction buffer was added to each sample. The plate was then read on a luminometer.

2.3 Animal studies

2.3.1 Home office project and personal licensing

All animal work undertaken was reviewed and approved of in project and personal licenses issued by the UK Home Office.

2.3.2 Animal genotyping

For routine genotyping, animals were ear-clipped at weaning and samples dispatched to Transnetyx molecular diagnostics for automated genotyping.

2.3.3 Lifeact GFP mice

The Lifeact GFP mouse was developed within the group by Dr Nicola Rath; GFP Lifeact was cloned into the pBigT plasmid and the animals were subsequently created by the Beatson transgenic facility. In order to achieve ubiquitous expression of Lifeact GFP, the mouse was crossed with a Deleter Cre mouse. GFP expression was verified by imaging the mouse using the IVIS® Spectrum *in vivo* imaging system. Thereafter, the mice were crossed with K14 KD:ER and K14 ROCK:ER mice, and the offspring phenotyped using GFP goggles. GFP positive

mice were crossed to achieve homozygous KD or ROCK expression (confirmed by western blot following treatment of primary keratinocytes with 4-hydroxytamoxifen).

2.3.4 Isolation of primary murine keratinocytes

Mice were euthanized either by cervical dislocation or by rising concentration of CO_2, and the tail was subsequently removed near the base. The tail was washed with Povidone-Iodine solution, PBS-AF (PBS with fluconazole and streptomycin), and 70% ethanol, and the skin was peeled off and placed in a 10% Dispase II solution. Following 90 minutes incubation at 37 °C, the epidermis was separated from the dermis, washed in PBS and minced with a scalpel. The minced epidermis was transferred to a 50 ml Falcon tube containing 10 ml of 0.25% trypsin and incubated for 10 minutes at 37 °C, then agitated by pipetting up and down. Filtered FBS was added and the mixture was passed through a 70 µm then a 40 µm cell strainer. The resulting solution was centrifuged in an Eppendorf 5804R centrifuge at 2,000 rpm for 5 minutes and the cell pellet was resuspended in PBS. Following further centrifugation, the cells were resuspended in Keratinocyte Growth Medium (KGM-2; 500 ml supplemented as below) and plated on PureCol-coated tissue culture dishes. The cells were maintained at 37 °C in a low (3%) O_2 incubator.

KGM-2 Supplement	Volume
Bovine pituitary extract	2 ml
Human epidermal growth factor	500 µl
Insulin	500 µl
Hydrocortisone	500 µl
Transferrin	500 µl
Epinephrine	500 µl
Gentamicin (GA-1000)	500 µl
Calcium chloride	83 µl

2.3.5 Treatment of primary murine keratinocytes

Following 24 – 48 hours in fully supplemented KGM-2 medium, keratinocytes were washed twice with PBS then cultured in keratinocyte basal medium (KBM) with no growth factors or antibiotics. 4-hydroxytamoxifen (1 μM) or ethanol vehicle was added to medium, and cells were cultured at 37 °C for 16 hours before imaging, or preparation of RNA and protein lysates.

2.3.6 Culturing cells in hanging drops

In order to co-culture keratinocytes and fibroblasts, a technique of culturing both cell types in a suspended drop of medium was used. To do this, primary keratinocytes were isolated from K14 KD:ER and ROCK:ER animals as previously described, and grown in 6-well plates. On the 3rd day of culture, the cells were trypsinised with 500 μl of 0.25% trypsin, and transferred to a 14 ml Falcon tube with 3.5 ml of complete medium. Simultaneously, NIH3T3 fibroblasts stably expressing a TGFβ reporter were trypsinised in the same manner. The Falcons were centrifuged (at 2000 rpm for keratinocytes, 1200 rpm for fibroblasts) for 5 minutes. The supernatant was removed, and the cells were resuspended in 8 ml of serum-free medium. After establishing the cell number with the Casy® Innovatis cell counter, both types of cell were centrifuged at 400 g for 5 minutes. The supernatant was removed, and thereafter the cells were dyed using red (keratinocytes) and green (fibroblasts) fluorescent cell linker kits for general cell membrane labelling (Sigma). In summary, this was achieved by adding 500 μl of diluent C from the kit to the cell pellet and pipetting to mix gently. Dye solution was prepared by adding 2 μl of dye to 500 μl of diluent C; this was added to the cell suspension and mixed. The resulting suspension was incubated at room temperature for 3 minutes, then 1 ml of serum was added, followed by a further incubation at room temperature for 1 minute. Subsequently, the cells were centrifuged at 400 g for 10 minutes, and then centrifuged at 400 g for 5 minutes 6 times, with the supernatant being aspirated and the cells resuspended in complete medium at each step to ensure complete removal of the dye solution. After the final centrifuge, the cells were resuspended to a concentration of 6 x 10^5 cells/ml.

Meanwhile, a 10 cm tissue culture dish was filled with 20 ml of sterile water, and the lid was wiped with damp tissue to eliminate static. The lid of the plate was inverted and 10 µl drops of cell suspension (consisting of 5 µl of keratinocytes and 5 µl of fibroblasts) were placed on the lid. The lid was flipped over and placed on the plate over the sterile water with the drops hanging down from the lid. Thereafter, images of the drops were taken using the Olympus FV1000 confocal microscope.

2.3.7 In vivo treatments

2.3.7.1 Topical tamoxifen

K14 ROCK:ER and K14 KD:ER mice had topical 4-hydroxytamoxifen (4-HT) applied to both ears once daily for 21 days at a dose of 500 µg/ear. 4-HT was prepared by dissolving 50 mg in 2 ml of 100% ethanol. Animals were euthanized following the final application of 4-HT and ears were collected for histology.

2.3.7.2 Tamoxifen diet

Baseline weight was recorded for K14 ROCK:ER and K14 KD:ER mice, and normal diet was replaced with tamoxifen diet. The weight of the animals was rechecked 3 times per week to ensure <10% weight loss and the animals were euthanized on day 36. Dorsal skin was shaved, dissected, placed in formalin and submitted to histology.

2.4 Epigenetics studies

2.4.1 Preparation of genomic DNA from tissue and cell lines

2.4.1.1 Preparation of genomic DNA from cell lines

Cells were trypsinised, centrifuged, and the supernatant removed to yield a cell pellet. The pellet was resuspended in 200 µl of PBS, and proteinase K (20 µl) and buffer AL (200 µl) added. The mixture was incubated at 56 °C for 10 minutes, followed by the addition of 200 µl of 100% ethanol.

2.4.1.2 Preparation of genomic DNA from tissue

Genomic DNA (gDNA) was prepared from paired frozen samples of colon tumour and normal colonic tissue. A 25 mg sample was minced and placed in a 1.5 ml microfuge tube. Subsequently, the QiaAMP Mini Kit was used to prepare gDNA following the manufacturer's instructions. Briefly, 180 µl of lysis buffer (ATL) and 20 µl of proteinase K were added, and the sample was placed in an Eppendorf Comfort Thermomixer and agitated at 56 °C for a minimum of 2 hours. 4 µl of RNAse A was added to the resulting mix to obtain RNA-free gDNA. 200 µl of binding buffer (AL) was added to the sample and incubated at 70 °C for 10 minutes, followed by brief centrifugation in an Eppendorf 5417R microfuge and the addition of 200 µl of 100% ethanol.

Subsequent steps of the protocol were essentially the same for both cells and tissue:

The mix was applied to a QiaAMP spin column and centrifuged at 8000 rpm for 1 minute. The filtrate was discarded, and the column was transferred to a clean collection tube. Following two wash steps with 500 µL of buffers AW1 and AW2 respectively, the column was incubated with elution buffer (AE) for 5 minutes at room temperature. The column was subsequently centrifuged at 8000 rpm for 1 minute to elute gDNA.

The concentration of the gDNA was determined using an Eppendorf BioSpectrometer; the sample was diluted in nuclease-free water and the absorbance at 260 nm was measured.

2.4.2 Bisulphite conversion of genomic DNA

Bisulphite conversion of gDNA was achieved using the EZ DNA Methylation Gold Kit (Zymo Research). In summary, the gDNA sample was made up to a volume of 20 µl with nucleotide-free water. 130 µl of CT conversion reagent was added to the gDNA sample and mixed, and the mixture was run in an MJ Research PTL-200 Peltier thermal cycler using the following programme:

Temperature	Time
98 °C	10 minutes
64 °C	2.5 hours
4 °C	Up to 20 hours

The sample was subsequently loaded into a Zymo spin column with 600 µl of M-binding buffer, mixed and centrifuged at 13,000 rpm for 30 seconds. After discarding the flow-through, 100 µl of M-wash buffer was applied to the column, followed by a further centrifuge and 20 minute incubation with 200 µl of M-desulphonation buffer. Following two additional wash steps with 200 µl of M-wash buffer, 10 µl of M-elution buffer was applied to the column, which was centrifuged at 13,000 rpm for 30 seconds in a fresh collection tube to elute the converted gDNA.

2.4.3 PCR (for bisulphite sequencing)

Oligonucleotides were designed using the Zymo Research primer design tool. The primer sequences are detailed below:

Promoter	Primer name	Sequence
Promoter A	LIMK2 Forward A	tttaaatatttggatttttggtatgttttgaaaggttg
Promoter A	LIMK2 Reverse A	aaaaatattacaataaaaaaaccaaatctatcccac
Promoter B	LIMK2 Forward B	tttagaggggtygtttgagtttttgagaattagggag
Promoter B	LIMK2 Reverse B	ataaaataaaccraaactaacaaataactccccatc

A 50µl PCR mix was set up in a 200µl PCR tube as follows:

Reagent	Volume (µl)
2x Reaction buffer Nuclease-free water Forward primer (10µM) Reverse primer (10µM) Template DNA (100ng) dNTPs Zymo Taq	25 18.1 2 2 2 0.5 0.4
Total	50

The mix was run on a PCR thermal cycler using the following programme:

Temperature	Time
94 °C	3 minutes
40 cycles of: 94 °C 46 °C or 49 °C (depending on promoter) 72 °C	 1 minute 1 minute 30 seconds
72 °C	10 minutes
4 °C	∞

Agarose gel electrophoresis was then utilised to confirm amplification of appropriately-sized PCR products.

2.4.4 Agarose gel electrophoresis

In order to make a 1% agarose gel, 1 g of agarose was added to 100 ml of 1xTBE in a 250 ml conical flask. The mix was microwaved at medium power for 3 minutes, and then swirled to ensure the agarose was fully dissolved. 1 µl of 2 µg/ml ethidium bromide was added and the mix was allowed to cool slightly. It was then poured into a gel tray with caster and comb, and left to set at room

temperature for 45-60 minutes. The gel was subsequently transferred to a Bio Rad gel tank, and 1xTBE was added, covering the gel by 1-2 mm. DNA samples were prepared with DNA loading buffer and added to the gel, with Hyperladders I and IV loaded simultaneously as markers. Gels were run at 100-120 V for 45-60 minutes. Bands were subsequently imaged on a Syngene Genius Bio Imaging Transilluminator with the GeneSnap programme.

2.4.5 PCR Product Purification

PCR products were purified using the Qiagen Qiaquick PCR purification kit, following the manufacturer's instructions. In summary, buffer PB was added to the PCR product (5 parts to 1 part), mixed, and applied to a Qiaquick Spin Column in a collection tube. The sample was centrifuged in an Eppendorf 5417R centrifuge at 13,200 rpm for 1 minute at room temperature. The flow-through was discarded and 750 µl of buffer PE was added to the Qiaquick column before centrifuging a further two times under the same conditions, with removal of flow-through between spins. The Qiaquick column was subsequently transferred to a clean collection tube, and 30 µl of Buffer EB was applied to the Qiaquick column membrane. Following 1 minute incubation at room temperature, the Qiaquick column was centrifuged for 1 minute at 13,200 rpm at room temperature. The resulting eluted DNA was run on an agarose gel to confirm purification of PCR product.

In the event of multiple products being visible on agarose gel electrophoresis, the Qiagen Gel Extraction Kit was utilised as follows: the appropriately sized band was excised from the gel with a scalpel and placed in a 1.5 ml Eppendorf tube. Three volumes of Buffer QG were then added to the gel band and the sample was incubated in a heat block at 50 °C for 10 minutes, with vortexing every 2-3 minutes. Following this, 1 volume of isopropanol was added to the sample and the mix was transferred to a Qiaquick Spin Column. This was centrifuged for 1 minute at 13,200 rpm, and the flow-through was discarded. 500 µl of Buffer QG was added to the Qiaquick column, which was centrifuged for 1 minute at 13,200 rpm, followed by the addition of 750 µl of Buffer PE and a further 1 minute centrifuge. The flow-through was discarded, and the Qiaquick column was centrifuged for 1 minute before being transferred to a clean

collection tube. The subsequent elution steps using Buffer EB were as per the PCR purification protocol.

2.4.6 Cloning, transforming and sequencing bisulphite-converted PCR products

The TOPO® TA cloning® kit was used to clone PCR products. Cloning reactions were set up in a PCR tube as follows:

Reagent	Volume
Fresh PCR product	4 µl
Salt solution	1 µl
TOPO vector	1 µl

The reagents were gently mixed, and incubated in a PCR thermal cycler for 30 minutes at 23 °C. The reaction was then placed on ice. 2 µl of the TOPO® cloning reaction was added to one vial of One Shot® chemically competent *E.coli* on ice and mixed gently. The mixture was incubated on ice for 30 minutes. Subsequently, the bacteria were heat-shocked by placing the vial in a 42 °C water bath for 30 seconds, then immediately placed on ice. 250 µl of room temperature SOC medium was added, and the mixture was transferred to a 15 ml polypropylene round-bottomed snap-cap tube. The tube was placed in a 37 °C shaking incubator for 1 hour.

Meanwhile, X-GAL (40 mg/ml in dimethylformamide) was spread over the surface of an ampicillin-containing agar plate and incubated at 37 °C until required. Following the 1 hour incubation, the transformation mixture was spread over the plate, which was then inverted and placed in a 37 °C incubator for a minimum of 16 hours.

Following incubation, blue-white selection was used to pick 10 white colonies per plate with an inoculation loop. Each colony was placed in a snap-cap tube with L-broth (5 ml) and ampicillin (5 µl) and incubated at 37 °C in a shaking incubator for at least 16 hours. The samples were then centrifuged in a Beckman Coulter J6-M1 centrifuge at 2000 rpm for 15 minutes at 4 °C; the supernatant was discarded and DNA was isolated from the resulting pellets using a Qiagen

8000 robot. DNA was sequenced on an Applied Biosystems sequencer. DNA sequencing reactions were set up, and the samples loaded and precipitated following the Applied Biosystems DNA sequencing protocol. DNA sequencing was performed by the Beatson Molecular Technology Services.

2.4.7 Restriction enzyme digestion

Digestion of DNA with restriction endonucleases was performed in REact 3 buffer 2 µl of 10 x) at 37 °C for 2 hours. 10 units of restriction enzyme (*EcoR I*) was added per 1 µg of DNA, and nuclease-free water was added to a total volume of 20 µl. The reaction was stopped by adding 5 µl of 10 x DNA loading buffer. Digestion of DNA was confirmed by agarose gel electrophoresis as previously described.

2.4.8 Analysis of sequencing results

DNA sequences were analysed on the CLC Genomics Workbench version 5.5.1.

2.4.9 Methylation specific PCR

Methylation-specific primers were designed for individual CpG islands within the promoter sequence using the Urogene Methprimer tool (Department of Urology, UCSF). One primer pair was specific to unmethylated and one to methylated DNA. The primer sequences are detailed below:

Primer name	Sequence
Unmethylated forward	tttgtattaaaaatataaaaattagtcga
Unmethylated reverse	gtactaaccaccatacccaacgta
Methylated forward	ttgtattaaaaatataaaaattagttga
Methylated reverse	catactaaccaccatacccaacata

Following bisulphite conversion of gDNA, a PCR reaction was set up in a 200 µl PCR tube, and run on a thermal cycler. Agarose gel electrophoresis was subsequently used to differentiate unmethylated and methylated bands.

2.5 Cellular protein extraction and analysis

2.5.1 Total cell lysate preparation

Cells are lysed to obtain soluble proteins. After placing the culture dish on ice, the cell culture medium was aspirated and the cells washed twice with ice-cold PBS. An appropriate volume of SDS lysis buffer was added to the culture dish (e.g. 30 µl per well of a 6-well plate), and a cell lifter used to scrape the cells from the surface of the dish. The resulting lysate was applied to a Qiagen Qiashredder column and centrifuged at 13,200 rpm for 1 minute. The homogenized lysate was transferred to a 1.5 ml Eppendorf microfuge tube and placed on dry ice for 1 minute. After thawing, the sample was centrifuged at 13,200 rpm for 15 minutes at 4 °C. The supernatant was transferred to a fresh tube and the protein concentration was determined.

2.5.2 Measurement of protein concentration

The Bicinchoninic acid (BCA) assay was used to determine the protein concentration of cell lysates. Protein standards were prepared using bovine serum albumin (stock concentration 2 mg/ml) in SDS lysis buffer at the following concentrations: 0.08, 0.1, 0.2, 0.4, 1 and 2 mg/ml. Samples were added to a Greiner Bio One 96 well plate: 10 µl of blank (SDS buffer alone) in triplicate, and 10 µl of standards and samples. 200 µl of developing solution (bicinchoninic acid and copper sulphate; 50:1) was added to each well, and the plate was incubated at 37 °C for 45-60 minutes. After equilibrating to room temperature, absorbance was measured on a Molecular Devices Microplate reader. A standard curve was plotted, and sample concentrations thus determined.

2.5.3 SDS-Polyacrylamide gel electrophoresis

Separation of protein samples by molecular weight was achieved by SDS-polyacrylamide gel electrophoresis. 8% Tris-glycine gels (recipe below) and NuPAGE Bis-Tris 4-12% gradient gels were used. Protein samples were prepared in SDS sample buffer and heated at 95 °C for 4 minutes. Samples were centrifuged briefly after heating, and loaded onto the gel alongside Precision Plus Protein™ All Blue molecular weight marker or Thermo Scientific PageRuler™ Prestained protein ladder. 8% gels were run in tanks containing 1 x

SDS running buffer at 90 V for 2 hours 45 minutes; Bis-Tris gels were run in tanks containing 1 x NuPAGE MES or MOPS running buffer (depending on the expected molecular weight of the protein of interest) at 160 V for approximately 1 hour 30 minutes. Subsequently, gels were used for western blotting.

Reagent	Separating gel	Stacking gel
Distilled water	46.4 ml	20.4 ml
30% Acrylamide mix	26.6 ml	5.1 ml
1.5 M Tris pH 8.8	25 ml	-
1.0 M Tris pH 6.8	-	3.75 ml
10% SDS	1 ml	300 µl
10% Ammonium persulphate	1 ml	300 µl
TEMED	60 µl	30 µl

2.5.4 Western blotting

Proteins were transferred to Protran™ nitrocellulose membrane in a Bio-Rad Mini Trans-Blot Cell® containing 1 x NuPAGE Transfer Buffer with 10-20% methanol. All transfers were run at 100 V for 1 hour. The membrane was stained with Ponceau red solution to verify equivalent loading, washed with distilled water, and blocked in 5% non-fat milk powder in TBS-T (TBS-TM) for 1 hour at room temperature. Primary antibodies were diluted to the desired concentration in TBS-TM) and membranes were incubated with the solution at 4 °C overnight. This was followed by three 5 minute washes in TBS-T, and 1 hour incubation in secondary antibody at the required concentration in TBS-TM at room temperature. The membrane was washed again: 10 minutes in TBS-T, 2 x 5 minutes in TBS-T, and 10 minutes in TBS. The membrane was then scanned using the LI-COR Odyssey CLx system, and protein bands were visualised and quantified using Image Studio version 3.1.

2.5.5 Preparation of nuclear and cytoplasmic extracts

Following trypsinisation, cells were harvested with serum-containing DMEM, transferred into a 14 ml Falcon tube and centrifuged at 500 g for 5 minutes in an Eppendorf 5804R centrifuge. The medium was removed, and the pellet resuspended in 1 ml of cold PBS and transferred to a 1.5 ml Eppendorf tube. This was centrifuged in an Eppendorf 5415 centrifuge at 500 g for 3 minutes at 4 °C, and the supernatant was removed, leaving the pellet as dry as possible.
Thereafter, the Thermoscientific NE-PER Nuclear and Cytoplasmic Extraction kit was used, following the manufacturer's instructions. In summary, the volume of the cell pellet was estimated, and an appropriate volume of CER I (cytoplasmic extraction reagent I), with protease inhibitor, was added. This was vortexed for 15 seconds, and incubated on ice for 10 minutes. Next, an appropriate volume of CER II was added, followed by vortexing for 5 seconds, and a 1 minute incubation on ice. The tube was again vortexed, and subsequently centrifuged at 13,200 rpm for 5 minutes at 4 °C. The supernatant (cytoplasmic extract) was transferred to a clean, pre-chilled tube and kept on ice. The remaining pellet was suspended in an appropriate volume of NER (nuclear extraction reagent) with added protease inhibitor and vortexed for 15 seconds every 10 minutes for a total of 40 minutes. Following this, the tube was centrifuged at 13,200 rpm at 4 °C for 10 minutes. The resulting supernatant (nuclear extract) was transferred to a clean, pre-chilled tube. Both cytoplasmic and nuclear extracts were homogenised using a Qiashredder spin column. Thereafter, the extracts were used for gel electrophoresis as previously described.

2.5.6 TGFβ ELISA

An R&D Systems Quantikine ELISA kit was used to detect TGFß in cell culture medium. In order to activate latent TGFß to the immunoreactive form, acid reactivation and neutralisation is necessary. This was achieved by adding 200 µl of cell culture supernatant to 40 µl of 1 N hydrochloric acid, mixing, and incubating at room temperature for 10 minutes. 20 µl of 1.2 N sodium hydroxide/0.5 M HEPES was then added to neutralise the sample. The standard stock solution was used to produce a two-fold dilution series at the following concentrations: 31.2, 62.5, 125, 250, 500, 1000 and 2000 pg/ml. Subsequently, 50 µl of assay diluent and 50 µl of standard or sample were added to each well

of the ELISA plate and incubated for 1 hour at room temperature. Following this, the plate was washed and 100 µl of TGFß 1 conjugate was added to each well. This was incubated for 2 hours at room temperature, followed by washing and incubation with colour reagents. Stop solution was added after 30 minutes, and the optical density of each well was determined with SoftMax Pro 4.8 software on a Molecular Devices Microplate Reader set to 450 nm wavelength.

2.5.7 TGFβ Bioassay

To determine the responsiveness of NIH3T3 TGFß reporter cells, cells were plated at 1 x 10^5 per well of a 24-well plate, in DMEM supplemented with FCS. 24 hours later, cells were washed with PBS, and serum-free medium was added. After 6 hours had elapsed, recombinant TGFß was added at a range of concentrations (from 20 pg/ml to 5 ng/ml). Cells were incubated at 37 °C for 16 hours. Subsequently, Promega luciferase reagents were prepared: a 1X solution of reporter lysis buffer was made up, and 10 ml of luciferase buffer was added to lypophilized luciferase substrate and mixed. Following this, the cells were washed with PBS and 100 µl of 1X reporter lysis buffer was added to each well. The plate was placed at -80 °C for 1 hour to ensure adequate cell lysis. After thawing, the plate was placed on a rocker at room temperature for approximately 5 minutes. The cells were scraped, and the lysates transferred to 1.5 ml Eppendorf tubes on ice. These were vortexed for 10 seconds, and centrifuged at 12,000 g for 2 minutes at 4 °C in an Eppendorf 5415 centrifuge. The supernatant was transferred to a fresh tube, and 40 µl of each sample was added to a 96-well white plate. The plate was placed on a Turner Biosystems Veritas™ Microplate Luminometer, and automated injectors used to add 40 µl of luciferase assay reagent per well; the readout was recorded by GloMax® software.

2.6 Microscopy

2.6.1 Histological tissue collection, fixation, processing and staining

Animals were euthanized by rising concentrations of CO_2 and tissues were immediately dissected and fixed by immersion in 10% buffer formaldehyde. The fixed tissue was subsequently processed by the Beatson Institute Histology

Service, which undertook paraffin embedding, sectioning and staining. Samples were de-waxed prior to staining by immersing in xylene, and then rehydrated in 97% ethanol and washed in deionised water. Slides were stained with haematoxylin and eosin (H&E). Additionally, samples were probed for the presence of TNC as follows: heat-induced antigen retrieval was performed with PT Module™ pH 8 EDTA retrieval buffer. After washing with Tris-buffered saline with tween (TBST), the samples were blocked with endogenous peroxidase for 5 minutes, washed again, and blocked with ImmPRESS™ normal goat serum for 30 minutes. Subsequently, the samples were incubated with mouse anti-TNC antibody (1:300; Sigma) for 40 minutes at room temperature. Following this, the slides were washed, and ImmPRESS™ anti-rat reagent was applied for 30 minutes. Thereafter, they were incubated with 3,3'-Diaminobenzidine tetrahydrochloride for 10 minutes, washed and counterstained with haematoxylin Z for 7 minutes. Finally, the slides were washed and mounted.

2.6.2 Immunofluorescence

Cells were plated on autoclaved 13 mm coverslips in 24 well plates; following treatment, medium was aspirated from the well and cells washed, fixed with 4% paraformaldehyde, permeabilised with 0.3% Triton X100 and blocked with 1% BSA. Primary antibody was diluted to the required concentration in 1% BSA and applied to the coverslip for 1 hour at room temperature. The coverslip was subsequently washed before being incubated with secondary antibody for 1 hour. Thereafter, the coverslip was washed, inverted on Vectashield™ mounting medium on a glass slide, and sealed with nail polish. Cells were imaged on a Zeiss 710 upright confocal microscope, using a 40X oil objective and 1,3 aperture.

2.6.3 Time lapse microscopy

K14 KD:ER Lifeact GFP and K14 ROCK:ER Lifeact GFP keratinocytes were isolated as described previously and plated on collagen-coated 6-well plates for 24 to 48 hours. They subsequently underwent serum starvation and treatment with 4HT (1 μM) or ethanol vehicle. Bright field differential interference contrast (DIC) and GFP fluorescent time lapse microscopy images were acquired with a 10X objective using a Nikon Eclipse Ti microscope (with Perfect Focus System) with a

heated stage and 5% CO_2 gas line. The plated cells were placed on the microscope immediately following treatment, and time lapse images were taken every 10 minutes for 24 hours using a CoolSNAP HQ2 camera with 0.3 aperture. The resulting images were analysed using MetaMorph® software.

2.7 Gene expression studies

2.7.1 Preparation of RNA from primary keratinocytes

In order to prepare RNA from primary keratinocytes, cultured cells were washed with PBS and trypsinised with 0.25% trypsin. Medium was added to the trypsinised cells, and the mix was centrifuged at 14,000 rpm for 10 minutes at 4 °C. The supernatant was removed, and RNA was isolated from the resulting cell pellet.

Using the RNeasy Kit (Qiagen), the cells were lysed with lysis buffer, then homogenised in a Qiashredder spin column. 70% ethanol was added to the resulting flow through, and the mix was passed through the RNeasy spin column to bind the RNA. Following a wash step, to reduce the possibility of DNA contamination the RNase-free DNase set was used to digest DNA on the spin column. The solution was prepared by adding 10µl of RNase-free DNase I to 70 µl of RNase-free buffer and mixing. This was then added directly to the column membrane and incubated at room temperature for 15 minutes. Subsequently, a further two wash steps were followed by elution of the RNA in RNase-free water.

2.7.2 Determination of RNA concentration and quality

Concentration of RNA samples was determined using the Qubit® Assay, comprising a fluorescent dye that binds to RNA and emits a signal that can be read in the Qubit® fluorometer.

To determine the integrity of RNA samples, the Agilent Bioanalyzer RNA 6000 kit was used. Gel matrix was filtered by applying to a spin column and centrifuging for 10 minutes at 4000 rpm in an Eppendorf 5417R microfuge. 1 µl of dye concentrate was added to a 65 µl aliquot of filtered gel, vortexed, and centrifuged at 13,200 rpm for 10 minutes. The gel-dye mix was applied to the

microfluidic chip, and RNA samples were loaded into the appropriate wells. The chip was vortexed, and run in an Agilent Bioanalyzer 2100.

2.7.3 Quantitative Real Time PCR

To carry out quantitative RT PCR, complementary DNA (cDNA) was prepared from RNA samples using the Quantitect Reverse Transcription kit. The initial step involved a genomic DNA elimination reaction, in which 2 µl of gDNA wipeout buffer was added to 1 µg of template RNA, and nuclease-free water added to a total volume of 14 µl. The mixture was incubated at 42 °C for 2 minutes in a PCR thermal cycler, and added to a reverse transcription mix, consisting of 1 µl of reverse transcriptase, 4 µl of RT buffer, and 1 µl of RT primer mix. The resulting solution was incubated in a thermal cycler as follows:

Temperature	Time
42 °C	15 minutes
95 °C	5 minutes

Thereafter, resulting cDNA samples were diluted to 1:5 with nuclease-free water; 10 µl of each sample was pooled and standards were prepared at the following concentrations: 0.01, 0.04, 0.2, 1. A reaction mixture was then prepared as follows (volumes for 1 reaction):

Component	Volume
Master mix	10 µl
Nuclease-free water	6.1 µl
Primer	2 µl
ROX passive reference dye	0.4 µl
Total	18.5 µl

NB. Master mix contains hot-start polymerase, SYBR green, PCR buffer, 5 mM $MgCl_2$, and dNTP mix.

The reaction mixture was then dispensed into a MicroAmp® Fast Optical 96 well reaction plate, and 1.5 µl of standard or sample was added to each well. The plate was covered with optically transparent sealing film, and run on an Applied Biosystems 7500 Fast Real-Time PCR System. Data were analysed on Applied Biosystems 7500 Software version 2.0.5.

2.7.4 RNA microarray

Affymetrix mouse gene 1.0 ST array was performed on RNA samples by the Molecular Core Biology Facility at the CRUK Manchester Institute.

2.7.5 RNA sequencing

Next-generation RNA sequencing was carried out on the Illumina® NextSeq 500 platform by the Beatson Institute Molecular Technology Services. Data were analysed by the Computational Biology department at the CRUK Beatson Institute.

3 The role of LIM kinases as potential tumour suppressor genes in colorectal cancer

3.1 LIM kinases in colorectal cancer

The LIM kinases (LIMK 1 & 2) play a downstream role in the Rho/ROCK pathway in the regulation of actin-myosin cytoskeletal dynamics; they act by phosphorylating cofilin on serine 3 and inactivating its F-actin severing function, thus regulating actin filament dynamics. It has been proposed that the balance of phosphorylated versus non-phosphorylated cofilin, under the influence of LIMKs, may participate in determining the metastatic potential of a cancer cell.
Using Oncomine®, it was identified that *LIMK2* expression was down-regulated in colorectal cancer (CRC), and a statistically significant reduction in LIMK2 levels in adenocarcinoma samples relative to normal colon tissue in CRC microarray datasets was observed (Figure 3-1). In addition, a progressive reduction in LIMK2 levels with increasing tumour stage was noted, and a statistically significant positive correlation between low LIMK2 levels and poor patient outcomes has been shown [224]. It was also found that LIMK2 expression in CRC cell lines is lower than levels observed in normal colon cell lines (Figure 3-2).

The “cell of origin” in CRC is understood to be the intestinal crypt stem cell, which functions as a self-renewing multipotent cell capable of regenerating the intestinal epithelium. *LIMK2* was found to impede intestinal stem cell proliferation in both *Drosophila melanogaster* and murine models, implying that reduced *LIMK2* expression may permit intestinal stem cells to proliferate without restraint.

Based on these findings, it was proposed that loss or silencing of *LIMK2* may play an important role in the initiation and progression of CRC.

A

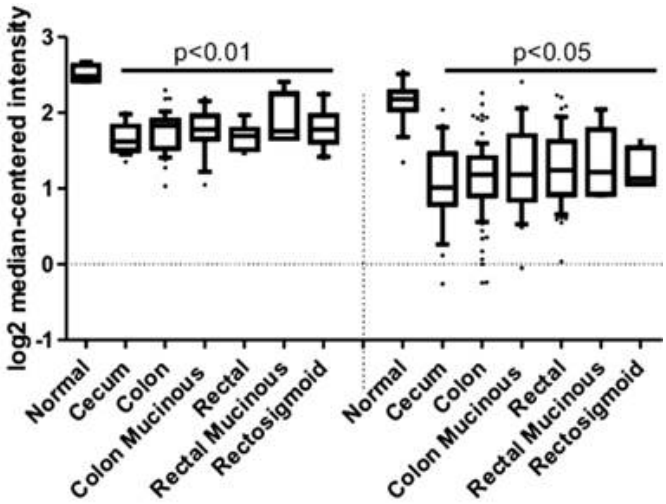

B

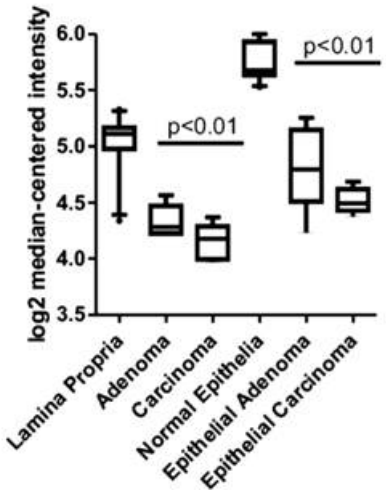

C

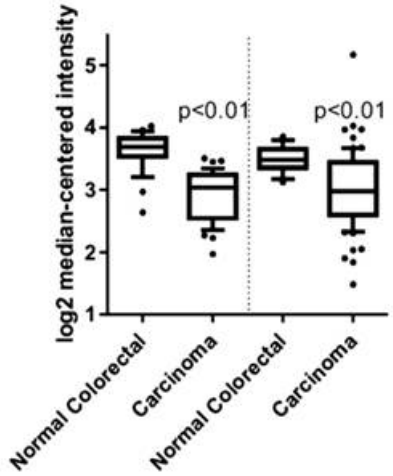

Figure 3-1 LIMK2 expression is down-regulated in colorectal cancer versus normal colonic tissue

A) Log^2 median-centred LIMK2 mRNA expression in normal versus adenocarcinoma tissue samples from Kaiser et al [462] (left side) and The Cancer Genome Atlas Network [463] (right side). B) Log^2 median-centred LIMK2 mRNA expression in microdissected healthy lamina propria or epithelia versus corresponding adenoma or carcinoma from Skrzypczak et al [464]. C) Log^2 median-centred LIMK2 mRNA expression in normal versus carcinoma samples from Skrzypczak et al [464] (left side) and Hong et al [465] (right side). Statistical significance was determined by one way analysis of variance followed by Tukey's post-hoc tests.

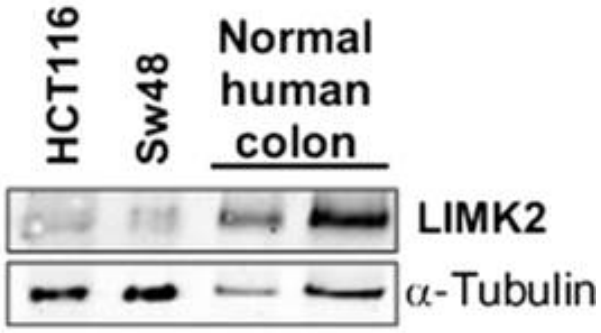

Figure 3-2 LIMK2 expression in normal colon versus CRC cell line.

Western blot of lysates prepared from HCT116 and SW48 (CRC cell lines) and from normal human colon confirms higher expression of LIMK2 in healthy colon tissue compared to colon cancer. α-tubulin served as a loading control.

3.2 Epigenetics

By a process known as DNA methylation, DNA molecules can be altered covalently by the attachment of methyl groups to cytosine bases; this modification has been shown to be as important as mutation in altering gene expression [270]. A class of enzymes known as maintenance methylases functions to maintain the methylation state of a DNA sequence through multiple rounds of DNA replication [466]; thus, DNA methylation can be considered a heritable property. However, as DNA methylation does not alter the nucleotide sequence it is regarded as an epigenetic, as opposed to genetic, mechanism. *De novo* DNA methylation also occurs, primarily during embryogenesis and cell differentiation [467]; it is mediated by DNMT3a and DNMT3b [468].

It is well established that the disruption of normal epigenetic patterns can occur in the early phases of tumorigenesis, and continue to accumulate throughout tumour progression [469]. Aberrant DNA methylation, with the excessive addition of methyl groups to the 5' position of cytosine nucleotides in gene promoter regions, leads to silencing of gene transcription. This is of particular relevance in the context of tumour suppressor genes [470]. Conversely, global hypomethylation can result in the expression of previously suppressed genes, and has been implicated in genetic instability and cancer progression.

3.3 Hypotheses

Thus, the hypotheses that *LIMK2* may function as a tumour suppressor gene in CRC and that its down-regulation may be under the influence of hypermethylation of the gene promoter region were proposed.

3.4 Assessing methylation status

To assess the methylation status of a DNA sequence, a number of options are available. These include (1) methylation-specific PCR (MSP) and (2) bisulphite sequencing, both of which entail initial conversion of DNA with sodium bisulphite, modifying unmethylated cytosines to uracil whilst leaving methylated cytosines unaltered. Thereafter, in the case of MSP, primers are designed that utilise the sequence differences following bisulphite conversion to amplify either

methylated or unmethylated DNA. Whilst this technique provides useful information on methylation of "blocks" of CpG dinucleotides, it has limitations in that it gives a fairly crude "yes or no" outcome. In contrast, bisulphite sequencing relies on the design of primers that do not contain CpGs, so that PCR amplification does not depend on methylation status; this provides an unbiased approach, with no presupposition of the degree of methylation of the sequence of interest. In addition, bisulphite sequencing enables a more accurate and detailed assessment of methylation status of individual CpGs within the sequence. I elected to adopt both approaches; however I chose to focus my efforts on bisulphite sequencing for the aforementioned reasons.

3.5 *LIMK2* promoters are methylated in CRC cell lines

3.5.1 Methylation-specific PCR

To establish if methylation status was influencing *LIMK2* expression, I cultured two human CRC cell lines: HCT 116 and SW48. These had previously been shown to have reduced LIMK2 levels compared with normal colon. I designed methylation-specific primers: one pair specific for methylated DNA and one pair specific for unmethylated DNA. I prepared genomic DNA from the cells; this was bisulphite converted, a process in which, on exposure to bisulphite, unmethylated C nucleotides undergo conversion to T nucleotides, while methylated CpGs are resistant to conversion and are unaltered. I carried out methylation-specific PCR on the converted samples, confirming that *LIMK2* promoter B is methylated (Figure 3-3).

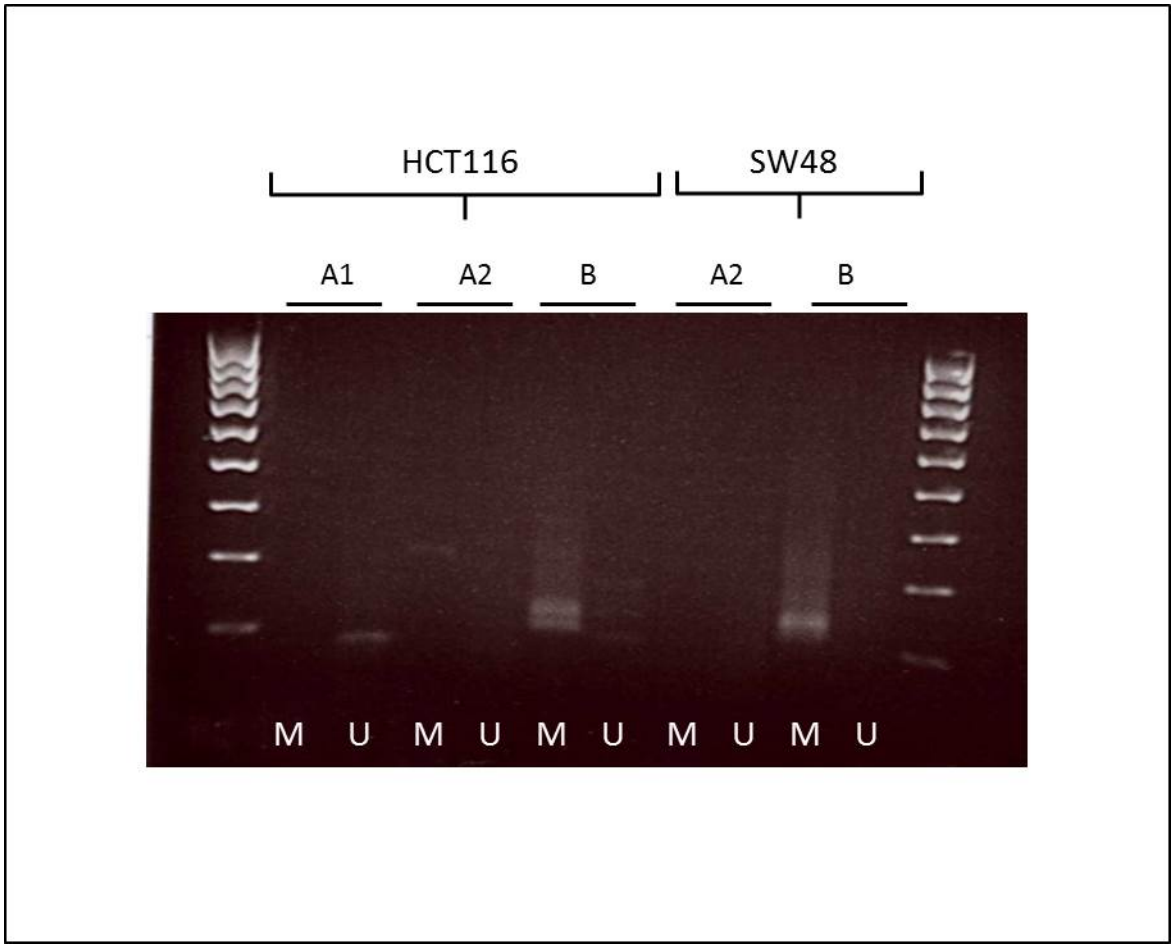

Figure 3-3 Methylation-specific PCR on CRC cell lines.

Genomic DNA was prepared from HCT116 and SW48 CRC cell lines. Following bisulphite conversion, PCR using primer pairs specific for methylated and unmethylated DNA was carried out. Primer pairs A1 and A2 were targeted to *LIMK2* promoter A; primer pair B was targeted to *LIMK2* promoter B. M = methylated, U = unmethylated. A band is visible in the appropriate location in the "methylated" primer B reaction, indicating that promoter B is predominantly methylated as opposed to unmethylated.

3.5.2 Bisulphite sequencing

To elucidate the degree of methylation, I went on to design oligonucleotides (using the Zymo Research bisulphite primer seeker programme) with the capability to amplify both methylated and non-methylated DNA (after identifying CG-rich sequences in the region of both *LIMK2* promoters). In order to optimise the bisulphite sequencing method, multiple primer pairs were designed and trialled. In addition, both temperature and magnesium gradients were utilised, as PCR on bisulphite-converted gDNA is notoriously difficult to perfect. Ultimately, the correct primer pair and optimal conditions with regard to temperature and magnesium concentration were established and used in all experiments going forward. I then performed PCR on the bisulphite-converted genomic DNA from HCT116 and SW48 cell lines, and carried out agarose gel electrophoresis on the PCR products. Following purification, the products were cloned, transformed and sequenced. On obtaining sequences for 10 clones from each cell line, I analysed the DNA sequences using the CLC Genomics Workbench (version 5.1.1). This enabled a direct comparison between the unmodified *LIMK2* promoter sequences, and the bisulphite converted promoter sequences. I could thus identify individual CpG subunits that had remained resistant to conversion and could therefore be deemed methylated. Analysing 10 separate clones allowed me to determine a map of the methylation status of the promoter regions in the CRC cell lines (Figure 3-4).

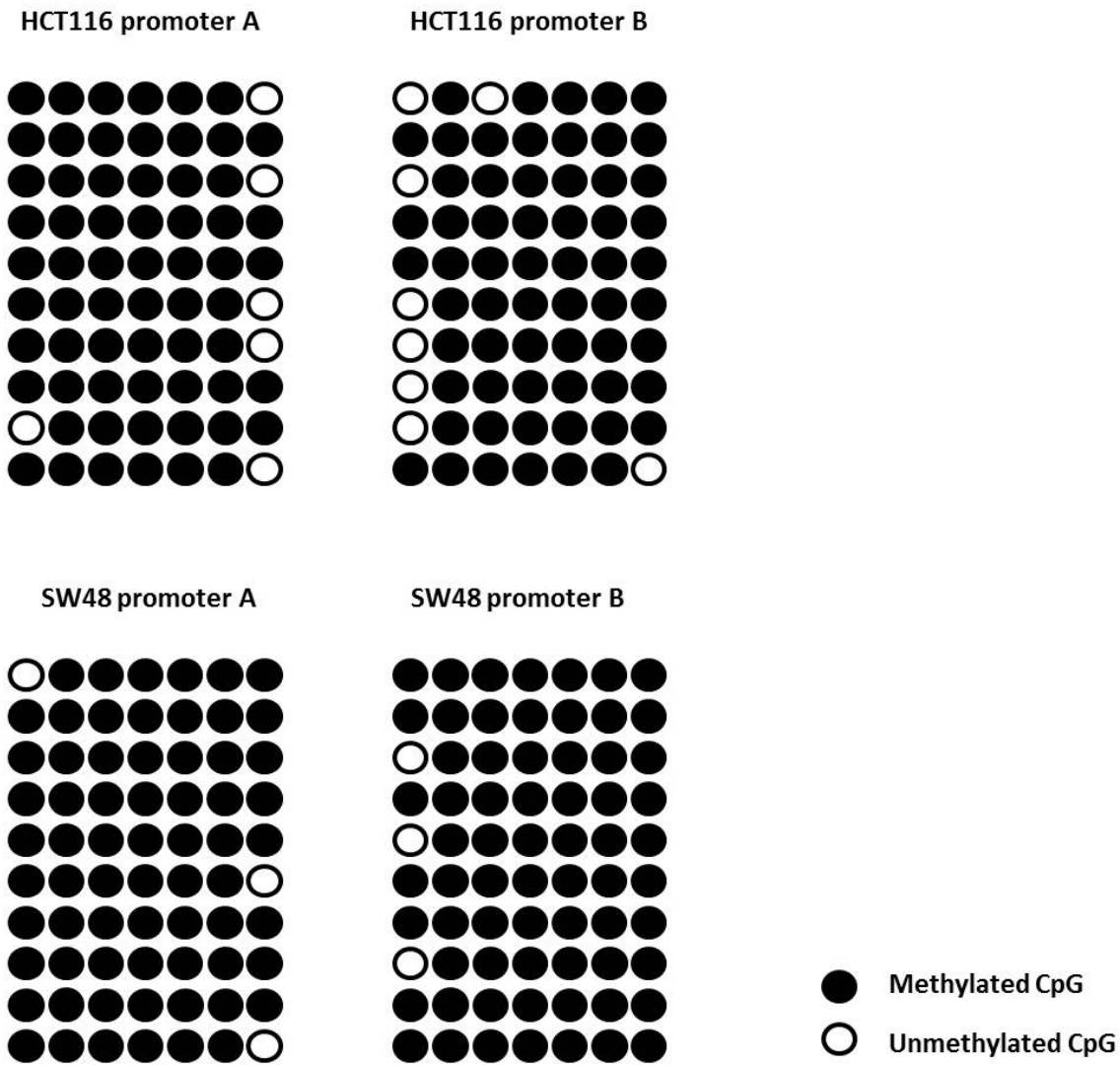

Figure 3-4 Schematic of methylation status of individual CpG dinucleotides

Each panel shows the methylation status of individual CpG dinucleotides as determined by bisulphite sequencing; each horizontal row represents a single clone. HCT116 promoter A demonstrates 94.3% CpG methylation; promoter B demonstrates 88.6% CpG methylation. SW48 promoter A and promoter B demonstrate 95.7% CpG methylation.

3.6 Treatment with DNMTi leads to upregulation of LIMK2 expression in CRC cell lines

It is well established that aberrant gene promoter methylation is a pivotal mechanism of tumour suppressor gene inactivation and many genes, including *p15INK4B* and E-cadherin [471,472], are inactivated by promoter hypermethylation. It has previously been shown that treatment with DNA methyltransferase (DNMT) inhibitors such as 5-AZA-2'-deoxycytidine causes re-expression of genes silenced through promoter hypermethylation. Both 5-Azacytidine (5-AZA) and 5-AZA-2'-deoxycytidine are converted to deoxynucleotide triphosphates and subsequently incorporated in place of cytosine as azacytosine into replicating DNA when cells are in S-phase [473]. DNA demethylation as a consequence of Azacytidine exposure is observed following extended drug exposure, typically 48 hours [474], a time period that permits a sufficient number of cell division cycles for incorporation into the DNA to occur [475]. Thus, in the presence of DNMT inhibitors, there is a progressive loss of DNA methylation as cells continue to grow and divide.

In order to determine if the reduction in LIMK2 levels observed in CRC cell lines is under epigenetic control, I again used HCT116 and SW48 cells. 24 hours after plating the cells in 6 well plates at 2 x 10^5 cells per well, I treated the cell lines with DNMT inhibitors, compounds that are capable of inhibiting the transfer of methyl groups to DNA by preventing the activity of DNA methyltransferases. I used the well-characterised DNMT inhibitor 5-Azacytidine (5-AZA; final concentration 10 μM), and the novel DNMT inhibitor RG108 (final concentration 100 μM), with dimethyl sulfoxide (DMSO) vehicle 1% as a control. Following 48 hours of treatment with the DNMT inhibitors, I confirmed by western blot that there was an increase in the protein level of LIMK2 when compared with the vehicle-treated SW48 cell line (Figure 3-5). This effect was not observed in the HCT116 cell line.

There is some evidence that genes that undergo demethylation following treatment with DNMT inhibitors display enrichment of transcription factor binding motifs; this may interfere with maintenance methylation at specific regions of the new DNA strand during replication and thus potentially facilitate non-random demethylation at specific loci [202,476]. It is therefore possible that

both direct and indirect effects of DNMT inhibition on *LIMK2* are responsible for the alterations in expression observed.

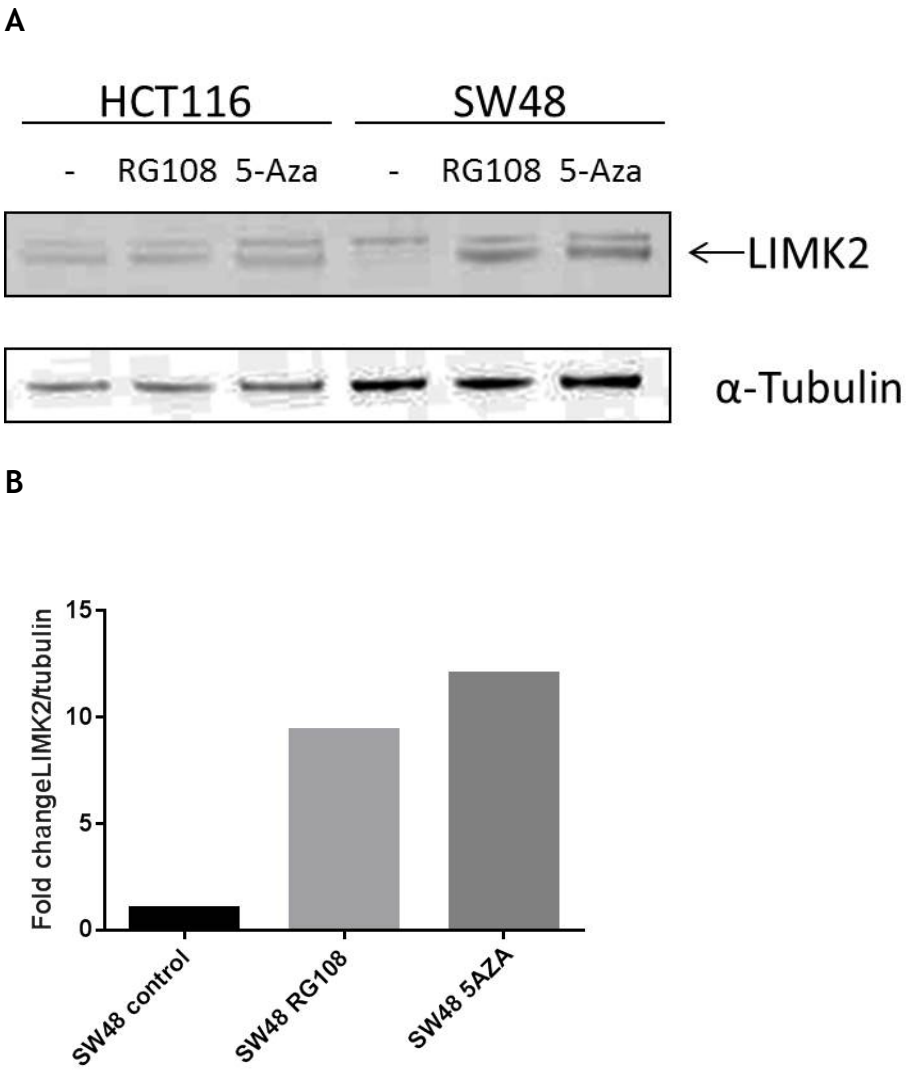

Figure 3-5 Treatment with DNMTi increases LIMK2 expression in CRC cell lines

A. Representative western blot showing an increase in LIMK2 levels in SW48 cells following 48 hours of treatment with the DNMT inhibitors 5-Azacytidine and RG108 versus DMSO vehicle control. α-tubulin was used as a loading control to ensure equivalent protein concentrations. All antibodies used at a concentration of 1:1000. B. Quantification of fold change in LIMK2 relative to α-tubulin in SW48 cells. Arbitrary units, n = 1.

3.7 Treatment with DNMTi reduces methylation of the *LIMK2* promoters in CRC cell lines

Having previously confirmed that DNMT inhibitor treatment led to increased protein levels of LIMK2, I next wanted to investigate the DNA methylation profile of the gene promoters following exposure to DNMT inhibition. In order to do so, I again used HCT116 and SW48 cells and treated them with 5-AZA and RG108. Vehicle-treated cells were again used as a comparator. Following 48 hours of treatment, I carried out bisulphite sequencing as described previously; this confirmed that the number of methylated CpG dinucleotides was lower in cells treated with 5-AZA than in those treated with vehicle (Figure 3-6).

A

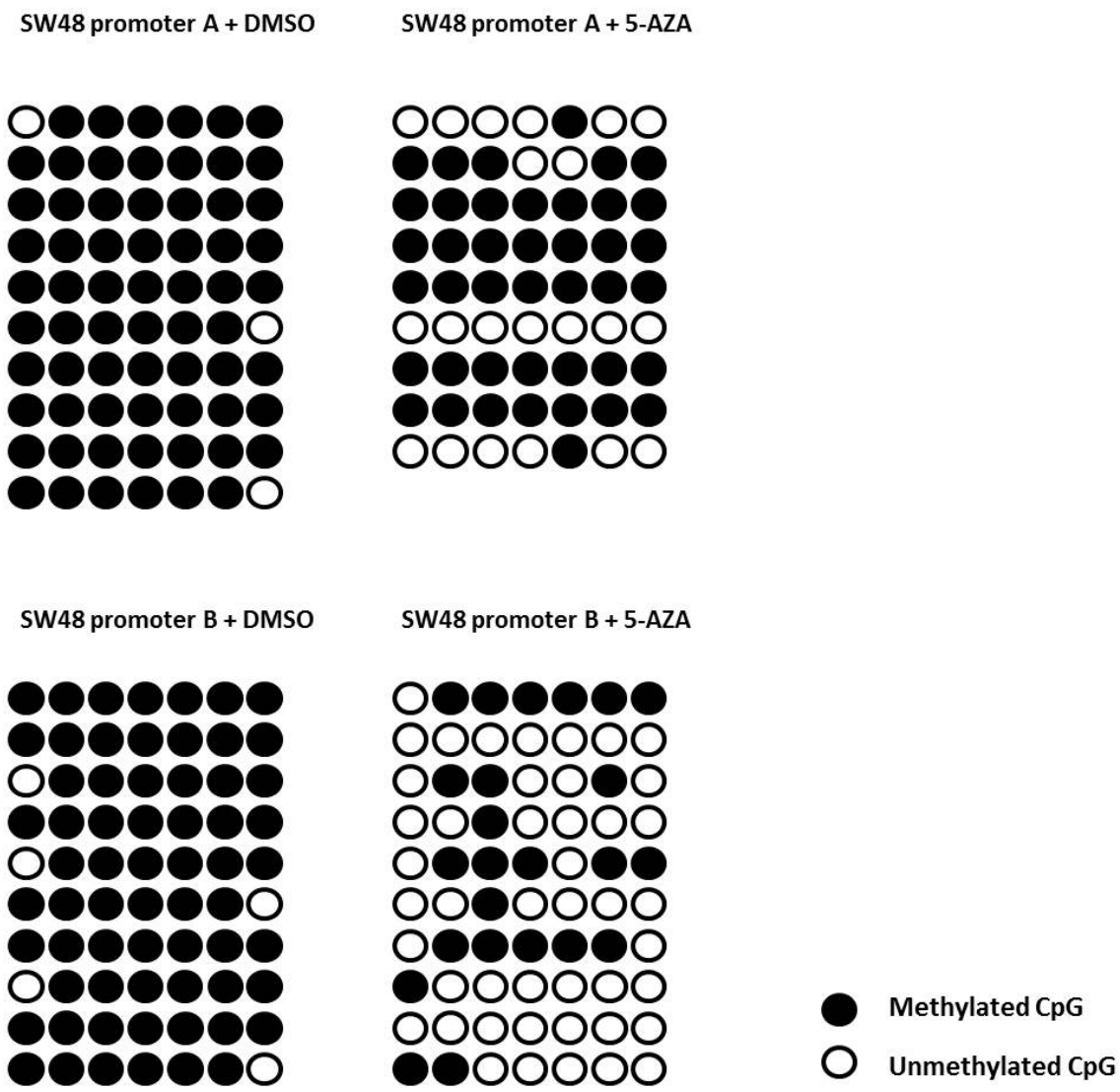
SW48 promoter A + DMSO
SW48 promoter A + 5-AZA
SW48 promoter B + DMSO
SW48 promoter B + 5-AZA
Methylated CpG
Unmethylated CpG

B

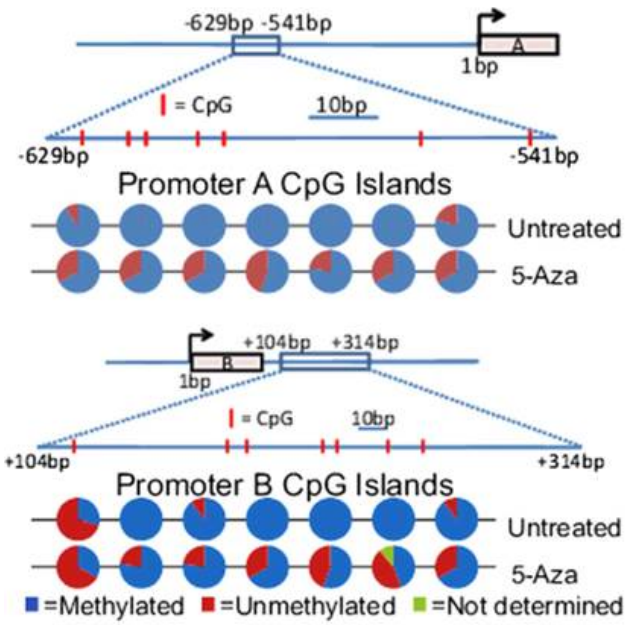

Figure 3-6 CpG methylation in CRC cell lines treated with 5-Azacytidine

SW48 cells were treated with 5-Azacytidine or DMSO vehicle for 48 hours. Subsequently, genomic DNA was prepared and bisulphite converted as described previously and, following amplification, PCR products were cloned and sequenced. A) Each panel shows the methylation status of individual CpG dinucleotides as determined by bisulphite sequencing; each horizontal row represents a single clone. B) The schematic shows the location of the CpG islands in relation to the transcriptional start sites for the *LIMK2a* and *LIMK2b* promoters. The pie charts show the degree of methylation of untreated CpG dinucleotides versus 5-Aza treated dinucleotides. The degree of methylation following DNMT inhibitor treatment decreased in both the *LIMK2a* promoter and *LIMK2b* promoter. With permission from Lourenço et al [224].

3.8 The *LIMK2* promoters are significantly more methylated in human CRC tumour samples than in normal colonic tissue

Having established that expression of *LIMK2* is dependent on the methylation status of the promoters *in vitro*, I next wished to investigate the role of methylation in human CRC. To do so, I obtained matched samples of normal colon and colonic adenocarcinoma (through collaboration with Professor Graeme Murray, Pathology Department, Aberdeen University). I initially wanted to investigate a range of stages of disease, to reflect the stepwise progression that occurs in the development of CRC. CRC is conventionally staged by the Duke's system (Dukes, C. E. (1932), The classification of cancer of the rectum. J. Pathol., 35: 323–332. doi: 10.1002/path.1700350303); however, I felt that Duke's stage C encompasses too many potential variables as the primary tumour can be of any degree of invasiveness in the presence of lymph node disease. Therefore, I elected to focus my efforts on Duke's stage A and stage B tumours. I acquired paired samples from 6 patients, 3 representing each different stage of CRC, with matched normal tissue from the same patients. I prepared genomic DNA from the healthy tissue and the tumour samples, and carried out bisulphite sequencing using primers for *LIMK2a* and *LIMK2b* promoters. After selecting 10 clones for each sample, I again used the CLC Genomics Workbench to analyse the degree of CpG methylation.

I discovered that normal colon samples had significantly lower CpG dinucleotide methylation than colon adenocarcinoma samples (Figures 3-7 and 3-8).

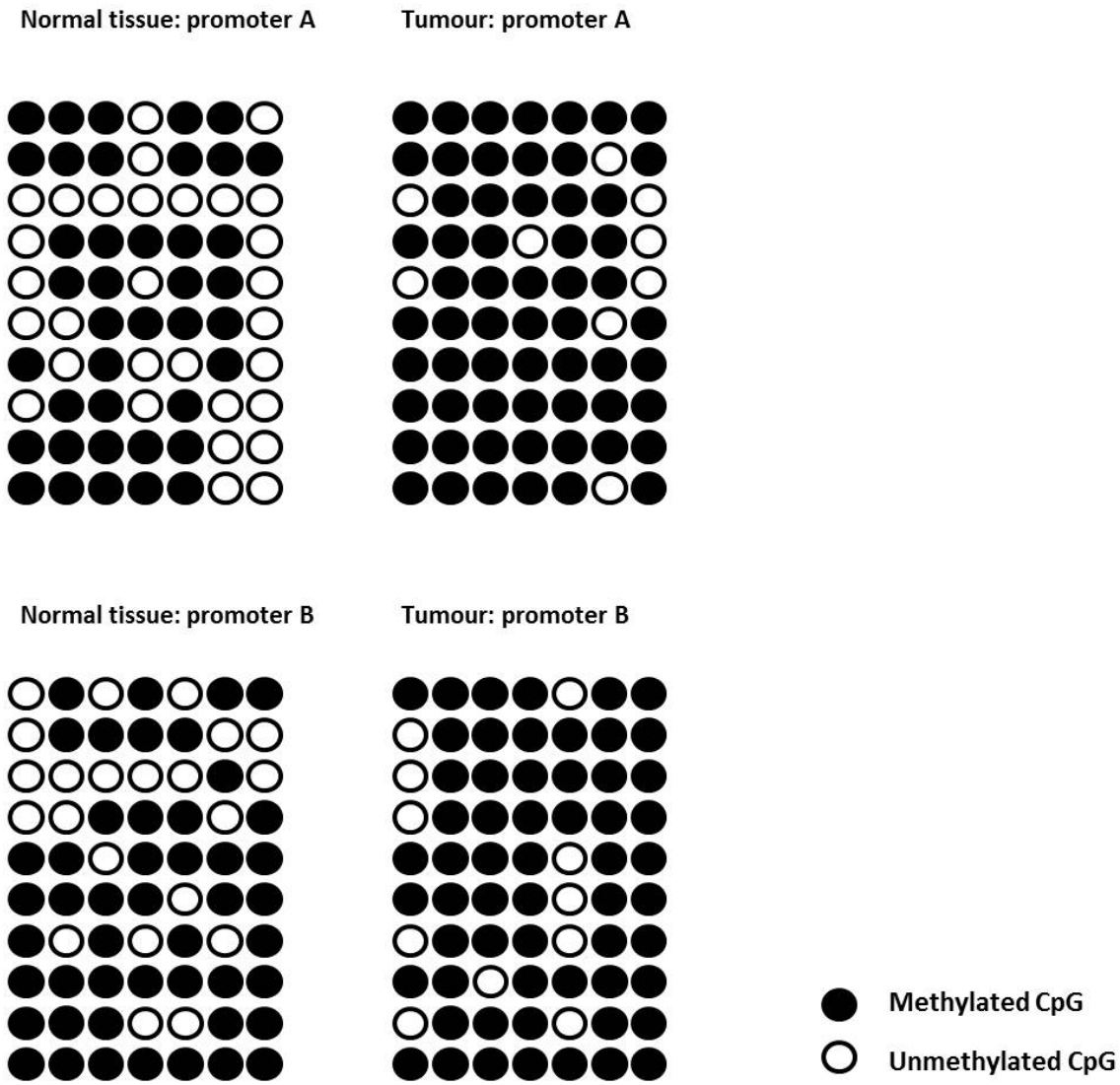

	% methylation normal	% methylation tumour
Promoter A	57.1	87.1
Promoter B	68.6	84.3

Figure 3-7 Tumour samples show a greater degree of methylation than matched healthy tissue
Bisulphite sequencing confirms that individual CpG dinucleotides display higher levels of methylation in tumour samples compared to healthy colon from the same individual.

A

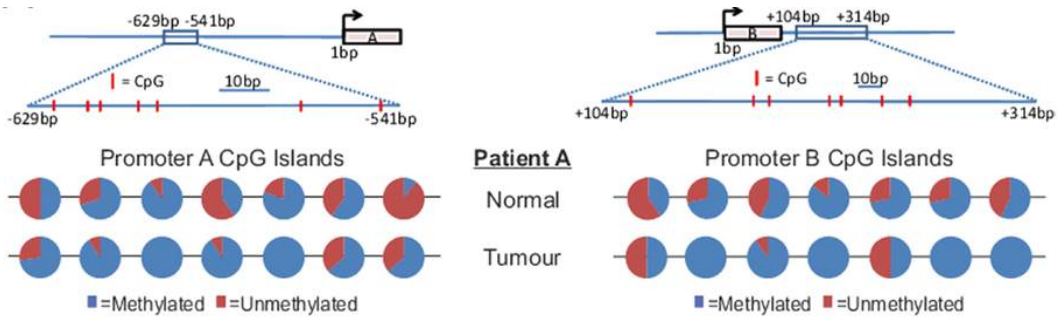

B

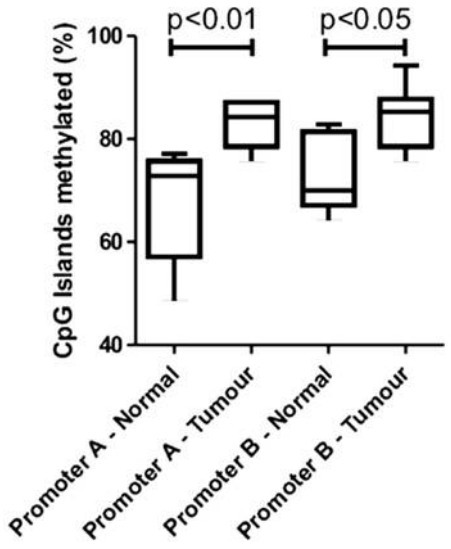

Figure 3-8 CpG methylation of *LIMK2a* and *LIMK2b* promoters in paired normal and tumour samples.

A) Schematic indicates the position of CpG islands relative to the transcriptional start site for each promoter. The pie charts indicate the proportion of methylation from multiple independent clones for each CpG island in the bisulphite-converted genomic DNA of a representative patient. B) Cumulative *LIMK2a* and *LIMK2b* promoter methylation from matched healthy and tumour tissue obtained from six patients with CRC. Statistical significance determined by one way analysis of variance followed by Tukey's post-hoc tests.

I next wanted to determine if a relationship existed between the stage of the tumour and the degree of methylation of CpG islands. I therefore analysed the degree of methylation of Duke's A versus Duke's B tumours, with the matched normal tissue also categorised as per the stage of the patient's tumour. I found a trend towards increasing methylation of the *LIMK2a* and *LIMK2b* promoters with increasing depth of invasion of the primary tumour (Figure 3-9).

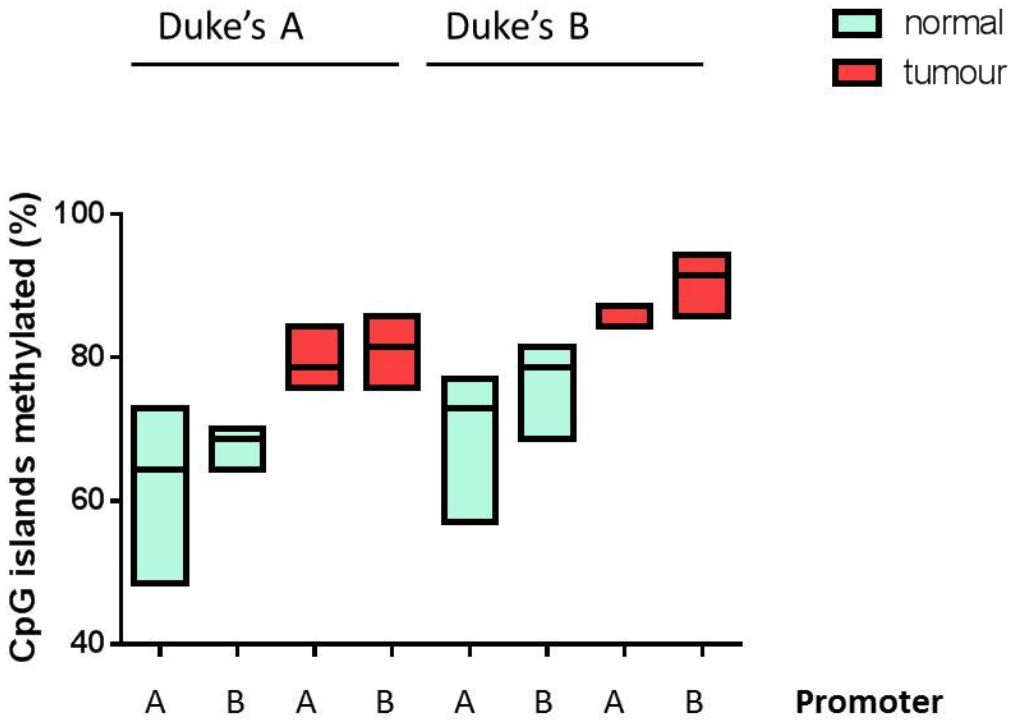

Figure 3-9 Methylation status of *LIMK2a* and *LIMK2b* promoters by Duke's stage

A trend towards increasing CpG methylation is observed in tumour samples obtained from patients with Duke's B tumours versus Duke's A tumours. Duke's A promoter A versus Duke's B promoter A: p = 0.0686. Duke's A promoter B versus Duke's B promoter B: p = 0.0682 (unpaired t test). A larger sample size would be necessary to establish if a significant relationship does exist between advancing tumour stage and degree of methylation.

3.9 LIMK2 deficiency in mouse models of colorectal cancer

I subsequently wanted to investigate whether *Limk2* deletion in a CRC animal model would promote the development and progression of CRC. This work was undertaken with Dr Filipe Lourenço. The *Limk2* knock-out mouse model was developed by obtaining Limk2 gene-trap embryonic stem cells from the European Conditional Mouse Mutagenesis Program (EUCOMM); the Beatson transgenic facility subsequently performed blastocyst injections using a standard approach. The gene-trap targeted the second intron of the *Limk2* gene, thus preventing the expression of a functional protein. Gene trapping is an approach through which a promoterless reporter construct is integrated into a gene expressed in an embryonic stem cell. The gene trap cassette is flanked with genomic sequences, enabling the insertion to be directed precisely into introns of genes by homologous recombination [477]. Genotyping of the mice was carried out by Transnetyx molecular diagnostics, with the desired phenotype (*Limk2*-KO) being present in 26.8% of animals at birth. Mice homozygous for gene-trapped *Limk2* loci were validated by immunofluorescence, which showed no Limk2 or phosphorylated cofilin expression in the intestine (compared with *Limk2*-WT mice) [224]. In the first experiment, performed by Dr Lourenço with my assistance, 8 – 12 week-old *Limk2* wild-type (WT) and knock-out mice underwent a single intraperitoneal injection of azoxymethane (AOM) solution at a dose of 12.5 mg/kg. AOM is metabolised by cytochrome P450, ultimately forming formaldehyde and a highly reactive alkylating species, resulting in alkylation of DNA. Following this, mice received drinking water with dextran sodium sulphate (DSS), an agent that is directly toxic to colonic epithelium, mimicking the chronic inflammatory state observed in inflammatory bowel disease in man (e.g. Crohn's disease or ulcerative colitis), and compounding the tumorigenic effects of AOM. It was found that *Limk2*-deficient mice experienced a greater degree of weight loss, and also were shown to have larger tumour foci with a greater propensity to invasiveness than WT mice [224].

Further to this work, we crossed the *Limk2* knock-out model with a genetically modified CRC model: Vilin Cre:ER, *Apc*$^{fl/+}$, *Kras* G12D mutant. Cre was induced with four daily intraperitoneal injections of tamoxifen, and I monitored the animals for evidence of weight loss and signs of gastrointestinal disease. There was no significant difference between the two groups in terms of survival or

extent of weight loss (Figure 3-10). This could possibly be explained by the high malignant potential of the mutant *Kras*, *Apc* heterozygous phenotype, which may not be modulated by the relatively small effect of loss of *Limk2*.

A

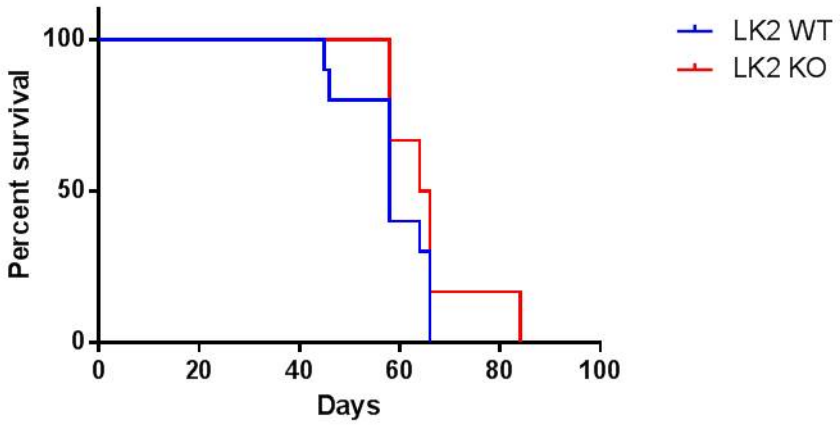

B

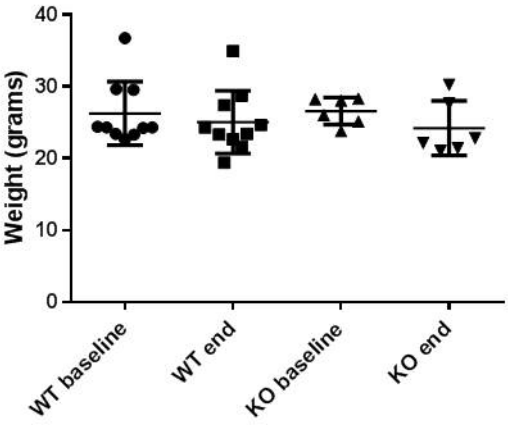

Figure 3-10 Loss of *Limk2* in a GM mouse model of CRC shows no significant difference in survival or weight loss

A)Kaplan Meier curve of survival in two cohorts of Vilin Cre:ER, $APC^{fl/+}$, KRAS G12D mutant mice, one expressing wild type (WT) *Limk2*, the other with *Limk2* knock out. Survival was not significantly altered between the groups. B) Baseline and final weights of the mice reveals no acceleration in weight loss in the *Limk2* KO group versus the *Limk2* WT group.

3.10 Summary

In summary, the results presented in this chapter show that:

- LIMK2 expression is downregulated in CRC when compared with normal colon tissue at the mRNA and protein level
- *LIMK2* promoters are methylated in CRC cell lines
- Treatment with DNMT inhibitors reverses this hypermethylation
- Primary colonic tumours display a greater degree of LIMK2 methylation than matched healthy colon tissue
- There is a trend towards increased methylation with increasing depth of invasion of primary tumour
- Loss of LIMK2 in an inflammation-related CRC mouse model predisposes to larger tumour foci with a greater depth of invasion
- Loss of LIMK2 in a GM mouse model with mutant KRAS and loss of APC does not give the same outcome

4 Modulation of the Actin Cytoskeleton Impacts on Extracellular Matrix Composition

Skin is an organ that is subject to external mechanical stress, prompting interactions between the cells of the dermis and epidermis, and the extracellular matrix. A conditionally active ROCK construct had previously been developed in the lab (Figure 4-1) [478]. In order to determine the impact of alterations in the actin cytoskeleton in the context of skin's response to differing levels of tension, genetically modified mice with a conditionally regulated oestrogen receptor (ER) fusion form of the ROCKII kinase domain under transcriptional control of the cytokeratin 14 (K14) promoter were previously developed in the laboratory [479]. This construct consisted of a modified ER, with a glycine to arginine point mutation at position 525, resulting in an inability to bind 17ß-oestradiol, but retained 4-HT-binding capacity; this was inserted in the *ROCK* II gene, in place of the Rho-binding domain, resulting in a ROCK II kinase domain that was responsive to 4-HT as opposed to RhoA-GTP [478]. Through targeting the K14 gene promoter to the hypoxanthine phosphoribosyltransferase (*Hprt*) gene locus, tissue-selective expression of conditionally active ROCKII:mER™ within a specific target tissue was possible (Figure 4-2); in this instance, as K14 is a cytokeratin that is expressed at high levels in the stratified epithelium of the epidermis, permitting skin localisation. A kinase dead control construct had also previously been created by point mutation (lysine 121 was altered to glycine in the ATP-binding pocket) [478]. *In vivo s*tudies with these mice previously revealed that ROCK activation leads to an elevation in skin stiffness and thickness [83]; however, the specific mechanisms by which this occurs have not yet been determined. I therefore sought to identify alterations in gene expression that occur as a consequence of ROCK activation in keratinocytes. The results of these investigations are presented in this chapter.

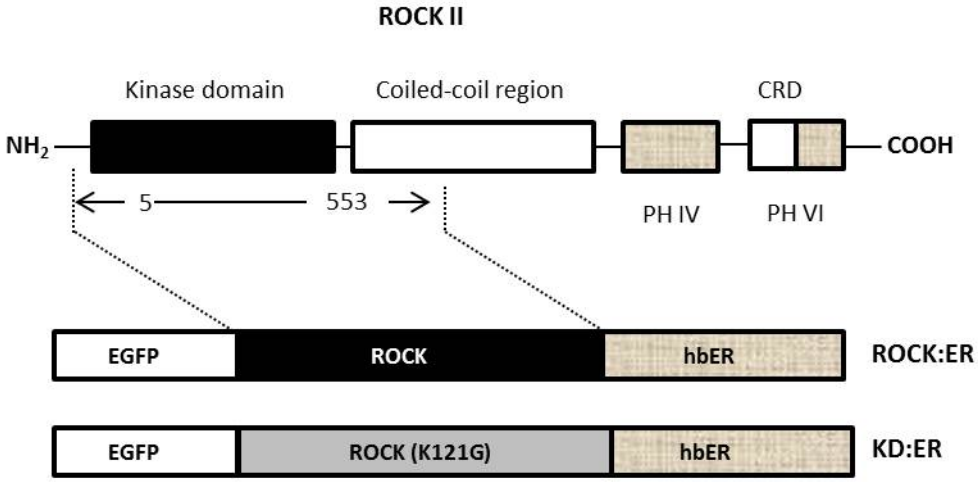

Figure 4-1 Schematic of ROCKII and the conditionally regulated ROCK:ER construct
PH: pleckstrin homology domain; CRD: cysteine-rich domain. Amino acids 5-553 were joined in frame to enhanced GFP (EGFP) and ER hormone-binding domain (hbER) to create the ROCK:ER fusion protein. A kinase dead version was created by altering lysine 121 to glycine (ROCK(K121G)). Adapted from Croft and Olson[478]

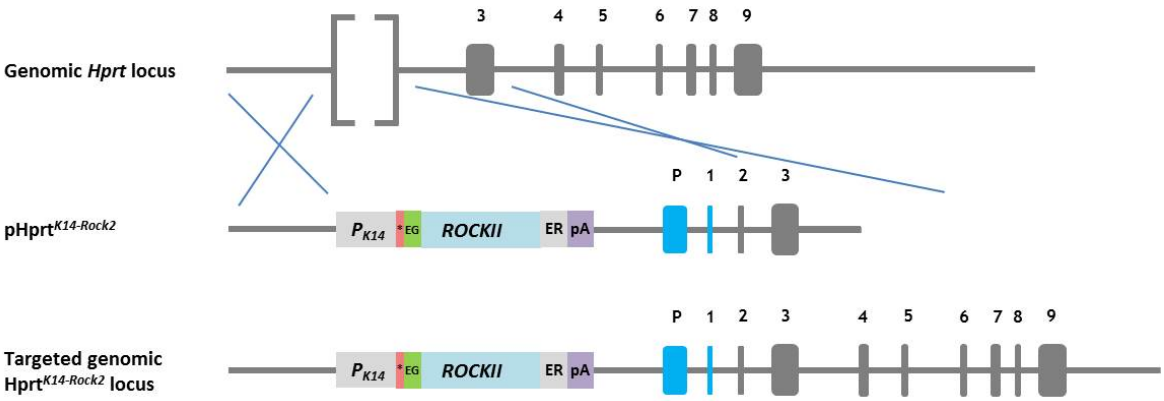

Figure 4-2 The gene targeting approach for developing K14-ROCKII:mER™ mice

A K14-ROCKII:mER™ expression cassette was targeted to the mutant mouse *Hprt* locus, with the promoter and first exon of human *HPRT* and the second exon of murine *Hprt* to reconstitute an active chimeric *Hprt* locus. EG: green fluorescent protein; *: ß globin intron; P_{K14}: K14 promoter sequence; ER: mER™ sequence; pA: K14 polyadenylation signal. This represents the ROCK2 kinase domain alone, not full length ROCK2. Not to scale. Adapted from Samuel et al [479].

4.1 Confirmation of ROCK activation in primary keratinocytes

In order to investigate the impact of ROCK activation *in vitro* in keratinocytes, I first wished to confirm that ROCK activation was induced by treatment with 4-hydroxytamoxifen (4-HT). I therefore isolated and cultured keratinocytes from the tail skin of ROCK:ER and control kinase dead (KD):ER mice. Following 16 hours of treatment with 4-HT or ethanol drug vehicle, I stained cells with Texas Red-conjugated Phalloidin and utilised confocal microscopy to visualise actin fibres. In cells with activated ROCK, these were apparent as stress fibres, while stress fibre formation was not evident in either the KD cells treated with 4-HT or the ROCK:ER cells treated with vehicle.

In addition, I prepared protein lysates from keratinocytes and used western blot to determine levels of phosphorylated myosin light chain (pMLC) in response to ROCK activation. This showed that pMLC was elevated in ROCK-activated cells (Figure 4-3).

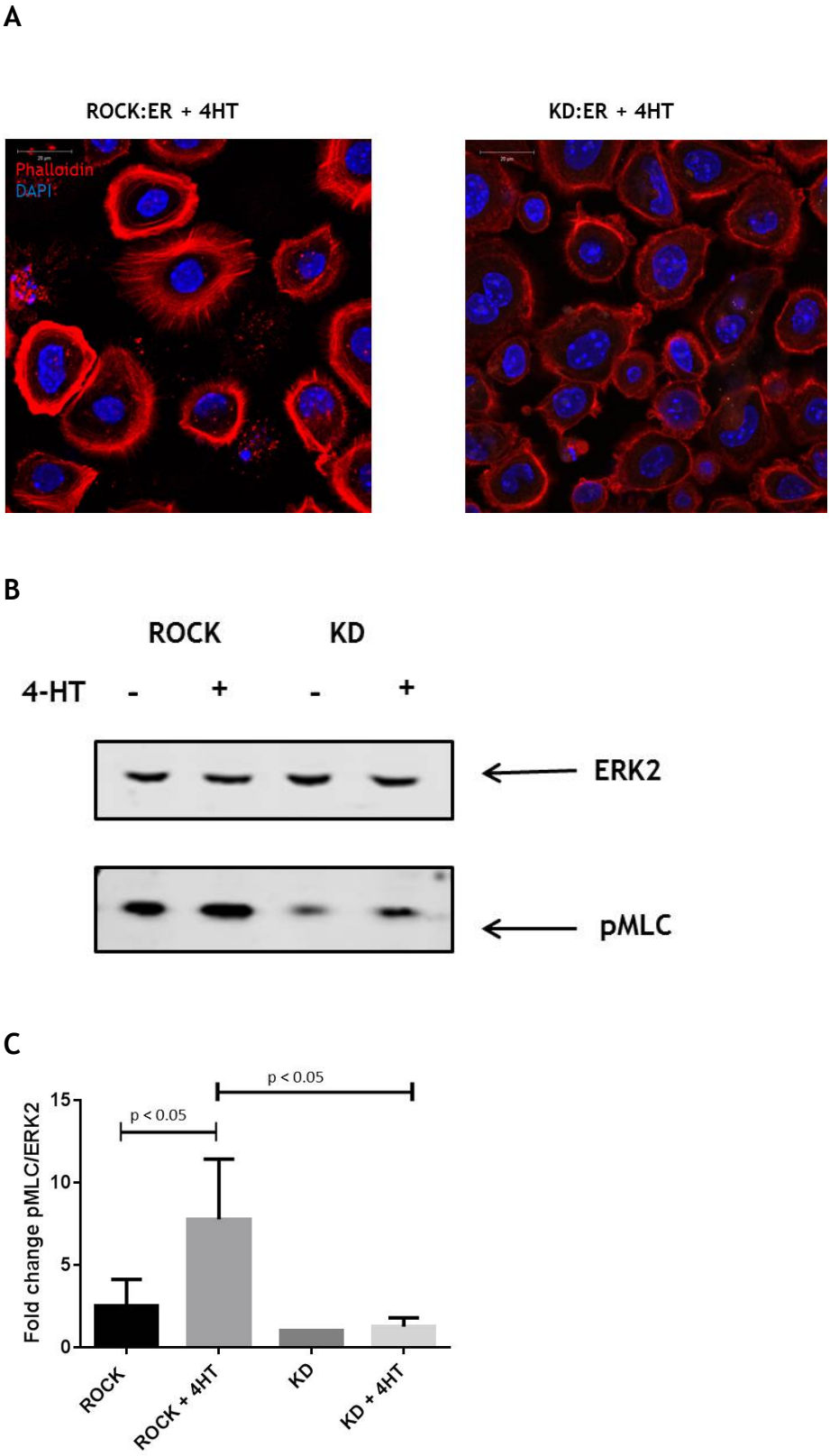

Figure 4-3 Confirmation of ROCK activation with 4-HT treatment
A) Confocal microscopy of primary keratinocytes shows Texas Red-conjugated phalloidin staining of actin fibres (1:500), with more intense phalloidin staining indicating increased cortical actin and a number of K14 ROCK:ER cells demonstrating stress fibre formation. DAPI is used to stain nuclei. B) Western blot confirms an increase in phosphorylated myosin light chain (pMLC) relative to total myosin light chain (MLC) following ROCK activation. The membrane was probed with antibodies against both phosphorylated myosin light chain (1:500) and total myosin light chain (1:1000). C) Quantification of fold change of pMLC relative to ERK. n = 4. Significance determined by unpaired t test.

4.2 Increases in extracellular matrix protein gene expression following ROCK activation

Having validated ROCK activation in keratinocytes, I next set out to investigate the alterations in gene expression observed in these cells when compared with control cells. Attempts had previously been made in the laboratory to investigate gene expression changes in tissue derived directly from transgenic mice treated with 4-HT; however, due to a high degree of inter-animal variability, this approach was not felt to be viable. In order to interrogate changes in primary cells, I again isolated and cultured primary keratinocytes, and treated them with 4-HT or ethanol vehicle. Thereafter, I prepared RNA from the cells, and Affymetrix gene expression microarray analysis was performed at the Cancer Research UK facility at the Paterson Institute. The results of the microarray were analysed by the Computational Biology Service at the Beatson Institute, and Ingenuity® Pathway Analysis was undertaken. This identified a number of possible networks of molecular relationships that may be contributing to the differences observed following ROCK activation, including the "cell movement network" (Figure 4-4). Numbering among the components of this network were the extracellular matrix glycoproteins tenascin C (*Tnc*) and thrombospondin-1 (*Thbs1*), and the plasminogen activator, urokinase receptor (*Plaur*) (which is upregulated in cutaneous squamous skin cancer [480], and also functions as a high-affinity receptor for the extracellular matrix glycoprotein vitronectin (VTN) [481]). TNC, THBS-1 and VTN are up-regulated at sites of physiological tissue-remodelling, e.g. during wound healing; in addition, these ECM proteins have been implicated in the permissive interplay between cancer cells and the tumour microenvironment. Of the ECM components I had identified, I decided to pursue investigation of TNC. This was in part due to evidence linking the expression of TNC to alterations in mechanical properties, and also due to the fact that TNC has been shown to be overexpressed in most solid tumours. It is believed to participate in a number of pro-tumorigenic processes, including:

- Supporting the capacity of some cancer types to form a metastatic niche [446]

- Promoting epithelial-mesenchymal transition [433-435]

- Mediating resistance to apoptosis [446,482]

To validate the gene expression changes observed in the microarray, I proceeded to carry out quantitative real-time PCR (q RT-PCR). This confirmed that ROCK activation by 4-HT led to an increase in *Tnc* transcripts (Figure 4-5).

The RNA microarray data is available at the following URL:

https://docs.google.com/spreadsheets/d/1hko3Tf9E34s6fR6mJhrjA8NpVvPl82mKSkoUcxDQsFc/edit?usp=sharing.

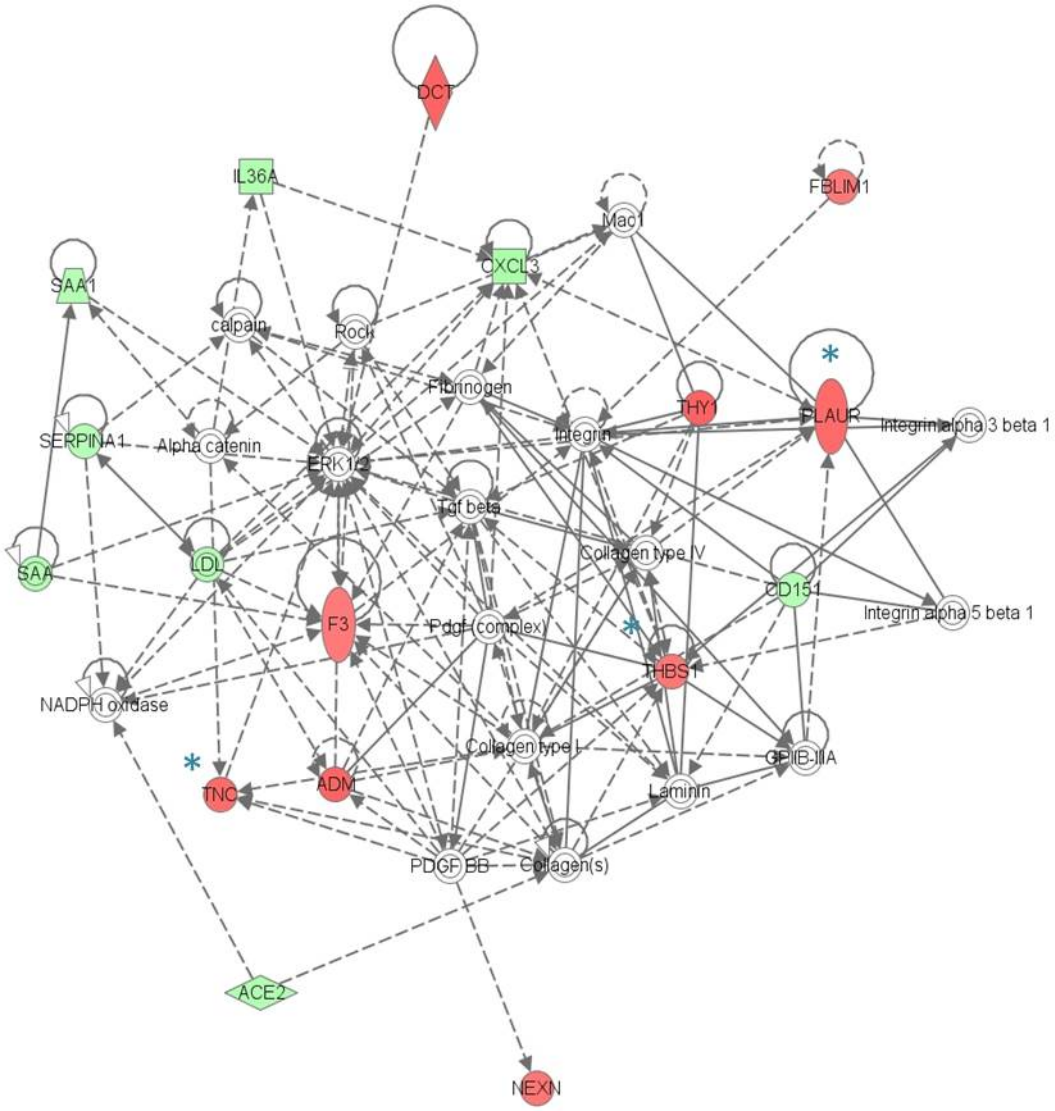

Figure 4-4 Ingenuity ® Pathway Analysis: Cell movement network

Following RNA isolation from primary keratinocytes +/- ROCK activation, Affymetrix gene expression microarray was performed. Pathway analysis shows changes in the cell movement network following activation of ROCK in primary keratinocytes. The network analysis identifies the upstream regulators that may be responsible for observed gene expression changes. IPA predicts which upstream regulators are activated or inhibited to explain the upregulated and downregulated genes. Red = upregulated; Green = downregulated. Tenascin C (*Tnc*), Thrombospondin 1 (*Thbs1*) and plasminogen activator, urokinase receptor (*Plaur*) are highlighted by *. Lines link genes with up or downstream relationships; solid line = direct relationship, dotted line = indirect relationship.

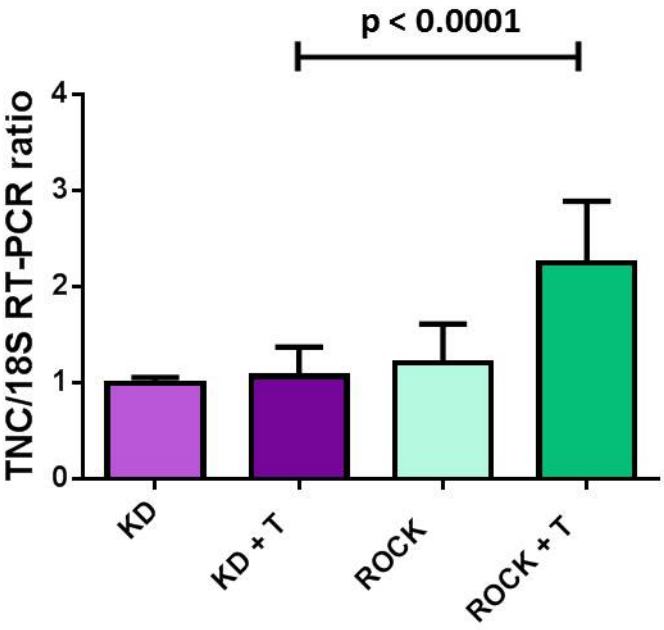

Figure 4-5 Increase in *TNC* RNA transcripts following ROCK activation of keratinocytes with 4-HT.

Replicates of paired primary keratinocytes isolated from K14 KD:ER and ROCK:ER animals, activated for 16 hours with 4-HT in serum-free medium. Fold change of *Tnc* transcripts is shown relative to *18s* abundance determined by q RT-PCR. Statistical significance of differences was determined by one-way ANOVA. n = 4.

4.3 Validation of TNC antibody

Having decided that TNC was a target I wished to pursue in further experiments, I next wanted to conduct studies of TNC on the protein level. In order to do so, I set out to validate the TNC antibody by probing tissues in which I expected to observe high levels of TNC expression. TNC is highly expressed during embryogenesis; therefore, I prepared protein lysates from wild type (WT) mouse embryonic fibroblasts (MEFs), and performed a western blot. This confirmed high levels of TNC expression. In adults, physiological TNC expression is limited to regions of the brain such as the hypothalamus, where it mediates neuron-glial interactions. I obtained TNC knock-out (KO) mice and, along with WT mice, dissected the brains and stained sections for TNC. This confirmed the presence of TNC in the hypothalamus of WT mice, and its absence in the hypothalamus of KO mice (Figure 4-6).

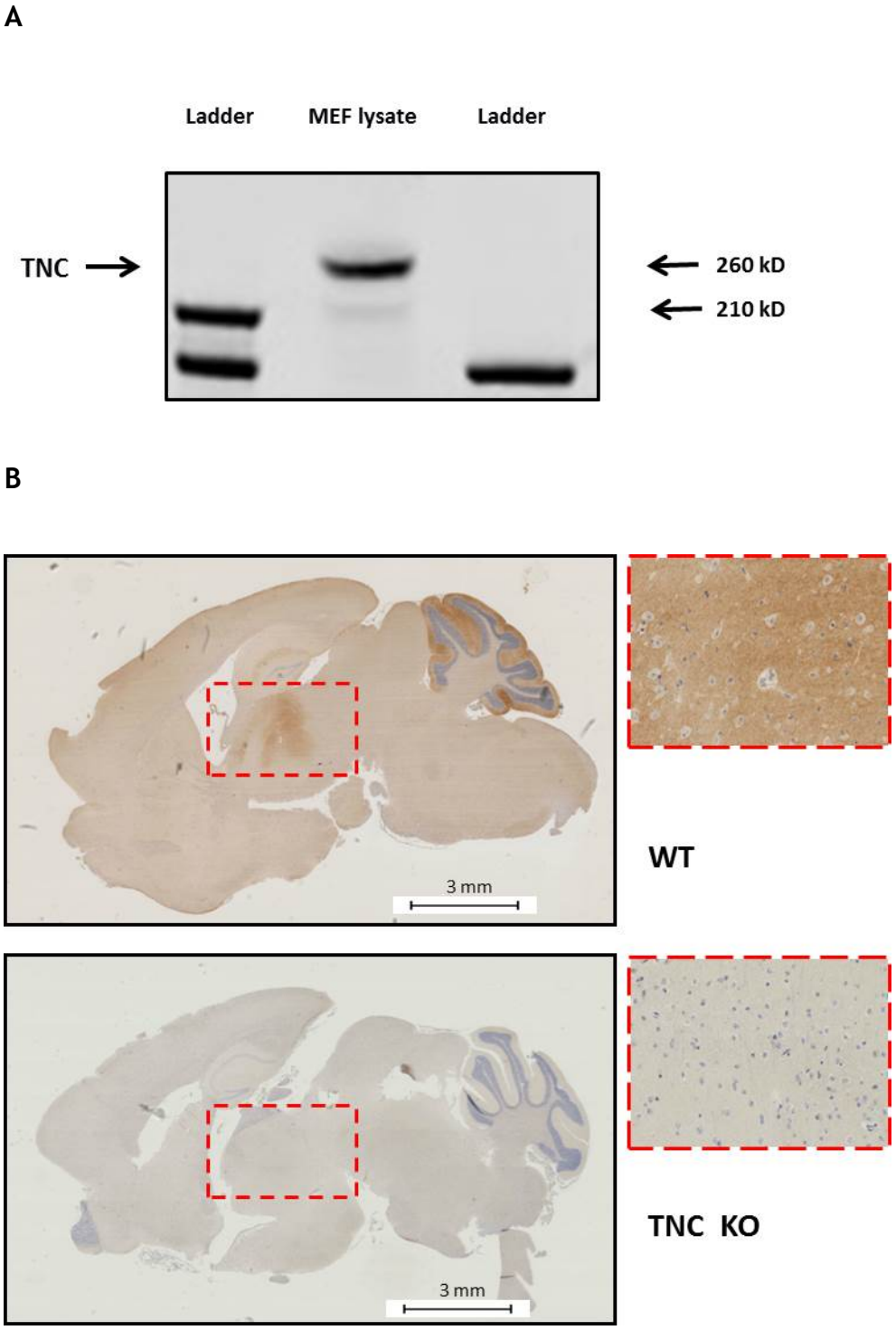

Figure 4-6 TNC antibody validation: western blot and immunohistochemistry.

A) Early-passage MEFs were cultured in 6-well plates. Cells were washed and lysed with SDS lysis buffer, and protein electrophoresis was performed. Following transfer, the membrane was probed for TNC expression (1:500). Two bands were visible, one of 260 kDA, and a fainter band (a probable splice variant) of 210 kDA. B) 11-month-old WT and TNC KO animals were euthanized humanely. The spinal cords were severed, the skull removed, and the entire brain dissected *en bloc* and placed in formalin. The brain was subsequently embedded in paraffin, sectioned, and stained for TNC. TNC expression was apparent in the hypothalamus of the WT animal, but not in that of the KO animal. Sections show whole brain, with the hypothalamus at higher magnification (20X).

4.4 ROCK activation leads to increased protein levels of TNC

I subsequently wished to determine if the increase I had observed in TNC RNA transcripts was translated to the protein level following ROCK activation. To do this, I utilised primary keratinocytes, isolated as described previously. I found that, following treatment with 4-HT, ROCK-activated keratinocytes had higher levels of TNC protein on western blot (Figure 4-7).

Having confirmed that TNC expression was influenced by ROCK activation, I wished to investigate the role TNC could be playing in squamous skin cancer. Using Oncomine®, I analysed data that revealed *TNC* was consistently overexpressed in squamous skin cancer (Figure 4-8). Furthermore, there was literature suggesting that TNC may be associated with a worse clinical prognosis in a number of cancer types. Consequently, I decided to further investigate the relationship between ROCK activation and TNC expression.

A

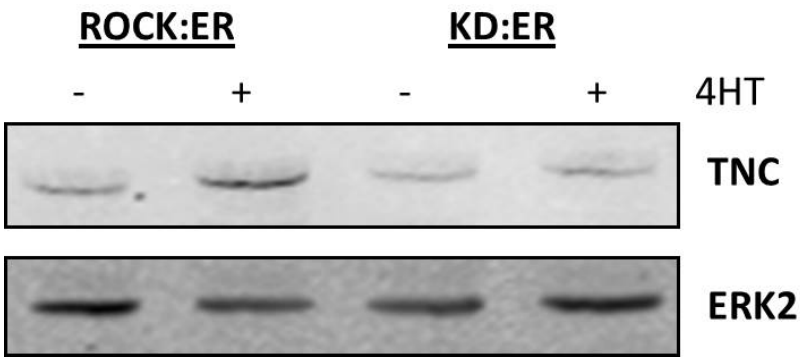

B

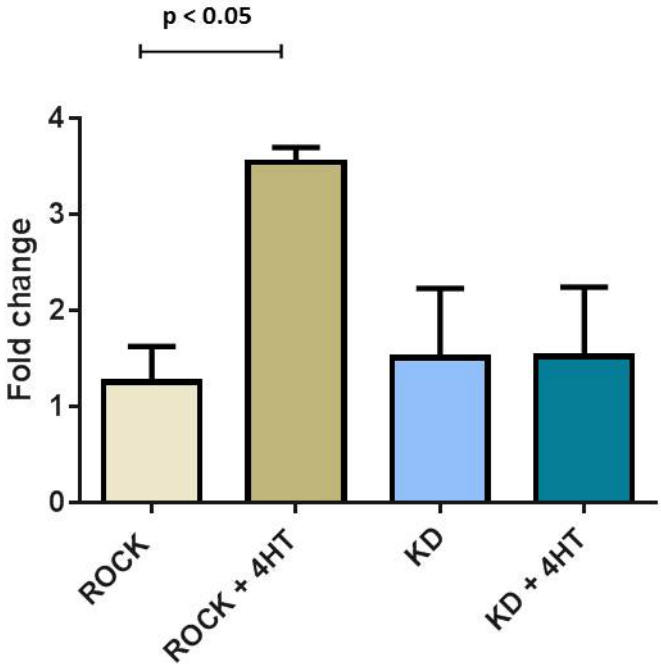

Figure 4-7 Tenascin C protein expression is increased in ROCK-activated cells.

Primary keratinocytes were isolated, cultured, and treated with 4-HT or ethanol vehicle. Lysates were prepared, and following protein electrophoresis and transfer, the membrane was probed for TNC (1:500) and ERK2 (loading control; 1:1000). A) Representative western blot showing increase in *Tnc* levels following treatment with 4-HT. B) Replicates of above (n = 2). Statistical significance determined by ANOVA.

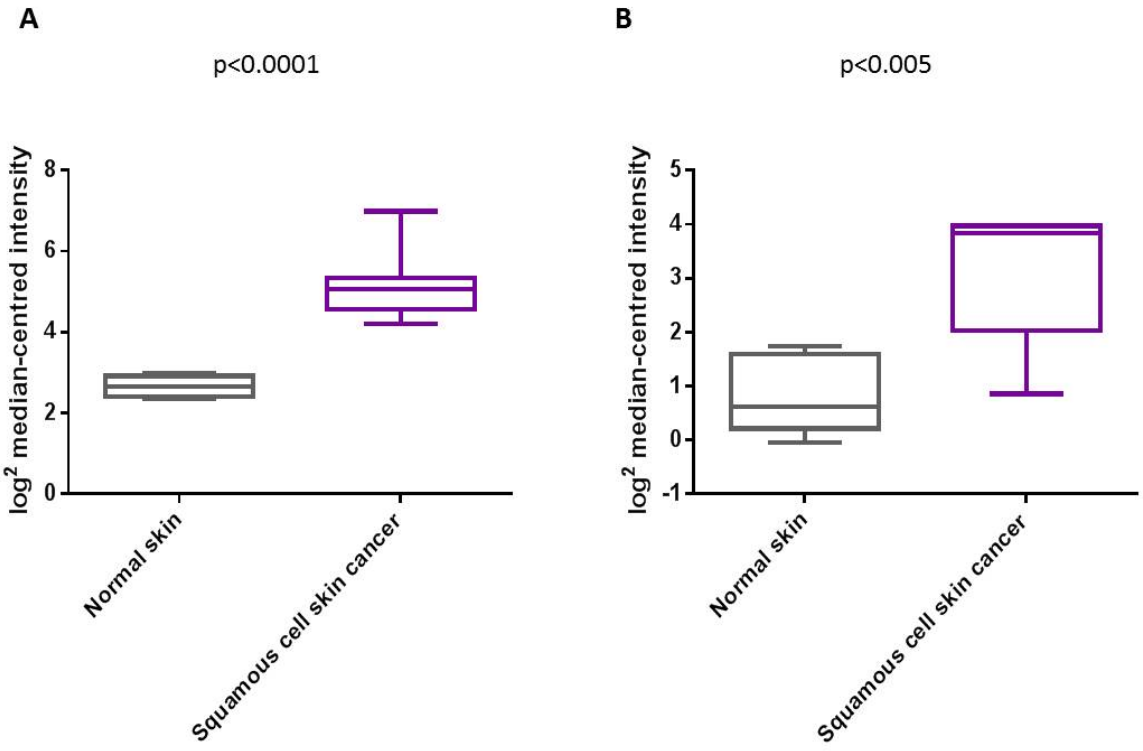

Figure 4-8 *TNC* expression is increased in squamous skin cancer versus normal skin samples

Log^2 median-centred *TNC* mRNA expression in normal versus squamous skin cancer samples from A) Riker et al [483] and B) Nindl et al [484]. Statistical significance of differences was determined by an unpaired t-test.

4.5 ROCK activation increases TNC expression in murine skin *in vivo*

Previous work carried out in the laboratory had revealed that ROCK activation led to an increase in skin thickness and stiffness. This work had used phosphorylation of MYPT1 in the epidermis to confirm ROCK activation [83,479]. I considered the possibility that TNC may be one of the components contributing to the observed thickening, and so decided to activate ROCK *in vivo*, using the K14 ROCK:ER animal model, and then examine the skin for TNC expression. In order to do so, I used two methods: the first of these was to commence K14 KD:ER and ROCK:ER animals on a tamoxifen diet. This was an attractive approach as it is less stressful for animals than topical or invasive (i.e. intraperitoneal) methods, can be continued for a relatively lengthy period and in theory should cause ubiquitous transgene expression. Age- and weight-matched animals were fed tamoxifen diet for a period of 36 days. The animals and the food were weighed 3 times per week to ensure that they were maintaining an adequate nutritional status; initially, both groups experienced a degree of weight loss. This is a common issue when using tamoxifen diet, but tends to be overcome after approximately one week, as was the case in this experiment. However, following stabilisation of the animals' weight, no subsequent weight gain was observed. At the end of the experimental period, the animals were humanely euthanized and the back skin was dissected and placed in formalin. Staining for haematoxylin and eosin (H&E), and TNC did not reveal any difference between the two groups. I suspected that this may reflect inadequate intake or reduced oral absorption due to the absence of weight gain, and therefore I considered an alternative approach, namely the topical application of 4-HT directly to the ear skin of K14 KD:ER and ROCK:ER mice. Six KD mice and five ROCK mice were treated, and 500 µg was applied to each ear daily for 21 days. Subsequently, the animals were humanely euthanized, and the ears were removed and placed in formalin, before being embedded in paraffin, sectioned and stained for H&E and TNC. In the ROCK-activated animals, I noted a substantial increase in TNC deposition in the junction between the epidermis and dermis (Figure 4-9).

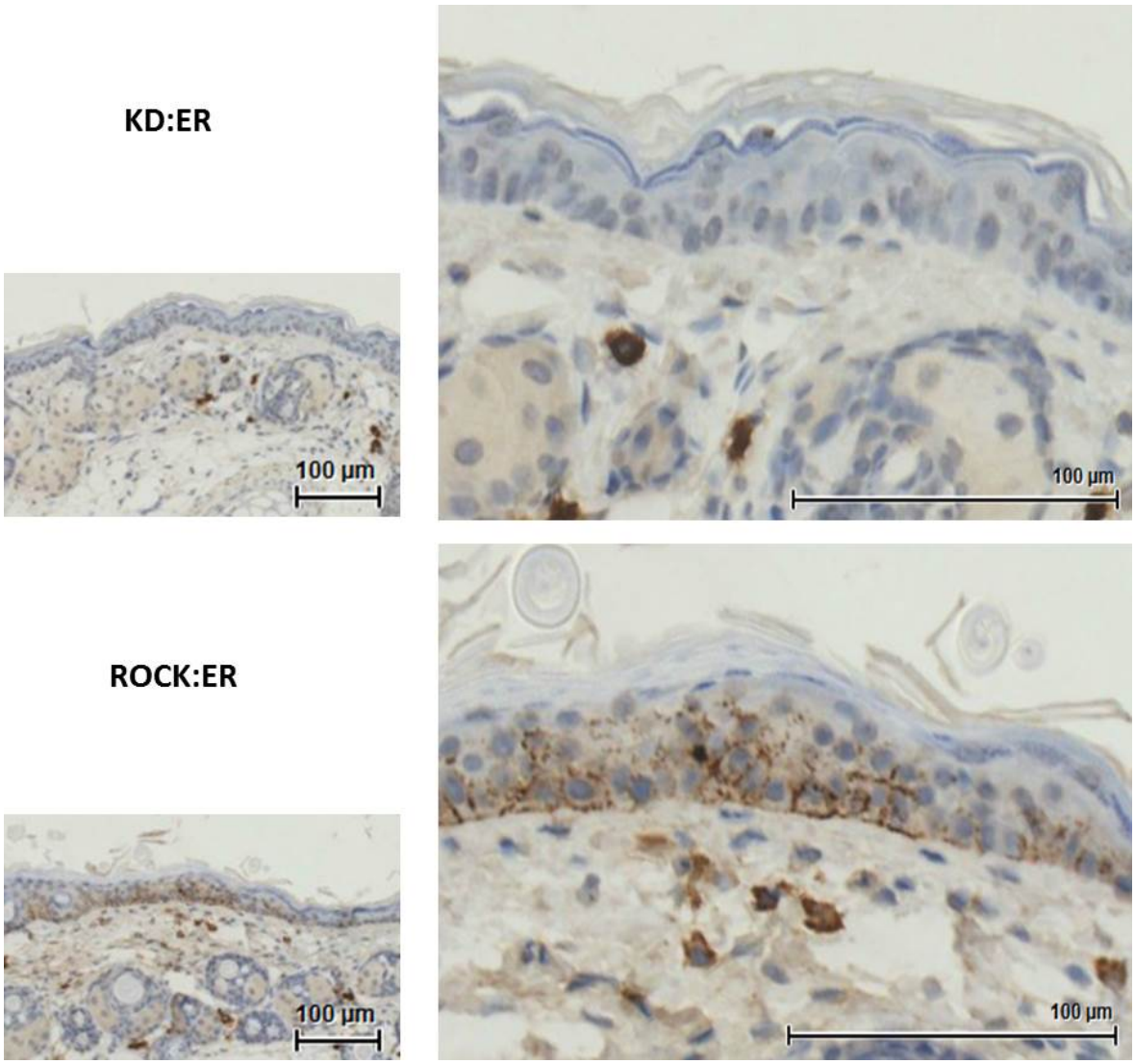

Figure 4-9 Increased TNC staining is localised to sites of cell-cell adhesion following ROCK-activation in keratinocytes.

K14 KD:ER and K14 ROCK:ER animals were treated with topical 4-HT for 36 days. At the completion of treatment, animals were humanely euthanized and the ears were processed at the Beatson Institute core histology facility. TNC staining was negligible in the KD:ER animals; distinct TNC staining was apparent at the sites of cell-cell adhesion in the ROCK:ER animals. Representative examples from one KD and one ROCK animal; total numbers, 6 KD:ER and 5 ROCK:ER animals.

4.5.1 ROCK activation in a tumorigenic model increases TNC deposition

In order to further investigate the interaction between ROCK activation and TNC expression in the context of malignancy, a collaboration was established between our laboratory and the laboratory of Dr David Greenhalgh in the Department of Dermatology, University of Glasgow, with a contribution by Ms Siti Masre, who established the crosses between genetically modified animal models and performed the application of topical 4-HT at the University of Glasgow animal facility. This involved animal models expressing various oncogenic driver mutations and loss of tumour suppressor genes, in isolation and in combination, including epidermis-specific expression of c-fos, H-RAS mutation, and PTEN deletion ($PTEN^{null}$). These tumour models were crossed with the K14 ROCK:ER model, and ROCK was activated by application of topical 4-HT. A comparison was made between the RAS/c-fos/$PTEN^{null}$ animals with and without ROCK:ER expression. Most animals, regardless of ROCK activation, developed papillomas following treatment with 4-HT for 8-10 weeks. However, following 13 weeks of 4-HT application, the animals expressing ROCK:ER exhibited malignant conversion and were observed to develop foci of squamous skin cancer. On obtaining sections from the malignant tumours, I carried out TNC staining and found a significant upregulation of TNC expression in the mutant RAS plus ROCK specimens (Figure 4-10). Rho has been shown to act downstream of RAS in transformed fibroblasts, relaying proliferative signals [485]. In murine models expressing oncogenic RAS and conditionally active ROCK, papillomas expressed low levels of TNC. Following malignant conversion to squamous cell cancers, which occurred only in ROCK-activated animals, TNC expression increased. The implication may be that, through the increased proliferation and cytoskeletal tension seen through RAS/ROCK co-operation, deposition of tumorigenic ECM components occurs.

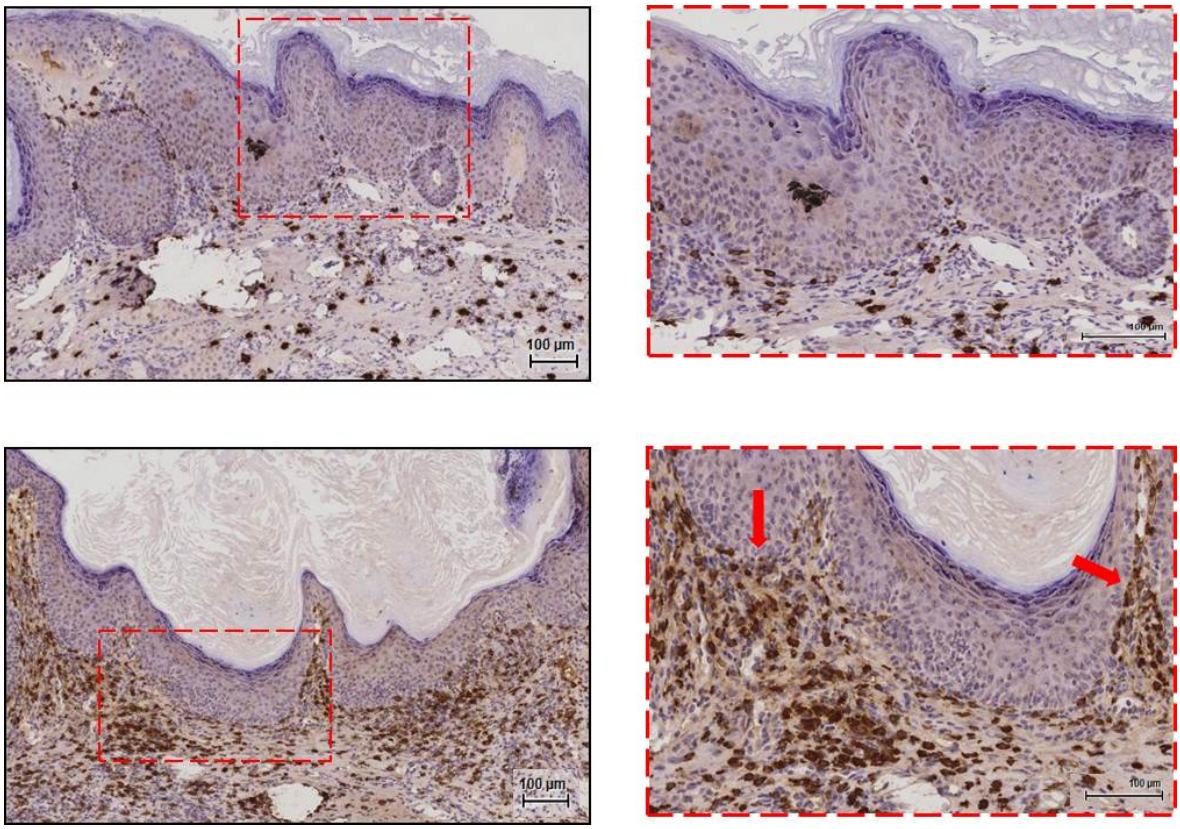

Figure 4-10 Increased TNC staining in a tumorigenic animal model with concurrent ROCK-activation.

Animals expressing mutant RAS in the epidermis were crossed with K14 ROCK:ER animals. ROCK activation was achieved by topical application of 4-HT for 13 weeks, and specimens of skin bearing papillomas with foci of malignant conversion were subsequently blocked, sectioned and stained for TNC. A significant increase in TNC deposition at the sites of cell-cell adhesion was observed in these animals compared with animals in which mutant RAS alone was present. The top panels show sections from animals expressing RAS treated with topical 4-HT. The lower panels show sections from animals expressing RAS and the ROCK:ER transgene treated with 4-HT. Scale bars represent 100 µm. Red arrows indicate the epidermal-dermal junction.

4.6 Investigating TGFβ as a contributing factor to ROCK-induced epidermal stiffening and thickening

As had previously been noted, ROCK activation was seen to increase stiffness and thickness of the epidermis through collagen and extracellular matrix deposition. This bears similarities to the process of fibrosis (an excess of connective tissue), which is observed:

- during wound healing (scar formation) [304]
- in rheumatological conditions such as systemic sclerosis (a multi-system autoimmune disorder characterised by the pathological accumulation of collagen)[486]
- within the tumour microenvironment in some cancer types (through the activation of cancer-associated fibroblasts) [312].

Keratinocytes and fibroblasts are known to interact in a number of ways, and it has been shown that fibroblasts can become activated to myofibroblasts through signalling pathways initiated by keratinocytes. In particular, increased mechanical tension and transforming growth factor beta (TGFß) activity are known to cause differentiation to a myofibroblast phenotype. These cells then have the capacity to synthesise collagen and other ECM components, leading to deposition of fibrotic tissue.

4.6.1 Investigating endogenous TGFβ levels

As I had observed that TNC expression appeared to be predominantly within the junction between the epidermis and dermis, I hypothesised that the keratinocytes within the epidermis may be prompting the dermal fibroblasts to produce TNC, along with other ECM components. I decided to investigate if ROCK activation, in addition to altering the mechanical tension of cells, may be contributing to TGFß signalling. In order to do so, I performed quantitative RT-PCR on cDNA prepared from ROCK activated keratinocytes with primers for *Tgfb*. This showed an increase in *Tgfb* transcripts following ROCK activation (Figure 4-11).

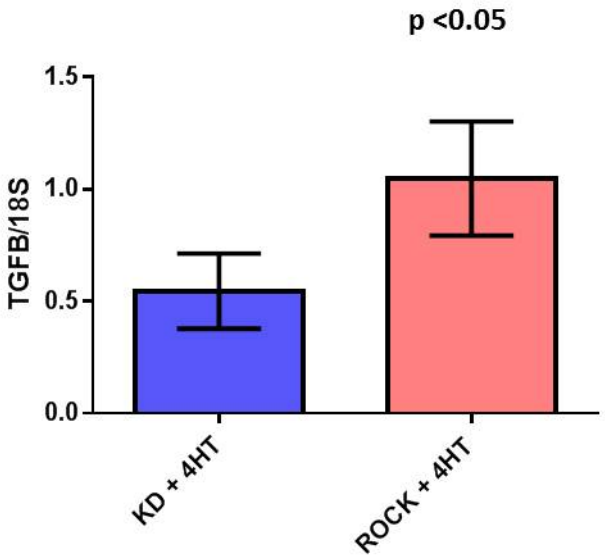

Figure 4-11 Increase in TGFβ transcripts following ROCK activation

RT-PCR (from 3 paired experiments) shows a statistically significant increase in TGFβ transcripts following ROCK activation in primary keratinocytes.

Subsequently, I isolated and cultured 3 pairs of primary keratinocytes from K14 KD:ER and ROCK:ER mice (the same type of cells and using the same technique as previously described). Following ROCK activation with 4-HT for 16 hours, I harvested the medium from the cells and, after using hydrochloric acid to activate latent TGFβ, went on to perform an enzyme-linked immunosorbent assay (ELISA). This did not show an increase in TGFβ1 levels in the ROCK-activated supernatant. However, I considered that this may be a consequence of culturing keratinocytes in isolation; I therefore attempted to develop a robust co-culture system to determine the impact of ROCK activation in keratinocytes on fibroblasts.

I initially adopted a “hanging drop” technique, in which primary keratinocytes were dyed and mixed with NIH3T3 fibroblasts and grown in a drop suspended from the lid of a cell culture dish. Unfortunately, it was not possible to maintain the viability of the primary cells in this context.

I went on to work with an NIH3T3 fibroblast cell line that had been stably transfected with a TGFβ reporter plasmid. This was a kind gift of Dr Gareth Inman, University of Dundee, Division of Cancer Research. Upon exposure to TGFβ, luciferase expression was induced and could be quantified on a luminometer. I first wanted to determine the sensitivity of the cell line; therefore, using recombinant human TGFβ (Peprotech), I established that the bioassay had a range of responsiveness from 50 pg/ml to 500 pg/ml (Figure 4-12). Thereafter, I cultured primary keratinocytes and reporter fibroblasts, activated ROCK in the keratinocytes, and carried out a luciferase reporter assay. No difference was apparent between co-cultured cells with or without ROCK activation, possibly as it was not feasible to activate latent TGFβ in a living cell system (Figure 4-13).

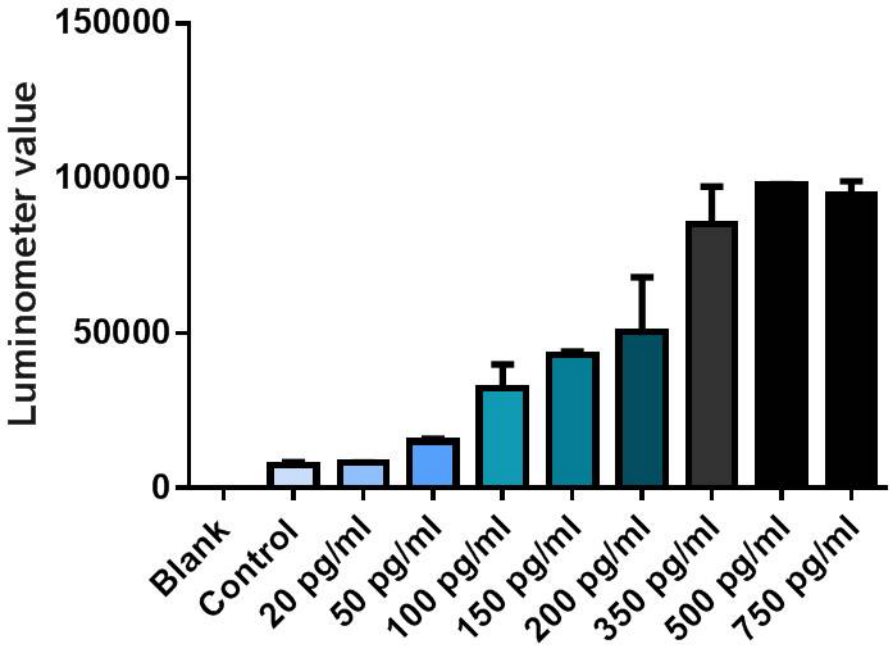

Figure 4-12 The TGFß bioassay has a range of responsiveness from 50 pg/ml to 500 pg/ml.

NIH3T3 fibroblasts had been selected to stably express a TGFß reporter. Serum-free medium with increasing concentrations of recombinant TGFß was added to the cells in a 24-well plate, and the cells were cultured at 37 °C overnight. Thereafter, a luciferase reporter assay was performed, and the read-out determined on a luminometer. At a concentration of 20 pg/ml, TGFß activity was not detectable. At concentrations above 500 pg/ml, there was no dose-response relationship. The sensitivity range was therefore determined to be 50 pg/ml to 500 pg/ml.

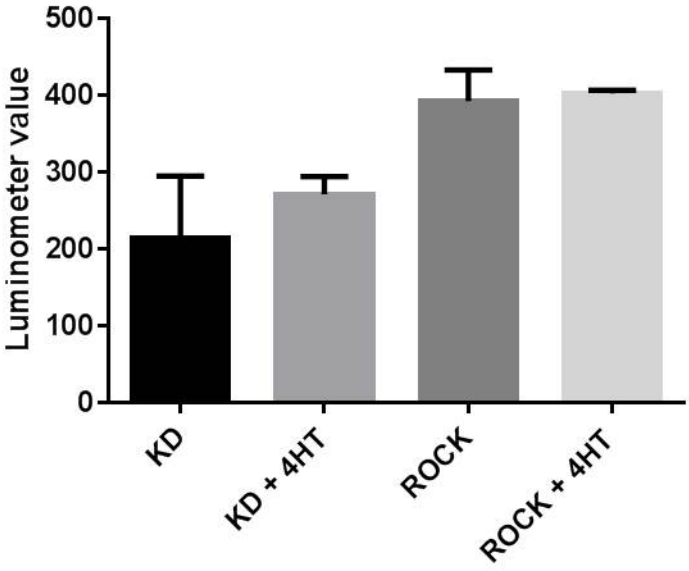

Figure 4-13 No increase in TGFß is detected following ROCK activation of primary keratinocytes using a fibroblast reporter system
Reporter NIH3T3 cells were established in culture. The following day primary ROCK:ER or KD keratinocytes were added to the fibroblast culture, and subsequently treated with 4-HT or vehicle. Thereafter a reporter luciferase assay was performed on the medium. Luminometer values are plotted, corrected for protein concentration. No statistically significant difference was apparent between each condition. n = 2.

4.6.2 Using exogenous TGFβ to investigate effects on the actin cytoskeleton and the extracellular matrix

As there appeared to be inherent difficulties in determining the part played by endogenous TGFß in the observed changes in epidermal composition, I elected to delineate the effect of adding exogenous recombinant TGFß (rTGFß) to cells. I serum starved parental NIH3T3 fibroblasts and added rTGFß at a range of concentrations (500 pg/ml to 10 ng/ml) for 16 hours. I subsequently prepared protein lysates, and following protein electrophoresis I probed the membrane with antibody against pMLC. This confirmed that at a dose of 10 ng/ml there was an increase in pMLC, indicating that TGFß also impacts turnover of the actin cytoskeleton (Figure 4-12).

I went on to determine if there was an additive effect of activating ROCK and treating cells with rTGFß. To do this, I used NIH3T3 fibroblasts expressing KD:ER or ROCK:ER transgenes, and added 4-HT alone, rTGFß alone, and both treatments together. Cell lysates were again prepared, and I carried out a western blot, probing for TNC and pMLC. This confirmed that the greatest increase in both pMLC and TNC was seen in those cells treated with rTGFß concurrent with ROCK activation (Figure 4-13). This suggested that both cellular mechanical tension and TGFß are participants in determining ECM component production, with a cumulative effect when both factors are present.

A

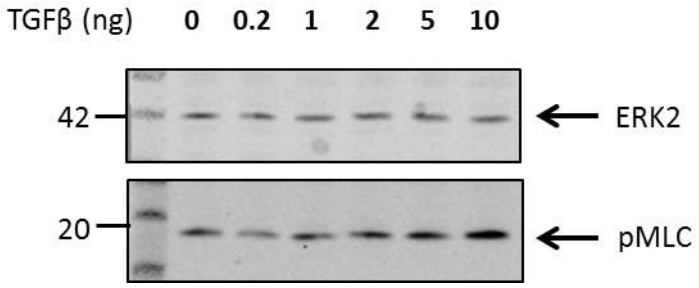

B

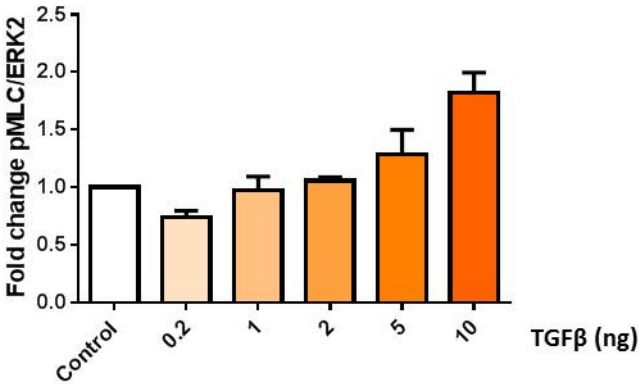

Figure 4-14 Phosphorylation of myosin light chain is increased following treatment with rTGFß

A) Representative western blot of NIH3T3 fibroblasts treated with rTGFß showing a dose-dependent increase in pMLC. Parental NIH3T3 fibroblasts were plated at $1x10^5$ cells per well of a 24-well plate. 24 hours later, serum-free medium was added with increasing concentrations of rTGFß (200 pg/ml, 1 ng/ml, 2 ng/ml, 5 ng/ml, 10 ng/ml). Cells were cultured at 37 °C for 24 hours, and protein lysates were made. The membrane was probed with pMLC antibody (1:500); ERK2 served as a loading control(1:1000). B) Quantification of western blots, showing the fold change in pMLC relative to ERK2 levels; n = 2. One-way ANOVA p = 0.0017.

A

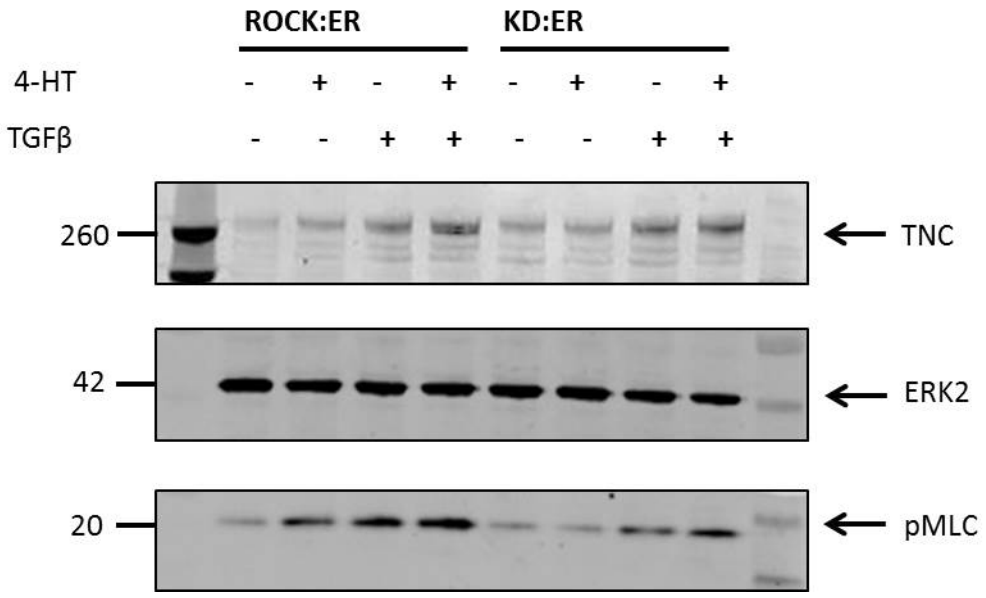

B

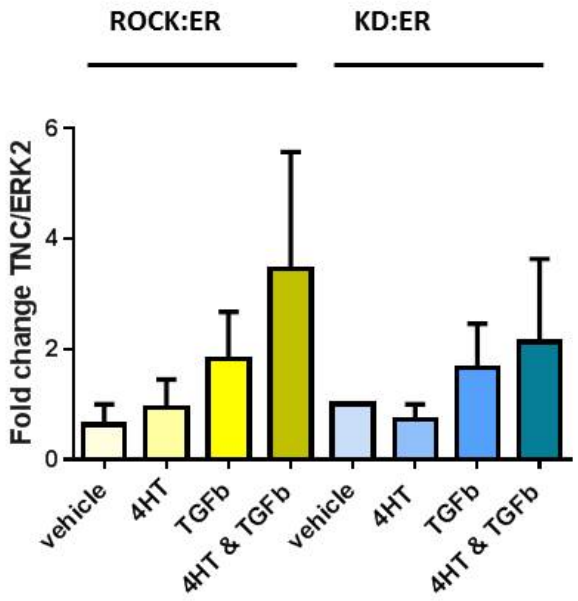

Figure 4-15 ROCK activation and TGFβ combine to increase pMLC and TNC expression

A) Representative western blot of NIH3T3 fibroblasts +/- ROCK activation and +/- TGFβ. NIH3T3 cells stably expressing the ROCK:ER or KD:ER transgene were plated at $3x10^5$ cells per well of a 6-well plate. 12 hours later, cells were washed with PBS, and serum-free medium plus 4-HT (1 μM)/ethanol vehicle +/- TGFβ (10 ng/ml) was added. Cells were incubated at 37 °C for 16 hours before lysates were prepared. The membrane was probed with antibodies against TNC (1:500) and pMLC (1:500), and ERK2 (1:1000) served as a loading control. The highest levels of TNC and pMLC were observed in ROCK-activated cells treated with TGFβ. B) Quantification of western blots, showing the fold change in TNC relative to ERK2 levels; n = 3. NS

4.7 Regulation of TNC expression

I undertook further review of the literature, which revealed that TNC is regulated by megakaryoblastic leukaemia 1 (MKL1; also known as myocardin-related transcription factor A (MRTFA)), a member of the myocardin-related transcription factor family. MKL1 interacts with serum response factor (SRF) to activate transcription of genes with serum response element (SRE)-containing promoters. In turn, MKL1 is regulated through its interaction with actin, remaining localised within the cytoplasm in association with G-actin when unstimulated, and translocating to the nucleus when the balance shifts towards F-actin production.

As a consequence, I sought to determine if ROCK transgene activation would cause MKL1 to accumulate within the nucleus and thus, by implication, induce TNC expression. To do so, I initially plated NIH3T3 ROCK:ER fibroblasts and activated ROCK with 4-HT for 16 hours; subsequently, I prepared nuclear and cytoplasmic extracts, using the Thermoscientific NE-PER Nuclear and Cytoplasmic Extraction kit. I went on to perform a western blot, probing for MKL1 in the nucleus (using Lamin A/C antibody to ensure that the extracts were entirely nuclear in origin) and in the cytoplasm (with GAPDH antibody to determine that extracts were cytoplasmic). I did not detect a discernible difference in MKL1 levels following ROCK activation; I hypothesised that this may have been as consequence of culturing the cells on a stiff (i.e. non-physiologically representative) surface. To further evaluate this, I plated NIH3T3 ROCK:ER fibroblasts on glass coverslips and activated ROCK with 4-HT for 16 hours before fixing and permeabilising cells, then probing with anti-MRTFA antibody (1:50 for 1 hour at room temperature; Santa Cruz). The cells were subsequently visualised on a Zeiss 710 upright confocal microscope. I felt that those ROCK-activated fibroblasts that exhibited marked stress fibre formation possibly demonstrated greater levels of perinuclear MRTFA staining, while vehicle treated cells showed predominantly cytoplasmic staining (Figure 4-14). The data are not sufficiently convincing to draw any conclusions, but this could be an area worthy of further investigation.

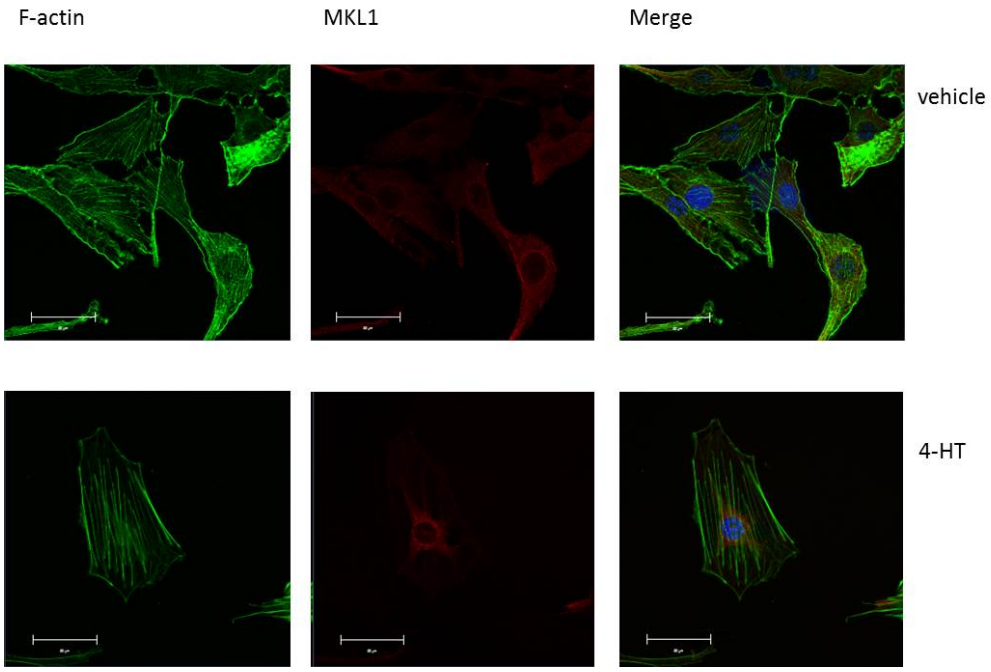

Figure 4-16 Perinuclear localisation of MKL1 following ROCK activation.

Representative immunofluorescence confocal images of serum-starved ROCK:ER NIH3T3 fibroblasts treated with 4-HT or ethanol vehicle and stained for F-actin (left panels) and MKL1 (centre panels). Cellular nuclei, stained with DAPI, are shown in blue in the merged images (right panels). Scale bars represent 20 μm. After plating on glass coverslips, cells were serum-starved and treated with 4-HT or ethanol vehicle for 16 hours, then fixed and stained as described previously. Confocal images were obtained using a Zeiss 710 upright confocal microscope. ROCK-activated cells with prominent stress fibre formation show possible localisation of MKL1 around the nucleus.

Next, to look specifically at the effect of ROCK activation on SRE, I obtained a plasmid construct: SRE fused to a secreted alkaline phosphatase (SEAP) reporter. This was a kind gift of Professor Ruth Chiquet-Ehrismann, Friedrich Miescher Institute for Biomedical Research, Basel. I transfected the plasmid into NIH3T3 cells with the KD:ER and ROCK:ER transgenes using Lipofectamine 2000, and following 16 hours of serum-starvation and treatment with 4-HT or ethanol vehicle, I determined the level of SEAP in the culture supernatant. In parallel, I transfected identical cells with secreted *Metridia* luciferase construct, to ensure transfection efficiency. I found there was a non-significant > 2-fold increase in SEAP activity in ROCK-activated cells compared with vehicle-treated or KD cells; *Metridia* luciferase activity remained relatively constant across all conditions (Figure 4-15). These results confirmed that SRE and MKL1 localisation are influenced by ROCK activation; this is borne out by the knowledge that Rho family members upregulate SRE gene expression [487].

A

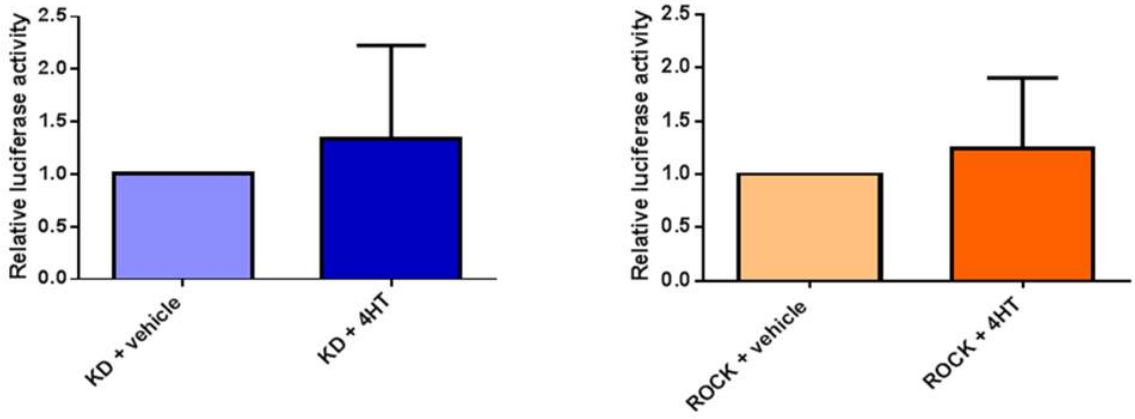

B

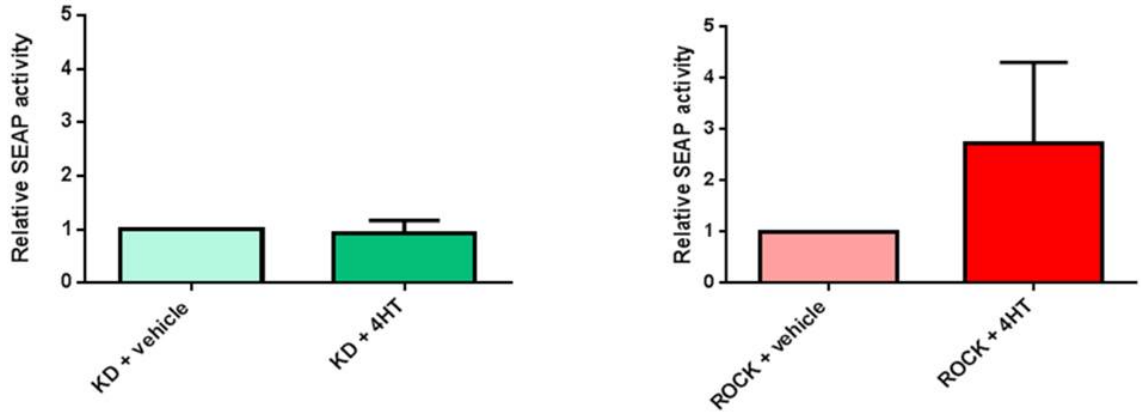

Figure 4-17 ROCK activation causes an increase in SRE-SEAP activity

NIH3T3 fibroblasts stably expressing the KD:ER or ROCK:ER transgene were transiently transfected with A) *Metridia* secreted luciferase plasmid or B) SRE-SEAP plasmid, then cultured in serum-free medium with 4-HT or ethanol vehicle for 16 hours. Luciferase reporter assay showed no difference following ROCK activation; SRE-SEAP levels were increased following ROCK activation. Results shown are for 4 independent experiments; the increase in SRE-SEAP following ROCK activation did not reach statistical significance (determined by unpaired t-test. p=0.071).

4.8 Altering the stiffness of the cell culture substrate impacts cell behaviour

Having observed that TGFß was capable of enhancing the effect of ROCK activation in terms of ECM component production, I next wished to investigate the impact of altering the tension of the surface that cells are cultured upon.

In order to perform these experiments, I obtained Excellness® biomimetic tissue culture plates of differing levels of stiffness, to replicate a physiological cellular environment. I chose to use 2 kPa plates, with a surface approximately analogous to fat or brain tissue, denoted “soft”, and 30 kPa plates, representing intestinal tissue, denoted “medium”. In addition, I used conventional plastic tissue culture dishes which, with a stiffness of >10,000 kPa are most similar to mammalian bone, and are denoted “hard”.

4.8.1 Levels of myosin light chain phosphorylation are increased in cells cultured on stiffer surfaces

First, I wanted to investigate whether simply culturing cells on a stiffer surface would be sufficient to promote an increase in phosphorylation of myosin light chain. To do this, I plated parental NIH3T3 fibroblasts at 1 x 10^5 cells in 3 cm dishes of differing stiffness for 24 hours. Subsequently, I used SDS lysis buffer to prepare protein lysates. Due to the nature of the soft polymer surface, it was not possible to use traditional cell scrapers; therefore, a pipette tip was used to lyse cells and transfer them to a column to undergo homogenisation. Thereafter, the protein concentration was determined, and the samples were run on a gradient gel. Following transfer, the membrane was probed with antibody against pMLC. This revealed that a consistently higher level of pMLC was seen in cells plated on a stiff surface when compared with those cultured on a softer substrate (Figure 4-16 A, B).

4.8.2 ROCK activation and stiff culture substrate have a cumulative effect

Next, I wanted to determine the effect of combining ROCK activation with culturing cells on a stiffer surface. This was an effort to replicate the cytoskeletal alterations a cell experiences when maintaining force equilibrium in

response to increasing external tension. I plated NIH3T3 cells with the ROCK:ER transgene stably expressed on both Excellness® plates (2 kPa and 30 kPa) and conventional tissue culture plates (>10,000 kPa). 24 hours after seeding, the cells were treated with serum-free medium containing 4-HT or ethanol vehicle for 16 hours. Subsequently, I prepared protein lysates and performed a western blot. This confirmed that, in cells plated on a stiff surface, ROCK activation had an additive effect, with the greatest level of pMLC observed in these conditions (Figure 4-16 C).

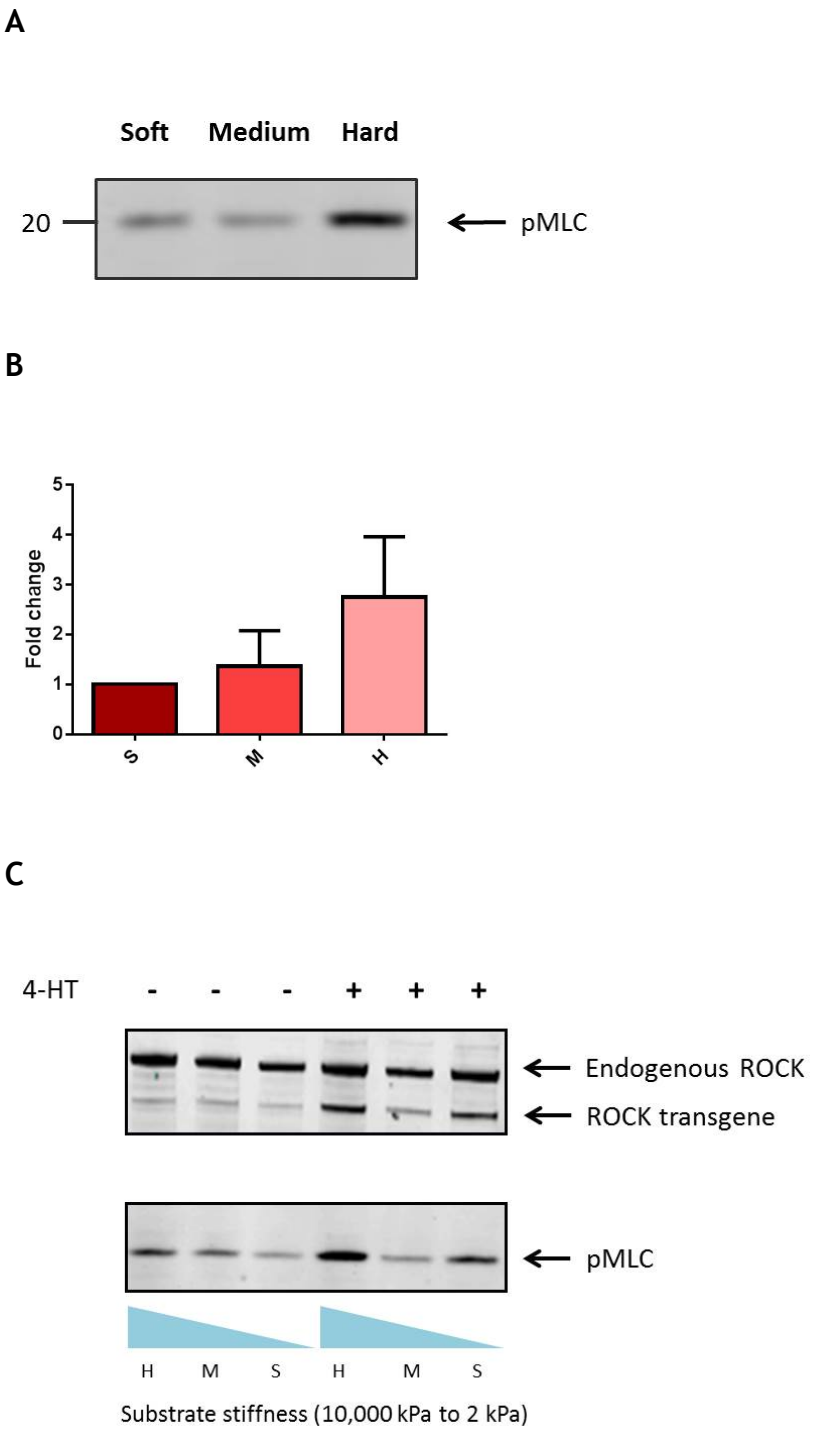

Figure 4-18 Cells grown on stiff culture substrates have increased levels of pMLC.

A) Representative western blot of parental NIH3T3 fibroblasts cultured on hard (conventional tissue culture plastic; >10,000 kPa), medium (30 kPa), and soft (2 kPa), substrates for 24 hours. Protein lysates were prepared and western blot carried out, showing that levels of pMLC were significantly higher in those cells cultured on the stiff substrate than those cultured on softer substrates. B) Graph of replicates showing quantification of fold change relative to loading control (ERK2); n=3. C) The experiment was repeated with NIH3T3 ROCK:ER fibroblasts; 4-HT or ethanol vehicle was added to serum-free medium on cells for 16 hours prior to harvesting protein lysates. The increase in pMLC was greatest in those cells in which ROCK activation occurred in the context of culture on a stiff surface. Endogenous ROCK acted as a loading control (1:1000).

4.8.3 The impact of differing levels of stiffness on TNC expression

The relationship between differing levels of stiffness, ROCK activation and TNC expression was less clear-cut, with a degree of variability between experiments. Taking this into account, I queried whether using rTGFß to treat cells on different substrates would enable subtle alterations in TNC expression to be more accurately determined. To do this, I plated parental NIH3T3 fibroblasts on different substrates (soft, medium and hard) and after 24 hours added serum-free medium +/- rTGFß. TNC levels were higher (as determined by western blot) in cells treated with rTGFß on all surfaces, but the greatest increase was observed in treated cells on a stiff surface (Figure 4-17). Thus, I concluded that a relationship exists between intra- and extracellular tension, TGFß, and synthesis of ECM components.

A

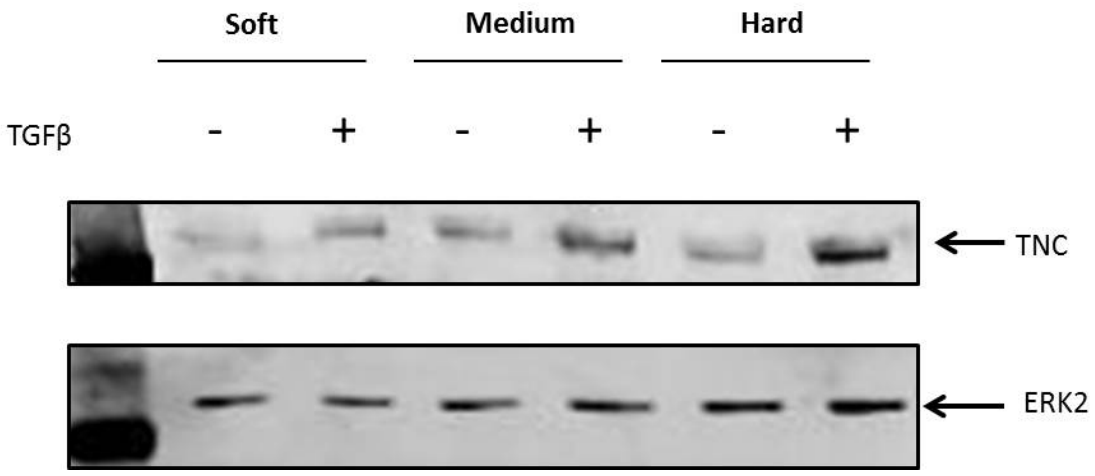

B

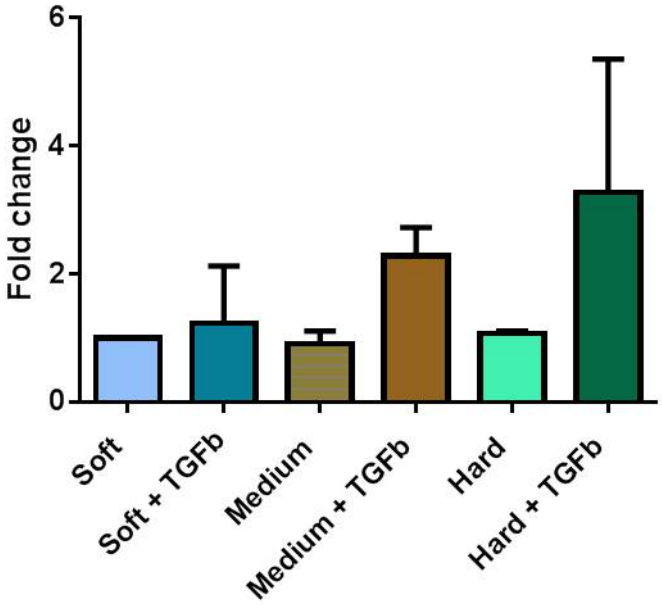

Figure 4-19 TNC expression is highest in cells plated on a stiff substrate and treated with rTGFß

A) Representative western blot showing increased levels of TNC in cells plated on a stiff substrate and treated with TGFß. NIH3T3 fibroblasts were plated on soft, medium and hard substrates (as previous) and treated with rTGFß for 16 hours. Subsequently, protein lysates were prepared and a western blot carried out to determine TNC levels. ERK2 was probed as a loading control. B) Quantification of fold change in TNC determined from 3 replicates of the experiment.

4.9 The transition from fibroblast to myofibroblast is triggered by alterations in the actin cytoskeleton

Next, I wanted to investigate the mechanism by which cells were producing ECM components. Evidence suggests that the activation of fibroblasts to myofibroblasts leads to the adoption of a pro-fibrotic phenotype; cells consequently exhibit enhanced secretory and contractile properties. α smooth muscle actin (α SMA) is the classic marker of myofibroblast activity, and can be used to illustrate the transition from quiescent fibroblast to activated cell. I therefore considered if the factors I had been investigating (1. cytoskeletal remodelling through intrinsic ROCK activation; 2. TGFß stimulation of cells; and 3. altering the stiffness of cell culture substrates) could, in isolation and/or combination be prompting the development of myofibroblasts and consequent production of TNC. I therefore used antibody raised against α SMA to investigate this. I found that ROCK activation in/TGFß treatment of cells plated on a soft or medium surface was sufficient to drive an increase in α SMA expression. However, cells plated on a stiff substrate displayed baseline higher levels of α SMA, with no discernible increase following ROCK activation (Figure 4-18) or TGFß exposure (Figure 4-19). This reinforces the integral role the cellular environment plays, illustrating that elements that affect the actin cytoskeleton have a different impact depending on the context in which the cell exists.

A

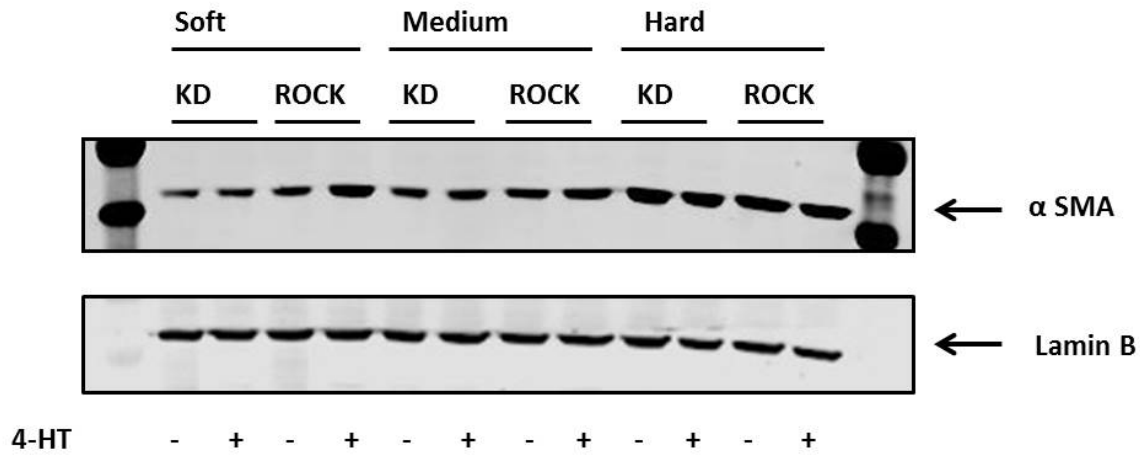

B

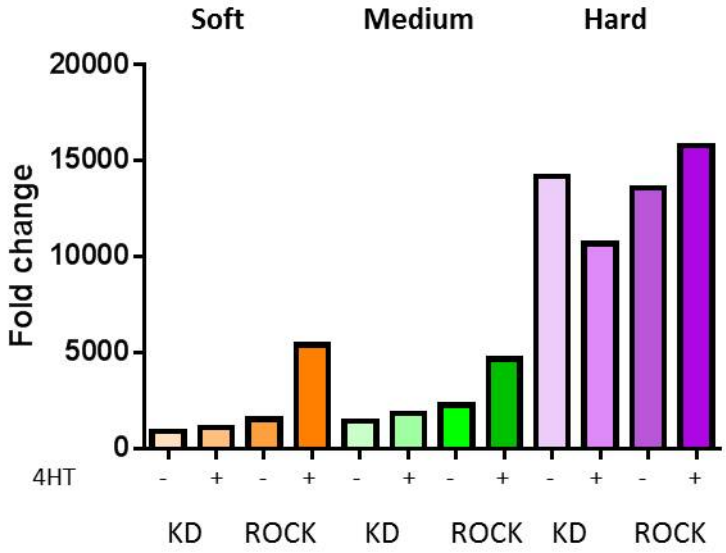

Figure 4-20 α SMA expression varies with substrate stiffness and ROCK activation

A) Representative western blot showing increased α SMA in ROCK-activated cells on a soft or medium stiffness substrate, and in all cells (+/- ROCK activation) plated on a stiff substrate. NIH3T3 fibroblasts expressing the KD:ER or ROCK:ER transgene were plated on soft, medium, and hard surfaces at a concentration of $1x10^5$ cells per plate, and treated with 4-HT(1 μM) or ethanol vehicle in serum-free medium for 16 hours. Protein lysates were prepared and, following gel electrophoresis and transfer, the membrane was probed with antibody against α SMA (1:200). Lamin B antibody was used as a loading control (1:500). B) Fold change in α SMA levels (relative to Lamin B; fold change in arbitrary units).

A

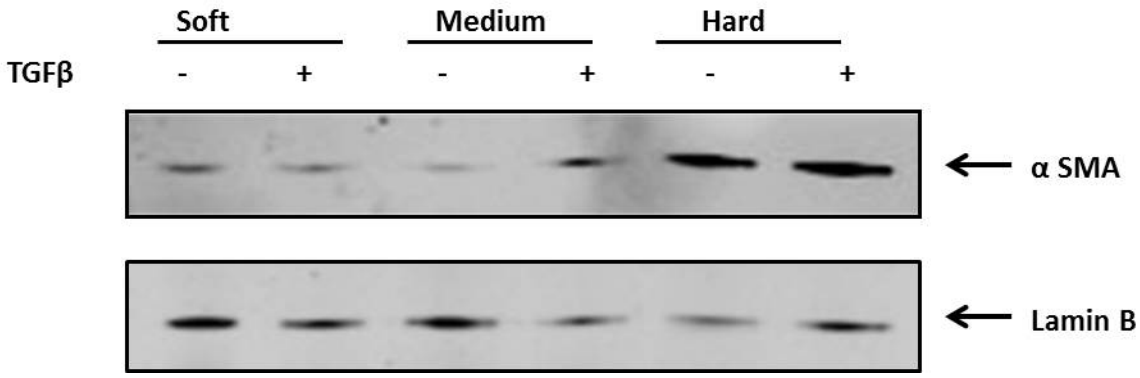

B

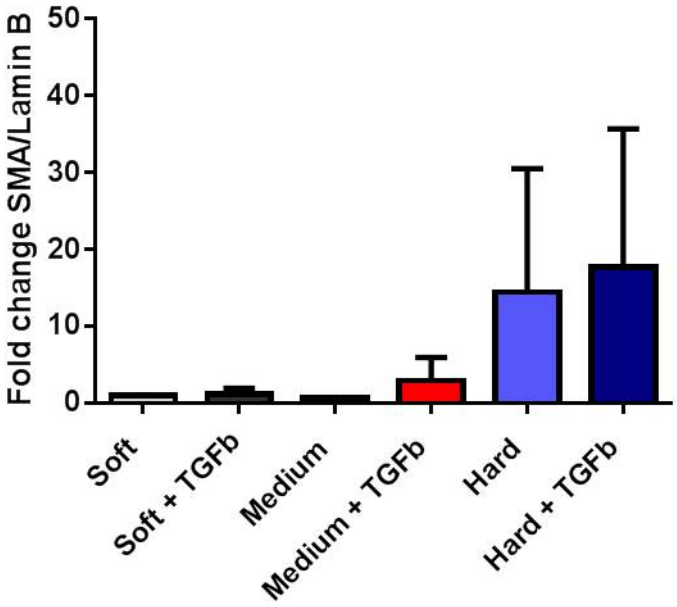

Figure 4-21 α SMA expression varies with substrate stiffness and TGFß treatment

A) Representative western blot showing increased α SMA in TGFß-treated cells on a medium stiffness substrate, and in cells plated on a stiff substrate regardless of TGFß exposure. Parental NIH3T3 fibroblasts were plated at $1x10^5$ cells per plate for 24 hours, before washing and adding serum-free medium +/- rTGFß (10 ng/ml). Western blot was performed on protein lysates, and the membrane was subsequently probed with α SMA antibody (1:200). Lamin B was probed as a loading control (1:500). B) Quantification of the fold change in α SMA in TGFß treated cells (n = 2).

4.10 Summary

In summary, the results presented in this chapter show that:

- ROCK activation in primary keratinocytes leads to increased ECM component expression
- TNC is one of these components
- ROCK activation *in vivo* also leads to increased TNC deposition in the epidermis and dermis of GM mice
- This effect is enhanced in a tumorigenic animal model with mutant RAS and ROCK activation
- A synergistic effect is observed between increased substrate stiffness, ROCK activation and exogenous TGFβ, suggesting a potential positive feedback cycle that may drive the transition of fibroblast to CAFs

5 RNA sequencing of ROCK-activated versus control epidermal keratinocytes

I undertook RNA sequencing in order to verify and expand on the results garnered by carrying out the ROCK-activated keratinocyte microarray experiments.

5.1 RNA quality control assessment

As previously described, I isolated primary keratinocytes from epidermis taken from the tails of K14 ROCK:ER mice; once established in culture, the cells were treated with 4-HT or ethanol vehicle for 16 hours. Thereafter, RNA was isolated from the cells and a quality control check was performed using the Agilent Bioanalyzer 2100. This assigns an RNA integrity number (RIN) to each sample, with 10 corresponding to a pure, non-degraded sample and 1 corresponding to a completely degraded sample. It is recommended that samples with an RIN of less than 7 are not utilised in experiments. This confirmed that the RNA was of sufficient quality to proceed to sequencing (Figure 5-1).

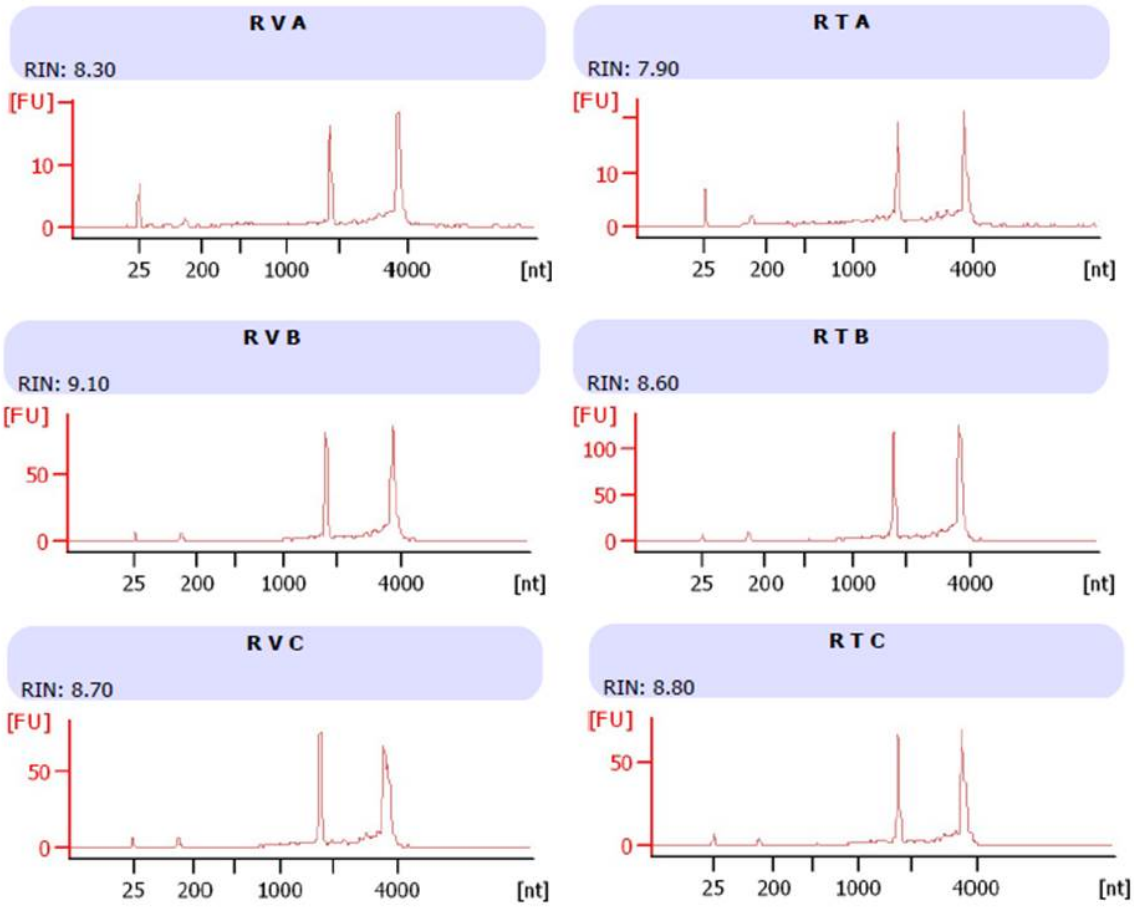

Figure 5-1 Agilent Bioanalyzer 2100 RNA read-out

Results from analysis of RNA isolated from primary keratinocytes confirmed that samples were sufficiently intact to proceed to further interrogation (RIN values ranging from 7.90 to 9.10).

5.2 RNA sequencing

Having confirmed that the RNA was of adequate integrity, RNA sequencing was performed on the Illumina® NextSeq 500 platform. This revealed alterations in gene expression in those cells treated with 4-HT when compared with cells treated with vehicle (Figure 5-2).

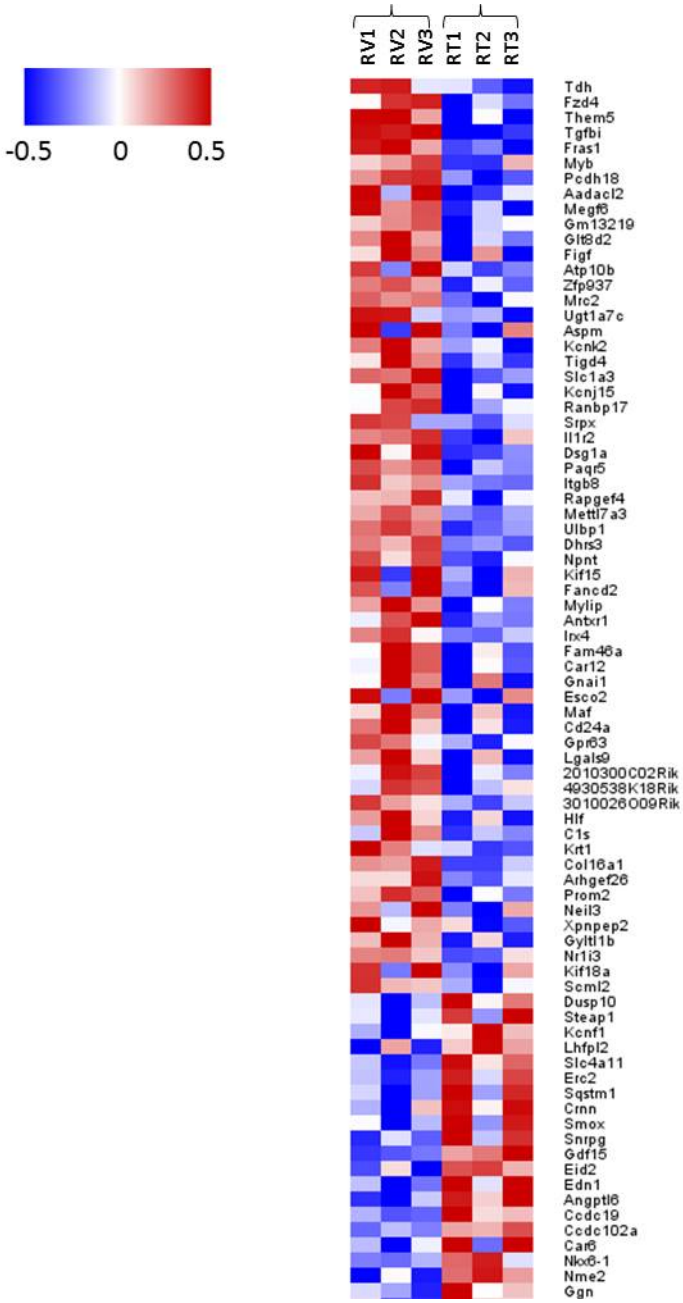

Figure 5-2 RNA sequencing heat map

Data analysis of RNA sequencing output confirms that genes are differentially expressed in keratinocytes with ROCK activation compared to those in which ROCK is not activated. The left hand columns (RV1, RV2 and RV3) represent three replicate experiments of cells treated with ethanol vehicle, while the right hand columns (RT1, RT2 and RT3) represent three replicate experiments of cells treated with 4-HT. Heat map generated by Gabriela Kalna, Computational Biology Department, CRUK Beatson Institute.

A number of common pathways and networks were found to demonstrate different expression levels. Those genes with biological functions related to cancer showed the most frequent alterations (Table 5-1), while genes belonging to the “connective tissue” and “cell-to-cell signalling/cellular growth and proliferation” networks also displayed aberrant expression (Table 5-2).

A

Category (biological functions)	No of genes differentially expressed	p value
Cancer	59	9.32E-07-1.79E-02
Cell-To-Cell Signaling and Interaction	2	2.46E-05-1.79E-02
Tissue Morphology	1	2.13E-04-1.79E-02
Organismal Development	1	2.13E-04-1.79E-02
Cellular Growth and Proliferation	1	2.99E-04-1.79E-02
Cellular Development	1	2.99E-04-1.79E-02

B

Category (biological functions)	No of genes differentially expressed	p value
Cancer, Dermatological Diseases and Conditions, Organismal Injury and Abnormalities	33	9.32E-07
Cancer, Organismal Injury and Abnormalities	13	1.03E-05
Cancer, Gastrointestinal Disease, Hepatic System Disease, Organismal Injury and Abnormalities	6	2.71E-04
Cancer, Gastrointestinal Disease, Organismal Injury and Abnormalities	5	2.82E-04
Cell-To-Cell Signaling and Interaction, Molecular Transport, Small Molecule Biochemistry	1	1.81E-04
Cellular Movement	1	5.71E-04
Cell Morphology	1	6.88E-04
Cell-To-Cell Signaling and Interaction, Cellular Growth and Proliferation	1	1.13E-03
Cell Death and Survival	1	1.29E-03
Inflammatory Disease, Inflammatory Response, Respiratory Disease	1	6.00E-03
Lipid Metabolism, Molecular Transport, Small Molecule Biochemistry	1	1.00E-02
Cellular Growth and Proliferation	1	1.26E-02

Table 5-1 RNA sequencing data analysis (biological functions)

Interrogation of RNA sequencing data shows that genes with specific biological functions more frequently display altered expression levels.

Category (networks)	No of genes differentially expressed
Connective Tissue Disorders, Hereditary Disorder, Ophthalmic Disease	12
Developmental Disorder, Organismal Injury and Abnormalities, Renal Hypoplasia	12
Cell-To-Cell Signaling and Interaction, Cellular Growth and Proliferation, Hematological System Development and Function	12
Cellular Development, Skeletal and Muscular System Development and Function, Tissue Development	6
Hematological Disease, Nutritional Disease, Cell Morphology	6
Cell Cycle, Cell-To-Cell Signaling and Interaction, Cellular Growth and Proliferation	5
Cancer, Gastrointestinal Disease, Organismal Injury and Abnormalities	5
Cancer, Organismal Injury and Abnormalities, Tumor Morphology	5
Connective Tissue Development and Function, Nervous System Development and Function, Organ Morphology	1
Developmental Disorder, Hereditary Disorder, Ophthalmic Disease	1

Table 5-2 RNA sequencing data analysis (networks)

Genes that participate in networks related to connective tissue disorders, developmental disorders, and cell-to-cell signalling demonstrated a greater degree of discordance between those cells with and without ROCK activation.

6 Lifeact GFP enables live cell imaging of dynamic alterations in the actin cytoskeleton

"Lifeact" is a 17-amino-acid peptide fused to GFP that is able to bind to F-actin, yet does not corrupt normal cellular behaviour. It displays selective, low-affinity binding to actin structures, permitting direct visualisation of the actin cytoskeleton [488]. Transgenic mice expressing Lifeact have been generated to permit the study of actin structures in primary cells and animal models [489].

Transgenic mice that express Lifeact fused to GFP had been generated by the Beatson Institute transgenic facility. This had been achieved through use of pROSA26, a generic targeting vector, which was used in association with pBigT to target the ROSA locus. The Lifeact GFP was sub-cloned into the pBigT vector; subsequently, a larger fragment from pBigT was placed into the pROSA26 vector. The final step involved the extraction of the targeting sequence and insertion into the mouse genome. Using a Deleter Cre mouse, I established matings that produced progeny displaying ubiquitous Lifeact GFP expression. Initially I ensured that mice were expressing Lifeact GFP with the IVIS® Spectrum *in vivo* imaging system (Figure 6-1); thereafter I used GFP goggles to confirm expression, with GFP being detected primarily in the murine tail and feet.

I subsequently bred the Lifeact GFP animals with K14 ROCK:ER and K14 KD:ER mice, ultimately to derive homozygous ROCK/KD animals with global Lifeact GFP expression. Thereafter, I isolated epidermal tail keratinocytes as previously described, and established the cells in culture. Following treatment with 4-HT, I captured live time-lapse imaging of the cells using a Nikon Eclipse Ti microscope (Figure 6-2). This proved to be a useful method to visualise dynamic alterations in the cytoskeleton in live cells, and is a technique that can hopefully be utilised further in the future. The hypothesis being tested was that deriving animals with conditional ROCK expression and Lifeact GFP expression would enable the direct visualisation of altered live cell behaviour in real time. I anticipated that, following ROCK activation, the keratinocytes would display greater levels of motility and enhanced proliferation; I did not have sufficient time to test this adequately.

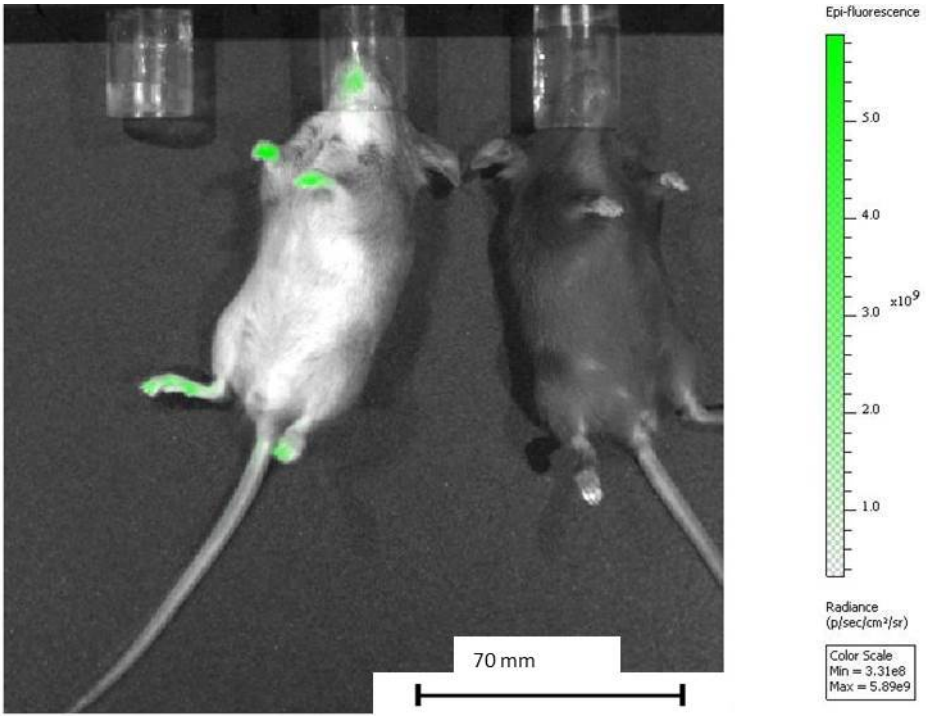

Figure 6-1 IVIS® Spectrum *in vivo* imaging system confirms Lifact GFP expression

The IVIS® imaging system permits live imaging of animals to ensure GFP expression. On the left is a Lifeact GFP mouse, with GFP evident in the feet and nose. On the right is a control mouse with no GFP expression evident.

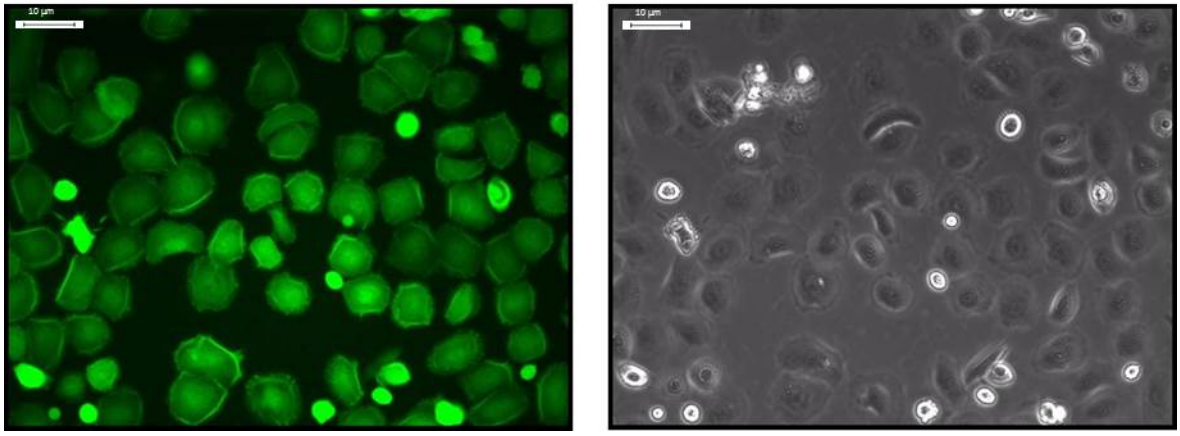

Figure 6-2 Lifeact GFP primary keratinocytes

Representative images of primary keratinocytes isolated from the epidermis of Lifeact GFP/ROCK:ER animals. The panel on the left shows cells visualised by fluorescent microscopy; the panel on the right shows the same cells under bright field microscopy. Images taken at 10X magnification.

7 Discussion

7.1 LIMK expression in colorectal cancer

7.1.1 Loss of LIMK in colorectal cancer versus other tumour types

The prevailing school of thought has long been that constituents of the Rho-ROCK pathway tend to be upregulated in cancer, due to their role in promoting cell motility. LIM kinase expression has been noted to be elevated in several cancer types, and shown to participate in tumour cell proliferation and invasion. Breast cancer cell lines expressing LIM kinase 1 demonstrate a proliferative, invasive phenotype with enhanced angiogenesis *in vitro* [107], while increased expression of LIMK1 in breast tumour xenografts promotes tumour growth [490]. A tumour-promoting role for the LIM kinases has also been identified in prostate cancer [108,491]. Furthermore, knockdown or inhibition of LIMK has been shown to reduce pancreatic cancer progression [110,492].

The assumption had been that, in the majority of cancer types, LIMK expression would directly correlate with the degree of invasiveness and aggression. However, when the role of actin cytoskeleton pathway members is examined out-with the conceptual framework of cell motility, it becomes clear that they participate in a range of other processes; indeed, the relative balance of the components may be the determinant of the metastatic potential of a cancer cell.

In response to cellular stress, such as ionising radiation or doxorubicin (a DNA-damaging chemotherapeutic agent that exerts a cytotoxic effect through intercalating DNA and binding to topoisomerase I and II) [493], the Rho-ROCK-LIMK pathway is activated [111]. *LIMK2* has previously been identified as a p53-responsive gene, and further studies have confirmed that *LIMK2* is a direct p53 target [111,112]. In turn, loss of *LIMK2* through knockdown or inhibition results in G2/M arrest when cells receive a genotoxic insult. Ultimately, it was shown that loss of *LIMK2* increases the sensitivity of cells to apoptosis through DNA-damage pathways. These findings are compatible with the knowledge that *LIMK2* regulates microtubule and spindle dynamics during mitosis [494]. The implication is that, in the context of colorectal cancer, where intestinal stem cells serve as

the cell of origin, silencing of LIMK through hypermethylation relieves constraints on gastrointestinal stem cell proliferation, thus facilitating tumorigenesis and tumour propagation.

There is evidence that downregulation of LIMK1 via diallyl disulphide compounds inhibits the migration and invasion of human CRC cell lines [495], thus highlighting the apparent disparate roles of LIMK1 and LIMK2 in the context of cancer. This should be borne in mind when considering the nuances of alterations in actin cytoskeleton pathway members and dynamics.

7.1.2 Prognostic and predictive factors in CRC

At present, a number of factors have been identified as prognostic and predictive markers of outcome in early stage CRC. These include pathological findings such as TNM staging, tumour perforation, degree of tumour differentiation and presence of lymphatic or vascular invasion [496], and evidence of pre-operative systemic inflammation (based on elevated serum C-reactive protein and/or hypoalbuminaemia) [497].

In advanced disease (inoperable locally advanced or metastatic), the presence of *KRAS* or *BRAF* mutations is deemed to be a negative prognostic indicator and is also predictive of a lack of response to EGFR inhibitor therapy such as cetuximab [163,498].

The ability to more accurately stratify patients by their risk of relapse/recurrence is a goal that has long been sought. It is becoming increasingly evident that CRC is a group of distinct entities, with some patients destined to have poor outcomes despite optimal adjuvant therapy, and some in whom the disease would be cured by surgery alone with no need to suffer the toxicities associated with systemic chemotherapy. Loss of LIMK2 is associated with poorer clinical outcomes; this could translate as a prospective prognostic biomarker, potentially being utilised as a method to determine which patients would derive the greatest benefit from adjuvant systemic treatment following surgical resection.

Furthermore, as loss of LIMK2 appears to play a pro-apoptotic role following treatment with DNA-damaging agents such as doxorubicin [111], this may influence the choice of cytotoxic agent used in the context of colorectal tumours with reduced LIMK2 expression. In addition, LIMK2 inhibition also appears to sensitise cells to a number of other compounds. These include Aurora A inhibitors, which synergise with shRNA-mediated silencing of LIMK2 to promote cell death [499], and RAS inhibitors, which co-operate with LIMK inhibition to reduce cell proliferation [500]. This could have future implications for the development of targeted, personalised cancer treatments for individual patients.

7.1.3 Mouse models of colorectal cancer

As stated in the CRC epigenetics section, an effect was noted in the AOM-DSS CRC model when LIMK2 was absent. The model I utilised (KRAS G12D mutant, APC mutant heterozygous) has a high propensity to malignant conversion, and therefore the effect of *Limk2* knock out was insufficient to produce a detectable difference. *Apc* mutant heterozygous mice, without KRAS mutation, are a good model for studying early events in CRC [501], and would possibly be appropriate for further investigation of the effect of *Limk2* loss.

7.1.4 Epigenetic manipulation in colorectal cancer

It has been shown that DNA hypomethylation inhibits intestinal tumorigenesis [502], consistent with my finding that hypermethylation, with consequent LIMK2 repression, accelerates colonic tumour progression. Treatment with DNMT inhibitors has been evaluated to a degree in CRC [503], where it was shown that DNMT inhibition potentiated the effects of standard cytotoxics on human CRC cell lines. The strategy of combining epigenetic therapies (including DNMT inhibitors and deacetylase inhibitors) with targeted therapies and chemotherapeutic agents in the treatment of solid tumours is one that is being continually evaluated in early phase clinical trials [504]. The knowledge that LIMK2 is hypermethylated could prove valuable in developing a predictive biomarker in CRC patients treated with epigenetic therapies.

7.2 Tumour microenvironment

I found that activating ROCK, and thus promoting actin stress fibre formation, led to the synthesis and deposition of ECM components, including TNC. As the density of the ECM increases, so does the mechanical tension within the stromal compartment and, as I showed in fibroblasts cultured on stiffer substrates, this alters the cellular phenotype to a more contractile myofibroblast, capable of depositing further ECM glycoproteins. This work was performed in a non-malignant context, but there is evidently considerable overlap between the alterations observed in benign fibrotic conditions and malignant desmoplastic tumour stroma. Certainly, ROCK inhibition has been evaluated and found to be effective in the reduction of hepatic fibrosis [505] and pulmonary fibrosis [506]. In the context of pancreatic ductal adenocarcinoma, a tumour type classically associated with desmoplasia and thus poor cytotoxic penetrance, ROCK inhibition has been utilised and found to reduce tumour collagen content (Whatcott Cancer Res 2012 (AACR abstract)). While other constituents of the stroma were not examined in this study, the question is raised: would ROCK inhibition reduce the TNC content of desmoplastic stroma? As previously outlined, a clear relationship exists between TNC and cancer progression; it would therefore be interesting to investigate the impact of ROCK inhibition on the TNC content of the tumour stroma and consequent tumour susceptibility to chemotherapeutic agents. It must be borne in mind that this work would need to be replicated in the cancer context to determine if the effects seen in fibrotic-like tissue are reproduced.

TNC knock out mice have been examined in cancer models, including the polyomavirus middle T breast cancer model [507]. It was found that the TNC null tumours formed smaller "nests", and the architecture of the stromal compartment was altered, with a significantly higher degree of immune cell (macrophage and monocyte) infiltration. This observation is of particular significance, given recent developments in the arena of cancer immunotherapy. It has been shown that stimulating the immune system, either through inhibition of the programmed death 1 (PD1) pathway or blockade of cytotoxic T-lymphocyte protein 4 (CTLA4), produces impressive responses in multiple tumour types, including melanoma, renal cancer and non-small cell lung cancer [508]. There appears to be a correlation between patients with pre-existing cellular

immune responses and degree and duration of tumour shrinkage [509]. The knowledge that ROCK inhibition may reduce stromal TNC and permit a greater number of immune cells to enter the tumour microenvironment could be utilised to enhance the effectiveness of immunotherapies in those patients who have mounted an inadequate innate immune response. As previously outlined, TNC also appears to function in both cancer and wound healing through the induction of pro-inflammatory cytokines and immune cell modulation. It may be that the balance of differing immune cells present in the tumour stroma is under the influence of TNC, and can impact on host-environment responses. As headway continues to be made with implementing immunotherapy in clinical practice, more information will be gathered regarding this possibility.

Recent work has found that K14 ROCK:ER mice display accelerated wound-healing with an associated increase in collage, periostin and TNC deposition when compared with K14 KD:ER mice [510], Interestingly, the authors sought the presence of TNC in unwounded skin of WT animals and animals deficient in 14-3-3ζ (a member of a family of phosphor-serine binding proteins; these mice also display rapid wound-healing). While they found that TNC was not detectable in unwounded skin, this was not examined in the ROCK-activated animals. I did not carry out any epidermal wounding studies, but it seems feasible that wound-healing in the context of ROCK-activation would indeed lead to higher levels of TNC deposition.

7.2.1 Gene expression: microarray versus RNA sequencing

There is a vast diversity of RNA expression from the genome; the transcriptome is dynamic, altering as a result of alternative splicing, post-transcriptional modifications, gene fusion, mutations, and changes in gene expression [511].

Gene expression microarrays utilise probes that target a specific sequence within an mRNA transcript of interest, producing a record of genes that are actively expressed at a unique time-point. Microarrays have the capacity to concurrently investigate over 10,000 transcripts, permitting identification of genes with differential expression levels in healthy versus diseased tissues, evolutionary changes in gene regulation within disparate species, pharmacogenomic profiling and interrogation of developmental processes [512].

Gene expression microarrays have tended to be a widely utilised approach due to their affordability and accessibility since their introduction in the 1990s.

However, there are limitations inherent to the use of gene expression microarray technology, as the ability to detect previously unidentified genes or transcripts is absent; consequently, alterations in their expression cannot be captured. Furthermore, transcripts present in low abundance may not be accurately detected due to background hybridisation.

In the first instance, I elected to perform a gene expression microarray using the Affymetrix Mouse Gene 1.0 ST array platform, as this technology has been extensively used; thus, the results have been repeatedly validated, and the tools available to analyse the output are more mature. This yielded interesting results, and triggered further interrogation of TNC as a gene of interest. While TNC is seen to be present in the invading front and microenvironment of several tumour types, further research continues to elucidate the function that TNC may serve in this context; for example, TNC has been observed to induce resistance to apoptosis in pancreatic cancer cells via ERK/NFκB pathway activation [482].

Technological advances have resulted in RNA sequencing becoming a more widely used technique to determine differential gene expression patterns. As the facility was available at the Beatson Institute Molecular Technology Service, I was keen to determine what new data could be garnered on the differences seen in ROCK-activated keratinocytes. In particular, the opportunity to detect new and unidentified genes, and transcripts with a low copy number was attractive.

7.2.2 RNA sequencing of ROCK-activated versus control epidermal keratinocytes

RNA sequencing was carried out on primary epidermal keratinocytes with and without ROCK activation. The finding that biological functions related to cancer show the most frequently altered gene expression patterns following ROCK activation is unsurprising given the high rate of somatic mutations in ROCK in numerous cancer types. RNA sequencing revealed differences in 65 genes with known functions; of those, 59 (90.8%) displayed “cancer” biological functions.

Upon further investigation, utilising Ingenuity® Pathway Analysis software, a number of networks were identified that showed differences in gene expression between the ROCK-activated and control cells. These included the "connective tissue disorders" network, confirming the previously noted relationship between ROCK activation, cytoskeletal contraction, and tissue fibrosis.

As previously noted, ROCK signalling induces integrin signalling and consequent epidermal hyperproliferation [83]; consistent with this, 18% of the noted genes were members of the "cell-to-cell signalling, cellular growth and proliferation" network.

A number of putative "hits" were identified through RNA sequencing that were of particular interest from the perspective of determining the pathways and mechanisms at play to facilitate the epidermal thickening identified in ROCK-activated animals. I have outlined the most intriguing of these below.

7.2.2.1 Growth differentiation factor 15

Growth differentiation factor 15 (*GDF15*), also known as macrophage inhibitory cytokine-1 (*MIC1*), belongs to the bone morphogenic protein group, which is in turn a member of the TGFβ family [513]. In conditions of health, the majority of tissues display low levels of GDF15 expression (macrophages and the placenta being notable exceptions [514]). In contrast, in chronic inflammatory states or following injury, GDF15 undergoes striking upregulation [515]. Furthermore, GDF15 is overexpressed in a number of solid tumours, including colon, prostate, breast, thyroid and pancreatic cancers [516], and a relationship has been observed between the presence of GDF15 in the primary tumour and GDF15 serum levels. High serum GDF15 levels are positively correlated with adverse clinical outcomes in both prostate and colon cancers [517,518].

In the context of prostatic malignancy, GDF15 is highly upregulated in the tumour stroma; fibroblasts expressing GDF15 appear to display a high degree of commonality with myofibroblasts, with α smooth muscle actin expression and increased deposition of extracellular matrix components noted in both. In addition, stromally-derived GDF15 appears to facilitate prostate cancer cell proliferation, invasion and migration [519].

In addition to the role of GDF15 in the tumour microenvironment, there is also evidence that GDF15 may contribute to fibrosis in benign pathologies. In particular, patients with the diffuse cutaneous variant of systemic sclerosis have increased GDF15 levels in the serum when compared with both healthy controls and patients with limited cutaneous systemic sclerosis [520]. The level of GDF15 correlates with disease activity [521], indicating a possible role for GDF15 in the pathogenesis of chronic fibrotic conditions.

I found that *GDF15* transcripts were 1.75-fold more abundant in ROCK-activated compared with control keratinocytes (p=0.00244). My finding that *GDF15* transcripts are more abundant in ROCK-activated keratinocytes could thus explain the thickening and stiffening noted in the epidermis *in vivo*, as *GDF15* expression effectively generates a myofibroblast phenotype and appears to have a pro-fibrotic effect on the skin.

7.2.2.2 Thymic stromal lymphopoietin

Thymic stromal lymphopoietin (*TSLP*) is a cytokine that belongs to the IL-7 family; it is largely expressed by the epithelial cells found on barrier surfaces (e.g. the skin and gut), where it is thought to function to maintain homeostasis through regulating immune cell activation [522].

An animal model with a *Tslp* transgene expressed specifically in epidermal keratinocytes was shown to spontaneously develop cutaneous lesions resembling atopic dermatitis [523], an inflammatory skin condition characterised by epidermal hypertrophy, hyperkeratosis, and dermal inflammatory cell infiltrates [524]. Subsequent studies have revealed that patients with diffuse cutaneous systemic sclerosis, a fibrotic skin condition, express high levels of TSLP within the skin. Further interrogation of the mechanisms at play suggests that TSLP may trigger pro-fibrotic and pro-inflammatory signalling; of note, there appears to be a degree of overlap between the effects of TSLP signalling and the alterations brought about by TGFß signalling [525].

In the context of malignancy, TSLP has been found to facilitate T helper immune responses that, in turn, stimulate a dialogue between cancer-associated fibroblasts, tumour cells and immune cells that promotes tumour progression [526].

Production of TSLP by CAFs in the tumour stroma surrounding pancreatic cancers appears to induce T helper-mediated inflammation, with a correlation being noted between TSLP production, T helper cell infiltrates and poor survival outcomes [527].

TSLP has also been shown to facilitate neo-angiogenesis in cervical cancer models; the addition of recombinant TSLP to cell culture media enhances HUVEC proliferation. Furthermore, TSLP derived from cervical cancer cell lines had a similar impact, while blocking TSLP with neutralising antibody reduced the production of markers of angiogenesis such as IL-6, IL-6 and VEGF [528].

Some evidence exists that TSLP may also participate in promoting tumour metastasis; it appears that TSLP mediates T helper responses to facilitate the escape of cells from the primary tumour. TSLP also apparently recruits regulatory T cells, which are necessary for the establishment of lung metastases in breast cancer [529].

These data indicate that TSLP promotes non-malignant tissue fibrosis; in addition, there is an apparent role for TSLP in cancer progression, through facilitation of an immune cell dialogue between the tumour and the microenvironment, via a pro-vascularisation function, and potentially by promoting tumour cell metastasis. I found that *Tslp* transcripts were 2.38-fold more abundant in ROCK-activated versus control keratinocytes (p=0.033). My finding that *Tslp* is upregulated in keratinocytes following ROCK-activation suggests that increased tissue tension may feed into these facets of cellular behaviour.

7.3 Final conclusion

I approached the investigation of the actin cytoskeleton in cancer in two distinct manners. In the first instance, using methylation studies including bisulphite sequencing, I identified epigenetic regulation as an important determinant of *LIMK2* expression in colorectal cancer, with consequent impact on clinical behaviour of the disease, and thus translational implications. The ability to more accurately determine subgroups of patients with a poor prognosis is a longstanding goal, as this would enable the intensification of treatment in those

patients in whom this was deemed necessary, while sparing those patients with a relatively favourable outlook the toxicity associated with many anti-cancer treatments. Testing colorectal tumours for the presence or absence of LIMK2 may be a step towards identifying prognostic biomarkers, and could be further evaluated in the clinical setting.

Following on from this, I chose to interrogate how the changes that occur in the cytoskeleton of cells within the tumour stromal compartment are brought about, and how these alterations in turn impact upon the microenvironment. The data I have presented in this thesis indicate that stromal cells become increasingly contractile as the surroundings become stiffer. This promotes the transformation of stromal fibroblasts to cancer-associated fibroblasts, leading to the synthesis and deposition of extracellular matrix components (including Tenascin C), compounding the raised level of mechanical tension. Thus, a positive feedback cycle is established within the stroma, with evidence implicating this as an adverse prognostic indicator in a number of tumour types.

This work was a continuation of a project previously carried out in the group that had used the epidermis as its model system. In a clinical context, this most closely resembles cutaneous squamous cell cancer; indeed there is evidence that increased stiffness of cSCC is associated with poor patient outcomes. As this is one of the most common types of malignancy encountered in clinical practice, the possibility that inhibition of ROCK could play a role in reducing stromal stiffness and thus potentially render inoperable tumours amenable to surgery is an intriguing one.

References

1. Hanahan D, Weinberg RA. Hallmarks of cancer: the next generation. *Cell*. Mar 4 2011;144(5):646-674.

2. Holmes KC, Popp D, Gebhard W, Kabsch W. Atomic model of the actin filament. *Nature*. Sep 6 1990;347(6288):44-49.

3. Wegner A. Head to tail polymerization of actin. *J Mol Biol*. Nov 1976;108(1):139-150.

4. Pollard TD, Borisy GG. Cellular motility driven by assembly and disassembly of actin filaments. *Cell*. Feb 21 2003;112(4):453-465.

5. Isenberg G, Aebi U, Pollard TD. An actin-binding protein from Acanthamoeba regulates actin filament polymerization and interactions. *Nature*. Dec 4 1980;288(5790):455-459.

6. Burridge K, Fath K, Kelly T, Nuckolls G, Turner C. Focal adhesions: transmembrane junctions between the extracellular matrix and the cytoskeleton. *Annu Rev Cell Biol*. 1988;4:487-525.

7. Hall A. The cytoskeleton and cancer. *Cancer Metastasis Rev*. Jun 2009;28(1-2):5-14.

8. Valencia A, Chardin P, Wittinghofer A, Sander C. The ras protein family: evolutionary tree and role of conserved amino acids. *Biochemistry*. May 14 1991;30(19):4637-4648.

9. Freeman JL, Abo A, Lambeth JD. Rac "insert region" is a novel effector region that is implicated in the activation of NADPH oxidase, but not PAK65. *J Biol Chem*. Aug 16 1996;271(33):19794-19801.

10. Wheeler AP, Ridley AJ. Why three Rho proteins? RhoA, RhoB, RhoC, and cell motility. *Exp Cell Res*. Nov 15 2004;301(1):43-49.

11. Kitzing TM, Wang Y, Pertz O, Copeland JW, Grosse R. Formin-like 2 drives amoeboid invasive cell motility downstream of RhoC. *Oncogene*. Apr 22 2010;29(16):2441-2448.

12. Van Aelst L, D'Souza-Schorey C. Rho GTPases and signaling networks. *Genes Dev*. Sep 15 1997;11(18):2295-2322.

13. Lamarche N, Hall A. GAPs for rho-related GTPases. *Trends Genet*. Dec 1994;10(12):436-440.

14. Olofsson B. Rho guanine dissociation inhibitors: pivotal molecules in cellular signalling. *Cell Signal*. Aug 1999;11(8):545-554.

15. Hoffman GR, Nassar N, Cerione RA. Structure of the Rho family GTP-binding protein Cdc42 in complex with the multifunctional regulator RhoGDI. *Cell*. Feb 4 2000;100(3):345-356.

16. Robbe K, Otto-Bruc A, Chardin P, Antonny B. Dissociation of GDP dissociation inhibitor and membrane translocation are required for efficient activation of Rac by the Dbl homology-pleckstrin homology region of Tiam. *J Biol Chem*. Feb 14 2003;278(7):4756-4762.

17. Liu M, Bi F, Zhou X, Zheng Y. Rho GTPase regulation by miRNAs and covalent modifications. *Trends Cell Biol*. Jul 2012;22(7):365-373.

18. Navarro-Lerida I, Sanchez-Perales S, Calvo M, et al. A palmitoylation switch mechanism regulates Rac1 function and membrane organization. *Embo J*. Feb 1 2012;31(3):534-551.

19. Loirand G, Guilluy C, Pacaud P. Regulation of Rho proteins by phosphorylation in the cardiovascular system. *Trends Cardiovasc Med*. Aug 2006;16(6):199-204.

20. Yarbrough ML, Li Y, Kinch LN, Grishin NV, Ball HL, Orth K. AMPylation of Rho GTPases by Vibrio VopS disrupts effector binding and downstream signaling. *Science*. Jan 9 2009;323(5911):269-272.

21. Schmidt G, Sehr P, Wilm M, Selzer J, Mann M, Aktories K. Gln 63 of Rho is deamidated by Escherichia coli cytotoxic necrotizing factor-1. *Nature*. Jun 12 1997;387(6634):725-729.

22. Doye A, Mettouchi A, Bossis G, et al. CNF1 exploits the ubiquitin-proteasome machinery to restrict Rho GTPase activation for bacterial host cell invasion. *Cell*. Nov 15 2002;111(4):553-564.

23. Ridley AJ, Paterson HF, Johnston CL, Diekmann D, Hall A. The small GTP-binding protein rac regulates growth factor-induced membrane ruffling. *Cell*. Aug 7 1992;70(3):401-410.

24. Nobes CD, Hall A. Rho, rac, and cdc42 GTPases regulate the assembly of multimolecular focal complexes associated with actin stress fibers, lamellipodia, and filopodia. *Cell*. Apr 7 1995;81(1):53-62.

25. Knaus UG, Wang Y, Reilly AM, Warnock D, Jackson JH. Structural requirements for PAK activation by Rac GTPases. *J Biol Chem*. Aug 21 1998;273(34):21512-21518.

26. Morreale A, Venkatesan M, Mott HR, et al. Structure of Cdc42 bound to the GTPase binding domain of PAK. *Nat Struct Biol*. May 2000;7(5):384-388.

27. Edwards DC, Sanders LC, Bokoch GM, Gill GN. Activation of LIM-kinase by Pak1 couples Rac/Cdc42 GTPase signalling to actin cytoskeletal dynamics. *Nat Cell Biol*. Sep 1999;1(5):253-259.

28. Sanders LC, Matsumura F, Bokoch GM, de Lanerolle P. Inhibition of myosin light chain kinase by p21-activated kinase. *Science*. Mar 26 1999;283(5410):2083-2085.

29. Rohatgi R, Ho HY, Kirschner MW. Mechanism of N-WASP activation by CDC42 and phosphatidylinositol 4, 5-bisphosphate. *J Cell Biol*. Sep 18 2000;150(6):1299-1310.

30. Riento K, Ridley AJ. Rocks: multifunctional kinases in cell behaviour. *Nat Rev Mol Cell Biol*. Jun 2003;4(6):446-456.

31. Leung T, Chen XQ, Manser E, Lim L. The p160 RhoA-binding kinase ROK alpha is a member of a kinase family and is involved in the reorganization of the cytoskeleton. *Mol Cell Biol*. Oct 1996;16(10):5313-5327.

32. Wen W, Liu W, Yan J, Zhang M. Structure basis and unconventional lipid membrane binding properties of the PH-C1 tandem of rho kinases. *J Biol Chem*. Sep 19 2008;283(38):26263-26273.

33. Amano M, Chihara K, Nakamura N, Kaneko T, Matsuura Y, Kaibuchi K. The COOH terminus of Rho-kinase negatively regulates rho-kinase activity. *J Biol Chem*. Nov 5 1999;274(45):32418-32424.

34. Nakagawa O, Fujisawa K, Ishizaki T, Saito Y, Nakao K, Narumiya S. ROCK-I and ROCK-II, two isoforms of Rho-associated coiled-coil forming protein serine/threonine kinase in mice. *FEBS Lett*. Aug 26 1996;392(2):189-193.

35. Amano M, Ito M, Kimura K, et al. Phosphorylation and activation of myosin by Rho-associated kinase (Rho-kinase). *J Biol Chem*. Aug 23 1996;271(34):20246-20249.

36. Rath N, Olson MF. Rho-associated kinases in tumorigenesis: re-considering ROCK inhibition for cancer therapy. *EMBO Rep*. Oct 2012;13(10):900-908.

37. Matsuoka T, Yashiro M. Rho/ROCK signaling in motility and metastasis of gastric cancer. *World journal of gastroenterology*. Oct 14 2014;20(38):13756-13766.

38. Kimura K, Ito M, Amano M, et al. Regulation of myosin phosphatase by Rho and Rho-associated kinase (Rho-kinase). *Science*. Jul 12 1996;273(5272):245-248.

39. Velasco G, Armstrong C, Morrice N, Frame S, Cohen P. Phosphorylation of the regulatory subunit of smooth muscle protein phosphatase 1M at Thr850 induces its dissociation from myosin. *FEBS Lett*. Sep 11 2002;527(1-3):101-104.

40. Scott RW, Olson MF. LIM kinases: function, regulation and association with human disease. *J Mol Med (Berl)*. Jun 2007;85(6):555-568.

41. Arber S, Barbayannis FA, Hanser H, et al. Regulation of actin dynamics through phosphorylation of cofilin by LIM-kinase. *Nature*. Jun 25 1998;393(6687):805-809.

42. Fujisawa K, Fujita A, Ishizaki T, Saito Y, Narumiya S. Identification of the Rho-binding domain of p160ROCK, a Rho-associated coiled-coil containing protein kinase. *J Biol Chem*. Sep 20 1996;271(38):23022-23028.

43. Takahashi N, Tuiki H, Saya H, Kaibuchi K. Localization of the gene coding for ROCK II/Rho kinase on human chromosome 2p24. *Genomics*. Jan 15 1999;55(2):235-237.

44. Shimizu Y, Thumkeo D, Keel J, et al. ROCK-I regulates closure of the eyelids and ventral body wall by inducing assembly of actomyosin bundles. *J Cell Biol*. Mar 14 2005;168(6):941-953.

45. Thumkeo D, Keel J, Ishizaki T, et al. Targeted disruption of the mouse rho-associated kinase 2 gene results in intrauterine growth retardation and fetal death. *Mol Cell Biol*. Jul 2003;23(14):5043-5055.

46. Amano M, Chihara K, Kimura K, et al. Formation of actin stress fibers and focal adhesions enhanced by Rho-kinase. *Science*. Feb 28 1997;275(5304):1308-1311.

47. Burridge K, Chrzanowska-Wodnicka M. Focal adhesions, contractility, and signaling. *Annu Rev Cell Dev Biol*. 1996;12:463-518.

48. Engler AJ, Sen S, Sweeney HL, Discher DE. Matrix elasticity directs stem cell lineage specification. *Cell*. Aug 25 2006;126(4):677-689.

49. Trybus KM. Assembly of cytoplasmic and smooth muscle myosins. *Curr Opin Cell Biol*. Feb 1991;3(1):105-111.

50. Gordon AM, Homsher E, Regnier M. Regulation of contraction in striated muscle. *Physiol Rev*. Apr 2000;80(2):853-924.

51. Heissler SM, Sellers JR. Various themes of myosin regulation. *J Mol Biol*. Jan 28 2016.

52. Kamm KE, Stull JT. The function of myosin and myosin light chain kinase phosphorylation in smooth muscle. *Annu Rev Pharmacol Toxicol*. 1985;25:593-620.

53. Ye LH, Kishi H, Nakamura A, et al. Myosin light-chain kinase of smooth muscle stimulates myosin ATPase activity without phosphorylating myosin light chain. *Proc Natl Acad Sci U S A*. Jun 8 1999;96(12):6666-6671.

54. Gao Y, Ye LH, Kishi H, et al. Myosin light chain kinase as a multifunctional regulatory protein of smooth muscle contraction. *IUBMB Life*. Jun 2001;51(6):337-344.

55. Qi D, Mitchell RW, Burdyga T, Ford LE, Kuo KH, Seow CY. Myosin light chain phosphorylation facilitates in vivo myosin filament reassembly after mechanical perturbation. *Am J Physiol Cell Physiol*. Jun 2002;282(6):C1298-1305.

56. O'Connell CB, Tyska MJ, Mooseker MS. Myosin at work: motor adaptations for a variety of cellular functions. *Biochim Biophys Acta*. May 2007;1773(5):615-630.

57. Somlyo AP, Somlyo AV. Signal transduction by G-proteins, rho-kinase and protein phosphatase to smooth muscle and non-muscle myosin II. *J Physiol*. Jan 15 2000;522 Pt 2:177-185.

58. Coleman ML, Sahai EA, Yeo M, Bosch M, Dewar A, Olson MF. Membrane blebbing during apoptosis results from caspase-mediated activation of ROCK I. *Nat Cell Biol*. Apr 2001;3(4):339-345.

59. Gilmore AP. Anoikis. *Cell Death Differ*. Nov 2005;12 Suppl 2:1473-1477.

60. Boudreau N, Sympson CJ, Werb Z, Bissell MJ. Suppression of ICE and apoptosis in mammary epithelial cells by extracellular matrix. *Science*. Feb 10 1995;267(5199):891-893.

61. Walsh SV, Hopkins AM, Chen J, Narumiya S, Parkos CA, Nusrat A. Rho kinase regulates tight junction function and is necessary for tight junction assembly in polarized intestinal epithelia. *Gastroenterology*. Sep 2001;121(3):566-579.

62. McKenzie JA, Ridley AJ. Roles of Rho/ROCK and MLCK in TNF-alpha-induced changes in endothelial morphology and permeability. *J Cell Physiol*. Oct 2007;213(1):221-228.

63. Sahai E, Marshall CJ. ROCK and Dia have opposing effects on adherens junctions downstream of Rho. *Nat Cell Biol*. Jun 2002;4(6):408-415.

64. Bhowmick NA, Ghiassi M, Bakin A, et al. Transforming growth factor-beta1 mediates epithelial to mesenchymal transdifferentiation through a RhoA-dependent mechanism. *Mol Biol Cell*. Jan 2001;12(1):27-36.

65. Pawlak G, Helfman DM. Post-transcriptional down-regulation of ROCKI/Rho-kinase through an MEK-dependent pathway leads to cytoskeleton disruption in Ras-transformed fibroblasts. *Mol Biol Cell*. Jan 2002;13(1):336-347.

66. Sahai E, Ishizaki T, Narumiya S, Treisman R. Transformation mediated by RhoA requires activity of ROCK kinases. *Curr Biol*. Feb 11 1999;9(3):136-145.

67. Chevrier V, Piel M, Collomb N, et al. The Rho-associated protein kinase p160ROCK is required for centrosome positioning. *J Cell Biol*. May 27 2002;157(5):807-817.

68. Croft DR, Olson MF. The Rho GTPase effector ROCK regulates cyclin A, cyclin D1, and p27Kip1 levels by distinct mechanisms. *Mol Cell Biol*. Jun 2006;26(12):4612-4627.

69. Ohgushi M, Sasai Y. Lonely death dance of human pluripotent stem cells: ROCKing between metastable cell states. *Trends Cell Biol*. May 2011;21(5):274-282.

70. Watanabe K, Ueno M, Kamiya D, et al. A ROCK inhibitor permits survival of dissociated human embryonic stem cells. *Nat Biotechnol*. Jun 2007;25(6):681-686.

71. Krawetz RJ, Li X, Rancourt DE. Human embryonic stem cells: caught between a ROCK inhibitor and a hard place. *Bioessays*. Mar 2009;31(3):336-343.

72. Rungsiwiwut R, Manolertthewan C, Numchaisrika P, et al. The ROCK inhibitor Y-26732 enhances the survival and proliferation of human

embryonic stem cell-derived neural progenitor cells upon dissociation. *Cells Tissues Organs*. 2013;198(2):127-138.

73. Greenman C, Stephens P, Smith R, et al. Patterns of somatic mutation in human cancer genomes. *Nature*. Mar 8 2007;446(7132):153-158.

74. Lochhead PA, Wickman G, Mezna M, Olson MF. Activating ROCK1 somatic mutations in human cancer. *Oncogene*. Apr 29 2010;29(17):2591-2598.

75. Lane J, Martin TA, Watkins G, Mansel RE, Jiang WG. The expression and prognostic value of ROCK I and ROCK II and their role in human breast cancer. *Int J Oncol*. Sep 2008;33(3):585-593.

76. Liu X, Choy E, Hornicek FJ, et al. ROCK1 as a potential therapeutic target in osteosarcoma. *J Orthop Res*. Aug 2011;29(8):1259-1266.

77. Wong CC, Wong CM, Tung EK, Man K, Ng IO. Rho-kinase 2 is frequently overexpressed in hepatocellular carcinoma and involved in tumor invasion. *Hepatology*. May 2009;49(5):1583-1594.

78. Kamai T, Tsujii T, Arai K, et al. Significant association of Rho/ROCK pathway with invasion and metastasis of bladder cancer. *Clin Cancer Res*. Jul 2003;9(7):2632-2641.

79. Provenzano PP, Inman DR, Eliceiri KW, et al. Collagen density promotes mammary tumor initiation and progression. *BMC Med*. 2008;6:11.

80. Mahadevan D, Von Hoff DD. Tumor-stroma interactions in pancreatic ductal adenocarcinoma. *Mol Cancer Ther*. Apr 2007;6(4):1186-1197.

81. Conklin MW, Eickhoff JC, Riching KM, et al. Aligned collagen is a prognostic signature for survival in human breast carcinoma. *Am J Pathol*. Mar 2011;178(3):1221-1232.

82. Whatcott CJ, Diep CH, Jiang P, et al. Desmoplasia in Primary Tumors and Metastatic Lesions of Pancreatic Cancer. *Clin Cancer Res*. Aug 1 2015;21(15):3561-3568.

83. Samuel MS, Lopez JI, McGhee EJ, et al. Actomyosin-mediated cellular tension drives increased tissue stiffness and beta-catenin activation to

induce epidermal hyperplasia and tumor growth. *Cancer Cell*. Jun 14 2011;19(6):776-791.

84. Ibbetson SJ, Pyne NT, Pollard AN, Olson MF, Samuel MS. Mechanotransduction pathways promoting tumor progression are activated in invasive human squamous cell carcinoma. *Am J Pathol*. Sep 2013;183(3):930-937.

85. Raviraj V, Fok S, Zhao J, et al. Regulation of ROCK1 via Notch1 during breast cancer cell migration into dense matrices. *BMC Cell Biol*. 2012;13:12.

86. Gaggioli C, Hooper S, Hidalgo-Carcedo C, et al. Fibroblast-led collective invasion of carcinoma cells with differing roles for RhoGTPases in leading and following cells. *Nat Cell Biol*. Dec 2007;9(12):1392-1400.

87. Sanz-Moreno V, Gaggioli C, Yeo M, et al. ROCK and JAK1 signaling cooperate to control actomyosin contractility in tumor cells and stroma. *Cancer Cell*. Aug 16 2011;20(2):229-245.

88. Neri S, Ishii G, Hashimoto H, et al. Podoplanin-expressing cancer-associated fibroblasts lead and enhance the local invasion of cancer cells in lung adenocarcinoma. *Int J Cancer*. Aug 15 2015;137(4):784-796.

89. Nagumo H, Sasaki Y, Ono Y, Okamoto H, Seto M, Takuwa Y. Rho kinase inhibitor HA-1077 prevents Rho-mediated myosin phosphatase inhibition in smooth muscle cells. *Am J Physiol Cell Physiol*. Jan 2000;278(1):C57-65.

90. Ishizaki T, Uehata M, Tamechika I, et al. Pharmacological properties of Y-27632, a specific inhibitor of rho-associated kinases. *Mol Pharmacol*. May 2000;57(5):976-983.

91. Sasaki Y, Suzuki M, Hidaka H. The novel and specific Rho-kinase inhibitor (S)-(+)-2-methyl-1-[(4-methyl-5-isoquinoline)sulfonyl]-homopiperazine as a probing molecule for Rho-kinase-involved pathway. *Pharmacol Ther*. Feb-Mar 2002;93(2-3):225-232.

92. Breitenlechner C, Gassel M, Hidaka H, et al. Protein kinase A in complex with Rho-kinase inhibitors Y-27632, Fasudil, and H-1152P: structural basis of selectivity. *Structure*. Dec 2003;11(12):1595-1607.

93. Wermke M, Camgoz A, Paszkowski-Rogacz M, et al. RNAi profiling of primary human AML cells identifies ROCK1 as a therapeutic target and nominates fasudil as an antileukemic drug. *Blood*. Jun 11 2015;125(24):3760-3768.

94. Fagan-Solis KD, Schneider SS, Pentecost BT, et al. The RhoA pathway mediates MMP-2 and MMP-9-independent invasive behavior in a triple-negative breast cancer cell line. *J Cell Biochem*. Jun 2013;114(6):1385-1394.

95. Abe H, Kamai T, Hayashi K, et al. The Rho-kinase inhibitor HA-1077 suppresses proliferation/migration and induces apoptosis of urothelial cancer cells. *BMC Cancer*. 2014;14:412.

96. Yang X, Di J, Zhang Y, et al. The Rho-kinase inhibitor inhibits proliferation and metastasis of small cell lung cancer. *Biomed Pharmacother*. Apr 2012;66(3):221-227.

97. Deng L, Li G, Li R, Liu Q, He Q, Zhang J. Rho-kinase inhibitor, fasudil, suppresses glioblastoma cell line progression in vitro and in vivo. *Cancer Biol Ther*. Jun 1 2010;9(11):875-884.

98. Chen W, Mao K, Hua-Huy T, Bei Y, Liu Z, Dinh-Xuan AT. Fasudil inhibits prostate cancer-induced angiogenesis in vitro. *Oncol Rep*. Dec 2014;32(6):2795-2802.

99. Zhang JG, Li XY, Wang YZ, et al. ROCK is involved in vasculogenic mimicry formation in hepatocellular carcinoma cell line. *PLoS One*. 2014;9(9):e107661.

100. Routhier A, Astuccio M, Lahey D, et al. Pharmacological inhibition of Rho-kinase signaling with Y-27632 blocks melanoma tumor growth. *Oncol Rep*. Mar 2010;23(3):861-867.

101. Ikebe C, Ohashi K, Fujimori T, et al. Mouse LIM-kinase 2 gene: cDNA cloning, genomic organization, and tissue-specific expression of two alternatively initiated transcripts. *Genomics*. Dec 15 1997;46(3):504-508.

102. Foletta VC, Moussi N, Sarmiere PD, Bamburg JR, Bernard O. LIM kinase 1, a key regulator of actin dynamics, is widely expressed in embryonic and adult tissues. *Exp Cell Res*. Apr 1 2004;294(2):392-405.

103. Acevedo K, Moussi N, Li R, Soo P, Bernard O. LIM kinase 2 is widely expressed in all tissues. *J Histochem Cytochem*. May 2006;54(5):487-501.

104. Bernstein BW, Bamburg JR. ADF/cofilin: a functional node in cell biology. *Trends Cell Biol*. Apr 2010;20(4):187-195.

105. Ghosh M, Song X, Mouneimne G, Sidani M, Lawrence DS, Condeelis JS. Cofilin promotes actin polymerization and defines the direction of cell motility. *Science*. Apr 30 2004;304(5671):743-746.

106. Gorovoy M, Niu J, Bernard O, et al. LIM kinase 1 coordinates microtubule stability and actin polymerization in human endothelial cells. *J Biol Chem*. Jul 15 2005;280(28):26533-26542.

107. Bagheri-Yarmand R, Mazumdar A, Sahin AA, Kumar R. LIM kinase 1 increases tumor metastasis of human breast cancer cells via regulation of the urokinase-type plasminogen activator system. *Int J Cancer*. Jun 1 2006;118(11):2703-2710.

108. Davila M, Frost AR, Grizzle WE, Chakrabarti R. LIM kinase 1 is essential for the invasive growth of prostate epithelial cells: implications in prostate cancer. *J Biol Chem*. Sep 19 2003;278(38):36868-36875.

109. Yoshioka K, Foletta V, Bernard O, Itoh K. A role for LIM kinase in cancer invasion. *Proc Natl Acad Sci U S A*. Jun 10 2003;100(12):7247-7252.

110. Vlecken DH, Bagowski CP. LIMK1 and LIMK2 are important for metastatic behavior and tumor cell-induced angiogenesis of pancreatic cancer cells. *Zebrafish*. Dec 2009;6(4):433-439.

111. Croft DR, Crighton D, Samuel MS, et al. p53-mediated transcriptional regulation and activation of the actin cytoskeleton regulatory RhoC to LIMK2 signaling pathway promotes cell survival. *Cell Res*. Apr 2011;21(4):666-682.

112. Hsu FF, Lin TY, Chen JY, Shieh SY. p53-Mediated transactivation of LIMK2b links actin dynamics to cell cycle checkpoint control. *Oncogene*. May 13 2010;29(19):2864-2876.

113. Vogelstein B, Fearon ER, Hamilton SR, et al. Genetic alterations during colorectal-tumor development. *N Engl J Med*. Sep 1 1988;319(9):525-532.

114. Lengauer C, Kinzler KW, Vogelstein B. Genetic instability in colorectal cancers. *Nature*. Apr 10 1997;386(6625):623-627.

115. Cottrell S, Bicknell D, Kaklamanis L, Bodmer WF. Molecular analysis of APC mutations in familial adenomatous polyposis and sporadic colon carcinomas. *Lancet*. Sep 12 1992;340(8820):626-630.

116. Rajagopalan H, Bardelli A, Lengauer C, Kinzler KW, Vogelstein B, Velculescu VE. Tumorigenesis: RAF/RAS oncogenes and mismatch-repair status. *Nature*. Aug 29 2002;418(6901):934.

117. Thiagalingam S, Lengauer C, Leach FS, et al. Evaluation of candidate tumour suppressor genes on chromosome 18 in colorectal cancers. *Nat Genet*. Jul 1996;13(3):343-346.

118. Baker SJ, Fearon ER, Nigro JM, et al. Chromosome 17 deletions and p53 gene mutations in colorectal carcinomas. *Science*. Apr 14 1989;244(4901):217-221.

119. Kinzler KW, Vogelstein B. Cancer-susceptibility genes. Gatekeepers and caretakers. *Nature*. Apr 24 1997;386(6627):761, 763.

120. Herman JG, Umar A, Polyak K, et al. Incidence and functional consequences of hMLH1 promoter hypermethylation in colorectal carcinoma. *Proc Natl Acad Sci U S A*. Jun 9 1998;95(12):6870-6875.

121. Segditsas S, Tomlinson I. Colorectal cancer and genetic alterations in the Wnt pathway. *Oncogene*. Dec 4 2006;25(57):7531-7537.

122. van der Klift H, Wijnen J, Wagner A, et al. Molecular characterization of the spectrum of genomic deletions in the mismatch repair genes MSH2, MLH1, MSH6, and PMS2 responsible for hereditary nonpolyposis colorectal cancer (HNPCC). *Genes Chromosomes Cancer*. Oct 2005;44(2):123-138.

123. Parsons R, Myeroff LL, Liu B, et al. Microsatellite instability and mutations of the transforming growth factor beta type II receptor gene in colorectal cancer. *Cancer Res*. Dec 1 1995;55(23):5548-5550.

124. Souza RF, Appel R, Yin J, et al. Microsatellite instability in the insulin-like growth factor II receptor gene in gastrointestinal tumours. *Nat Genet*. Nov 1996;14(3):255-257.

125. Rampino N, Yamamoto H, Ionov Y, et al. Somatic frameshift mutations in the BAX gene in colon cancers of the microsatellite mutator phenotype. *Science*. Feb 14 1997;275(5302):967-969.

126. Toyota M, Ahuja N, Ohe-Toyota M, Herman JG, Baylin SB, Issa JP. CpG island methylator phenotype in colorectal cancer. *Proc Natl Acad Sci U S A*. Jul 20 1999;96(15):8681-8686.

127. Walther A, Johnstone E, Swanton C, Midgley R, Tomlinson I, Kerr D. Genetic prognostic and predictive markers in colorectal cancer. *Nat Rev Cancer*. Jul 2009;9(7):489-499.

128. Ponz de Leon M, Benatti P, Borghi F, et al. Aetiology of colorectal cancer and relevance of monogenic inheritance. *Gut*. Jan 2004;53(1):115-122.

129. Lynch HT, Shaw MW, Magnuson CW, Larsen AL, Krush AJ. Hereditary factors in cancer. Study of two large midwestern kindreds. *Arch Intern Med*. Feb 1966;117(2):206-212.

130. Pedroni M, Sala E, Scarselli A, et al. Microsatellite instability and mismatch-repair protein expression in hereditary and sporadic colorectal carcinogenesis. *Cancer Res*. Feb 1 2001;61(3):896-899.

131. Aarnio M, Sankila R, Pukkala E, et al. Cancer risk in mutation carriers of DNA-mismatch-repair genes. *Int J Cancer*. Apr 12 1999;81(2):214-218.

132. Vasen HF, Watson P, Mecklin JP, Lynch HT. New clinical criteria for hereditary nonpolyposis colorectal cancer (HNPCC, Lynch syndrome) proposed by the International Collaborative group on HNPCC. *Gastroenterology*. Jun 1999;116(6):1453-1456.

133. Gardner EJ. A genetic and clinical study of intestinal polyposis, a predisposing factor for carcinoma of the colon and rectum. *Am J Hum Genet*. Jun 1951;3(2):167-176.

134. Groden J, Thliveris A, Samowitz W, et al. Identification and characterization of the familial adenomatous polyposis coli gene. *Cell*. Aug 9 1991;66(3):589-600.

135. Bulow S. Familial polyposis coli. *Dan Med Bull*. Mar 1987;34(1):1-15.

136. Hernegger GS, Moore HG, Guillem JG. Attenuated familial adenomatous polyposis: an evolving and poorly understood entity. *Dis Colon Rectum*. Jan 2002;45(1):127-134; discussion 134-126.

137. Al-Tassan N, Chmiel NH, Maynard J, et al. Inherited variants of MYH associated with somatic G:C-->T:A mutations in colorectal tumors. *Nat Genet*. Feb 2002;30(2):227-232.

138. Crohn BB, Ginzburg L, Oppenheimer GD. Landmark article Oct 15, 1932. Regional ileitis. A pathological and clinical entity. By Burril B. Crohn, Leon Ginzburg, and Gordon D. Oppenheimer. *Jama*. Jan 6 1984;251(1):73-79.

139. Baumgart DC, Carding SR. Inflammatory bowel disease: cause and immunobiology. *Lancet*. May 12 2007;369(9573):1627-1640.

140. Franchimont D, Vermeire S, El Housni H, et al. Deficient host-bacteria interactions in inflammatory bowel disease? The toll-like receptor (TLR)-4 Asp299gly polymorphism is associated with Crohn's disease and ulcerative colitis. *Gut*. Jul 2004;53(7):987-992.

141. Eaden JA, Abrams KR, Mayberry JF. The risk of colorectal cancer in ulcerative colitis: a meta-analysis. *Gut*. Apr 2001;48(4):526-535.

142. Gupta RB, Harpaz N, Itzkowitz S, et al. Histologic inflammation is a risk factor for progression to colorectal neoplasia in ulcerative colitis: a cohort study. *Gastroenterology*. Oct 2007;133(4):1099-1105; quiz 1340-1091.

143. Xie J, Itzkowitz SH. Cancer in inflammatory bowel disease. *World J Gastroenterol*. Jan 21 2008;14(3):378-389.

144. Triantafillidis JK, Nasioulas G, Kosmidis PA. Colorectal cancer and inflammatory bowel disease: epidemiology, risk factors, mechanisms of carcinogenesis and prevention strategies. *Anticancer Res*. Jul 2009;29(7):2727-2737.

145. Fukata M, Chen A, Vamadevan AS, et al. Toll-like receptor-4 promotes the development of colitis-associated colorectal tumors. *Gastroenterology*. Dec 2007;133(6):1869-1881.

146. Roessner A, Kuester D, Malfertheiner P, Schneider-Stock R. Oxidative stress in ulcerative colitis-associated carcinogenesis. *Pathol Res Pract*. 2008;204(7):511-524.

147. Fantini MC, Pallone F. Cytokines: from gut inflammation to colorectal cancer. *Curr Drug Targets*. May 2008;9(5):375-380.

148. Lengauer C, Kinzler KW, Vogelstein B. Genetic instabilities in human cancers. *Nature*. Dec 17 1998;396(6712):643-649.

149. Thibodeau SN, Bren G, Schaid D. Microsatellite instability in cancer of the proximal colon. *Science*. May 7 1993;260(5109):816-819.

150. Merok MA, Ahlquist T, Royrvik EC, et al. Microsatellite instability has a positive prognostic impact on stage II colorectal cancer after complete resection: results from a large, consecutive Norwegian series. *Ann Oncol*. May 2013;24(5):1274-1282.

151. Soreide K, Janssen EA, Soiland H, Korner H, Baak JP. Microsatellite instability in colorectal cancer. *Br J Surg*. Apr 2006;93(4):395-406.

152. Popat S, Hubner R, Houlston RS. Systematic review of microsatellite instability and colorectal cancer prognosis. *J Clin Oncol*. Jan 20 2005;23(3):609-618.

153. Guastadisegni C, Colafranceschi M, Ottini L, Dogliotti E. Microsatellite instability as a marker of prognosis and response to therapy: a meta-analysis of colorectal cancer survival data. *Eur J Cancer*. Oct 2010;46(15):2788-2798.

154. Munemitsu S, Albert I, Souza B, Rubinfeld B, Polakis P. Regulation of intracellular beta-catenin levels by the adenomatous polyposis coli (APC) tumor-suppressor protein. *Proc Natl Acad Sci U S A*. Mar 28 1995;92(7):3046-3050.

155. Morin PJ, Sparks AB, Korinek V, et al. Activation of beta-catenin-Tcf signaling in colon cancer by mutations in beta-catenin or APC. *Science*. Mar 21 1997;275(5307):1787-1790.

156. Sansom OJ, Reed KR, Hayes AJ, et al. Loss of Apc in vivo immediately perturbs Wnt signaling, differentiation, and migration. *Genes Dev*. Jun 15 2004;18(12):1385-1390.

157. Stamos JL, Weis WI. The beta-catenin destruction complex. *Cold Spring Harb Perspect Biol*. Jan 2013;5(1):a007898.

158. Xing Y, Clements WK, Kimelman D, Xu W. Crystal structure of a beta-catenin/axin complex suggests a mechanism for the beta-catenin destruction complex. *Genes Dev*. Nov 15 2003;17(22):2753-2764.

159. Roberts DM, Pronobis MI, Poulton JS, et al. Deconstructing the sscatenin destruction complex: mechanistic roles for the tumor suppressor APC in regulating Wnt signaling. *Mol Biol Cell*. Jun 1 2011;22(11):1845-1863.

160. Koinuma K, Yamashita Y, Liu W, et al. Epigenetic silencing of AXIN2 in colorectal carcinoma with microsatellite instability. *Oncogene*. Jan 5 2006;25(1):139-146.

161. Downward J. Targeting RAS signalling pathways in cancer therapy. *Nat Rev Cancer*. Jan 2003;3(1):11-22.

162. Weisenberger DJ, Siegmund KD, Campan M, et al. CpG island methylator phenotype underlies sporadic microsatellite instability and is tightly associated with BRAF mutation in colorectal cancer. *Nat Genet*. Jul 2006;38(7):787-793.

163. Richman SD, Seymour MT, Chambers P, et al. KRAS and BRAF mutations in advanced colorectal cancer are associated with poor prognosis but do not preclude benefit from oxaliplatin or irinotecan: results from the MRC FOCUS trial. *J Clin Oncol*. Dec 10 2009;27(35):5931-5937.

164. Sarli L, Bottarelli L, Bader G, et al. Association between recurrence of sporadic colorectal cancer, high level of microsatellite instability, and loss of heterozygosity at chromosome 18q. *Dis Colon Rectum*. Sep 2004;47(9):1467-1482.

165. Schmitt CA, Thaler KR, Wittig BM, Kaulen H, Meyer zum Buschenfelde KH, Dippold WG. Detection of the DCC gene product in normal and malignant colorectal tissues and its relation to a codon 201 mutation. *Br J Cancer*. Feb 1998;77(4):588-594.

166. Rodrigues S, De Wever O, Bruyneel E, Rooney RJ, Gespach C. Opposing roles of netrin-1 and the dependence receptor DCC in cancer cell invasion, tumor growth and metastasis. *Oncogene*. Aug 16 2007;26(38):5615-5625.

167. Heldin CH, Miyazono K, ten Dijke P. TGF-beta signalling from cell membrane to nucleus through SMAD proteins. *Nature*. Dec 4 1997;390(6659):465-471.

168. Alazzouzi H, Alhopuro P, Salovaara R, et al. SMAD4 as a prognostic marker in colorectal cancer. *Clin Cancer Res*. Apr 1 2005;11(7):2606-2611.

169. Papageorgis P, Cheng K, Ozturk S, et al. Smad4 inactivation promotes malignancy and drug resistance of colon cancer. *Cancer Res*. Feb 1 2011;71(3):998-1008.

170. Fearon ER, Vogelstein B. A genetic model for colorectal tumorigenesis. *Cell*. Jun 1 1990;61(5):759-767.

171. Westra JL, Boven LG, van der Vlies P, et al. A substantial proportion of microsatellite-unstable colon tumors carry TP53 mutations while not showing chromosomal instability. *Genes Chromosomes Cancer*. Jun 2005;43(2):194-201.

172. Munro AJ, Lain S, Lane DP. P53 abnormalities and outcomes in colorectal cancer: a systematic review. *Br J Cancer*. Feb 14 2005;92(3):434-444.

173. Hoosein NM, McKnight MK, Levine AE, et al. Differential sensitivity of subclasses of human colon carcinoma cell lines to the growth inhibitory effects of transforming growth factor-beta 1. *Exp Cell Res*. Apr 1989;181(2):442-453.

174. Riggins GJ, Kinzler KW, Vogelstein B, Thiagalingam S. Frequency of Smad gene mutations in human cancers. *Cancer Res*. Jul 1 1997;57(13):2578-2580.

175. Akhurst RJ, Derynck R. TGF-beta signaling in cancer--a double-edged sword. *Trends Cell Biol*. Nov 2001;11(11):S44-51.

176. Friedman E, Gold LI, Klimstra D, Zeng ZS, Winawer S, Cohen A. High levels of transforming growth factor beta 1 correlate with disease progression in human colon cancer. *Cancer Epidemiol Biomarkers Prev*. Jul-Aug 1995;4(5):549-554.

177. Calon A, Espinet E, Palomo-Ponce S, et al. Dependency of colorectal cancer on a TGF-beta-driven program in stromal cells for metastasis initiation. *Cancer Cell*. Nov 13 2012;22(5):571-584.

178. Herman JG, Baylin SB. Gene silencing in cancer in association with promoter hypermethylation. *N Engl J Med*. Nov 20 2003;349(21):2042-2054.

179. Ahuja N, Mohan AL, Li Q, et al. Association between CpG island methylation and microsatellite instability in colorectal cancer. *Cancer Res*. Aug 15 1997;57(16):3370-3374.

180. Burri N, Shaw P, Bouzourene H, et al. Methylation silencing and mutations of the p14ARF and p16INK4a genes in colon cancer. *Lab Invest*. Feb 2001;81(2):217-229.

181. Hernandez-Blazquez FJ, Habib M, Dumollard JM, et al. Evaluation of global DNA hypomethylation in human colon cancer tissues by immunohistochemistry and image analysis. *Gut*. Nov 2000;47(5):689-693.

182. Jordan CT, Guzman ML, Noble M. Cancer stem cells. *N Engl J Med*. Sep 21 2006;355(12):1253-1261.

183. Barker N, van Es JH, Kuipers J, et al. Identification of stem cells in small intestine and colon by marker gene Lgr5. *Nature*. Oct 25 2007;449(7165):1003-1007.

184. Barker N, Ridgway RA, van Es JH, et al. Crypt stem cells as the cells-of-origin of intestinal cancer. *Nature*. Jan 29 2009;457(7229):608-611.

185. Vermeulen L, De Sousa EMF, van der Heijden M, et al. Wnt activity defines colon cancer stem cells and is regulated by the microenvironment. *Nat Cell Biol*. May 2010;12(5):468-476.

186. van der Flier LG, van Gijn ME, Hatzis P, et al. Transcription factor achaete scute-like 2 controls intestinal stem cell fate. *Cell*. Mar 6 2009;136(5):903-912.

187. Jubb AM, Hoeflich KP, Haverty PM, Wang J, Koeppen H. Ascl2 and 11p15.5 amplification in colorectal cancer. *Gut*. Nov 2011;60(11):1606-1607; author reply 1607.

188. Zhu R, Yang Y, Tian Y, et al. Ascl2 knockdown results in tumor growth arrest by miRNA-302b-related inhibition of colon cancer progenitor cells. *PLoS One*. 2012;7(2):e32170.

189. Jung P, Sato T, Merlos-Suarez A, et al. Isolation and in vitro expansion of human colonic stem cells. *Nat Med*. Oct 2011;17(10):1225-1227.

190. Merlos-Suarez A, Barriga FM, Jung P, et al. The intestinal stem cell signature identifies colorectal cancer stem cells and predicts disease relapse. *Cell Stem Cell*. May 6 2011;8(5):511-524.

191. Fre S, Huyghe M, Mourikis P, Robine S, Louvard D, Artavanis-Tsakonas S. Notch signals control the fate of immature progenitor cells in the intestine. *Nature*. Jun 16 2005;435(7044):964-968.

192. Anderson EC, Wong MH. Caught in the Akt: regulation of Wnt signaling in the intestine. *Gastroenterology*. Sep 2010;139(3):718-722.

193. Zhang Y, Li B, Ji ZZ, Zheng PS. Notch1 regulates the growth of human colon cancers. *Cancer*. Nov 15 2010;116(22):5207-5218.

194. Kosinski C, Li VS, Chan AS, et al. Gene expression patterns of human colon tops and basal crypts and BMP antagonists as intestinal stem cell niche factors. *Proc Natl Acad Sci U S A*. Sep 25 2007;104(39):15418-15423.

195. Lombardo Y, Scopelliti A, Cammareri P, et al. Bone morphogenetic protein 4 induces differentiation of colorectal cancer stem cells and increases their response to chemotherapy in mice. *Gastroenterology*. Jan 2011;140(1):297-309.

196. He XC, Zhang J, Tong WG, et al. BMP signaling inhibits intestinal stem cell self-renewal through suppression of Wnt-beta-catenin signaling. *Nat Genet*. Oct 2004;36(10):1117-1121.

197. Powell DW, Adegboyega PA, Di Mari JF, Mifflin RC. Epithelial cells and their neighbors I. Role of intestinal myofibroblasts in development, repair, and cancer. *Am J Physiol Gastrointest Liver Physiol*. Jul 2005;289(1):G2-7.

198. Pinchuk IV, Beswick EJ, Saada JI, et al. Human colonic myofibroblasts promote expansion of CD4+ CD25high Foxp3+ regulatory T cells. *Gastroenterology*. Jun 2011;140(7):2019-2030.

199. Yeung TM, Gandhi SC, Bodmer WF. Hypoxia and lineage specification of cell line-derived colorectal cancer stem cells. *Proc Natl Acad Sci U S A*. Mar 15 2011;108(11):4382-4387.

200. Mathieu J, Zhang Z, Zhou W, et al. HIF induces human embryonic stem cell markers in cancer cells. *Cancer Res.* Jul 1 2011;71(13):4640-4652.

201. de Sousa EMF, Colak S, Buikhuisen J, et al. Methylation of cancer-stem-cell-associated Wnt target genes predicts poor prognosis in colorectal cancer patients. *Cell Stem Cell.* Nov 4 2011;9(5):476-485.

202. Gebhard C, Benner C, Ehrich M, et al. General transcription factor binding at CpG islands in normal cells correlates with resistance to de novo DNA methylation in cancer cells. *Cancer Res.* Feb 15 2010;70(4):1398-1407.

203. Behrens J, Vakaet L, Friis R, et al. Loss of epithelial differentiation and gain of invasiveness correlates with tyrosine phosphorylation of the E-cadherin/beta-catenin complex in cells transformed with a temperature-sensitive v-SRC gene. *J Cell Biol.* Feb 1993;120(3):757-766.

204. Bendardaf R, Elzagheid A, Lamlum H, Ristamaki R, Collan Y, Pyrhonen S. E-cadherin, CD44s and CD44v6 correlate with tumour differentiation in colorectal cancer. *Oncol Rep.* May 2005;13(5):831-835.

205. Elzagheid A, Algars A, Bendardaf R, et al. E-cadherin expression pattern in primary colorectal carcinomas and their metastases reflects disease outcome. *World J Gastroenterol.* Jul 21 2006;12(27):4304-4309.

206. Zumbrunn J, Kinoshita K, Hyman AA, Nathke IS. Binding of the adenomatous polyposis coli protein to microtubules increases microtubule stability and is regulated by GSK3 beta phosphorylation. *Curr Biol.* Jan 9 2001;11(1):44-49.

207. Rosin-Arbesfeld R, Ihrke G, Bienz M. Actin-dependent membrane association of the APC tumour suppressor in polarized mammalian epithelial cells. *Embo J.* Nov 1 2001;20(21):5929-5939.

208. Watanabe T, Wang S, Noritake J, et al. Interaction with IQGAP1 links APC to Rac1, Cdc42, and actin filaments during cell polarization and migration. *Dev Cell.* Dec 2004;7(6):871-883.

209. Kawasaki Y, Senda T, Ishidate T, et al. Asef, a link between the tumor suppressor APC and G-protein signaling. *Science*. Aug 18 2000;289(5482):1194-1197.

210. Kawasaki Y, Sato R, Akiyama T. Mutated APC and Asef are involved in the migration of colorectal tumour cells. *Nat Cell Biol*. Mar 2003;5(3):211-215.

211. van der Flier A, Sonnenberg A. Function and interactions of integrins. *Cell Tissue Res*. Sep 2001;305(3):285-298.

212. Ziegler WH, Gingras AR, Critchley DR, Emsley J. Integrin connections to the cytoskeleton through talin and vinculin. *Biochem Soc Trans*. Apr 2008;36(Pt 2):235-239.

213. Otey CA, Pavalko FM, Burridge K. An interaction between alpha-actinin and the beta 1 integrin subunit in vitro. *J Cell Biol*. Aug 1990;111(2):721-729.

214. Cabodi S, Di Stefano P, Leal Mdel P, et al. Integrins and signal transduction. *Adv Exp Med Biol*. 2010;674:43-54.

215. Nemeth JA, Nakada MT, Trikha M, et al. Alpha-v integrins as therapeutic targets in oncology. *Cancer Invest*. Oct 2007;25(7):632-646.

216. Denadai MV, Viana LS, Affonso RJ, Jr., et al. Expression of integrin genes and proteins in progression and dissemination of colorectal adenocarcinoma. *BMC Clin Pathol*. 2013;13:16.

217. Enns A, Korb T, Schluter K, et al. Alphavbeta5-integrins mediate early steps of metastasis formation. *Eur J Cancer*. May 2005;41(7):1065-1072.

218. Ha SY, Shin J, Kim JH, et al. Overexpression of integrin alphav correlates with poor prognosis in colorectal cancer. *J Clin Pathol*. Jul 2014;67(7):576-581.

219. Sahai E, Marshall CJ. RHO-GTPases and cancer. *Nat Rev Cancer*. Feb 2002;2(2):133-142.

220. Ohata H, Ishiguro T, Aihara Y, et al. Induction of the stem-like cell regulator CD44 by Rho kinase inhibition contributes to the maintenance of colon cancer-initiating cells. *Cancer Res*. Oct 1 2012;72(19):5101-5110.

221. Rodrigues P, Macaya I, Bazzocco S, et al. RHOA inactivation enhances Wnt signalling and promotes colorectal cancer. *Nat Commun*. 2014;5:5458.

222. Braga VM, Machesky LM, Hall A, Hotchin NA. The small GTPases Rho and Rac are required for the establishment of cadherin-dependent cell-cell contacts. *J Cell Biol*. Jun 16 1997;137(6):1421-1431.

223. Scott RW, Hooper S, Crighton D, et al. LIM kinases are required for invasive path generation by tumor and tumor-associated stromal cells. *J Cell Biol*. Oct 4 2010;191(1):169-185.

224. Lourenco FC, Munro J, Brown J, et al. Reduced LIMK2 expression in colorectal cancer reflects its role in limiting stem cell proliferation. *Gut*. Mar 2014;63(3):480-493.

225. Ratushny V, Gober MD, Hick R, Ridky TW, Seykora JT. From keratinocyte to cancer: the pathogenesis and modeling of cutaneous squamous cell carcinoma. *J Clin Invest*. Feb 2012;122(2):464-472.

226. Ziegler A, Jonason AS, Leffell DJ, et al. Sunburn and p53 in the onset of skin cancer. *Nature*. Dec 22-29 1994;372(6508):773-776.

227. Ortonne JP. From actinic keratosis to squamous cell carcinoma. *Br J Dermatol*. Apr 2002;146 Suppl 61:20-23.

228. Campbell C, Quinn AG, Ro YS, Angus B, Rees JL. p53 mutations are common and early events that precede tumor invasion in squamous cell neoplasia of the skin. *J Invest Dermatol*. Jun 1993;100(6):746-748.

229. Brash DE, Rudolph JA, Simon JA, et al. A role for sunlight in skin cancer: UV-induced p53 mutations in squamous cell carcinoma. *Proc Natl Acad Sci U S A*. Nov 15 1991;88(22):10124-10128.

230. Kubo Y, Urano Y, Yoshimoto K, et al. p53 gene mutations in human skin cancers and precancerous lesions: comparison with immunohistochemical analysis. *J Invest Dermatol*. Apr 1994;102(4):440-444.

231. Pierceall WE, Goldberg LH, Tainsky MA, Mukhopadhyay T, Ananthaswamy HN. Ras gene mutation and amplification in human nonmelanoma skin cancers. *Mol Carcinog*. 1991;4(3):196-202.

232. Spencer JM, Kahn SM, Jiang W, DeLeo VA, Weinstein IB. Activated ras genes occur in human actinic keratoses, premalignant precursors to squamous cell carcinomas. *Arch Dermatol*. Jul 1995;131(7):796-800.

233. Khavari PA. Modelling cancer in human skin tissue. *Nat Rev Cancer*. Apr 2006;6(4):270-280.

234. Ridky TW, Chow JM, Wong DJ, Khavari PA. Invasive three-dimensional organotypic neoplasia from multiple normal human epithelia. *Nat Med*. Dec 2010;16(12):1450-1455.

235. Dajee M, Lazarov M, Zhang JY, et al. NF-kappaB blockade and oncogenic Ras trigger invasive human epidermal neoplasia. *Nature*. Feb 6 2003;421(6923):639-643.

236. Lazarov M, Kubo Y, Cai T, et al. CDK4 coexpression with Ras generates malignant human epidermal tumorigenesis. *Nat Med*. Oct 2002;8(10):1105-1114.

237. Dotto GP. Notch tumor suppressor function. *Oncogene*. Sep 1 2008;27(38):5115-5123.

238. Okuyama R, Nguyen BC, Talora C, et al. High commitment of embryonic keratinocytes to terminal differentiation through a Notch1-caspase 3 regulatory mechanism. *Dev Cell*. Apr 2004;6(4):551-562.

239. Lefort K, Mandinova A, Ostano P, et al. Notch1 is a p53 target gene involved in human keratinocyte tumor suppression through negative regulation of ROCK1/2 and MRCKalpha kinases. *Genes Dev*. Mar 1 2007;21(5):562-577.

240. Nicolas M, Wolfer A, Raj K, et al. Notch1 functions as a tumor suppressor in mouse skin. *Nat Genet*. Mar 2003;33(3):416-421.

241. South AP, Purdie KJ, Watt SA, et al. NOTCH1 mutations occur early during cutaneous squamous cell carcinogenesis. *J Invest Dermatol*. Oct 2014;134(10):2630-2638.

242. Kowal-Vern A, Criswell BK. Burn scar neoplasms: a literature review and statistical analysis. *Burns*. Jun 2005;31(4):403-413.

243. O'Byrne KJ, Dalgleish AG. Chronic immune activation and inflammation as the cause of malignancy. *Br J Cancer*. Aug 17 2001;85(4):473-483.

244. Coussens LM, Werb Z. Inflammation and cancer. *Nature*. Dec 19-26 2002;420(6917):860-867.

245. Erez N, Truitt M, Olson P, Arron ST, Hanahan D. Cancer-Associated Fibroblasts Are Activated in Incipient Neoplasia to Orchestrate Tumor-Promoting Inflammation in an NF-kappaB-Dependent Manner. *Cancer Cell*. Feb 17 2010;17(2):135-147.

246. Griffin JR, Wriston CC, Peters MS, Lehman JS. Decreased expression of intercellular adhesion molecules in acantholytic squamous cell carcinoma compared with invasive well-differentiated squamous cell carcinoma of the skin. *Am J Clin Pathol*. Apr 2013;139(4):442-447.

247. Perez OD, Kinoshita S, Hitoshi Y, et al. Activation of the PKB/AKT pathway by ICAM-2. *Immunity*. Jan 2002;16(1):51-65.

248. Sabeh F, Li XY, Saunders TL, Rowe RG, Weiss SJ. Secreted versus membrane-anchored collagenases: relative roles in fibroblast-dependent collagenolysis and invasion. *J Biol Chem*. Aug 21 2009;284(34):23001-23011.

249. Sasaki T, Fassler R, Hohenester E. Laminin: the crux of basement membrane assembly. *J Cell Biol*. Mar 29 2004;164(7):959-963.

250. Ryan MC, Christiano AM, Engvall E, et al. The functions of laminins: lessons from in vivo studies. *Matrix Biol*. Dec 1996;15(6):369-381.

251. Yamamoto H, Itoh F, Iku S, Hosokawa M, Imai K. Expression of the gamma(2) chain of laminin-5 at the invasive front is associated with recurrence and poor prognosis in human esophageal squamous cell carcinoma. *Clin Cancer Res*. Apr 2001;7(4):896-900.

252. Katayama M, Sekiguchi K. Laminin-5 in epithelial tumour invasion. *J Mol Histol*. Mar 2004;35(3):277-286.

253. Waterman EA, Sakai N, Nguyen NT, et al. A laminin-collagen complex drives human epidermal carcinogenesis through phosphoinositol-3-kinase activation. *Cancer Res*. May 1 2007;67(9):4264-4270.

254. Franz M, Hansen T, Richter P, et al. Complex formation of the laminin-5 gamma2 chain and large unspliced tenascin-C in oral squamous cell carcinoma in vitro and in situ: implications for sequential modulation of extracellular matrix in the invasive tumor front. *Histochem Cell Biol*. Jul 2006;126(1):125-131.

255. Hennings H, Glick AB, Lowry DT, Krsmanovic LS, Sly LM, Yuspa SH. FVB/N mice: an inbred strain sensitive to the chemical induction of squamous cell carcinomas in the skin. *Carcinogenesis*. Nov 1993;14(11):2353-2358.

256. Lelli KM, Slattery M, Mann RS. Disentangling the many layers of eukaryotic transcriptional regulation. *Annu Rev Genet*. 2012;46:43-68.

257. Ong CT, Corces VG. Enhancer function: new insights into the regulation of tissue-specific gene expression. *Nat Rev Genet*. Apr 2011;12(4):283-293.

258. Spitz F, Furlong EE. Transcription factors: from enhancer binding to developmental control. *Nat Rev Genet*. Sep 2012;13(9):613-626.

259. Lee TI, Young RA. Transcriptional regulation and its misregulation in disease. *Cell*. Mar 14 2013;152(6):1237-1251.

260. Littlewood TD, Kreuzaler P, Evan GI. All things to all people. *Cell*. Sep 28 2012;151(1):11-13.

261. Kotake Y, Nakagawa T, Kitagawa K, et al. Long non-coding RNA ANRIL is required for the PRC2 recruitment to and silencing of p15(INK4B) tumor suppressor gene. *Oncogene*. Apr 21 2011;30(16):1956-1962.

262. Lu J, Getz G, Miska EA, et al. MicroRNA expression profiles classify human cancers. *Nature*. Jun 9 2005;435(7043):834-838.

263. Calin GA, Sevignani C, Dumitru CD, et al. Human microRNA genes are frequently located at fragile sites and genomic regions involved in cancers. *Proc Natl Acad Sci U S A*. Mar 2 2004;101(9):2999-3004.

264. Weber B, Stresemann C, Brueckner B, Lyko F. Methylation of human microRNA genes in normal and neoplastic cells. *Cell Cycle*. May 2 2007;6(9):1001-1005.

265. Chang TC, Wentzel EA, Kent OA, et al. Transactivation of miR-34a by p53 broadly influences gene expression and promotes apoptosis. *Mol Cell*. Jun 8 2007;26(5):745-752.

266. Sass S, Dietmann S, Burk UC, et al. MicroRNAs coordinately regulate protein complexes. *BMC Syst Biol*. 2011;5:136.

267. Glickman MH, Ciechanover A. The ubiquitin-proteasome proteolytic pathway: destruction for the sake of construction. *Physiol Rev*. Apr 2002;82(2):373-428.

268. Pray TR, Parlati F, Huang J, et al. Cell cycle regulatory E3 ubiquitin ligases as anticancer targets. *Drug Resist Updat*. Dec 2002;5(6):249-258.

269. Hanahan D, Weinberg RA. The hallmarks of cancer. *Cell*. Jan 7 2000;100(1):57-70.

270. Bird A. DNA methylation patterns and epigenetic memory. *Genes Dev*. Jan 1 2002;16(1):6-21.

271. Jones PA, Laird PW. Cancer epigenetics comes of age. *Nat Genet*. Feb 1999;21(2):163-167.

272. Jones PA, Baylin SB. The fundamental role of epigenetic events in cancer. *Nat Rev Genet*. Jun 2002;3(6):415-428.

273. Herman JG. Hypermethylation of tumor suppressor genes in cancer. *Semin Cancer Biol*. Oct 1999;9(5):359-367.

274. Rideout WM, 3rd, Coetzee GA, Olumi AF, Jones PA. 5-Methylcytosine as an endogenous mutagen in the human LDL receptor and p53 genes. *Science*. Sep 14 1990;249(4974):1288-1290.

275. Gibney ER, Nolan CM. Epigenetics and gene expression. *Heredity (Edinb)*. Jul 2010;105(1):4-13.

276. Antequera F, Bird A. CpG islands. *Exs*. 1993;64:169-185.

277. Bird AP, Wolffe AP. Methylation-induced repression--belts, braces, and chromatin. *Cell*. Nov 24 1999;99(5):451-454.

278. Bestor TH. The host defence function of genomic methylation patterns. *Novartis Found Symp*. 1998;214:187-195; discussion 195-189, 228-132.

279. Knudson AG. Two genetic hits (more or less) to cancer. *Nat Rev Cancer*. Nov 2001;1(2):157-162.

280. Esteller M, Fraga MF, Guo M, et al. DNA methylation patterns in hereditary human cancers mimic sporadic tumorigenesis. *Hum Mol Genet*. Dec 15 2001;10(26):3001-3007.

281. Kuismanen SA, Holmberg MT, Salovaara R, de la Chapelle A, Peltomaki P. Genetic and epigenetic modification of MLH1 accounts for a major share of microsatellite-unstable colorectal cancers. *Am J Pathol*. May 2000;156(5):1773-1779.

282. Lee WH, Morton RA, Epstein JI, et al. Cytidine methylation of regulatory sequences near the pi-class glutathione S-transferase gene accompanies human prostatic carcinogenesis. *Proc Natl Acad Sci U S A*. Nov 22 1994;91(24):11733-11737.

283. Yoo CB, Jones PA. Epigenetic therapy of cancer: past, present and future. *Nat Rev Drug Discov*. Jan 2006;5(1):37-50.

284. Muller CI, Ruter B, Koeffler HP, Lubbert M. DNA hypermethylation of myeloid cells, a novel therapeutic target in MDS and AML. *Curr Pharm Biotechnol*. Oct 2006;7(5):315-321.

285. Walsh CP, Chaillet JR, Bestor TH. Transcription of IAP endogenous retroviruses is constrained by cytosine methylation. *Nat Genet*. Oct 1998;20(2):116-117.

286. Narayan A, Ji W, Zhang XY, et al. Hypomethylation of pericentromeric DNA in breast adenocarcinomas. *Int J Cancer*. Sep 11 1998;77(6):833-838.

287. Qu G, Dubeau L, Narayan A, Yu MC, Ehrlich M. Satellite DNA hypomethylation vs. overall genomic hypomethylation in ovarian epithelial tumors of different malignant potential. *Mutat Res*. Jan 25 1999;423(1-2):91-101.

288. Widschwendter M, Jiang G, Woods C, et al. DNA hypomethylation and ovarian cancer biology. *Cancer Res*. Jul 1 2004;64(13):4472-4480.

289. Furuichi Y, Wataya Y, Hayatsu H, Ukita T. Chemical modification of tRNA-Tyr-yeast with bisulfite. A new method to modify isopentenyladenosine residue. *Biochem Biophys Res Commun*. Dec 9 1970;41(5):1185-1191.

290. Shapiro R, DiFate V, Welcher M. Deamination of cytosine derivatives by bisulfite. Mechanism of the reaction. *J Am Chem Soc*. Feb 6 1974;96(3):906-912.

291. Raizis AM, Schmitt F, Jost JP. A bisulfite method of 5-methylcytosine mapping that minimizes template degradation. *Anal Biochem*. Mar 20 1995;226(1):161-166.

292. Herman JG, Graff JR, Myohanen S, Nelkin BD, Baylin SB. Methylation-specific PCR: a novel PCR assay for methylation status of CpG islands. *Proc Natl Acad Sci U S A*. Sep 3 1996;93(18):9821-9826.

293. Frommer M, McDonald LE, Millar DS, et al. A genomic sequencing protocol that yields a positive display of 5-methylcytosine residues in individual DNA strands. *Proc Natl Acad Sci U S A*. Mar 1 1992;89(5):1827-1831.

294. Jain RK. Normalizing tumor microenvironment to treat cancer: bench to bedside to biomarkers. *J Clin Oncol*. Jun 10 2013;31(17):2205-2218.

295. Beil M, Micoulet A, von Wichert G, et al. Sphingosylphosphorylcholine regulates keratin network architecture and visco-elastic properties of human cancer cells. *Nat Cell Biol*. Sep 2003;5(9):803-811.

296. Paszek MJ, Weaver VM. The tension mounts: mechanics meets morphogenesis and malignancy. *J Mammary Gland Biol Neoplasia*. Oct 2004;9(4):325-342.

297. Padera TP, Stoll BR, Tooredman JB, Capen D, di Tomaso E, Jain RK. Pathology: cancer cells compress intratumour vessels. *Nature*. Feb 19 2004;427(6976):695.

298. Akiri G, Sabo E, Dafni H, et al. Lysyl oxidase-related protein-1 promotes tumor fibrosis and tumor progression in vivo. *Cancer Res*. Apr 1 2003;63(7):1657-1666.

299. Egeblad M, Rasch MG, Weaver VM. Dynamic interplay between the collagen scaffold and tumor evolution. *Curr Opin Cell Biol*. Oct 2010;22(5):697-706.

300. Parsons JT, Horwitz AR, Schwartz MA. Cell adhesion: integrating cytoskeletal dynamics and cellular tension. *Nat Rev Mol Cell Biol*. Sep 2010;11(9):633-643.

301. Wozniak MA, Desai R, Solski PA, Der CJ, Keely PJ. ROCK-generated contractility regulates breast epithelial cell differentiation in response to the physical properties of a three-dimensional collagen matrix. *J Cell Biol*. Nov 10 2003;163(3):583-595.

302. Chiquet M, Gelman L, Lutz R, Maier S. From mechanotransduction to extracellular matrix gene expression in fibroblasts. *Biochim Biophys Acta*. May 2009;1793(5):911-920.

303. Wynn TA. Common and unique mechanisms regulate fibrosis in various fibroproliferative diseases. *J Clin Invest*. Mar 2007;117(3):524-529.

304. Hinz B, Phan SH, Thannickal VJ, Galli A, Bochaton-Piallat ML, Gabbiani G. The myofibroblast: one function, multiple origins. *Am J Pathol*. Jun 2007;170(6):1807-1816.

305. Wells RG, Discher DE. Matrix elasticity, cytoskeletal tension, and TGF-beta: the insoluble and soluble meet. *Sci Signal*. 2008;1(10):pe13.

306. Junker JP, Kratz C, Tollback A, Kratz G. Mechanical tension stimulates the transdifferentiation of fibroblasts into myofibroblasts in human burn scars. *Burns*. Nov 2008;34(7):942-946.

307. Aarabi S, Bhatt KA, Shi Y, et al. Mechanical load initiates hypertrophic scar formation through decreased cellular apoptosis. *Faseb J*. Oct 2007;21(12):3250-3261.

308. Wipff PJ, Rifkin DB, Meister JJ, Hinz B. Myofibroblast contraction activates latent TGF-beta1 from the extracellular matrix. *J Cell Biol*. Dec 17 2007;179(6):1311-1323.

309. Wight TN, Potter-Perigo S. The extracellular matrix: an active or passive player in fibrosis? *Am J Physiol Gastrointest Liver Physiol*. Dec 2011;301(6):G950-955.

310. Farazi PA, DePinho RA. Hepatocellular carcinoma pathogenesis: from genes to environment. *Nat Rev Cancer*. Sep 2006;6(9):674-687.

311. Archontogeorgis K, Steiropoulos P, Tzouvelekis A, Nena E, Bouros D. Lung cancer and interstitial lung diseases: a systematic review. *Pulm Med*. 2012;2012:315918.

312. Radisky DC, Kenny PA, Bissell MJ. Fibrosis and cancer: do myofibroblasts come also from epithelial cells via EMT? *J Cell Biochem*. Jul 1 2007;101(4):830-839.

313. Daniels CE, Jett JR. Does interstitial lung disease predispose to lung cancer? *Curr Opin Pulm Med*. Sep 2005;11(5):431-437.

314. Neaud V, Faouzi S, Guirouilh J, et al. Human hepatic myofibroblasts increase invasiveness of hepatocellular carcinoma cells: evidence for a role of hepatocyte growth factor. *Hepatology*. Dec 1997;26(6):1458-1466.

315. Quante M, Tu SP, Tomita H, et al. Bone marrow-derived myofibroblasts contribute to the mesenchymal stem cell niche and promote tumor growth. *Cancer Cell*. Feb 15 2011;19(2):257-272.

316. Nielsen BS, Sehested M, Timshel S, Pyke C, Dano K. Messenger RNA for urokinase plasminogen activator is expressed in myofibroblasts adjacent to cancer cells in human breast cancer. *Lab Invest*. Jan 1996;74(1):168-177.

317. Bisson C, Blacher S, Polette M, et al. Restricted expression of membrane type 1-matrix metalloproteinase by myofibroblasts adjacent to human breast cancer cells. *Int J Cancer*. May 20 2003;105(1):7-13.

318. Offersen BV, Nielsen BS, Hoyer-Hansen G, et al. The myofibroblast is the predominant plasminogen activator inhibitor-1-expressing cell type in human breast carcinomas. *Am J Pathol*. Nov 2003;163(5):1887-1899.

319. Ohtani H, Motohashi H, Sato H, Seiki M, Nagura H. Dual over-expression pattern of membrane-type metalloproteinase-1 in cancer and stromal cells in human gastrointestinal carcinoma revealed by in situ hybridization and immunoelectron microscopy. *Int J Cancer*. Nov 27 1996;68(5):565-570.

320. Cirri P, Chiarugi P. Cancer associated fibroblasts: the dark side of the coin. *Am J Cancer Res*. 2011;1(4):482-497.

321. Gallagher PG, Bao Y, Prorock A, et al. Gene expression profiling reveals cross-talk between melanoma and fibroblasts: implications for host-tumor interactions in metastasis. *Cancer Res*. May 15 2005;65(10):4134-4146.

322. Bergfeld SA, DeClerck YA. Bone marrow-derived mesenchymal stem cells and the tumor microenvironment. *Cancer Metastasis Rev*. Jun 2010;29(2):249-261.

323. Schor SL, Haggie JA, Durning P, et al. Occurrence of a fetal fibroblast phenotype in familial breast cancer. *Int J Cancer*. Jun 15 1986;37(6):831-836.

324. Kuperwasser C, Chavarria T, Wu M, et al. Reconstruction of functionally normal and malignant human breast tissues in mice. *Proc Natl Acad Sci U S A*. Apr 6 2004;101(14):4966-4971.

325. Bhowmick NA, Chytil A, Plieth D, et al. TGF-beta signaling in fibroblasts modulates the oncogenic potential of adjacent epithelia. *Science*. Feb 6 2004;303(5659):848-851.

326. Wang W, Li Q, Yamada T, et al. Crosstalk to stromal fibroblasts induces resistance of lung cancer to epidermal growth factor receptor tyrosine kinase inhibitors. *Clin Cancer Res*. Nov 1 2009;15(21):6630-6638.

327. Gerber PA, Hippe A, Buhren BA, Muller A, Homey B. Chemokines in tumor-associated angiogenesis. *Biol Chem*. Dec 2009;390(12):1213-1223.

328. Hynes RO. The extracellular matrix: not just pretty fibrils. *Science*. Nov 27 2009;326(5957):1216-1219.

329. Roy R, Yang J, Moses MA. Matrix metalloproteinases as novel biomarkers and potential therapeutic targets in human cancer. *J Clin Oncol*. Nov 1 2009;27(31):5287-5297.

330. Kalluri R, Weinberg RA. The basics of epithelial-mesenchymal transition. *J Clin Invest*. Jun 2009;119(6):1420-1428.

331. Matsumoto K, Nakamura T. Hepatocyte growth factor and the Met system as a mediator of tumor-stromal interactions. *Int J Cancer*. Aug 1 2006;119(3):477-483.

332. Paszek MJ, Zahir N, Johnson KR, et al. Tensional homeostasis and the malignant phenotype. *Cancer Cell*. Sep 2005;8(3):241-254.

333. Levental KR, Yu H, Kass L, et al. Matrix crosslinking forces tumor progression by enhancing integrin signaling. *Cell*. Nov 25 2009;139(5):891-906.

334. Zaman MH, Trapani LM, Sieminski AL, et al. Migration of tumor cells in 3D matrices is governed by matrix stiffness along with cell-matrix adhesion and proteolysis. *Proc Natl Acad Sci U S A*. Jul 18 2006;103(29):10889-10894.

335. Pankov R, Yamada KM. Fibronectin at a glance. *J Cell Sci*. Oct 15 2002;115(Pt 20):3861-3863.

336. Kaplan RN, Riba RD, Zacharoulis S, et al. VEGFR1-positive haematopoietic bone marrow progenitors initiate the pre-metastatic niche. *Nature*. Dec 8 2005;438(7069):820-827.

337. Kobayashi N, Miyoshi S, Mikami T, et al. Hyaluronan deficiency in tumor stroma impairs macrophage trafficking and tumor neovascularization. *Cancer Res*. Sep 15 2010;70(18):7073-7083.

338. De Wever O, Nguyen QD, Van Hoorde L, et al. Tenascin-C and SF/HGF produced by myofibroblasts in vitro provide convergent pro-invasive signals to human colon cancer cells through RhoA and Rac. *Faseb J*. Jun 2004;18(9):1016-1018.

339. Solis MA, Chen YH, Wong TY, Bittencourt VZ, Lin YC, Huang LL. Hyaluronan regulates cell behavior: a potential niche matrix for stem cells. *Biochem Res Int*. 2012;2012:346972.

340. Kauppila S, Stenback F, Risteli J, Jukkola A, Risteli L. Aberrant type I and type III collagen gene expression in human breast cancer in vivo. *J Pathol*. Nov 1998;186(3):262-268.

341. Hasebe T, Sasaki S, Imoto S, Mukai K, Yokose T, Ochiai A. Prognostic significance of fibrotic focus in invasive ductal carcinoma of the breast: a prospective observational study. *Mod Pathol*. May 2002;15(5):502-516.

342. Hwang RF, Moore T, Arumugam T, et al. Cancer-associated stromal fibroblasts promote pancreatic tumor progression. *Cancer Res*. Feb 1 2008;68(3):918-926.

343. Malik R, Lelkes PI, Cukierman E. Biomechanical and biochemical remodeling of stromal extracellular matrix in cancer. *Trends Biotechnol*. Apr 2015;33(4):230-236.

344. Butcher DT, Alliston T, Weaver VM. A tense situation: forcing tumour progression. *Nat Rev Cancer*. Feb 2009;9(2):108-122.

345. Croft DR, Sahai E, Mavria G, et al. Conditional ROCK activation in vivo induces tumor cell dissemination and angiogenesis. *Cancer Res*. Dec 15 2004;64(24):8994-9001.

346. Provenzano PP, Keely PJ. Mechanical signaling through the cytoskeleton regulates cell proliferation by coordinated focal adhesion and Rho GTPase signaling. *J Cell Sci*. Apr 15 2011;124(Pt 8):1195-1205.

347. Suresh S. Biomechanics and biophysics of cancer cells. *Acta Biomater*. Jul 2007;3(4):413-438.

348. Ridley AJ, Schwartz MA, Burridge K, et al. Cell migration: integrating signals from front to back. *Science*. Dec 5 2003;302(5651):1704-1709.

349. Ingber DE. Tensegrity-based mechanosensing from macro to micro. *Prog Biophys Mol Biol*. Jun-Jul 2008;97(2-3):163-179.

350. Nelson CM, Vanduijn MM, Inman JL, Fletcher DA, Bissell MJ. Tissue geometry determines sites of mammary branching morphogenesis in organotypic cultures. *Science*. Oct 13 2006;314(5797):298-300.

351. Chiquet-Ehrismann R, Kalla P, Pearson CA, Beck K, Chiquet M. Tenascin interferes with fibronectin action. *Cell*. May 6 1988;53(3):383-390.

352. Gherzi R, Carnemolla B, Siri A, Ponassi M, Balza E, Zardi L. Human tenascin gene. Structure of the 5'-region, identification, and characterization of the transcription regulatory sequences. *J Biol Chem*. Feb 17 1995;270(7):3429-3434.

353. Pas J, Wyszko E, Rolle K, et al. Analysis of structure and function of tenascin-C. *Int J Biochem Cell Biol*. 2006;38(9):1594-1602.

354. Jones FS, Jones PL. The tenascin family of ECM glycoproteins: structure, function, and regulation during embryonic development and tissue remodeling. *Dev Dyn*. Jun 2000;218(2):235-259.

355. Prieto AL, Edelman GM, Crossin KL. Multiple integrins mediate cell attachment to cytotactin/tenascin. *Proc Natl Acad Sci U S A*. Nov 1 1993;90(21):10154-10158.

356. Chung CY, Murphy-Ullrich JE, Erickson HP. Mitogenesis, cell migration, and loss of focal adhesions induced by tenascin-C interacting with its cell surface receptor, annexin II. *Mol Biol Cell*. Jun 1996;7(6):883-892.

357. Saito Y, Imazeki H, Miura S, et al. A peptide derived from tenascin-C induces beta1 integrin activation through syndecan-4. *J Biol Chem*. Nov 30 2007;282(48):34929-34937.

358. Chiquet-Ehrismann R, Matsuoka Y, Hofer U, Spring J, Bernasconi C, Chiquet M. Tenascin variants: differential binding to fibronectin and distinct distribution in cell cultures and tissues. *Cell Regul*. Nov 1991;2(11):927-938.

359. Swindle CS, Tran KT, Johnson TD, et al. Epidermal growth factor (EGF)-like repeats of human tenascin-C as ligands for EGF receptor. *J Cell Biol*. Jul 23 2001;154(2):459-468.

360. Chiquet-Ehrismann R. Tenascins. *Int J Biochem Cell Biol*. Jun 2004;36(6):986-990.

361. Webb CM, Zaman G, Mosley JR, Tucker RP, Lanyon LE, Mackie EJ. Expression of tenascin-C in bones responding to mechanical load. *J Bone Miner Res*. Jan 1997;12(1):52-58.

362. Mackie EJ, Halfter W, Liverani D. Induction of tenascin in healing wounds. *J Cell Biol*. Dec 1988;107(6 Pt 2):2757-2767.

363. Midwood KS, Orend G. The role of tenascin-C in tissue injury and tumorigenesis. *J Cell Commun Signal*. Dec 2009;3(3-4):287-310.

364. Orend G, Chiquet-Ehrismann R. Tenascin-C induced signaling in cancer. *Cancer Lett*. Dec 8 2006;244(2):143-163.

365. Schalkwijk J, Van Vlijmen I, Oosterling B, et al. Tenascin expression in hyperproliferative skin diseases. *Br J Dermatol*. Jan 1991;124(1):13-20.

366. Midwood KS, Williams LV, Schwarzbauer JE. Tissue repair and the dynamics of the extracellular matrix. *Int J Biochem Cell Biol*. Jun 2004;36(6):1031-1037.

367. Lowy CM, Oskarsson T. Tenascin C in metastasis: A view from the invasive front. *Cell Adh Migr*. 2015;9(1-2):112-124.

368. Midwood K, Sacre S, Piccinini AM, et al. Tenascin-C is an endogenous activator of Toll-like receptor 4 that is essential for maintaining inflammation in arthritic joint disease. *Nat Med*. Jul 2009;15(7):774-780.

369. Seyger MM, van Pelt JP, van den Born J, Latijnhouwers MA, de Jong EM. Epicutaneous application of leukotriene B4 induces patterns of tenascin and a heparan sulfate proteoglycan epitope that are typical for psoriatic lesions. *Arch Dermatol Res*. May 1997;289(6):331-336.

370. Hauzenberger D, Olivier P, Gundersen D, Ruegg C. Tenascin-C inhibits beta1 integrin-dependent T lymphocyte adhesion to fibronectin through the binding of its fnIII 1-5 repeats to fibronectin. *Eur J Immunol*. May 1999;29(5):1435-1447.

371. Clark RA, Erickson HP, Springer TA. Tenascin supports lymphocyte rolling. *J Cell Biol*. May 5 1997;137(3):755-765.

372. Puente Navazo MD, Valmori D, Ruegg C. The alternatively spliced domain TnFnIII A1A2 of the extracellular matrix protein tenascin-C suppresses activation-induced T lymphocyte proliferation and cytokine production. *J Immunol*. Dec 1 2001;167(11):6431-6440.

373. Betz P, Nerlich A, Tubel J, Penning R, Eisenmenger W. Localization of tenascin in human skin wounds--an immunohistochemical study. *Int J Legal Med*. 1993;105(6):325-328.

374. Kaarteenaho-Wiik R, Lakari E, Soini Y, Pollanen R, Kinnula VL, Paakko P. Tenascin expression and distribution in pleural inflammatory and fibrotic diseases. *J Histochem Cytochem*. Sep 2000;48(9):1257-1268.

375. Imanaka-Yoshida K, Hiroe M, Yasutomi Y, et al. Tenascin-C is a useful marker for disease activity in myocarditis. *J Pathol*. Jul 2002;197(3):388-394.

376. Latijnhouwers M, Bergers M, Ponec M, Dijkman H, Andriessen M, Schalkwijk J. Human epidermal keratinocytes are a source of tenascin-C during wound healing. *J Invest Dermatol*. May 1997;108(5):776-783.

377. Gerritsen MJ, Elbers ME, de Jong EM, van de Kerkhof PC. Recruitment of cycling epidermal cells and expression of filaggrin, involucrin and tenascin in the margin of the active psoriatic plaque, in the uninvolved skin of psoriatic patients and in the normal healthy skin. *J Dermatol Sci*. Mar 1997;14(3):179-188.

378. Schenk S, Bruckner-Tuderman L, Chiquet-Ehrismann R. Dermo-epidermal separation is associated with induced tenascin expression in human skin. *Br J Dermatol*. Jul 1995;133(1):13-22.

379. Ishii K, Imanaka-Yoshida K, Yoshida T, Sugimura Y. Role of stromal tenascin-C in mouse prostatic development and epithelial cell differentiation. *Dev Biol*. Dec 15 2008;324(2):310-319.

380. McClain SA, Simon M, Jones E, et al. Mesenchymal cell activation is the rate-limiting step of granulation tissue induction. *Am J Pathol*. Oct 1996;149(4):1257-1270.

381. Trebaul A, Chan EK, Midwood KS. Regulation of fibroblast migration by tenascin-C. *Biochem Soc Trans*. Aug 2007;35(Pt 4):695-697.

382. Clark RA. Biology of dermal wound repair. *Dermatol Clin*. Oct 1993;11(4):647-666.

383. El-Karef A, Yoshida T, Gabazza EC, et al. Deficiency of tenascin-C attenuates liver fibrosis in immune-mediated chronic hepatitis in mice. *J Pathol*. Jan 2007;211(1):86-94.

384. Nakao N, Hiraiwa N, Yoshiki A, Ike F, Kusakabe M. Tenascin-C promotes healing of Habu-snake venom-induced glomerulonephritis: studies in knockout congenic mice and in culture. *Am J Pathol*. May 1998;152(5):1237-1245.

385. Tanaka R, Seki Y, Saito Y, et al. Tenascin-C-derived peptide TNIIIA2 highly enhances cell survival and platelet-derived growth factor (PDGF)-dependent cell proliferation through potentiated and sustained activation of integrin alpha5beta1. *J Biol Chem*. Jun 20 2014;289(25):17699-17708.

386. End P, Panayotou G, Entwistle A, Waterfield MD, Chiquet M. Tenascin: a modulator of cell growth. *Eur J Biochem*. Nov 1 1992;209(3):1041-1051.

387. Chiquet M, Fambrough DM. Chick myotendinous antigen. II. A novel extracellular glycoprotein complex consisting of large disulfide-linked subunits. *J Cell Biol*. Jun 1984;98(6):1937-1946.

388. Ramos DM, Chen B, Regezi J, Zardi L, Pytela R. Tenascin-C matrix assembly in oral squamous cell carcinoma. *Int J Cancer*. Mar 2 1998;75(5):680-687.

389. Faissner A, Kruse J, Kuhn K, Schachner M. Binding of the J1 adhesion molecules to extracellular matrix constituents. *J Neurochem*. Mar 1990;54(3):1004-1015.

390. Kii I, Nishiyama T, Li M, et al. Incorporation of tenascin-C into the extracellular matrix by periostin underlies an extracellular meshwork architecture. *J Biol Chem*. Jan 15 2010;285(3):2028-2039.

391. Day JM, Olin AI, Murdoch AD, et al. Alternative splicing in the aggrecan G3 domain influences binding interactions with tenascin-C and other extracellular matrix proteins. *J Biol Chem*. Mar 26 2004;279(13):12511-12518.

392. Latijnhouwers MA, Bergers M, Van Bergen BH, Spruijt KI, Andriessen MP, Schalkwijk J. Tenascin expression during wound healing in human skin. *J Pathol*. Jan 1996;178(1):30-35.

393. Ingber DE. Mechanical signaling and the cellular response to extracellular matrix in angiogenesis and cardiovascular physiology. *Circ Res.* Nov 15 2002;91(10):877-887.

394. Canfield AE, Schor AM. Evidence that tenascin and thrombospondin-1 modulate sprouting of endothelial cells. *J Cell Sci.* Feb 1995;108 (Pt 2):797-809.

395. Nomi M, Miyake H, Sugita Y, Fujisawa M, Soker S. Role of growth factors and endothelial cells in therapeutic angiogenesis and tissue engineering. *Curr Stem Cell Res Ther.* Sep 2006;1(3):333-343.

396. Sumioka T, Fujita N, Kitano A, Okada Y, Saika S. Impaired angiogenic response in the cornea of mice lacking tenascin C. *Invest Ophthalmol Vis Sci.* Apr 2011;52(5):2462-2467.

397. Ballard VL, Sharma A, Duignan I, et al. Vascular tenascin-C regulates cardiac endothelial phenotype and neovascularization. *Faseb J.* Apr 2006;20(6):717-719.

398. Hinz B. The myofibroblast: paradigm for a mechanically active cell. *J Biomech.* Jan 5 2010;43(1):146-155.

399. Desmouliere A, Redard M, Darby I, Gabbiani G. Apoptosis mediates the decrease in cellularity during the transition between granulation tissue and scar. *Am J Pathol.* Jan 1995;146(1):56-66.

400. Fassler R, Sasaki T, Timpl R, Chu ML, Werner S. Differential regulation of fibulin, tenascin-C, and nidogen expression during wound healing of normal and glucocorticoid-treated mice. *Exp Cell Res.* Jan 10 1996;222(1):111-116.

401. Abergel RP, Pizzurro D, Meeker CA, et al. Biochemical composition of the connective tissue in keloids and analysis of collagen metabolism in keloid fibroblast cultures. *J Invest Dermatol.* May 1985;84(5):384-390.

402. Zouboulis CC, Blume U, Buttner P, Orfanos CE. Outcomes of cryosurgery in keloids and hypertrophic scars. A prospective consecutive trial of case series. *Arch Dermatol.* Sep 1993;129(9):1146-1151.

403. Dalkowski A, Schuppan D, Orfanos CE, Zouboulis CC. Increased expression of tenascin C by keloids in vivo and in vitro. *Br J Dermatol*. Jul 1999;141(1):50-56.

404. Dvorak HF. Tumors: wounds that do not heal. Similarities between tumor stroma generation and wound healing. *N Engl J Med*. Dec 25 1986;315(26):1650-1659.

405. Ronnov-Jessen L, Petersen OW, Bissell MJ. Cellular changes involved in conversion of normal to malignant breast: importance of the stromal reaction. *Physiol Rev*. Jan 1996;76(1):69-125.

406. Chiquet-Ehrismann R, Mackie EJ, Pearson CA, Sakakura T. Tenascin: an extracellular matrix protein involved in tissue interactions during fetal development and oncogenesis. *Cell*. Oct 10 1986;47(1):131-139.

407. Latijnhouwers MA, Pfundt R, de Jongh GJ, Schalkwijk J. Tenascin-C expression in human epidermal keratinocytes is regulated by inflammatory cytokines and a stress response pathway. *Matrix Biol*. Aug 1998;17(4):305-316.

408. Mackie EJ, Abraham LA, Taylor SL, Tucker RP, Murphy LI. Regulation of tenascin-C expression in bone cells by transforming growth factor-beta. *Bone*. Apr 1998;22(4):301-307.

409. Mettouchi A, Cabon F, Montreau N, et al. The c-Jun-induced transformation process involves complex regulation of tenascin-C expression. *Mol Cell Biol*. Jun 1997;17(6):3202-3209.

410. Yamamoto K, Dang QN, Kennedy SP, Osathanondh R, Kelly RA, Lee RT. Induction of tenascin-C in cardiac myocytes by mechanical deformation. Role of reactive oxygen species. *J Biol Chem*. Jul 30 1999;274(31):21840-21846.

411. Gebb SA, Jones PL. Hypoxia and lung branching morphogenesis. *Adv Exp Med Biol*. 2003;543:117-125.

412. Tucker RP, Chiquet-Ehrismann R. The regulation of tenascin expression by tissue microenvironments. *Biochim Biophys Acta*. May 2009;1793(5):888-892.

413. Sarasa-Renedo A, Chiquet M. Mechanical signals regulating extracellular matrix gene expression in fibroblasts. *Scand J Med Sci Sports*. Aug 2005;15(4):223-230.

414. Siri A, Knauper V, Veirana N, Caocci F, Murphy G, Zardi L. Different susceptibility of small and large human tenascin-C isoforms to degradation by matrix metalloproteinases. *J Biol Chem*. Apr 14 1995;270(15):8650-8654.

415. Imai K, Kusakabe M, Sakakura T, Nakanishi I, Okada Y. Susceptibility of tenascin to degradation by matrix metalloproteinases and serine proteinases. *FEBS Lett*. Sep 26 1994;352(2):216-218.

416. Kusagawa H, Onoda K, Namikawa S, et al. Expression and degeneration of tenascin-C in human lung cancers. *Br J Cancer*. 1998;77(1):98-102.

417. Cai M, Onoda K, Takao M, et al. Degradation of tenascin-C and activity of matrix metalloproteinase-2 are associated with tumor recurrence in early stage non-small cell lung cancer. *Clin Cancer Res*. Apr 2002;8(4):1152-1156.

418. Huang W, Chiquet-Ehrismann R, Moyano JV, Garcia-Pardo A, Orend G. Interference of tenascin-C with syndecan-4 binding to fibronectin blocks cell adhesion and stimulates tumor cell proliferation. *Cancer Res*. Dec 1 2001;61(23):8586-8594.

419. Taraseviciute A, Vincent BT, Schedin P, Jones PL. Quantitative analysis of three-dimensional human mammary epithelial tissue architecture reveals a role for tenascin-C in regulating c-met function. *Am J Pathol*. Feb 2010;176(2):827-838.

420. Fukunaga-Kalabis M, Martinez G, Nguyen TK, et al. Tenascin-C promotes melanoma progression by maintaining the ABCB5-positive side population. *Oncogene*. Nov 18 2010;29(46):6115-6124.

421. Vollmer G. Biologic and oncologic implications of tenascin-C/hexabrachion proteins. *Crit Rev Oncol Hematol*. Apr 1997;25(3):187-210.

422. von Holst A. Tenascin C in stem cell niches: redundant, permissive or instructive? *Cells Tissues Organs*. 2008;188(1-2):170-177.

423. Garcion E, Faissner A, ffrench-Constant C. Knockout mice reveal a contribution of the extracellular matrix molecule tenascin-C to neural precursor proliferation and migration. *Development*. Jul 2001;128(13):2485-2496.

424. Nie S, Gurrea M, Zhu J, et al. Tenascin-C: a novel candidate marker for cancer stem cells in glioblastoma identified by tissue microarrays. *J Proteome Res*. Feb 6 2015;14(2):814-822.

425. Klein G, Beck S, Muller CA. Tenascin is a cytoadhesive extracellular matrix component of the human hematopoietic microenvironment. *J Cell Biol*. Nov 1993;123(4):1027-1035.

426. Ohta M, Sakai T, Saga Y, Aizawa S, Saito M. Suppression of hematopoietic activity in tenascin-C-deficient mice. *Blood*. Jun 1 1998;91(11):4074-4083.

427. Ruiz C, Huang W, Hegi ME, et al. Growth promoting signaling by tenascin-C [corrected]. *Cancer Res*. Oct 15 2004;64(20):7377-7385.

428. Orend G, Chiquet-Ehrismann R. Adhesion modulation by antiadhesive molecules of the extracellular matrix. *Exp Cell Res*. Nov 25 2000;261(1):104-110.

429. Woods A, Longley RL, Tumova S, Couchman JR. Syndecan-4 binding to the high affinity heparin-binding domain of fibronectin drives focal adhesion formation in fibroblasts. *Arch Biochem Biophys*. Feb 1 2000;374(1):66-72.

430. Orend G, Huang W, Olayioye MA, Hynes NE, Chiquet-Ehrismann R. Tenascin-C blocks cell-cycle progression of anchorage-dependent fibroblasts on fibronectin through inhibition of syndecan-4. *Oncogene*. Jun 19 2003;22(25):3917-3926.

431. Midwood KS, Schwarzbauer JE. Tenascin-C modulates matrix contraction via focal adhesion kinase- and Rho-mediated signaling pathways. *Mol Biol Cell*. Oct 2002;13(10):3601-3613.

432. Ohh M, Yauch RL, Lonergan KM, et al. The von Hippel-Lindau tumor suppressor protein is required for proper assembly of an extracellular fibronectin matrix. *Mol Cell*. Jun 1998;1(7):959-968.

433. Maschler S, Grunert S, Danielopol A, Beug H, Wirl G. Enhanced tenascin-C expression and matrix deposition during Ras/TGF-beta-induced progression of mammary tumor cells. *Oncogene*. Apr 29 2004;23(20):3622-3633.

434. Takahashi Y, Sawada G, Kurashige J, et al. Tumor-derived tenascin-C promotes the epithelial-mesenchymal transition in colorectal cancer cells. *Anticancer Res*. May 2013;33(5):1927-1934.

435. Nagaharu K, Zhang X, Yoshida T, et al. Tenascin C induces epithelial-mesenchymal transition-like change accompanied by SRC activation and focal adhesion kinase phosphorylation in human breast cancer cells. *Am J Pathol*. Feb 2011;178(2):754-763.

436. Deryugina EI, Bourdon MA. Tenascin mediates human glioma cell migration and modulates cell migration on fibronectin. *J Cell Sci*. Mar 1996;109 (Pt 3):643-652.

437. Nishio T, Kawaguchi S, Yamamoto M, Iseda T, Kawasaki T, Hase T. Tenascin-C regulates proliferation and migration of cultured astrocytes in a scratch wound assay. *Neuroscience*. 2005;132(1):87-102.

438. Wilson KE, Bartlett JM, Miller EP, et al. Regulation and function of the extracellular matrix protein tenascin-C in ovarian cancer cell lines. *Br J Cancer*. May 1999;80(5-6):685-692.

439. Yoshida T, Yoshimura E, Numata H, Sakakura Y, Sakakura T. Involvement of tenascin-C in proliferation and migration of laryngeal carcinoma cells. *Virchows Arch*. Nov 1999;435(5):496-500.

440. Herold-Mende C, Mueller MM, Bonsanto MM, Schmitt HP, Kunze S, Steiner HH. Clinical impact and functional aspects of tenascin-C expression during glioma progression. *Int J Cancer*. Mar 20 2002;98(3):362-369.

441. Katenkamp K, Berndt A, Hindermann W, et al. mRNA expression and protein distribution of the unspliced tenascin-C isoform in prostatic adenocarcinoma. *J Pathol*. Jul 2004;203(3):771-779.

442. Kaarteenaho-Wiik R, Soini Y, Pollanen R, Paakko P, Kinnula VL. Over-expression of tenascin-C in malignant pleural mesothelioma. *Histopathology*. Mar 2003;42(3):280-291.

443. Ilmonen S, Jahkola T, Turunen JP, Muhonen T, Asko-Seljavaara S. Tenascin-C in primary malignant melanoma of the skin. *Histopathology*. Oct 2004;45(4):405-411.

444. Aishima S, Taguchi K, Terashi T, Matsuura S, Shimada M, Tsuneyoshi M. Tenascin expression at the invasive front is associated with poor prognosis in intrahepatic cholangiocarcinoma. *Mod Pathol*. Oct 2003;16(10):1019-1027.

445. Hancox RA, Allen MD, Holliday DL, et al. Tumour-associated tenascin-C isoforms promote breast cancer cell invasion and growth by matrix metalloproteinase-dependent and independent mechanisms. *Breast Cancer Res*. 2009;11(2):R24.

446. Oskarsson T, Acharyya S, Zhang XH, et al. Breast cancer cells produce tenascin C as a metastatic niche component to colonize the lungs. *Nat Med*. Jul 2011;17(7):867-874.

447. O'Connell JT, Sugimoto H, Cooke VG, et al. VEGF-A and Tenascin-C produced by S100A4+ stromal cells are important for metastatic colonization. *Proc Natl Acad Sci U S A*. Sep 20 2011;108(38):16002-16007.

448. Oskarsson T, Massague J. Extracellular matrix players in metastatic niches. *Embo J*. Jan 18 2012;31(2):254-256.

449. Minn AJ, Gupta GP, Siegel PM, et al. Genes that mediate breast cancer metastasis to lung. *Nature*. Jul 28 2005;436(7050):518-524.

450. Gurbuz I, Ferralli J, Roloff T, Chiquet-Ehrismann R, Asparuhova MB. SAP domain-dependent Mkl1 signaling stimulates proliferation and cell migration by induction of a distinct gene set indicative of poor prognosis in breast cancer patients. *Mol Cancer*. 2014;13:22.

451. Parekh K, Ramachandran S, Cooper J, Bigner D, Patterson A, Mohanakumar T. Tenascin-C, over expressed in lung cancer down regulates effector functions of tumor infiltrating lymphocytes. *Lung Cancer*. Jan 2005;47(1):17-29.

452. Juhasz A, Bardos H, Repassy G, Adany R. Characteristic distribution patterns of tenascin in laryngeal and hypopharyngeal cancers. *Laryngoscope*. Jan 2000;110(1):84-92.

453. Van Obberghen-Schilling E, Tucker RP, Saupe F, Gasser I, Cseh B, Orend G. Fibronectin and tenascin-C: accomplices in vascular morphogenesis during development and tumor growth. *Int J Dev Biol*. 2011;55(4-5):511-525.

454. Tanaka K, Hiraiwa N, Hashimoto H, Yamazaki Y, Kusakabe M. Tenascin-C regulates angiogenesis in tumor through the regulation of vascular endothelial growth factor expression. *Int J Cancer*. Jan 1 2004;108(1):31-40.

455. Chiquet M, Fambrough DM. Chick myotendinous antigen. I. A monoclonal antibody as a marker for tendon and muscle morphogenesis. *J Cell Biol*. Jun 1984;98(6):1926-1936.

456. Chiquet-Ehrismann R, Tannheimer M, Koch M, et al. Tenascin-C expression by fibroblasts is elevated in stressed collagen gels. *J Cell Biol*. Dec 1994;127(6 Pt 2):2093-2101.

457. Trachslin J, Koch M, Chiquet M. Rapid and reversible regulation of collagen XII expression by changes in tensile stress. *Exp Cell Res*. Mar 15 1999;247(2):320-328.

458. Chiquet M, Sarasa-Renedo A, Tunc-Civelek V. Induction of tenascin-C by cyclic tensile strain versus growth factors: distinct contributions by

Rho/ROCK and MAPK signaling pathways. *Biochim Biophys Acta*. Sep 17 2004;1693(3):193-204.

459. Wang DZ, Li S, Hockemeyer D, et al. Potentiation of serum response factor activity by a family of myocardin-related transcription factors. *Proc Natl Acad Sci U S A*. Nov 12 2002;99(23):14855-14860.

460. Sotiropoulos A, Gineitis D, Copeland J, Treisman R. Signal-regulated activation of serum response factor is mediated by changes in actin dynamics. *Cell*. Jul 23 1999;98(2):159-169.

461. Asparuhova MB, Ferralli J, Chiquet M, Chiquet-Ehrismann R. The transcriptional regulator megakaryoblastic leukemia-1 mediates serum response factor-independent activation of tenascin-C transcription by mechanical stress. *Faseb J*. Oct 2011;25(10):3477-3488.

462. Kaiser S, Park YK, Franklin JL, et al. Transcriptional recapitulation and subversion of embryonic colon development by mouse colon tumor models and human colon cancer. *Genome Biol*. 2007;8(7):R131.

463. Comprehensive molecular characterization of human colon and rectal cancer. *Nature*. Jul 19 2012;487(7407):330-337.

464. Skrzypczak M, Goryca K, Rubel T, et al. Modeling oncogenic signaling in colon tumors by multidirectional analyses of microarray data directed for maximization of analytical reliability. *PLoS One*. 2010;5(10).

465. Hong Y, Downey T, Eu KW, Koh PK, Cheah PY. A 'metastasis-prone' signature for early-stage mismatch-repair proficient sporadic colorectal cancer patients and its implications for possible therapeutics. *Clin Exp Metastasis*. Feb 2010;27(2):83-90.

466. Bestor T, Laudano A, Mattaliano R, Ingram V. Cloning and sequencing of a cDNA encoding DNA methyltransferase of mouse cells. The carboxyl-terminal domain of the mammalian enzymes is related to bacterial restriction methyltransferases. *J Mol Biol*. Oct 20 1988;203(4):971-983.

467. Monk M. Changes in DNA methylation during mouse embryonic development in relation to X-chromosome activity and imprinting. *Philos Trans R Soc Lond B Biol Sci*. Jan 30 1990;326(1235):299-312.

468. Robertson KD, Uzvolgyi E, Liang G, et al. The human DNA methyltransferases (DNMTs) 1, 3a and 3b: coordinate mRNA expression in normal tissues and overexpression in tumors. *Nucleic Acids Res*. Jun 1 1999;27(11):2291-2298.

469. Baylin SB, Esteller M, Rountree MR, Bachman KE, Schuebel K, Herman JG. Aberrant patterns of DNA methylation, chromatin formation and gene expression in cancer. *Hum Mol Genet*. Apr 2001;10(7):687-692.

470. Garinis GA, Patrinos GP, Spanakis NE, Menounos PG. DNA hypermethylation: when tumour suppressor genes go silent. *Hum Genet*. Aug 2002;111(2):115-127.

471. Melki JR, Vincent PC, Brown RD, Clark SJ. Hypermethylation of E-cadherin in leukemia. *Blood*. May 15 2000;95(10):3208-3213.

472. Boultwood J, Wainscoat JS. Gene silencing by DNA methylation in haematological malignancies. *Br J Haematol*. Jul 2007;138(1):3-11.

473. Stresemann C, Lyko F. Modes of action of the DNA methyltransferase inhibitors azacytidine and decitabine. *International journal of cancer*. Jul 1 2008;123(1):8-13.

474. Bender CM, Gonzalgo ML, Gonzales FA, Nguyen CT, Robertson KD, Jones PA. Roles of cell division and gene transcription in the methylation of CpG islands. *Mol Cell Biol*. Oct 1999;19(10):6690-6698.

475. Jones PA, Taylor SM. Cellular differentiation, cytidine analogs and DNA methylation. *Cell*. May 1980;20(1):85-93.

476. Hagemann S, Heil O, Lyko F, Brueckner B. Azacytidine and decitabine induce gene-specific and non-random DNA demethylation in human cancer cell lines. *PLoS One*. 2011;6(3):e17388.

477. Friedel RH, Plump A, Lu X, et al. Gene targeting using a promoterless gene trap vector ("targeted trapping") is an efficient method to mutate a large fraction of genes. *Proc Natl Acad Sci U S A*. Sep 13 2005;102(37):13188-13193.

478. Croft DR, Olson MF. Conditional regulation of a ROCK-estrogen receptor fusion protein. *Methods Enzymol*. 2006;406:541-553.

479. Samuel MS, Munro J, Bryson S, Forrow S, Stevenson D, Olson MF. Tissue selective expression of conditionally-regulated ROCK by gene targeting to a defined locus. *Genesis*. Jul 2009;47(7):440-446.

480. Romer J, Pyke C, Lund LR, Ralfkiaer E, Dano K. Cancer cell expression of urokinase-type plasminogen activator receptor mRNA in squamous cell carcinomas of the skin. *J Invest Dermatol*. Mar 2001;116(3):353-358.

481. Wei Y, Waltz DA, Rao N, Drummond RJ, Rosenberg S, Chapman HA. Identification of the urokinase receptor as an adhesion receptor for vitronectin. *J Biol Chem*. Dec 23 1994;269(51):32380-32388.

482. Shi M, He X, Wei W, Wang J, Zhang T, Shen X. Tenascin-C induces resistance to apoptosis in pancreatic cancer cell through activation of ERK/NF-kappaB pathway. *Apoptosis*. Jun 2015;20(6):843-857.

483. Riker AI, Enkemann SA, Fodstad O, et al. The gene expression profiles of primary and metastatic melanoma yields a transition point of tumor progression and metastasis. *BMC Med Genomics*. 2008;1:13.

484. Nindl I, Dang C, Forschner T, et al. Identification of differentially expressed genes in cutaneous squamous cell carcinoma by microarray expression profiling. *Mol Cancer*. 2006;5:30.

485. Qiu RG, Chen J, McCormick F, Symons M. A role for Rho in Ras transformation. *Proc Natl Acad Sci U S A*. Dec 5 1995;92(25):11781-11785.

486. Ihn H. Scleroderma, fibroblasts, signaling, and excessive extracellular matrix. *Curr Rheumatol Rep*. Apr 2005;7(2):156-162.

487. Hill CS, Wynne J, Treisman R. The Rho family GTPases RhoA, Rac1, and CDC42Hs regulate transcriptional activation by SRF. *Cell*. Jun 30 1995;81(7):1159-1170.

488. Riedl J, Crevenna AH, Kessenbrock K, et al. Lifeact: a versatile marker to visualize F-actin. *Nat Methods*. Jul 2008;5(7):605-607.

489. Riedl J, Flynn KC, Raducanu A, et al. Lifeact mice for studying F-actin dynamics. *Nat Methods*. Mar 2010;7(3):168-169.

490. McConnell BV, Koto K, Gutierrez-Hartmann A. Nuclear and cytoplasmic LIMK1 enhances human breast cancer progression. *Mol Cancer*. 2011;10:75.

491. Mardilovich K, Gabrielsen M, McGarry L, et al. Elevated LIM kinase 1 in nonmetastatic prostate cancer reflects its role in facilitating androgen receptor nuclear translocation. *Mol Cancer Ther*. Jan 2015;14(1):246-258.

492. Rak R, Haklai R, Elad-Tzfadia G, Wolfson HJ, Carmeli S, Kloog Y. Novel LIMK2 Inhibitor Blocks Panc-1 Tumor Growth in a mouse xenograft model. *Oncoscience*. 2014;1(1):39-48.

493. Gewirtz DA. A critical evaluation of the mechanisms of action proposed for the antitumor effects of the anthracycline antibiotics adriamycin and daunorubicin. *Biochem Pharmacol*. Apr 1 1999;57(7):727-741.

494. Sumi T, Hashigasako A, Matsumoto K, Nakamura T. Different activity regulation and subcellular localization of LIMK1 and LIMK2 during cell cycle transition. *Exp Cell Res*. Apr 15 2006;312(7):1021-1030.

495. Zhou Y, Su J, Shi L, Liao Q, Su Q. DADS downregulates the Rac1-ROCK1/PAK1-LIMK1-ADF/cofilin signaling pathway, inhibiting cell migration and invasion. *Oncol Rep*. Feb 2013;29(2):605-612.

496. Petersen VC, Baxter KJ, Love SB, Shepherd NA. Identification of objective pathological prognostic determinants and models of prognosis in Dukes' B colon cancer. *Gut*. Jul 2002;51(1):65-69.

497. McMillan DC, Crozier JE, Canna K, Angerson WJ, McArdle CS. Evaluation of an inflammation-based prognostic score (GPS) in patients undergoing resection for colon and rectal cancer. *Int J Colorectal Dis*. Aug 2007;22(8):881-886.

498. Roth AD, Tejpar S, Delorenzi M, et al. Prognostic role of KRAS and BRAF in stage II and III resected colon cancer: results of the translational study on the PETACC-3, EORTC 40993, SAKK 60-00 trial. *J Clin Oncol*. Jan 20 2010;28(3):466-474.

499. Johnson EO, Chang KH, Ghosh S, et al. LIMK2 is a crucial regulator and effector of Aurora-A-kinase-mediated malignancy. *J Cell Sci*. Mar 1 2012;125(Pt 5):1204-1216.

500. Mashiach-Farkash E, Rak R, Elad-Sfadia G, et al. Computer-based identification of a novel LIMK1/2 inhibitor that synergizes with salirasib to destabilize the actin cytoskeleton. *Oncotarget*. Jun 2012;3(6):629-639.

501. Robanus-Maandag EC, Koelink PJ, Breukel C, et al. A new conditional Apc-mutant mouse model for colorectal cancer. *Carcinogenesis*. May 2010;31(5):946-952.

502. Laird PW, Jackson-Grusby L, Fazeli A, et al. Suppression of intestinal neoplasia by DNA hypomethylation. *Cell*. Apr 21 1995;81(2):197-205.

503. Flis S, Gnyszka A, Flis K. DNA methyltransferase inhibitors improve the effect of chemotherapeutic agents in SW48 and HT-29 colorectal cancer cells. *PLoS One*. 2014;9(3):e92305.

504. Brown R, Curry E, Magnani L, Wilhelm-Benartzi CS, Borley J. Poised epigenetic states and acquired drug resistance in cancer. *Nat Rev Cancer*. Nov 2014;14(11):747-753.

505. Tada S, Iwamoto H, Nakamuta M, et al. A selective ROCK inhibitor, Y27632, prevents dimethylnitrosamine-induced hepatic fibrosis in rats. *Journal of hepatology*. Apr 2001;34(4):529-536.

506. Bei Y, Hua-Huy T, Duong-Quy S, et al. Long-term treatment with fasudil improves bleomycin-induced pulmonary fibrosis and pulmonary

hypertension via inhibition of Smad2/3 phosphorylation. *Pulmonary pharmacology & therapeutics*. Dec 2013;26(6):635-643.

507. Talts JF, Wirl G, Dictor M, Muller WJ, Fassler R. Tenascin-C modulates tumor stroma and monocyte/macrophage recruitment but not tumor growth or metastasis in a mouse strain with spontaneous mammary cancer. *J Cell Sci*. Jun 1999;112 (Pt 12):1855-1864.

508. Brahmer JR, Tykodi SS, Chow LQ, et al. Safety and activity of anti-PD-L1 antibody in patients with advanced cancer. *N Engl J Med*. Jun 28 2012;366(26):2455-2465.

509. Herbst RS, Soria JC, Kowanetz M, et al. Predictive correlates of response to the anti-PD-L1 antibody MPDL3280A in cancer patients. *Nature*. Nov 27 2014;515(7528):563-567.

510. Kular J, Scheer KG, Pyne NT, et al. A Negative Regulatory Mechanism Involving 14-3-3zeta Limits Signaling Downstream of ROCK to Regulate Tissue Stiffness in Epidermal Homeostasis. *Dev Cell*. Dec 21 2015;35(6):759-774.

511. Maher CA, Kumar-Sinha C, Cao X, et al. Transcriptome sequencing to detect gene fusions in cancer. *Nature*. Mar 5 2009;458(7234):97-101.

512. Liotta L, Petricoin E. Molecular profiling of human cancer. *Nat Rev Genet*. Oct 2000;1(1):48-56.

513. Yokoyama-Kobayashi M, Saeki M, Sekine S, Kato S. Human cDNA encoding a novel TGF-beta superfamily protein highly expressed in placenta. *J Biochem*. Sep 1997;122(3):622-626.

514. Lawton LN, Bonaldo MF, Jelenc PC, et al. Identification of a novel member of the TGF-beta superfamily highly expressed in human placenta. *Gene*. Dec 5 1997;203(1):17-26.

515. Breit SN, Johnen H, Cook AD, et al. The TGF-beta superfamily cytokine, MIC-1/GDF15: a pleotrophic cytokine with roles in inflammation, cancer and metabolism. *Growth Factors*. Oct 2011;29(5):187-195.

516. Bauskin AR, Brown DA, Kuffner T, et al. Role of macrophage inhibitory cytokine-1 in tumorigenesis and diagnosis of cancer. *Cancer Res.* May 15 2006;66(10):4983-4986.

517. Brown DA, Stephan C, Ward RL, et al. Measurement of serum levels of macrophage inhibitory cytokine 1 combined with prostate-specific antigen improves prostate cancer diagnosis. *Clin Cancer Res.* Jan 1 2006;12(1):89-96.

518. Brown DA, Ward RL, Buckhaults P, et al. MIC-1 serum level and genotype: associations with progress and prognosis of colorectal carcinoma. *Clin Cancer Res.* Jul 2003;9(7):2642-2650.

519. Bruzzese F, Hagglof C, Leone A, et al. Local and systemic protumorigenic effects of cancer-associated fibroblast-derived GDF15. *Cancer Res.* Jul 1 2014;74(13):3408-3417.

520. Yanaba K, Asano Y, Tada Y, Sugaya M, Kadono T, Sato S. Clinical significance of serum growth differentiation factor-15 levels in systemic sclerosis: association with disease severity. *Mod Rheumatol.* Sep 2012;22(5):668-675.

521. Lambrecht S, Smith V, De Wilde K, et al. Growth differentiation factor 15, a marker of lung involvement in systemic sclerosis, is involved in fibrosis development but is not indispensable for fibrosis development. *Arthritis Rheumatol.* Feb 2014;66(2):418-427.

522. Taylor BC, Zaph C, Troy AE, et al. TSLP regulates intestinal immunity and inflammation in mouse models of helminth infection and colitis. *J Exp Med.* Mar 16 2009;206(3):655-667.

523. Yoo J, Omori M, Gyarmati D, et al. Spontaneous atopic dermatitis in mice expressing an inducible thymic stromal lymphopoietin transgene specifically in the skin. *J Exp Med.* Aug 15 2005;202(4):541-549.

524. Jariwala SP, Abrams E, Benson A, Fodeman J, Zheng T. The role of thymic stromal lymphopoietin in the immunopathogenesis of atopic dermatitis. *Clin Exp Allergy.* Nov 2011;41(11):1515-1520.

525. Christmann RB, Mathes A, Affandi AJ, et al. Thymic stromal lymphopoietin is up-regulated in the skin of patients with systemic sclerosis and induces profibrotic genes and intracellular signaling that overlap with those induced by interleukin-13 and transforming growth factor beta. *Arthritis Rheum*. May 2013;65(5):1335-1346.

526. Grivennikov SI, Greten FR, Karin M. Immunity, inflammation, and cancer. *Cell*. Mar 19 2010;140(6):883-899.

527. De Monte L, Reni M, Tassi E, et al. Intratumor T helper type 2 cell infiltrate correlates with cancer-associated fibroblast thymic stromal lymphopoietin production and reduced survival in pancreatic cancer. *J Exp Med*. Mar 14 2011;208(3):469-478.

528. Xie F, Meng YH, Liu LB, et al. Cervical carcinoma cells stimulate the angiogenesis through TSLP promoting growth and activation of vascular endothelial cells. *Am J Reprod Immunol*. Jul 2013;70(1):69-79.

529. Olkhanud PB, Rochman Y, Bodogai M, et al. Thymic stromal lymphopoietin is a key mediator of breast cancer progression. *J Immunol*. May 15 2011;186(10):5656-5662.